NTNU
Norwegian University of
Science and Technology

Screw Extrusion from various Binary Al-XMg Feed Materials

Effects of Heat Treatment on Microstructure

Tarjei Berulfsen

Materials Science and Engineering
Submission date: June 2016
Supervisor: Hans Jørgen Roven, IMTE
Co-supervisor: Oddvin Reiso, IMT
Kristian Grøtta Skorpen, IMT

Norwegian University of Science and Technology
Department of Materials Science and Engineering

Preface

This is a master thesis done at NTNU in the spring semester of 2016, at the Department of Materials Science and Engineering. The project has been carried out in cooperation with Hydro Aluminium.

NTNU, June 24, 2016
Tarjei Berulfsen

Acknowledgment

I would like to thank the following persons for their great help during this master thesis.

Kristian Grøtta Skorpen, for his assistance during experimental work, useful tips for specimen preparation, and theoretical discussions.

Trygve Schance, for tutoring me on lab equipment.

Yingda Yu, for patient tutoring on the SEM.

Kristin Høydalsvik Wells and Magnus Rotan for help with XRD.

And last, Hans Jørgen Roven, for guidance and encouraging words.

Tarjei Berulfsen

(T.B)

Aims

The primary goal with this work is to produce and characterize screw extruded profiles from two different feed stock materials.

The first feed stock material is granulates, machined from DC cast billets. The second feed stock material is re-melted DC cast billets, that subsequently are rapidly solidified to ribbons. Both feed stock materials have the same chemical composition spanning from Al-5wt%Mg to Al-10wt%Mg.

A secondary goal with this work is to explore the effects of homogenization parameters on particles and phases present in the material, and microstructure in general. In addition, the screw extrusion method is still new. Therefore, gathering information that will further the progress of this method is also a secondary goal.

Abstract

Three direct chill (DC) cast aluminium-magnesium (Al-Mg) alloys, with 5, 8, and 10 wt% magnesium, have been used as base materials. These base materials were either rapidly solidified by melt spinning, or granulated by machining DC cast billets. Finally, the rapidly solidified and machined feed stock materials have been screw extruded. This is a novel extrusion method developed at NTNU in cooperation with Hydro Aluminium.

In addition, various homogenization treatments have been examined. This was done in order to determine whether it is possible to eliminate the brittle intermetallic beta phase, by subjecting the cast material to a heating schedule in an air circulation furnace and quenching in water.

The investigated materials have been characterized by optical microscopy, hardness measurements, scanning electron microscopy and x-ray diffraction.

It has been found that screw extrusion produces profiles with good mechanical properties, compared to conventional ram extruded profiles. The grain size was much smaller, by approximately 50µm. In addition,the ultimate tensile strength of screw extruded Al-8wt%Mg was comparable to conventional extruded Al-10wt%Mg.

The homogenized DC cast material shows presence of beta particles in the first stage of the heat treatment schedule, but not in the last stage. It has also been found that time has an effect on the precipitation of the intermetallic beta phase. A DC cast sample homogenized at 430°C for four hours showed presence of beta, but a DC cast sample homogenized at 430°C for one week, did not. Homogenization time and temperature was also found to have a rather complex influence on the large amount of porosity already present in the DC cast material.

Sammendrag

Tre direkt kjølte (DC) støpte aluminium-magnesium (Al-Mg) legeringer med henholdsvis 5, 8, og 10 wt% magnesium har vært brukt som basismaterialer. Disse basismaterialene har vært brukt til å lage to foringsmaterialer. Basismaterialet har vært omsmeltet og hurtigkjølt ved smeltespinningsmetoden, og i tillegg maskinert til spon. Disse to foringsmaterialene har så blitt skrueekstrudert. Dette er en ny type ekstrudering av aluminium, utviklet av Hydro Aluminium i samarbeid med NTNU.

Basismaterialet har også vært homogenisert ved diverse varmebehandlingparametre. Dette har vært gjort for å se om det er mulig å eliminere den sprø og uønskede beta fasen ved varmebehandling i en luftsirkulasjonsovn, etterfulgt av bråkjøling i vann.

Materialene som har vært undersøkt har blitt karakterisert ved hjelp av optisk mikrografi, hardhetsmålinger, elektronmikroskopi, og røntgendiffraksjon.

Skrueekstrudering ga profiler med gode mekaniske egenskaper sammenlignet med konvensjonelle stempelekstruderte profiler. Kornstørrelsen var ca. 50µm mindre for skrueekstruderte profiler sammenlignet med stempelekstruderte profiler. Strekkfastheten var også høyere for de skrueekstruderte profilene. Strekkfastheten til begge de skrueekstruderte Al-8wt%Mg profilene kunne sammenlignes med stempelekstrudert Al-10wt%Mg.

Det homogeniserte basismaterialet viste betapartikler etter den første delen av varmebehandlingen, men ikke etter den andre delen. Det har også blitt oppdaget at tid har en effekt på mengde betapartikler. En DC-støpt prøve som ble homogenisert på 430°C i fire timer viste betapartikler. Det viste ikke en DC-støpt prøve som ble homogenisert ved 430°C i én uke. Homogeniseringstid og temperatur har også vist å ha en relativt kompleks innvirkning på porøsitet, som det var mye av i basismaterialet.

Contents

1 | Introduction

Aluminum (Al) is a light material, and of interest in many industries, construction and transportation being two major industries with interest. Adding alloying elements to aluminum is an easy way of drastically changing its properties, while still maintaining the low weight. Magnesium(Mg) as an alloying element gives a great contribution to strength. Mg has a hexagonal close-packed (HCP)-structure, which is more difficult to deform than aluminums face centered cubic(FCC) structure and it greatly contributes to work hardening effects.

The wrought 5xxx, and cast 5xx.x systems of alloys, are the primary Al-Mg system, and the magnesium content ranges from 0.5-13 wt% Mg. A key part of any high magnesium containing aluminum alloy, is to get magnesium in solid solution. This introduces a lattice strain in the aluminum matrix, which interacts with dislocations and strengthens the material. Generally, more magnesium in solid solution is better, however, achieving this can be difficult. Maximum solid solution of magnesium in aluminum is 17.3 wt% at 450°C, however, when cooling down, most of the magnesium will diffuse and form precipitates on the grain boundaries, lowering the mechanical properties. Increasing the cooling rate, increases the amount of magnesium in solid solution. Therefore, developing knowledge and methods on increasing the cooling rate of Al-Mg is of great interest. One such method, is the melt spinning method, explained in more detail in section 2.2. Melt spinning produces thin ribbons, like gift wrapping ribbons. The cooling rate of melt spinning is significantly higher than for conventional casting, and can produce alloys of high magnesium content. Another way, is heat treating Al-Mg alloys at higher temperature, until Mg is in solid solution through solid diffusion, and quenching in water.

A novel consolidation method developed at NTNU, in cooperation with Hydro aluminium, is

screw extrusion, see section 2.3 for more detail. This method already sees widespread use in the plastics industry, and is an interesting extrusion method for aluminum. Since screw extrusion is continuous, if proven successful, the process would be both energy, and time saving, in addition to giving a larger degree of freedom.

In this project, three different alloys have been produced, Al-5, 8, and 10 wt% Mg via melt spinning, with the goal of having as much magnesium in solid solution as possible. Al-5, 8, and 10%Mg as cast material have also been machined to granules. The machined granules and the melt spun material have then been consolidated via the screw extrusion method, with the goal of producing continuous profiles with good mechanical properties. In addition, Al-5, 8, and 10wt%Mg as cast material has been homogenized, and quenched. The resulting specimens have then been characterized by hardness testing, optical microscopy, SEM, and XRD. The homogenization investigation were conducted in order to reveal whether one can optimize the Mg-containing particle content versus Mg in solid solution.

For the sake of simplicity, Al-5, 8, 10%Mg will be interchangeably used in stead of Al-5, 8, 10wt%Mg from this point onward.

2 | Theoretical background

This chapter will give the reader insight into the theoretical background of the different analytical methods used to characterize the material, and mechanisms that might occur and will change the properties of the material.

2.1 The Al-Mg alloy system

Aluminium is a light element, with a density of $2.7 g/cm^3$, a lattice parameter of 4.0412 Å, and face centered (FCC) crystal structure. Magnesium is also a light element, with a density of 1.738 g/cm^3, a lattice parameter of 3.210 Å, and a hexagonal-close packed (HCP) crystal structure, which is less easily deformed than aluminium's FCC crystal structure. Data gathered from Murray (1982).

By adding small amounts of Mg to aluminium, and keeping it in solid solution, one can improve the mechanical properties of aluminium, which in its pure state, are quite poor. Mg in solid solution strains the lattice, and hinders dislocations from moving freely, improving the strength of aluminium.

A phase of interest in the Al-Mg system is the beta Al_3Mg_2 phase. This phase is very large, with a lattice parameter of 28.239 Å, and a unit cell of 1168 atoms (Samson, 1965). This phase is precipitated on grain boundaries and triple points upon cooling from liquid, in an Al-Mg alloy, and is generally unwanted, as it is brittle, and lowers the mechanical properties.

The Al-Mg phase diagram is shown in figure 2.1. In the Al rich area of the phase diagram, one can see the eutectic temperature is 450 °C, the eutectic composition is at 36.1 wt%, and the max

solubility of Mg in Al is 17.3 wt% Mg. Pure Al-Mg alloys are mostly used as wrought, non-heat treatable alloys, classified as the 5xxx series, due to the formation of the brittle Mg_5Al_8 β phase on dislocations and grain boundaries upon annealing. Used in its wrought state however, Al-Mg alloys have excellent corrosion resistance, surface quality, good weldability, and moderate strength, and achieving a super saturated solid up to 5 wt% Mg upon quenching is relatively easy. Although cast Al-Mg alloys are rare, low Mg cast alloys, classified as the 5xx.x series, and wrought heat treatable alloys with other alloying elements are made.

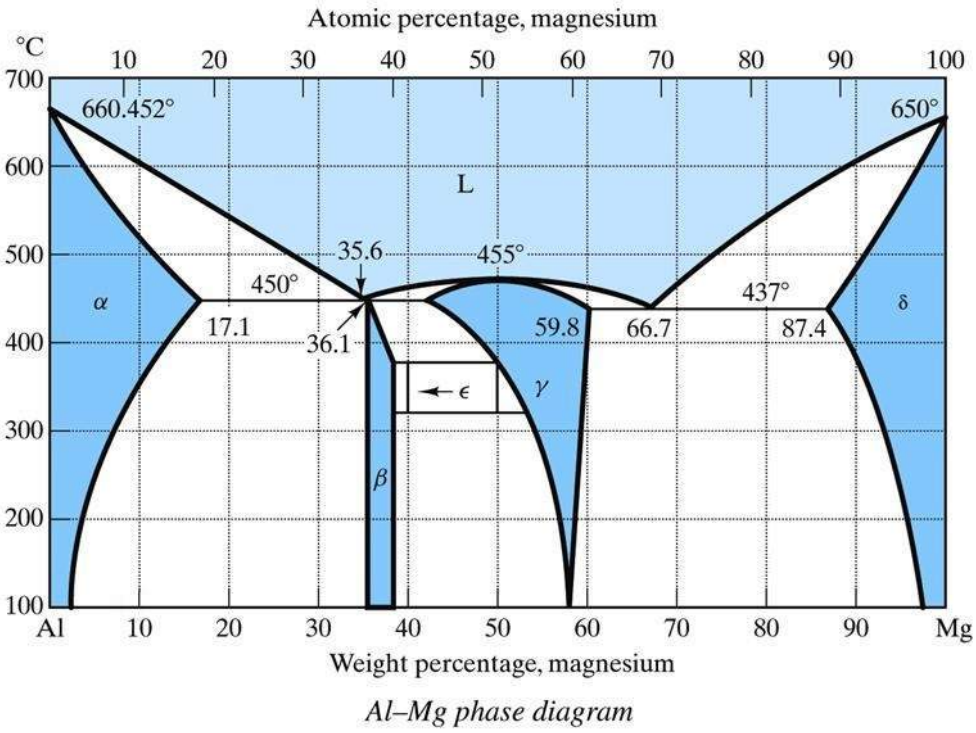

Figure 2.1: Al-Mg phase diagram (Kaufmyn (2016)).

2.2 Melt spinning

Melt spinning has been used as an engineering method since the late 1800s, one of the first reports of using rapid solidification, was E. M. Lang, who in 1871 used a simple chill block-melt spinning process to produce solder wire, however, melt spinning is still not a common industrial production method. One company that does utilize melt spinning as a production method

however, is RSP technology, who produce several different alloys, and claims applications such as automotive, aerospace, and electronics

Rapid solidification(RS) can be achieved by many methods, a few to be mentioned, are the atomization method, laser method, and single drop splat method. These methods produce very high solidification rates, but are more suited to the research environment, than the industrial environment. Melt spinning however, is an excellent production method for industrial use. A schematic of the basic principles can be seen in figure 2.2. Melt spinning is a semi-continuous batch process with a typical cooling rate of 10^6k/s, and only stops when there is no more melt left in the crucible. The method produces continuous ribbons of 0.x mm thickness, with width being dependent on the slit opening, usually in the mm range.

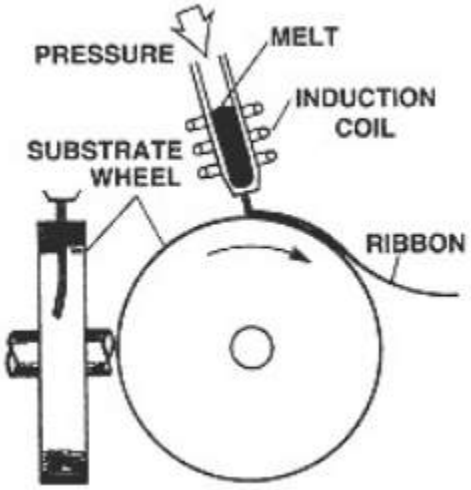

Figure 2.2: Schematic of a melt spinner Leibermann (1993).

Rapid quenching can be done from vapour, liquid, or solid state. The cooling rate of solid state quenching depends largely on the dimensions of the specimens. Quenching of steel in water, can yield rates up to 1000 K/s, where you start to run the risk of cracking. However, with very small dimensions, and cooling with high speed gas, cooling rates of 10 000-20 000 K/s can be achieved Míšek (1968). Cooling rates for vapour quenching are difficult to measure, but are generally higher than liquid quenching.

Pol Duwez is universally regarded as the man who spawned the new field of rapid solidification from liquid. He performed many experiments during the 1950s and 1960s, and proved that one

can achieve a metastable solid phase, from two stable phases. The definitive proof came when he made a metastable phase, from the two stable phases Ag and Cu, by rapidly solidifying a 25 mg liquid drop propelled against the inside of a high speed rotating copper cylinder Duwez et al. (1960).

In later years, there are several great contributors to the field of rapid solidification, three of which are John W. Cahn, Professor William Kurz, and Dr. William J. Boettinger.

During rapidsolidification, there is no longer a local equilibrium between the solid/liquidus interface. At low solidification rates, the chemical potential of element A and element B are equal at the solidification front.

$$\mu_{A,liquidus} = \mu_{A,solidus}, \qquad \mu_{B,liquidus} = \mu_{B,solidus} \tag{2.1}$$

At high solidification rates, this is no longer the case, and the interaction between solid and liquid, can no longer be explained by conventional solidification theory. An overview of what happens at higher undercoolings, can be seen in figure 2.3, from Boettinger and Coriell (1986). The metastable phases created at higher solidification rates, can be precipitation hardened, which is an important property of RS alloys.

In general, rapid solidification causes several microstructural changes, which according to Grant (1992), are:

- Sharply decreased segregation.
- Highly refined grain sizes.
- Much higher alloy contents.
- Highly increased metastable solid solubility.
- Production of new metastable phases.
- Formation of amorphous structures in selected metallic composites.

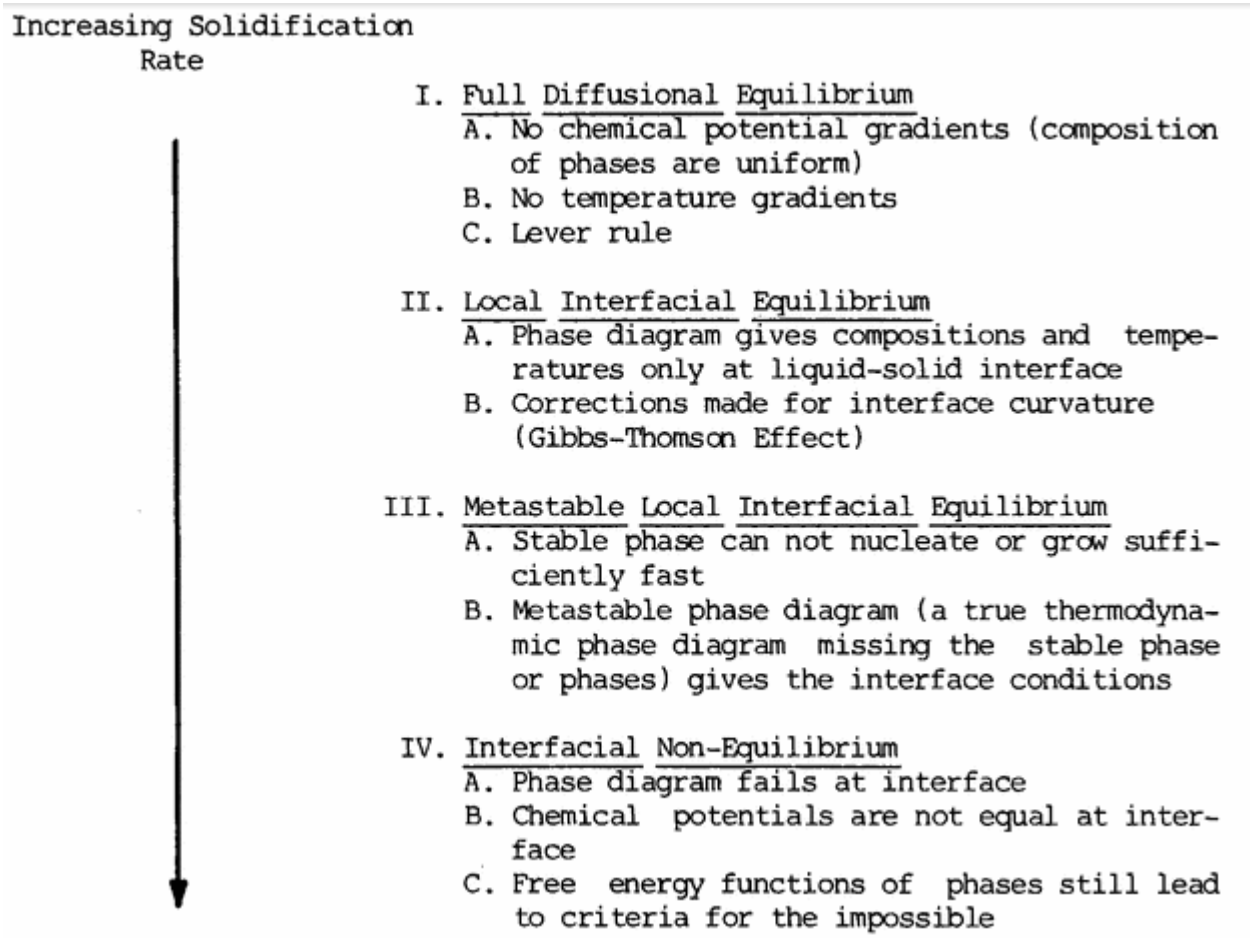

Figure 2.3: Effect of cooling rate on microstructure (Boettinger and Coriell (1986)).

2.3 Screw extrusion

Conventional extrusion methods for aluminium are discontinuous, where the material is loaded in the form of a billet, and pushed through the die, at elevated pressure and temperature. There are several different ways of performing conventional extrusion. Some of these are given in figure 2.4. The major difference, is whether extrusion goes through a stationary die, or if the die moves towards a stationary chamber.

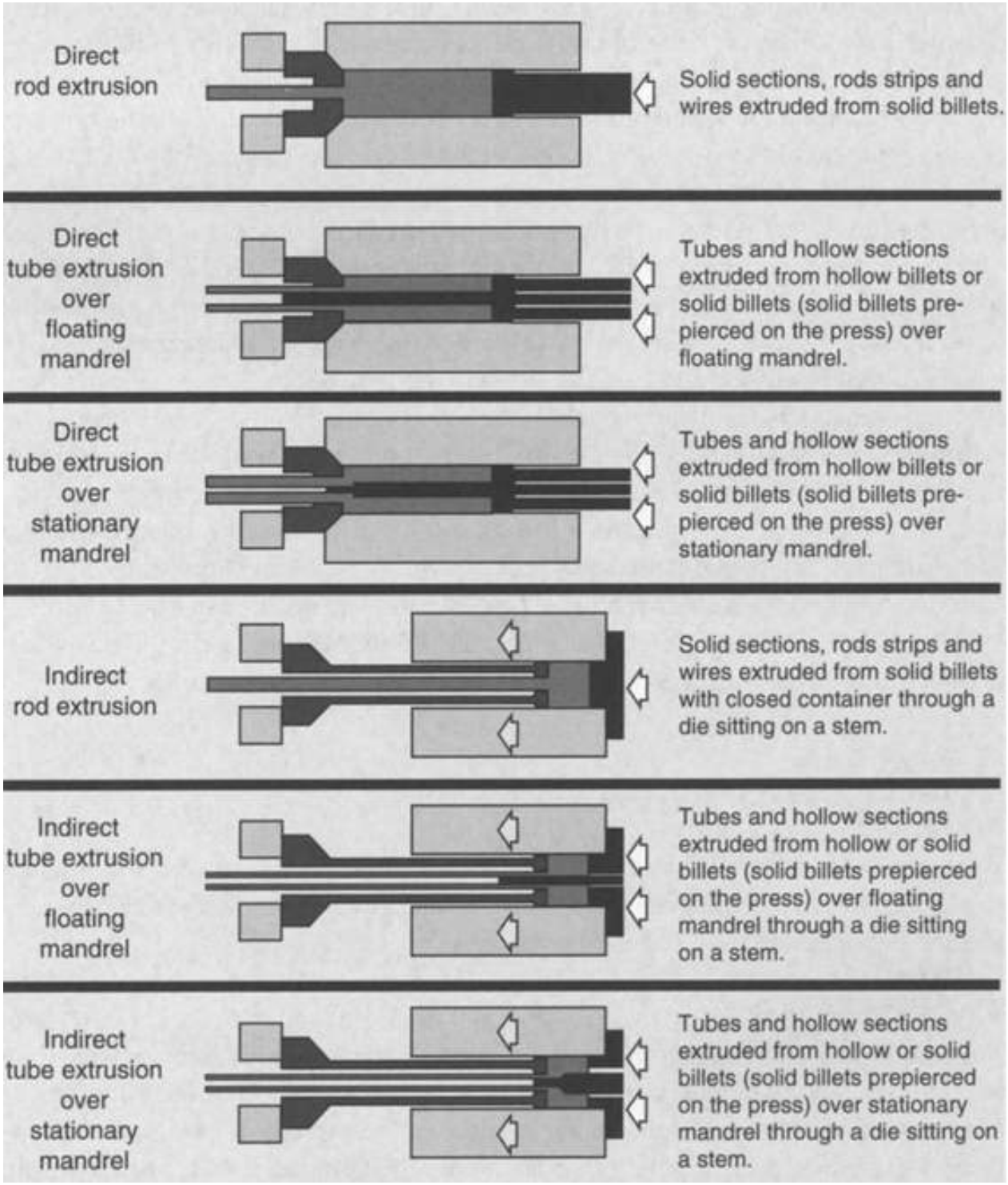

Figure 2.4: Different conventional extrusion methods (Sheppard (2013)).

Quite differently, a novel extrusion method has been developed by Hydro in cooperation with NTNU (Werenskiold et al., 2008). The patent schematic is shown in figure 2.5. This method

lets aluminium be continuously fed into the extrusion chamber, and consolidated by a screw of either one, or two flights. A schematic can be seen in figure 2.6. Literature on the subject of screw extrusion, has not been written outside NTNU, but several masters thesis' (Skorpen (2011), Bilsbak (2012), Mauland (2013), Pedersen (2013), Stedje (2014)), 2 articles (Widerøe and Welo (2013), Skorpen et al. (2014)), and a doctoral thesis (Widerøe, Fredrik (2012)), have been written, to examine the principles of screw extrusion of aluminium.

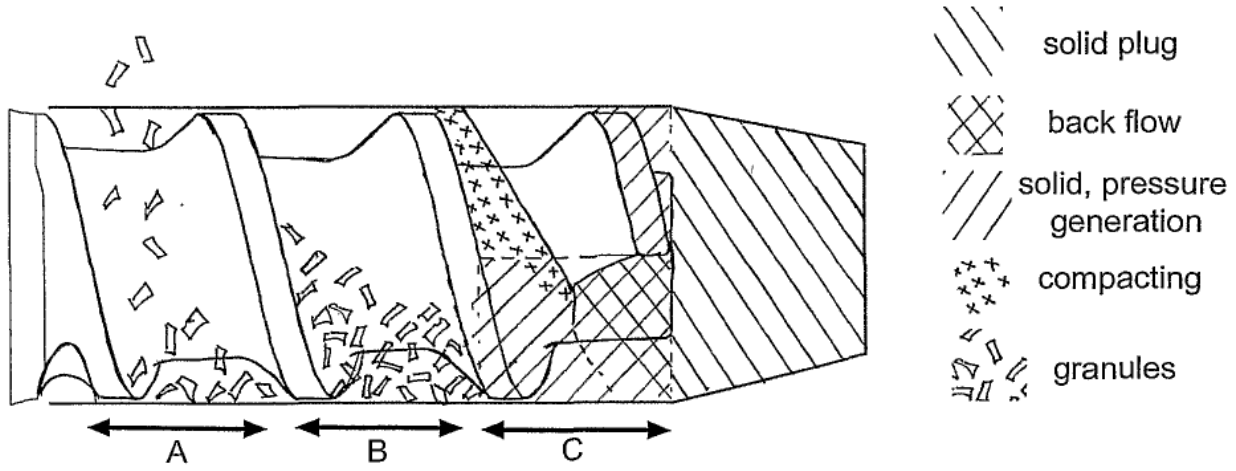

Figure 2.5: Patent schematic by Werenskiold et al. (2008).

The main attractions of the screw extrusion method, is that it is a solid state continuous process, where you can use either one, or several metals in granulate form. This means that you can not only consolidate one metal, or alloy, but several, which opens up the possibilities of metal composites, which was explored in Skorpen et al. (2014) and Pedersen (2013). The latter did not see a successful consolidation into composite from, but saw an almost full diffusion of Mg into the Al matrix. The extruded profiles did however have matching mechanical properties to other Al-Mg alloys. Skorpen et al. (2014) did achieve a composite structure with an Al-Mg alloy, with better mechanical properties with increasing Mg-content, up to 12.5 wt%, where the properties decreased, but this may be due to difficulties with the extrusion process, and not the content of Mg.

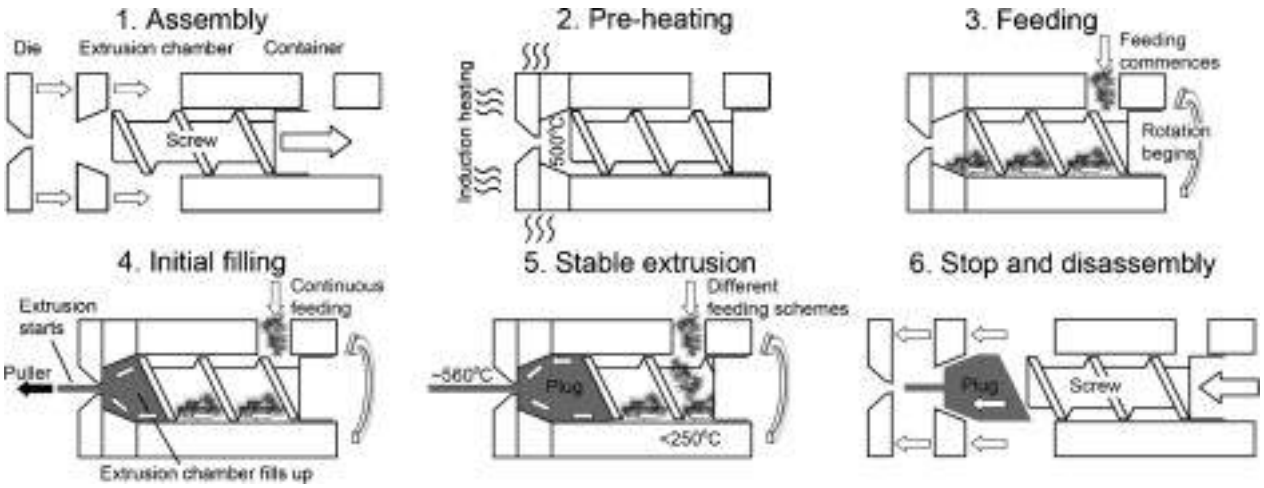

Figure 2.6: Schematic of screw extruder. The extruder is assembled, and preheating is performed to aid with consolidation. Feeding is commenced, and when enough material has filled up the extrusion chamber and the pressure is high enough, extrusion begins. After extrusion, the extruder is disassembled, the left over plug is removed, and the parts that were in contact with metal, are submerged in lye to remove left over oxides (Widerøe and Welo (2013)).

2.4 Homogenization

Homogenization is achieved through heating of metals at a higher temperature than the solvus temperature of the primary alloying element, in order to eliminate unwanted low temperature eutectics.

Homogenization results in several positive effects (Polmear and St. John, 2005):

- Reduction of microsegregation effects.
- Removal of unwanted low temperature eutectics, which lowers the mechanical properties.
- Controlled precipitation of elements that are dissolved during solidification.

To homogenize an Al-Mg alloy, it is necessary with heat treatment at a temperature higher than the solvus temperature of Mg for that particular alloy. For an Al-10%Mg alloy, this would be approximately 350°C, see figure 2.1. This would however take a very long time. Two parameters affect homogenization greatly, namely time and temperature. To homogenize at 350°C, one would need to homogenize for a very long time. Raising the temperature, reduces the time.

Therefore, a temperature close to the solidus temperature is often used.

The mechanism for homogenization, is diffusion of alloying elements from grain boundaries to grain centers. Time to complete homogenization depends on the diffusion rate of the alloying element. Diffusion rate is highly dependent on temperature, which is why raising the temperature shortens the homogenization temperature.

2.5 Recrystallization

Recovery, recrystallization, and grain growth are all related terms, and are important mechanisms to understand when dealing with heavily deformed materials. Both recovery and recrystallization are competing processes, and once full recrystallization has happened, recovery can no longer happen.

Annealing at higher temperatures, will first introduce recovery. Recovery is the motion of dislocations by glide, climb, and cross-slip, which will either meet an opposingly signed dislocation, and cancel each other out, or they will arrange themselves in a way, that will lower the total amount of energy in the material, and create subgrains, as illustrated in figure 2.7.

Annealing at a higher temperature than where recovery happens, introduces recrystallization. Recrystallization is the initiation of new grains at the boundaries of grains, subgrains, particles„ and strain fields. These new grains will grow at the expense of the original grains, driven by the dislocation density, and results in much larger grains than in the original material. A representation of recrystallization can be seen in the last figures of figure 2.8c-e. After recrystallization is finished, additional abnormal grain growth can sometimes happen, often called second recrystallization, 2.8f,(Slámová et al. (2004)).

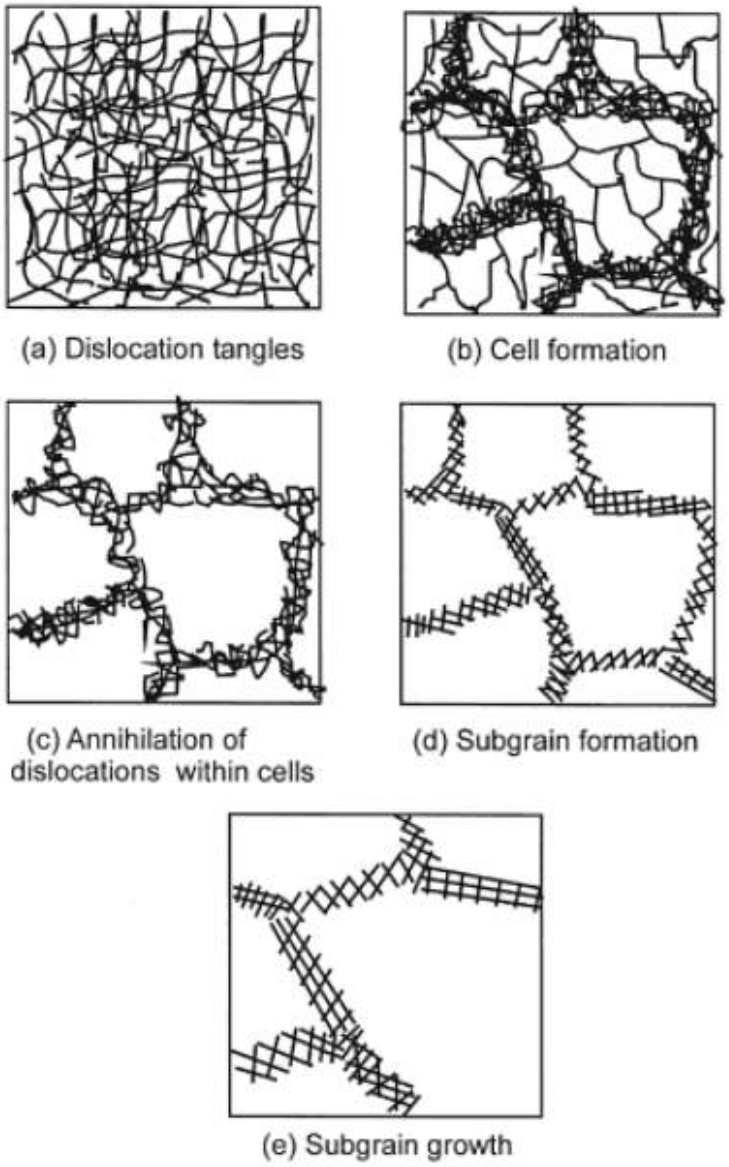

Figure 2.7: a) Dislocation tangles after plastic deformation. b)-e) Are characteristic sub-structures successively heating the aluminium in state a) at higher temperature, or for a longer time (Rollett et al. (2004)).

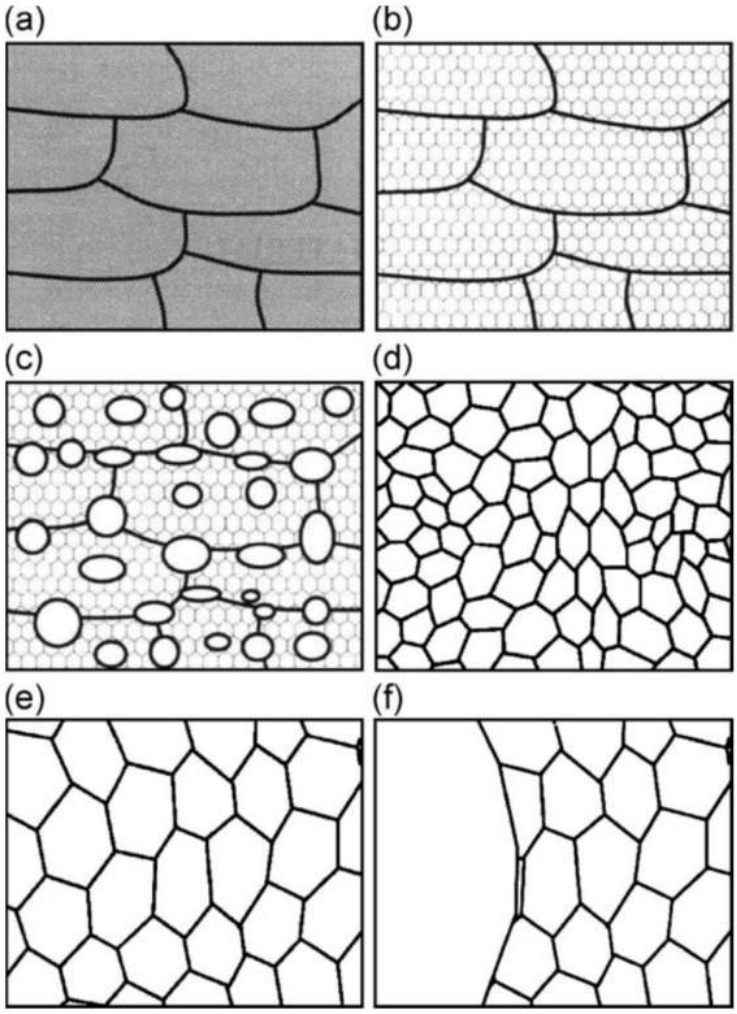

Figure 2.8: (a,b) Recovery, (c-e) recrystallization, (f) and abnormal grain growth (Slámová et al., 2004).

2.6 Diffusion

An atom can occupy a substitutional site in a metal matrix, substituting an atom in the crystal lattice, or an interstitial site in the metal matrix, occupying a site in between the crystal lattice, either in the center of a lattice edge, or center of the lattice, also called octahedral sites. Examples of substitutional and interstitial atom placement is seen in figure 2.9. As such, movement of atoms, also called diffusion, can be either substitutional or interstitial. Movement of interstitial atoms happen approximately random, in every direction, since the solution is often so dilute

that every nearby interstitial site is vacant. Substitutional atoms are much larger, and require a vacancy to move, and therefore require more energy than an interstitial atom to move.

In theory, given enough energy, atoms will move until the concentration of substitutional/interstitial elements is equal in the entire matrix, since this gives the preferred lowest amount of Gibbs free energy. However, there are grain boundaries, dislocations, and phase boundaries that changes this. If the material is under compressive strain, this area would have a smaller percentage of substitutional elements that are larger than the matrix, than the bulk material. In addition to diffusing to the defects, movement along these defects is also greater than in the bulk material. Under elevated temperature, movement along grain boundaries and free surfaces will be the dominant diffusion mechanism (Porter et al., 2009). Typical diffusion coefficients for Mg in Al, are $0.6710^{-}10cm^{2}sek^{-}1$ for Al-10%Mg, and $1.8510^{-}10cm^{2}sek^{-}1$ for Al-14.5%Mg, at 420 °C (Singh, 1970). Which shows that diffusion of Mg in Al increases with increasing Mg content at higher temperatures.

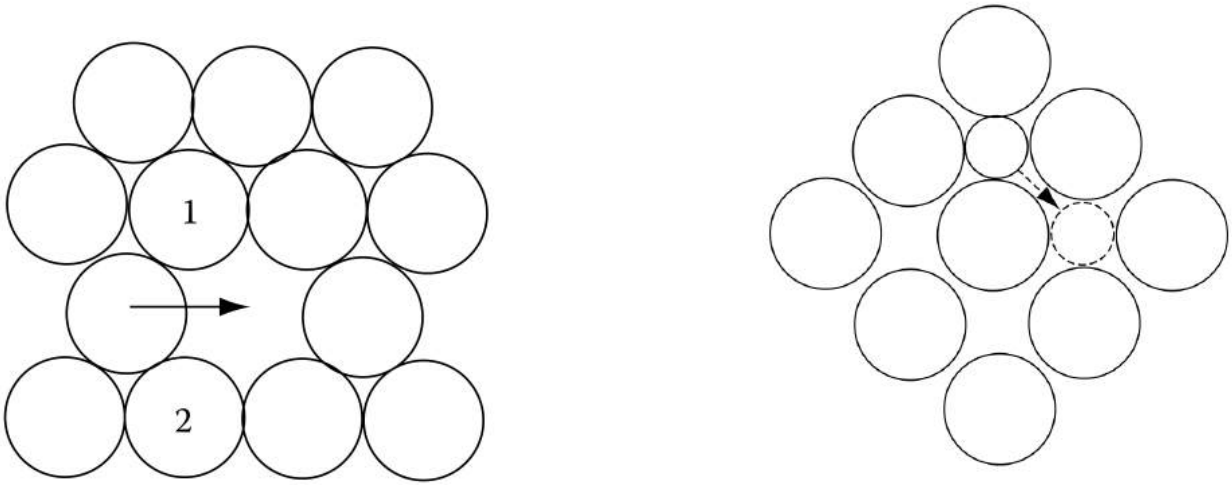

(a) Substitutional movement of atoms.

(b) Interstitial movement of atoms.

Figure 2.9: a) Movement of a substitutional atom to a nearby vacancy, given enough vibrational energy, b) movement of an interstitial atom given enough vibrational energy (Porter et al. (2009)).

2.7 Pore development during heating due to hydrogen

Porosity in aluminium will decrease its fatigue properties, as well as its general mechanical properties. Al-Mg alloys are mostly used in wrought state, where porosity will in most cases disappear during plastic deformation. However, some processing methods like high vacuum systems, might drastically reduce the porosity, and not remove it completely.

The solubility of hydrogen in aluminium can be seen in figure 2.10. The solubility is very high in the liquid state ,0.69 ppm at 660 °C, however, it is very low in the solid state, only 0.039 ppm (Friedrich et al. (2006)). This means that one should be very careful during solidification, to avoid pore formation. Upon heating , hydrogen would diffuse into the material again, and cluster into pores or eventually internal cracks.

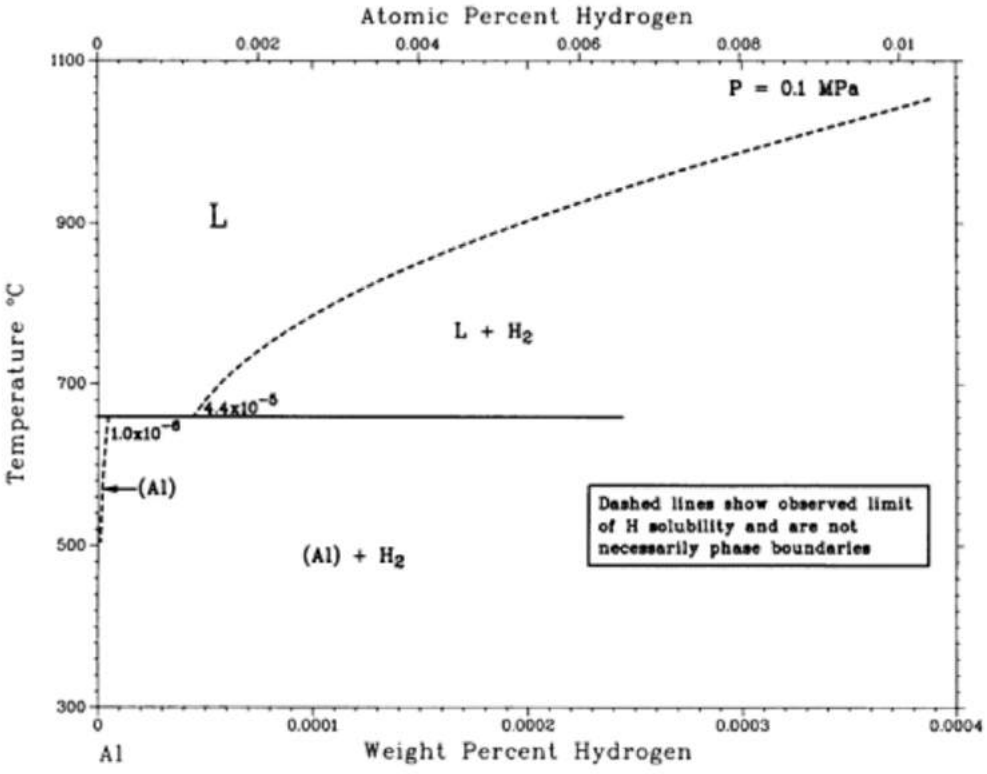

Figure 2.10: Al-Mg phase diagram (San-Martin and Manchester (1992)).

The following is a summary of the findings of Chaijaruwanich et al. (2007) when examining the effects of heat treatment on porosity in Al-Mg alloys. Three direct chill (DC) cast Al-Mg alloys,

containing 2, 4, and 6 wt% Mg, were heat treated at 530 °C for 0, 1, 10, and 100 hours. Metallographic results showed an increase in porosity density and size both with homogenization time, and Mg content. The increase in mean pore size with homogenization time indicated that inter-pore Ostwald ripening had occurred, however, the increase in pore density contradicted this. X-ray microtomography (XMT), a 3D imaging technique, confirmed the inter-pore Ostwald ripening causing pore coarsening, in addition to the pore density with homogenization time. The Ostawald ripening is shown in figure 2.11.

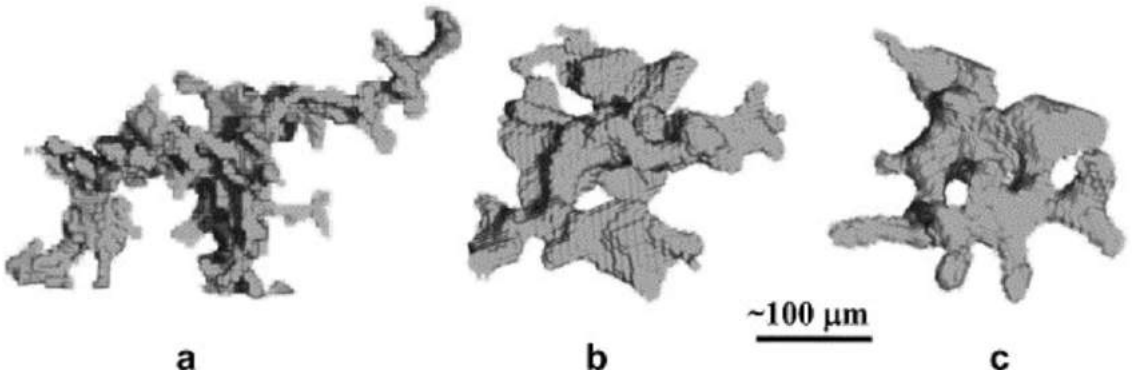

Figure 2.11: Pore morphology in a Al-6%Mg alloy a) as cast, and b) homogenized for 10 hours, and c) homogenized for 100 hours, at 530 °C. The mechanism for the coarsening of the pores is Ostwald ripening. X-ray microtomography (Chaijaruwanich et al., 2007).

2.8 Vickers Hardness

Hardness is an important factor when evaluating the properties of a material. Inhomogeneous hardness is an indication of an inhomogeneous material, and high hardness gives an indication of high strength. There are three types of hardness measurement, scratch, indentation, and rebound hardness. Scratch hardness shows resistance to friction by a sharp object, indentation hardness shows resistance to compression from a sharp object, and rebound hardness measures the rebound height of a sharp object dropped on the material. For metallography purposes, indentation hardness is the most commonly used.

There are several ways of measuring indentation hardness. A brief mention of commonly used tests is given here. Rockwell hardness (HR) testing uses a ball indenter, and determines hardness based on depth after loading from a preload, and deloading to the preload again. Commonly

used for plastics. Brinell hardness (HB) testing is performed with a ball indenter, and hardness is measured based on the diameter of the indentation. Knoop microhardness (HK) testing is performed with a pyramidal diamond indenter with a 7:1 length to width ratio, and measuring the two diagonals of the indentation. HK testing is used for very brittle materials, or thin sheets of metal.

Vickers hardness (HV) testing is the most commonly used indentation method for metals and the one used in this thesis. A pointed square diamond with 136°between the sides of the pyramid is pressed into the metal with a predetermined load, for a predetermined length of time, and unloaded. The hardness is determined by measuring the diagonals of the indentation, and using the formula.

$$HV = \frac{F}{A} = \frac{F}{\frac{d^2}{2sin(136°/2)}},$$

which can be approximated to

$$\frac{1.8544F}{d^2}, \tag{2.2}$$

where F is kilograms of force (kgf), A is the surface area of the indentation in square mm and d is the average of the two diagonals of the indentation. The minimum distance between indentations should be 2.5 the diagonal (E92-16 (2016)). Vickers hardness is independent of load, and gives the same result with 0.5 kgf and 1 kgf, however, there is a slight incaccuracy below 200gf (gram force) Instron (2016).

2.9 Scanning electron microscopy

Scanning electron microscopy (SEM), is a method of determining either topography, composition, or crystallography of a material. By the help of magnets, electrons are accelerated towards the sample by a voltage difference, several signals are emitted or reflected, collected by detectors, and analyzed by a computer, to form a picture. A simple schematic can be seen in figure

2.12. When the electrons hit the surface of the material, the different signals are seen in figure 2.13.

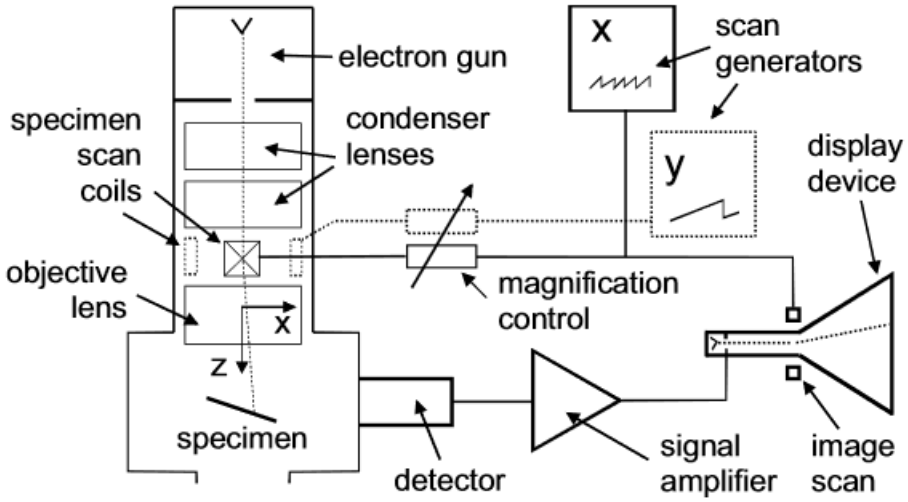

Figure 2.12: Basic principles of a SEM (The Science Education Scenter at Carleston College (2016)).

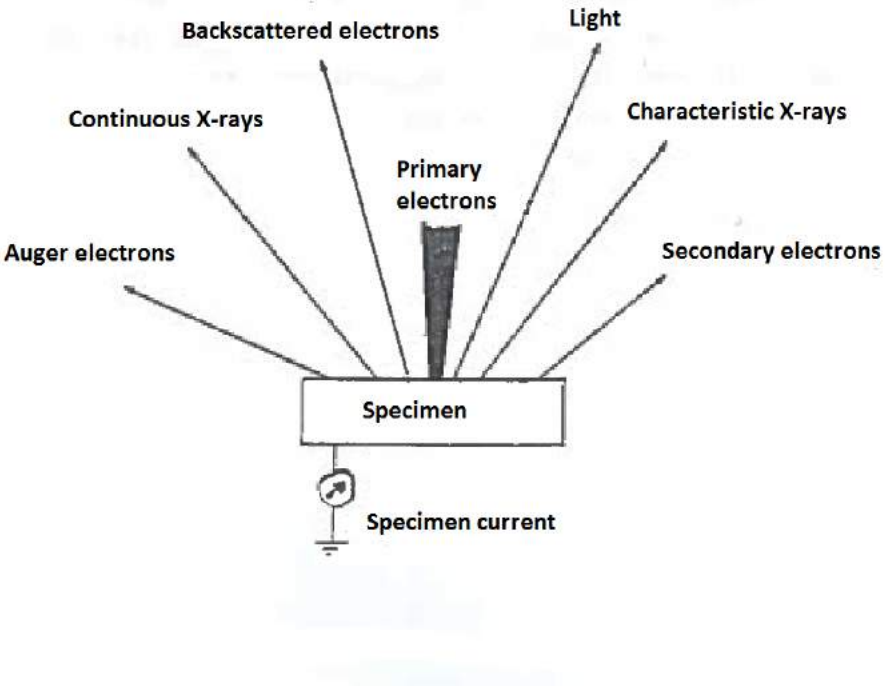

Figure 2.13: A representation of the different signals that are emitted/reflected from a specimen when hit by primary electrons in a SEM (Hjelen (1986)).

The most commonly used signals, are secondary electrons (topography), backscattered electrons (topography, composition, and crystallography), and X-rays (composition). The secondary electrons (SE) are ejected from the k-shell after interaction with the primary electrons, and emitted back from the surface, and collected by a detector. The emission volume of secondary electrons is very small, compared to the other signals, which makes it ideal for viewing topography.

Backscattered electrons are primary electrons which have interacted with the specimen, lost some energy, and been reflected back from the specimen surface. They have a larger volume than secondary electrons, which is approximately 5λ Hjelen (1986), and are used primarily for determining phase distribution. A heavier element will reflect a larger portion of backscatter electrons, see figure 2.14, making it more white, when seen in the CRT screen. This can be used to for instance determining where different phases are, and how large they are.

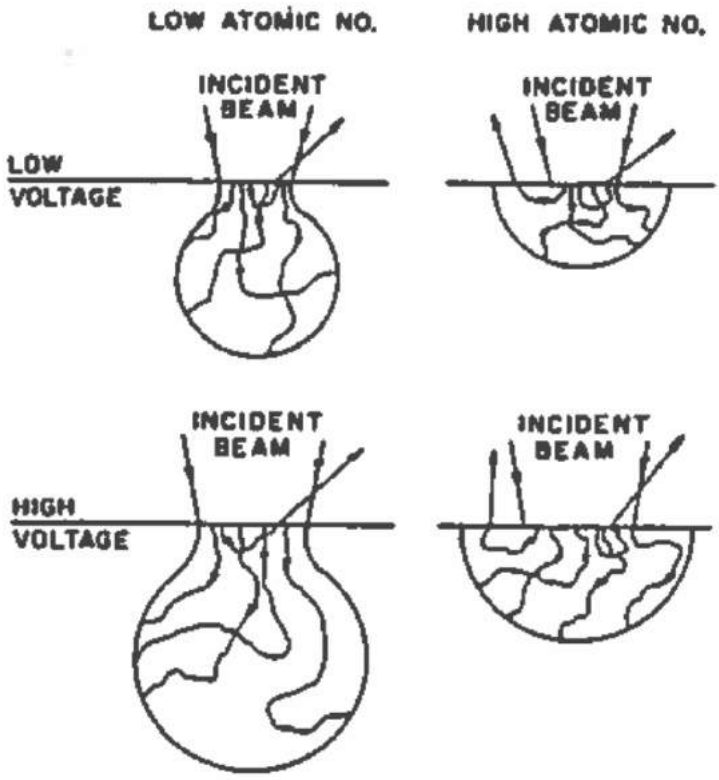

Figure 2.14: Illustration of the emission volume of backscatter electrons. The larger volume is caused by a material with a lower atomic number (Hjelen (1986)).

Characteristic X-rays are produced by primary electrons interacting with the inner orbitals of the material, exciting the atoms, which then emit characteristic X-rays. The emission volume is larger than both backscatter and secondary electrons. A comparison of all three can be seen in figure 2.15. This signal can be used to determine the chemical composition, both quantitatively and qualitatively. Two different detectors are used to analyze the X-rays, energy dispersive spectrometer (EDS), which uses a solid state detector, and wavelength dispersive spectrometer (WDS), which uses a crystal and Bragg diffraction. WDS is slower than EDS, has more moving parts, and can not check the entire spectrum at once, as EDS is capable of, but WDS has a higher resolution and is generally more precise.

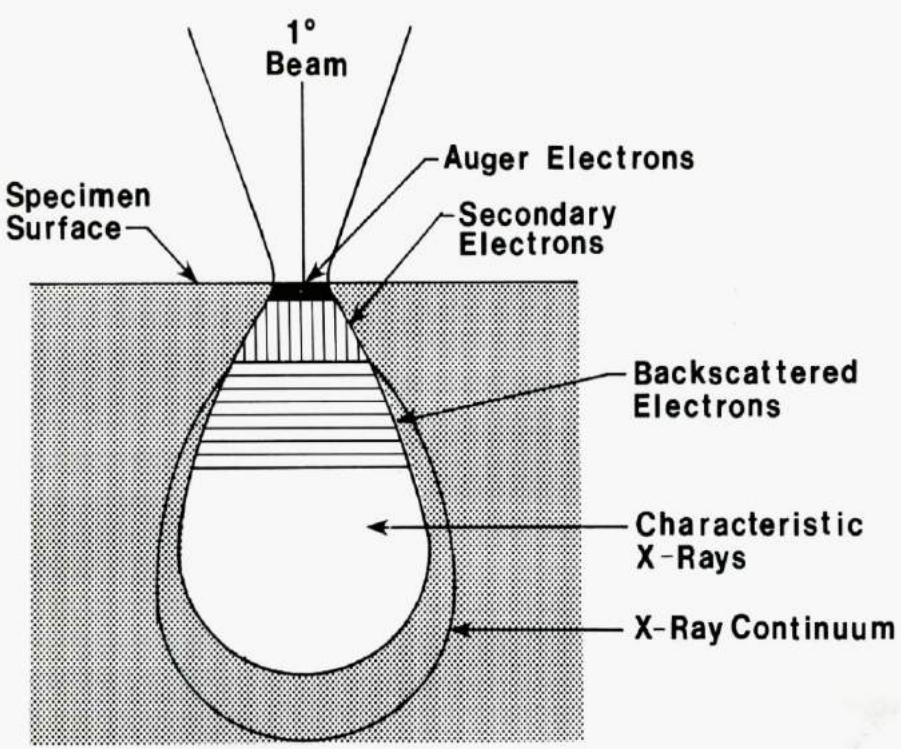

Figure 2.15: Illustration of the emission volume of the different signals. Notice how much smaller the secondary electron volume is compared to the backscattered electrons (Northeastern University (2016)).

2.10 X-ray diffraction

X-ray diffraction (XRD) is a characterization method used to determine the composition of crystalline (or amorphous) materials, which includes, but is not limited to, ceramics, metals, rock, and DNA. Incoming X-rays are elastically diffracted by the atoms in certain crystallographic planes, figure 2.16b, and received by a detector, which moves, and counts the amount of incoming x-rays at certain angles, often recording 2θ, figure 2.16a. The resulting patterns can then be matched with existing reference patterns, to determine the phases present in the material. The space between diffracting planes, d, is given by the well known Bragg's law,

$$n\lambda = 2d_{hkl}sin\theta_{hkl}, \tag{2.3}$$

where n is a positive integer, often 1, λ is the wavelength of the x-rays, θ is the angle of the x-rays, and hkl is the orientation of the crystallographic plane.

In addition, one can determine the amount of dislocations with a high resolution XRD. Lin et al. (2015) reported a dislocation density close to severely deformed aluminium processed by equal-channel angular pressing (ECAP), measured by XRD. Lin et al. (2015) states that peak broadening is the result of either small size of the diffracted crystallites, micro strain caused by dislocations, or instrumental broadening, and found a density in RS ribbons of $1.3x10^{14}m^{-2}$, which is comparable to that of aluminium processed by ECAP, which was reported to be in the range of $10^{14} - 10^{15}$ Lin et al. (2015).

Another use of the XRD, is to determine the degree of alloying element in solid solution. The XRD-pattern from an aluminium alloy with 5 wt% Mg, would have the same peaks as pure aluminium, only shifted to the left towards lower 2θ due to the higher lattice constant caused by Mg in solid solution Zha (2014).

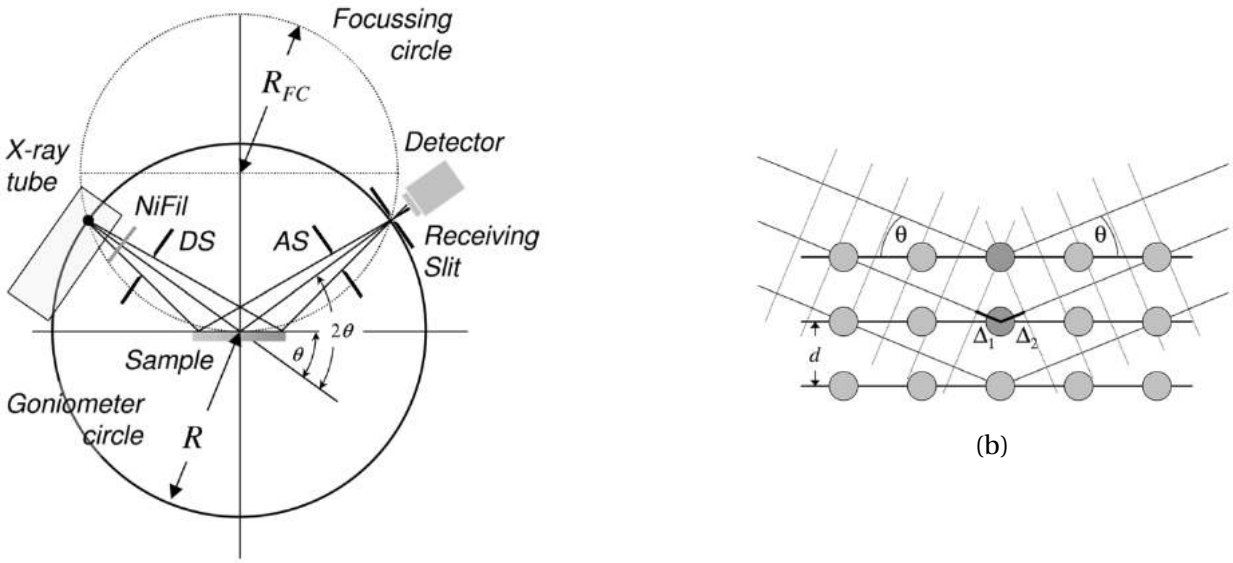

(a) (b)

Figure 2.16: a) A typical X-ray diffractometer. X-rays are reflected, and collected by the receiver at different angles. b) Bragg diffraction (Birkholz, 2006).

2.11 Tensile testing

A typical way of testing the mechanical properties of a material, is tensile testing. An elongated tensile specimen, is mounted in a testing machine, and pulled in uniaxial tension, at constant speed, until fracture. The pulling force is recorded. One can then calculate engineering stress, and strain. Engineering stress is given by force/original cross section, and strain is change in length/original length. These values are plotted in a graph, as the one seen in figure 2.17, and can give great knowledge on the mechanical properties of a material. One can extract several useful values from a stress-strain curve. The elastic zone is the area before the yield strain. Ultimate tensile strength (UTS) is maximum stress the material undergoes. Strain at fracture is how for the material strains before fracturing. A high UTS shows high strength and a high strain at fracture shows high ductility.

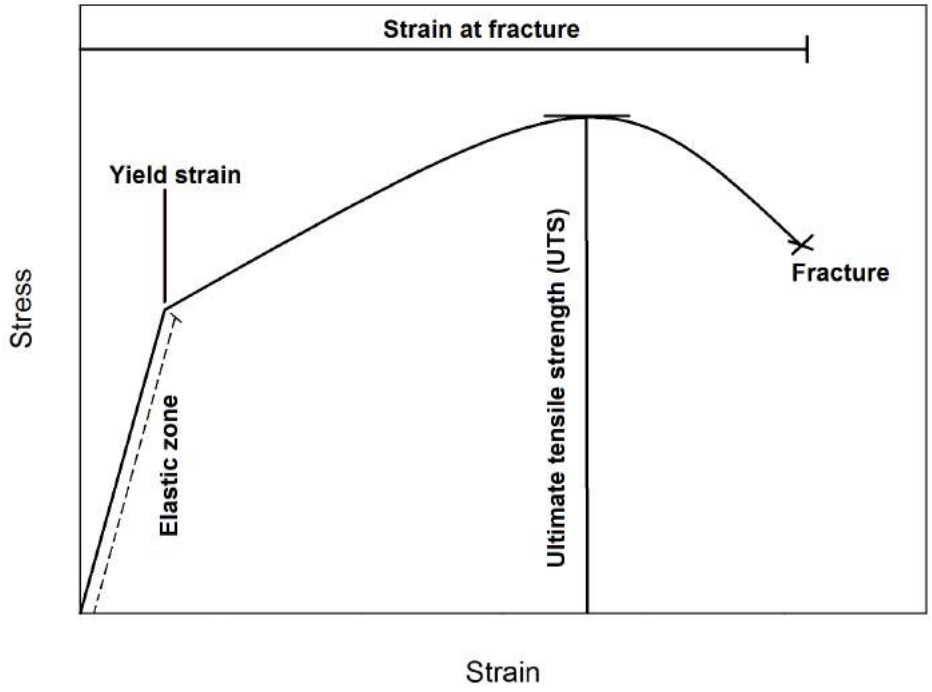

Figure 2.17: Typical stress-strain curve from a tensile test.

2.12 The Portevin–Le Chatelier effect

The Portevin–Le Chatelier effect can be seen in stress-strain curves, as a sharp drop in stress at a critical strain, and further serration in the curve, which might increase or decrease depending on material, temperature, and strain rate, until fracture. An example is seen in figure 2.18.

The main cause of the PLC effect in Al-Mg alloys is related to dynamic strain aging, due to Mg in solid solution. Mobile dislocations interact with solute Mg atoms, are temporarily stopped, a sharp increase in stress is seen, before the stress is so high that the dislocations start to move, and a sharp decrease is seen in stress. This interaction is what happens when a serrations is seen in the stress-strain curve.

Two important factors for degree of serration, is solute concentration, and grain size. Increased solute concentration increase serration density and amplitude, due to more dislocation solute atom interactions, and decreased grain size causes larger amplitude, due to the grain size de-

pendency of dislocation density.

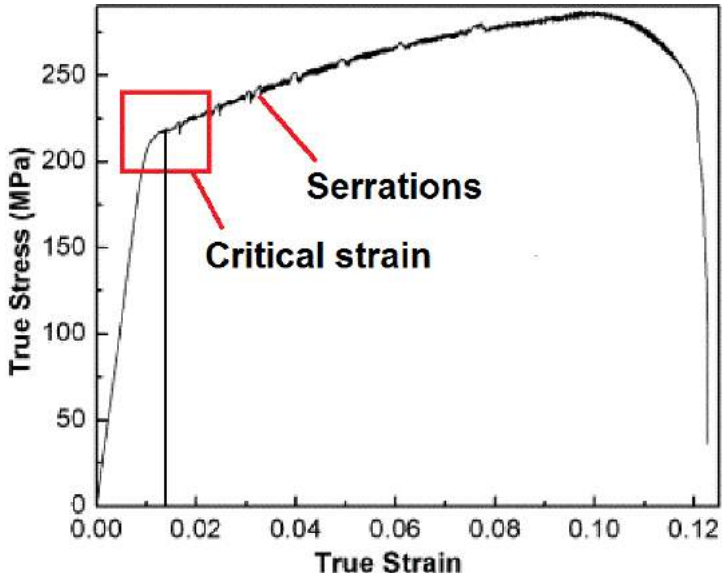

Figure 2.18: Typical stress-strain curve for an Al-2.5%Mg profile exhibiting the PLC effect. Serrations start at a critical strain, and are seen to a varying degree until fracture (Chatterjee et al., 2009).

2.13 Fracture Mechanisms

Fracture happens when a material is subject to such a large force, that the inter atomic bindings separate, and the material goes to fracture. Flaws in a material, like cracks, inclusions, or brittle phases will cause stress concentrations, that will cause the material to fracture prematurely.

For metals, there are 3 common fracture mechanisms:

- Ductile fracture.
- Cleavage fracture, often called brittle fracture, and it is transgranular.
- Intergranular fracture.

These mechanisms are illustrated in figure 2.19. Ductile fracture initiates at inclusions or second phase particles, when the applied load is large enough to separate them from the matrix, and create voids. These voids coalesce during further strain, and grow until fracture, an illus-

tration and explanation of this is given in figure 2.20. The resulting fracture will consist of microvoids/dimples near the middle of the uniaxial test unit, a smoother surface near the edges, and a cone shaped appearance. A SEM image of micro voids formed during ductile fracture can be seen in figure 2.21.

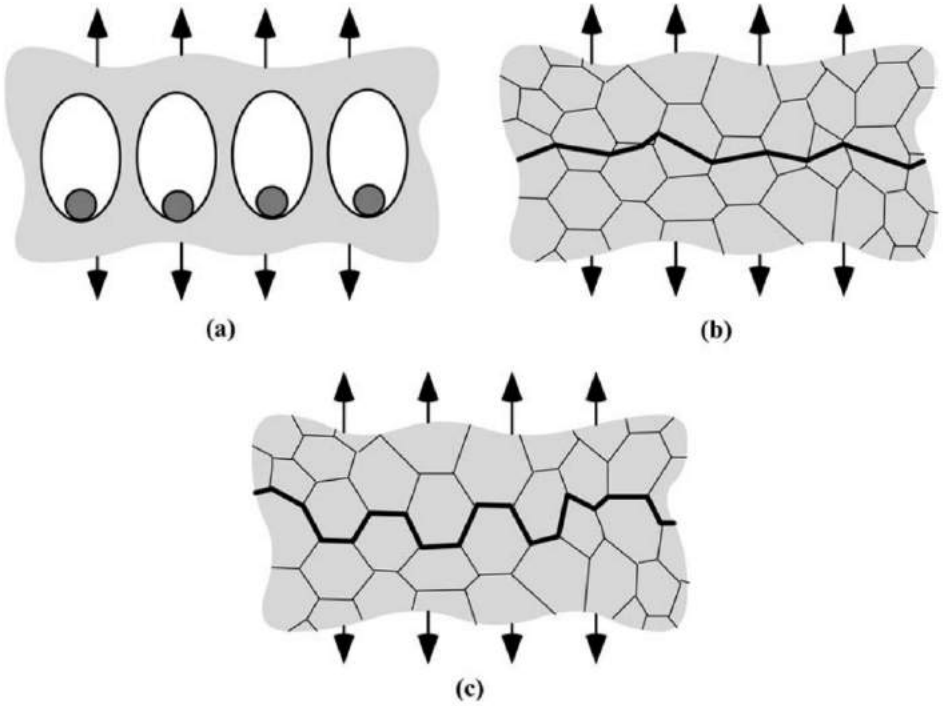

Figure 2.19: Three fracture mechanisms in metals. a) ductile fracture by void nucleation, b) cleaveage fracture through grains, and c) intergranular fracture (Anderson, 2005).

In the case of porosity, the metal will already have several flaws, as porosity seldom occurs singularly, and the cross section is effectively smaller. This creates large stress concentrations, and a short travel length for cracks, and a normally ductile material, would experience a higher fraction of brittle fracture, with increasing amount of porosity.

Cleavage, often called brittle fracture, seen in figure 2.19 b) and figure 2.23, can be defined as rapid crack propagation in a preferred crystallographic direction, where the packing density is the lowest, since there are fewer bonds to break. The crack propagation goes through grains, in the plane that is preferred, and changes direction every time it crosses a grain boundary. Although cleavage is often entirely brittle, it can be preceded by large scale plastic deformation. As several cracks propagate, there follows a tearing between the planes. This demands more energy

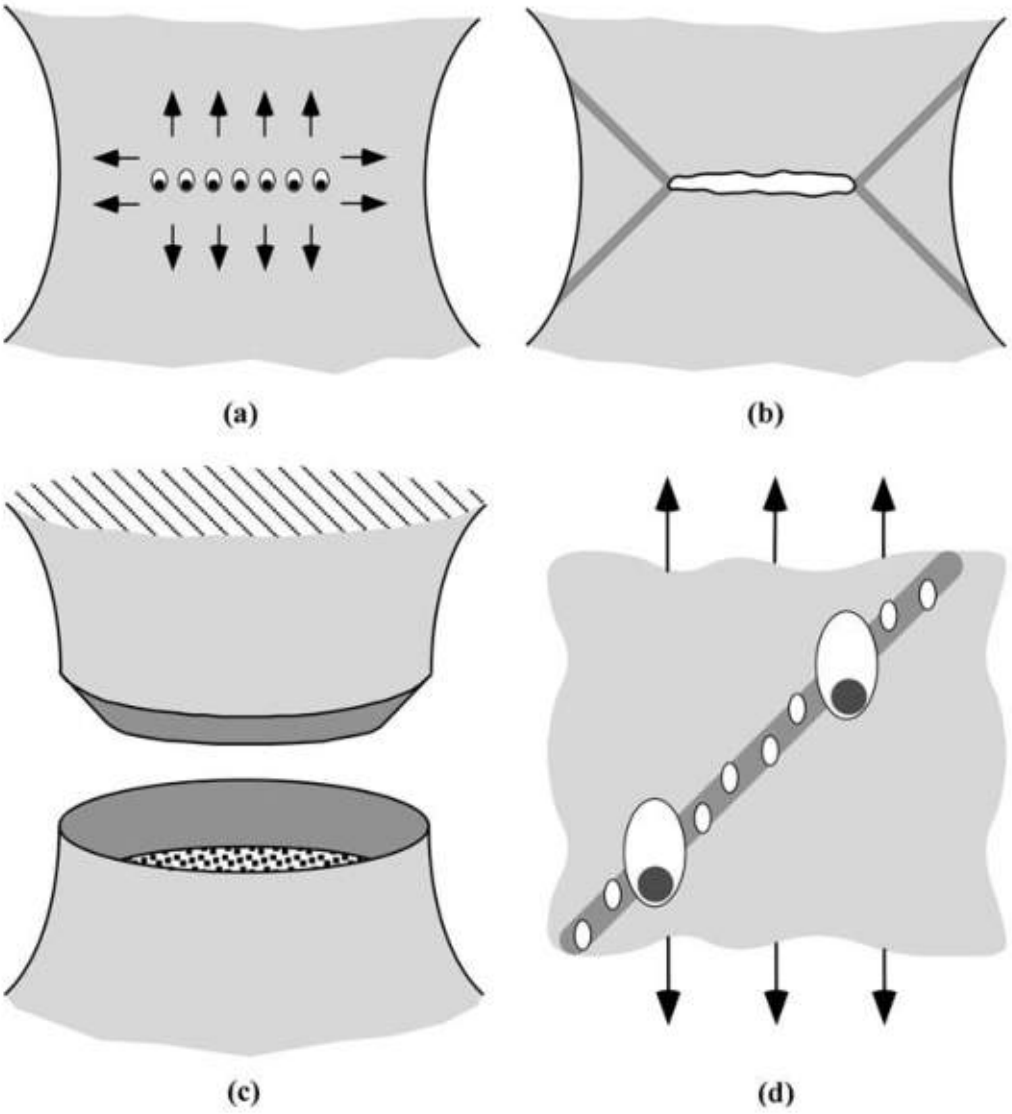

Figure 2.20: During uniaxial tension, micro voids will form in the middle of the specimen(a), since the stress is higher in the middle than in the outer ring. These micro voids coalesce after further strain, and produce a penny shaped flaw (b). This flaw produces strain concentration lines 45° from the flaw, where micro voids can form and coalesce (d). The high strain causes the micro voids around much smaller and numerous particles, which rapidly causes an instability, and subsequent fracture with a cone shaped appearance, with a much smoother fracture surface at the outer ring, than the inner penny shaped flaw (Anderson, 2005).

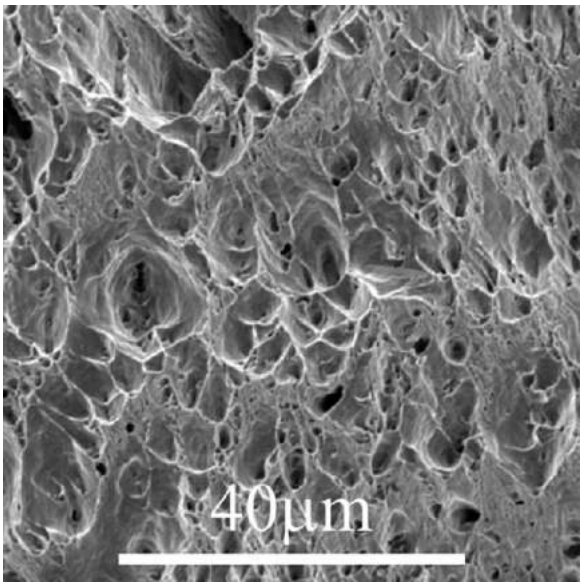

Figure 2.21: Micro voids caused by ductile fracture in an Al-Mg-Si alloy, as seen in the SEM (Clark (2016)).

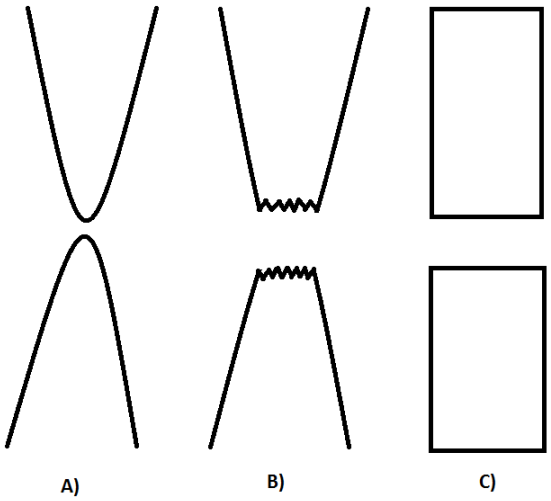

Figure 2.22: Degree of fracture. a) Is completely ductile and typical for soft metals and soft polymers, b) exhibits the classical cup and cone shape typical for most ductile materials, and is moderately ductile, c) is completely brittle and common for cold steels and ceramics.

than simply propagating a simple crack, which causes cracks to converge and become one. This makes it possible to follow the direction of cracking, and determine the origin of fracture.

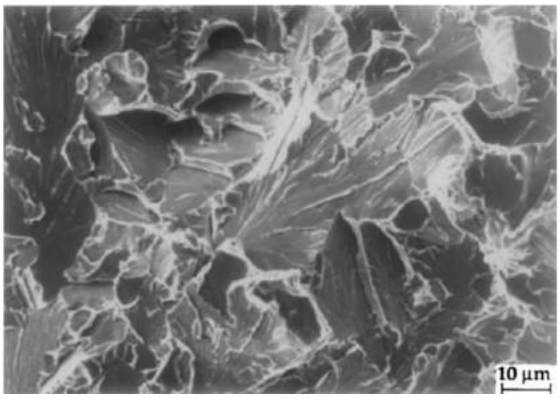

Figure 2.23: Typical SEM image of a brittle fracture surface (Anderson, 2005).

3 | Experimental procedures

This chapter details the experimental setup used during this work.

3.1 Investigated materials

Materials used can be seen in table 3.1. They were delivered 25/01/2010 by Hydro Sunndal, as 95mm diameter bolts. These were machined into shavings of approximately 10x4x0.5mm, to be used for reference when extruding, and cut into 10x9.5cm pieces to be used for melt spinning. It should be mentioned that the Al-5%Mg granulates were machined incorrectly, without the use of alcohol as coolant, and contained large amounts of oxides on the surface of the transverse plane. The granules were machined at Finmekanisk verksted, NTNU, and can be seen in figure 3.1.

Figure 3.1: Machined granulates from DC cast billets.

Conventional extruded material was manufactured in laboratory scale, at the Department of Engineering Design and Materials. Equipment was pre-heated to 430 °C, and a bolt with cross section 10mm, was extruded into a water basin. Extrusion speeds was 100, 50, and 10 mm/s for Al-5%Mg, Al-8%Mg, and Al-10%Mg respectively. The ram to die opening ratio was 100 to 1.

Table 3.1: Composition and heat treatment of as cast material, as specified by manufacturer, Hydro Sunndal.

Alloy	wt% Mg	wt% Fe	wt% Si	wt% Ti	$T_{Homogenized}$[°C]	$Time_{Homogenized}$[h]
Al5% Mg	5.047	0.0569	0.0526	0.0047	500	3
Al8% Mg	7.991	0.062	0.0574	0.0045	480	3
Al10 % Mg	9.988	0.0585	0.0601	0.0046	480	3

3.2 Specimen preparation

Al-Mg alloys are relatively ductile, and care must be taken during metallographic preparation. This section details metallographic preparation. Several standardized methods were performed, and the method which gave the best result was used.

Whenever casting was needed, Struers EpoFix at a ratio of 25/3 resin to hardener, and appropriate mounting size was used. EpoFix requires both mixing for 90 seconds, and storage for 8-12 hours, in a fume hood.

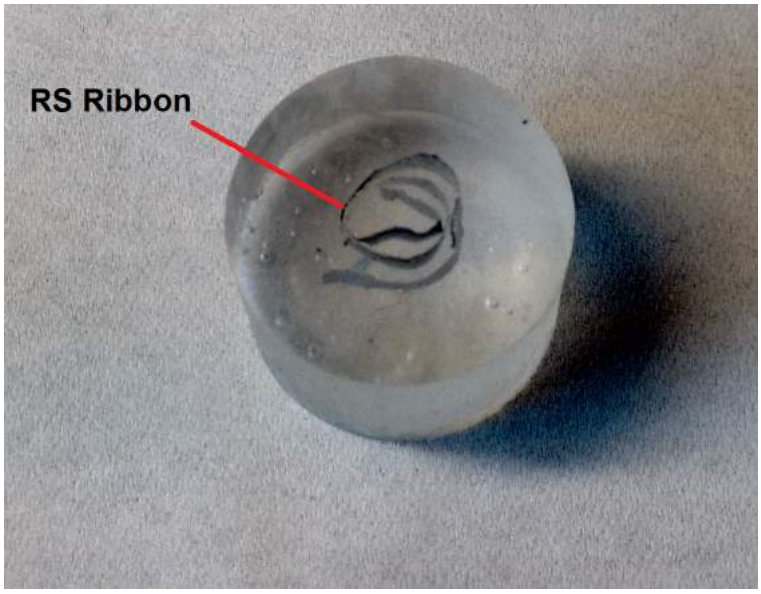

Figure 3.2: Illustration of how the ribbons were cast in epoxy. The transverse direction is in the normal direction of the figure.

Cutting of small samples was performed with a Struers Accutom-5 and parameters as shown in table 3.2, while the bolts were cut with a Struers Labotom discotom. The extruded profiles were cut in the longitudinal and transverse direction as shown in figure 3.6. To create the heat treated samples, a cross section of about 2 cm of the cast bolts were cut off with the discotom, which were cut into smaller cubes with dimensions roughly 2x2x4 cm for homogenization with the discotom, see figure 3.3, and further cut into cross sections with the accutom, before being cast in epoxy.

Grinding was done with #FEPA 300-4000 and the machine used was a ATM Saphir 330. Polishing

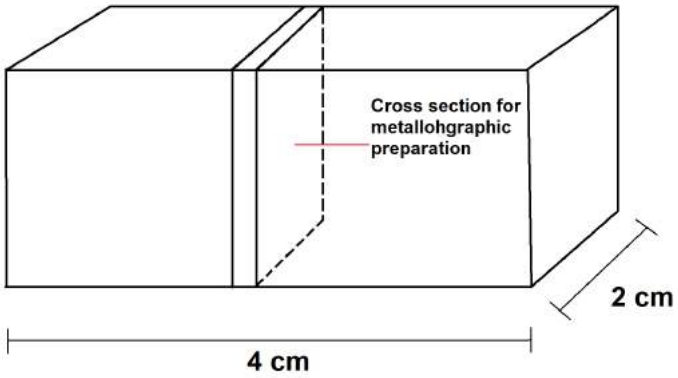

Figure 3.3: Dimensions of cubes for homogenization. The cross section was cast in epoxy.

Table 3.2: Parameters used on the accutom when cutting the extruded profiles.

Force limit	MEDIUM
Wheel speed	3000 RPM
Feed rate	0.080 mm/s

was performed with 6, 3, and 1 μm diamonds in a slurry solution on canvas, the machine used was a Struers DP-U3, to appropriate degree for the application to be used. Specimens for hardness testing has been grinded/polished to a much coarser degree than specimens for optical microscopy, as this is time saving. For specimens with high fraction of porosity, machines handling 6 samples at a time, rotating with the grinding/polishing paper, was used in place of hand polishing. An explanation of this is given in appendix B. The machines were Struers RotoPol-31 coupled with Struers RotoForce-4 for grinding, and Struers TegraPol-31 connected to a Struers TegraForce-5 and TegraDoser-5 for polishing. The grinding papers used were #FEPA 300, 800, 1200, while polishing was performed with 9, 3, and 1 μm diamond slurry solutions, and final polishing was performed with Struers OP-S 0.04 μm colloidal SiC suspension.

SEM samples must be conducting. Therefore, SEM samples were covered in aluminium foil, where epoxy was showing as seen in figure 3.5, and for samples such as the RS ribbons seen in figure 3.2, where it was very difficult to cover all the epoxy with foil, the samples were coated with a thin layer of carbon, using a Cressington 208 carbon coater. Microprobe specimen preparation was performed in the same way as for SEM.

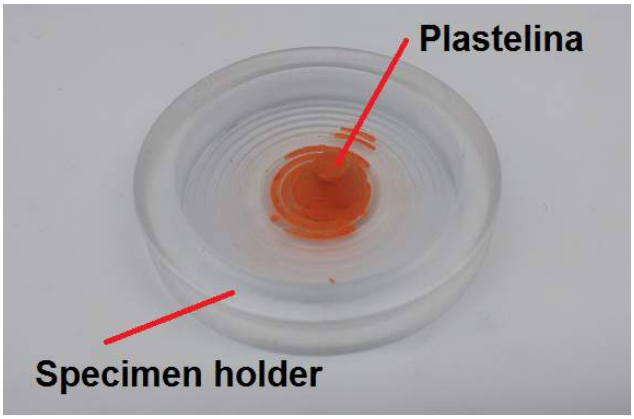

Figure 3.4: XRD sample holder.

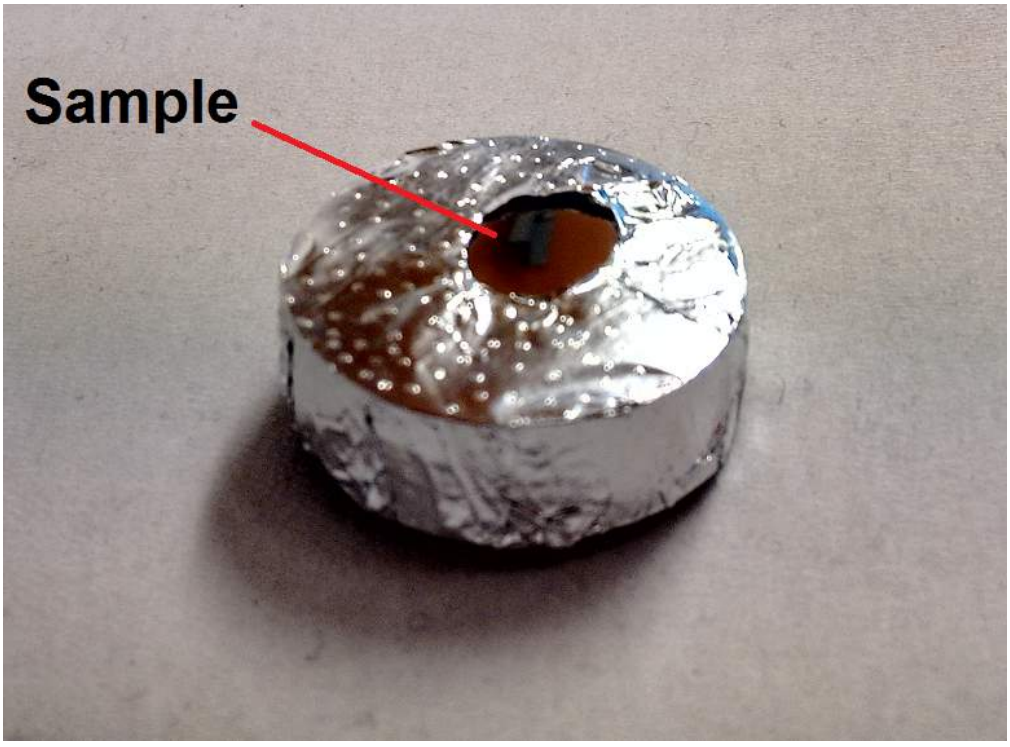

Figure 3.5: Example of preparation of SEM sample. The middle part of the square sample is not covered in aluminium foil, but the rest is, to avoid overcharging of the epoxy.

For XRD, it is not important with a well polished surface, as is the norm for most other metallographic investigations, however, it is important with a flat surface. As such, the specimens were directly ground at #FEPA 4000.

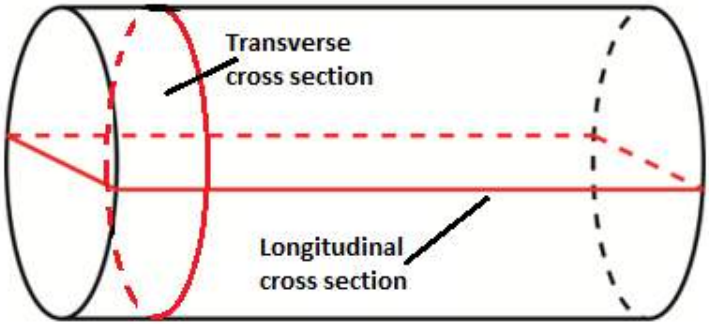

Figure 3.6: Illustration of how extruded profiles were cut in the transverse and longtitudal direction, courtesy of Stedje (2014).

Anodizing

To anodize the samples, a metal beaker was filled with ca. 200 ml of 5% HB_4, and connected to the negative input of the power supply, a TTI QL355, the positive input was connected to a clamp for all the samples except the ribbons, which connected to a platina wire. The power supply was set to 20 volts, and 1 amp, and power turned on. The samples were submerged in 5% HB_4 for 90 seconds, taken out, and rinsed in water in a nearby beaker. In addition, for all samples except ribbons, a Heidolph MR 1000 magnetic stirrer was used.

Since it is difficult to clamp the epoxy cast ribbons, they were submerged, ribbon side up, and a platina wire was placed on the end of the spiral as a conducter, see figure 3.2. The remaining samples, were clamped, and submerged 50-75 % sideways.

3.3 Optical microscopy and SEM

The optical microscope used, was a Leica MEF4M. Several magnifications were used, with a sub parallel lambda plate when imaging the anodized samples. When a picture was desired, ProgRes CapturePro was used in conjunction with a digital camera connected to the microscope, to capture the image. A scale bar was added as reference, as can be seen in the bottom right of

the resulting images in the next section. Panorama pictures were taken at 2.5X-10X each, and connected together with Photoshop Elements 14.

Test specimens cast in epoxy were degassed at 75 °C over night when for use in SEM and micro probe. SEM pictures were taken using a Zeiss FESEM Ultra 55 limited edition. When an SE image was taken, a low aperture, medium voltage, and high voltage mode off, was used. When EDS scans were made, a high aperture, medium voltage, and high voltage mode on, was used. Micro probe measurements were performed by Morten P. Raanes, at the department of Materials Science and Engineering. 2 linescans were taken across the RS ribbons, for each alloy. The end points were put outside the edge of the ribbon, so the resulting graphs will have a drop off near the edges.

3.4 Grain size measurement

To measure the grain size, optical micrographs were opened in iSolution DT, and the distance from one grain boundary, through several grains, and to another grain boundary, was measured, see figure 3.7. ASTM E112-13 was followed, which means at least 50 grains were measured to from the grain size. All images used for measuring of grain size, were taken in the middle of the respective samples, except for RS ribbons, which were measured at the wheel side, 10 to 20 µm from the edge.

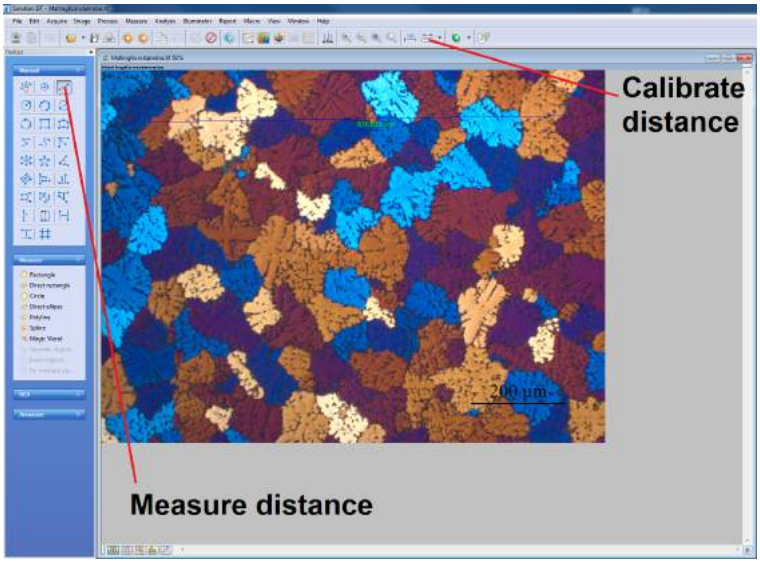

Figure 3.7: iSolution Dt was the program used for grain size measurement.

3.5 Hardness measurements

All micro hardness testing was performed with a Leica VMHTMOT, and all indentation times were 15 seconds.

Hardness of the as cast material was taken at random, with 50 gf.

Hardness of the screw extruded machined granulates was taken in a line from the center, to the edge, with 8 indentations evenly spaced. The load was 15 gf. The next line of measurements was taken at a distance an order of magnitude away.

Hardness measurements of conventional extruded profiles were taken in the same manner as screw extruded profiles, but only 3 measurements from center to edge were taken.

Homogenized samples were hardness tested from the edge, and 1 mm inwards, in the fashion shown in figure 3.8, with 500 gf.

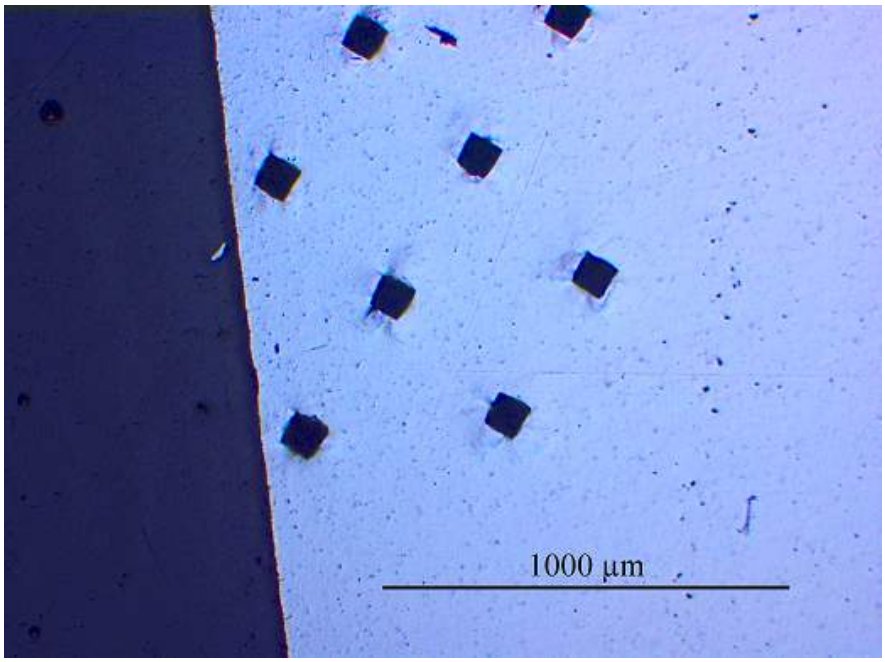

Figure 3.8: Optical micrograph of the hardness indentations performed on a homogenized samples. 24 indentations were performed for each condition.

3.6 Rapid solidification by melt spinning

The materials where melt spun using an "Advanced melt spinner" from "Marko materials,Inc", with slight modifications. Schematic of the melt spinner used in this project, can be seen in figure 3.9a. Parameters that were controlled during melt spinning were pressure inside the crucible, speed of copper wheel, and temperature of crucible by induction heating. The parameters used for the different alloys, can be seen in figure C.1-C.3. An example of the ribbons produced can be seen in figure 3.10.

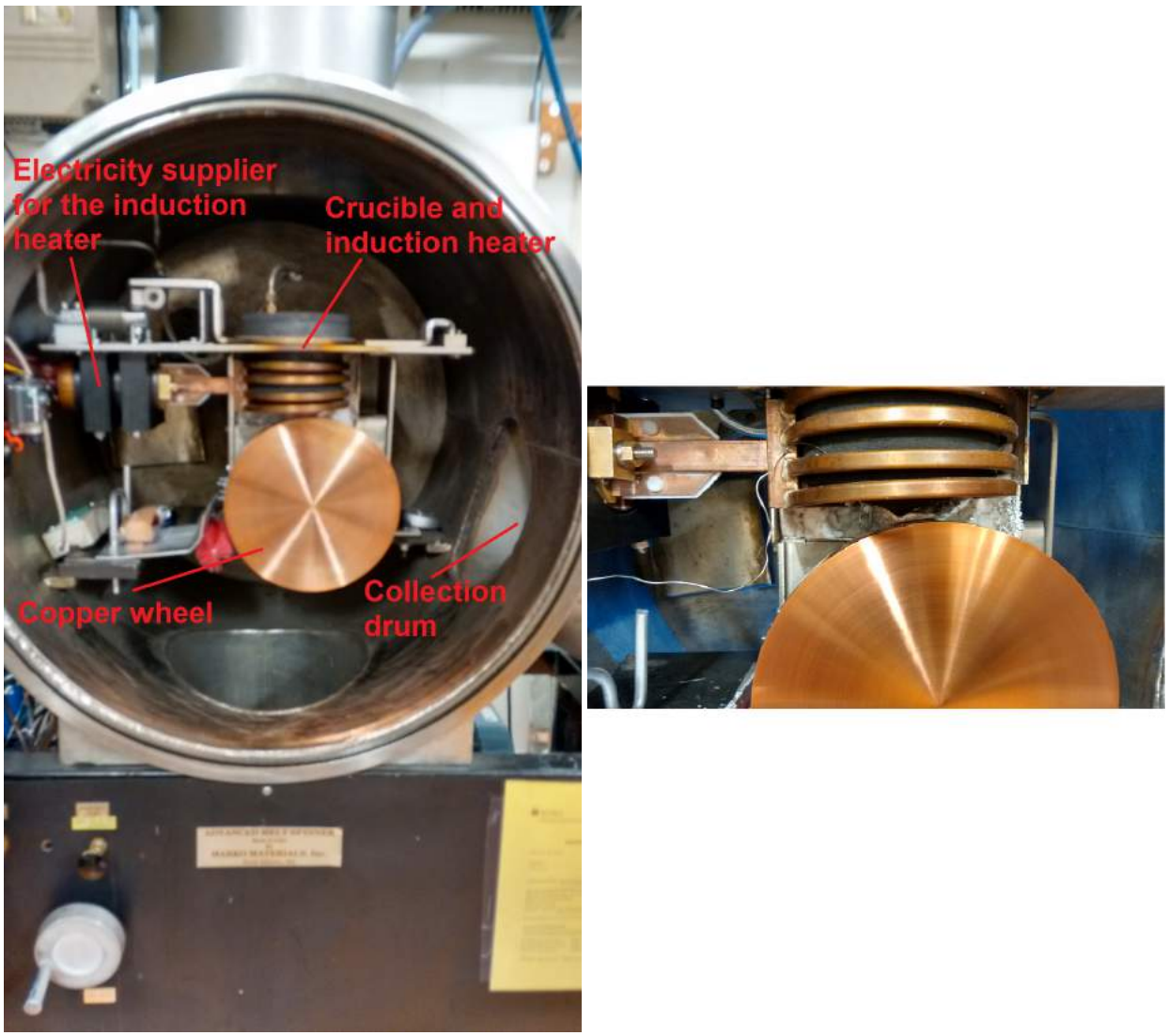

(a) (b)

Figure 3.9: Images of the melt spinner used in this work. The aluminium is melted via induction heating, and fed onto the copper wheel. The melt quickly cools, is slung off the wheel, and is collected in the collection drum.

Figure 3.10: RS ribbons produced by melt spinning.

3.7 Screw extrusion

To utilize the ribbons for screw extrusion, they were granulated, using an ATM Brovig Getecha RS1600 with an 8mm sieve, seen in figure 3.11a, and resulting granulates are seen in figure 3.11b. The knives rotate, and cut the ribbons, which after several passes of the knives, will be small enough, to fall through the sieve. One pass through the granulator did however not produce sufficiently small granulates, and 2-4 passes were necessary.

Screw extrusion was done according to patent Werenskiold et al. (2008). Schematic can be seen in figure 2.6. Several approximate values of ranges that were tried to be kept, can be seen in table 3.3, and the full parameters for the RS feed material, can be seen in figure C.4-C.6. A 10mm die was used for all profiles, the feed opening was flushed with argon, and the profiles were water cooled on exit from the die. In between use, the screw, and other parts subject to contact with aluminium, were disassembled and submerged in a lye solution over night to remove left over oxides.

SCREW EXTRUDED RS RIBBONS

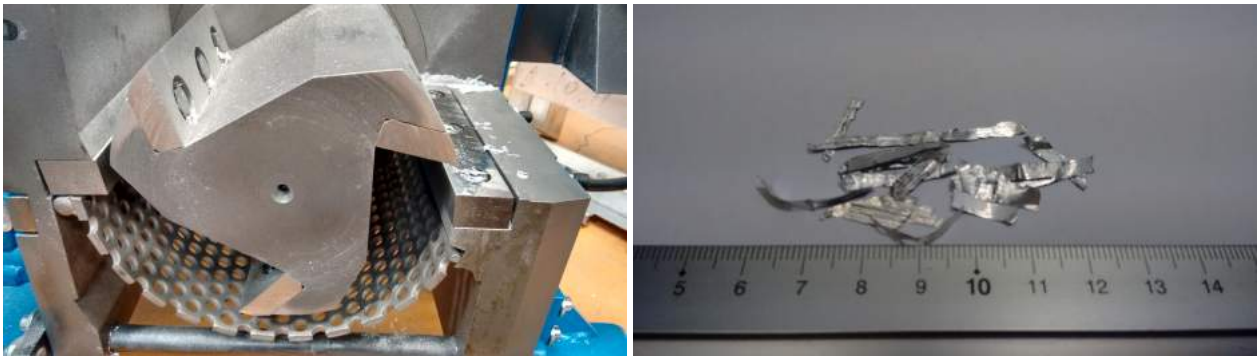

(a) ATM Brovig Getecha RS1600 with an 8mm sieve. (b) RS granulates.

Figure 3.11: a) ATM Brovig Getecha RS1600 with an 8mm sieve used to granulate the RS ribbons. The knives rotate, and cut the ribbons, which gradually fall through the sieve. b) The resulting granulates produced by the granulator.

Table 3.3: Approximate values controlled during under screw extrusion.

Die temperature °C	Feed rate [g/min]	Moment[kNm]
430-440	10-25	10-15

3.8 Homogenization

Homogenization was performed in order to determine if it is possible to completely eliminate the presence of the beta phase, or if not, how much it is possible to reduce it by.

Homogenization of as cast Al-XMg DC specimens was performed in Nabertherm N11/R air circulation furnace, up to 13 hours. The entire homogenization schedule can be seen in figure 3.12, samples were quenched after 5, 8, 9, 10, 11, and 13 hours. An initial homogenization was performed, where samples were held at 430 °C for 4 hours, both with, and without aluminium foil covering the samples, to see if there was any difference. Any discernable differnce was not seen. Results of this test can be seen in appendix E.During the full homogenization schedule, all the samples were covered in aluminium foil. In addition, some specimens covered in aluminium foil were held at 430 °C for 1 week, to see if there was any difference compared to holding for 4 hours. Quenching was performed in water. For further reference, the different homogenization schedules are given a number:

- Homogenization schedule 1: Homogenization at 430 °C for 4 hours, and immediately quenched in water.
- Homogenization schedule 2: Homogenization at 430 °C for 4 hours, then raised to 490 °C during a time period of 7 hours, and immediately quenched in water.
- Homogenization schedule 3: Homogenization at 430 °C for 1 week, and immediately quenched in water.

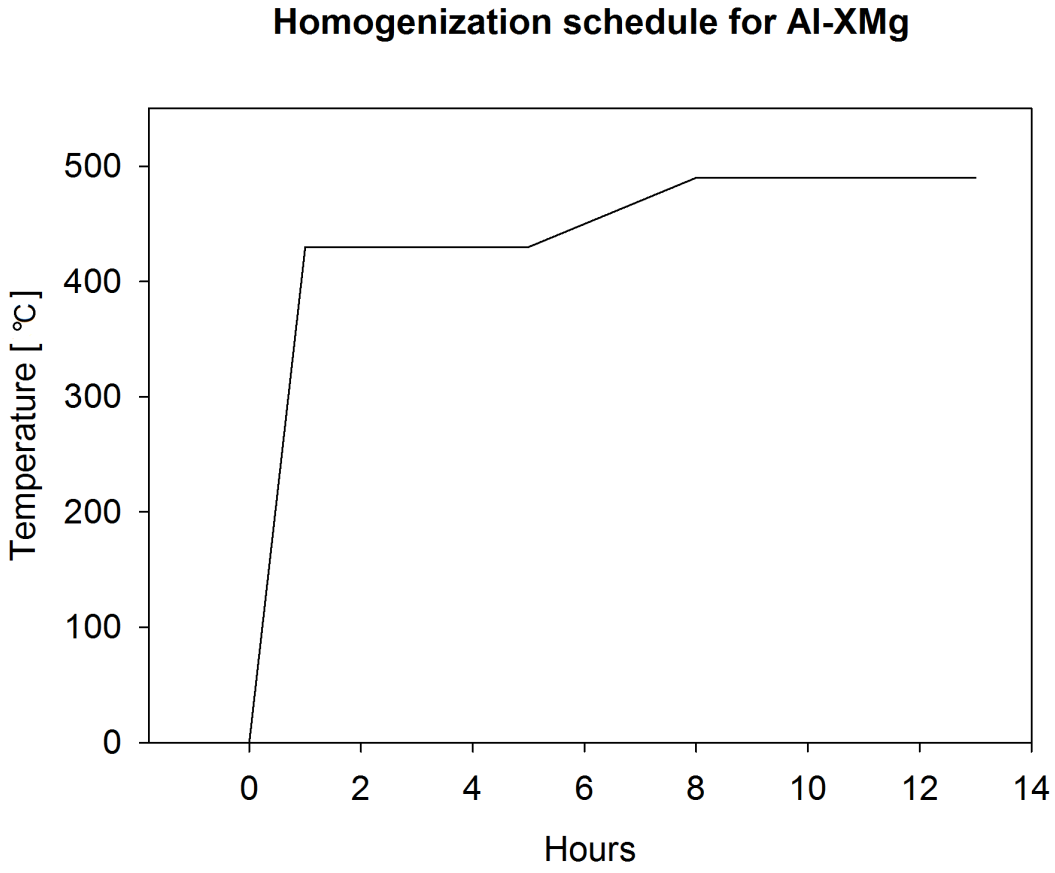

Figure 3.12: Homogenization schedule that the Al-XMg material followed.

3.9 X-ray diffraction (XRD)

XRD is used to determine which crystallographic phases are present in a material. The investigated material was characterized with XRD in the hopes that it would be possible to determine

the amount of beta phase in the investigated materials.

XRD measurements were performed with a Bruker D8 Advance DaVinci X-ray Diffractometer, Da Vinci 1. DIFFRAC.EVA was used to create the XRD plots, while the TOPAS program was used to implement the Rietveld refinement method to estimate the lattice parameters. Deep specimen holders were used, with plastelina to build up the height, so the samples were level with the sample holder. Start and end angles were 20°, and 80°, and the step size was 0.013°, with 72.96 s per step.

3.10 Tensile testing

Tensile testing was performed with a 100KN MTS Universal Testing Machine, seen in figure 3.13b, by PhD student Kristian Grøtta Skorpen. Strain rate was 2mm/min. The tensile specimens were round, with dimensions as shown in figure 3.13a.

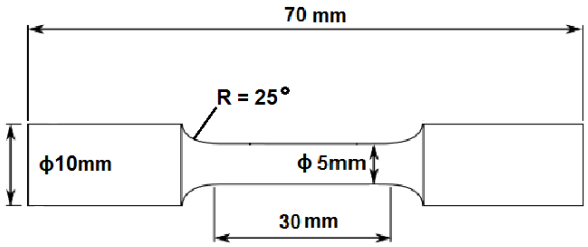

(a) Dimensions of the round tensile test specimens.

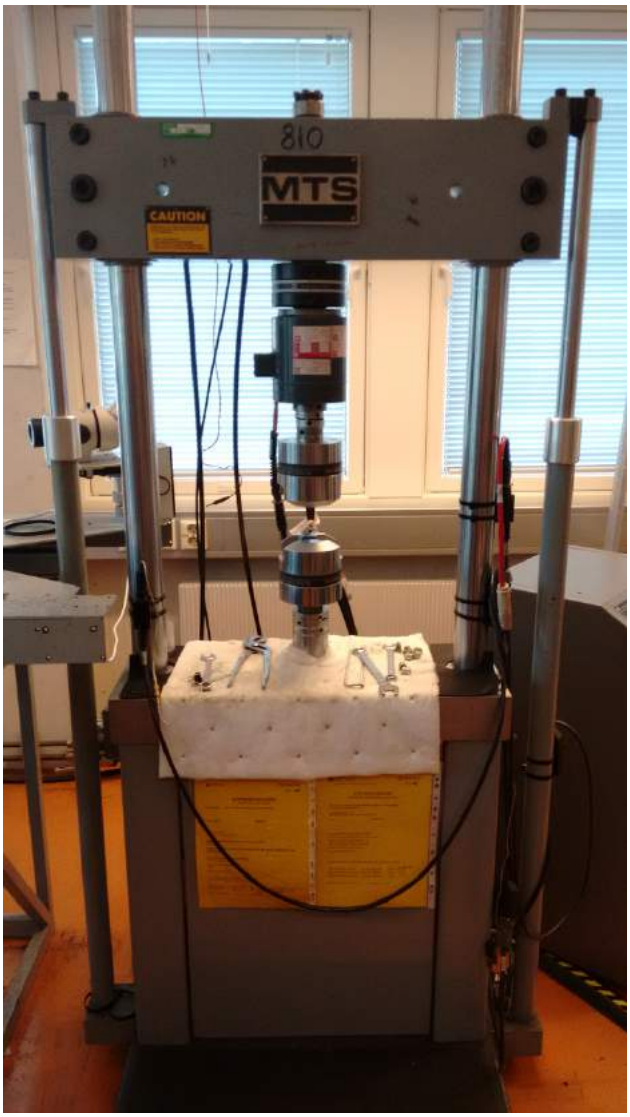

(b) Tensile machine used. 100KN MTS Universal Testing Machine.

4 | Results

An overview of the different materials produced from the as cast material received, can be seen in figure 4.1. A project on the same subject as this thesis was performed and written during the autumn of 2015. During this project work, the RS material and screw extruded RS/machined granulates material was made. Optical micrograph specimens have been metallographically prepared to a more satisfactory degree, based on experiences made during the autumn project, however some of the hardness measurements are referenced in this thesis, and mention will be made when they are.

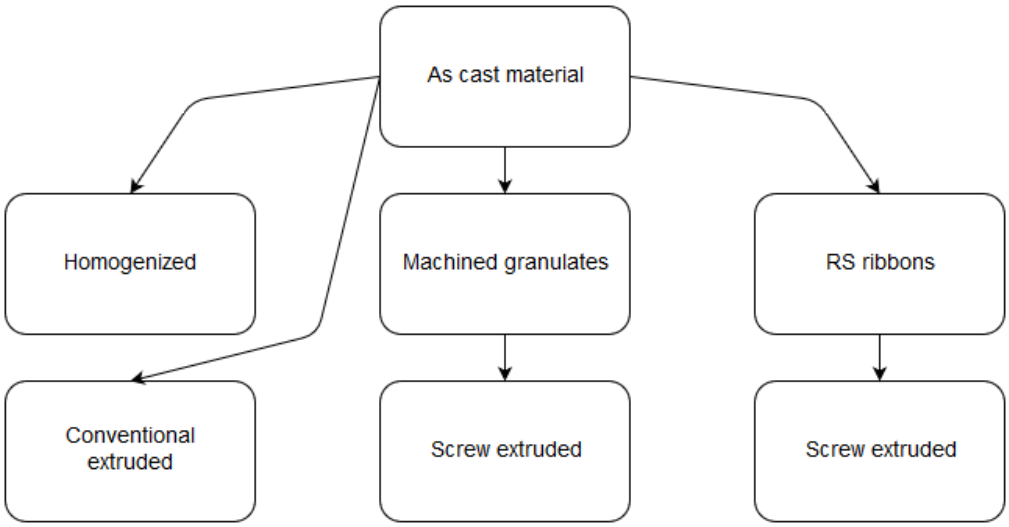

Figure 4.1: An overview of the different characterized materials.

4.1 Microstructure

This section presents bright and polarized light microscopy images, as this is an easy way of presenting microstructure in a good way.

As cast material

Micrographs of the as cast material can be seen in figures 4.2-4.3. A fair amount of porosity can be seen, both spherical, and disordered in shape. The light grey particles pointed out in figure 4.2f, are confirmed by EDS in section 4.4 to be beta particles. A clear increase in beta particles with increasing Mg content can be seen. The beta particles are clearly visible in all alloys. An increase in beta particle density, and decrease in grain size, is seen with increasing Mg content.

AS CAST

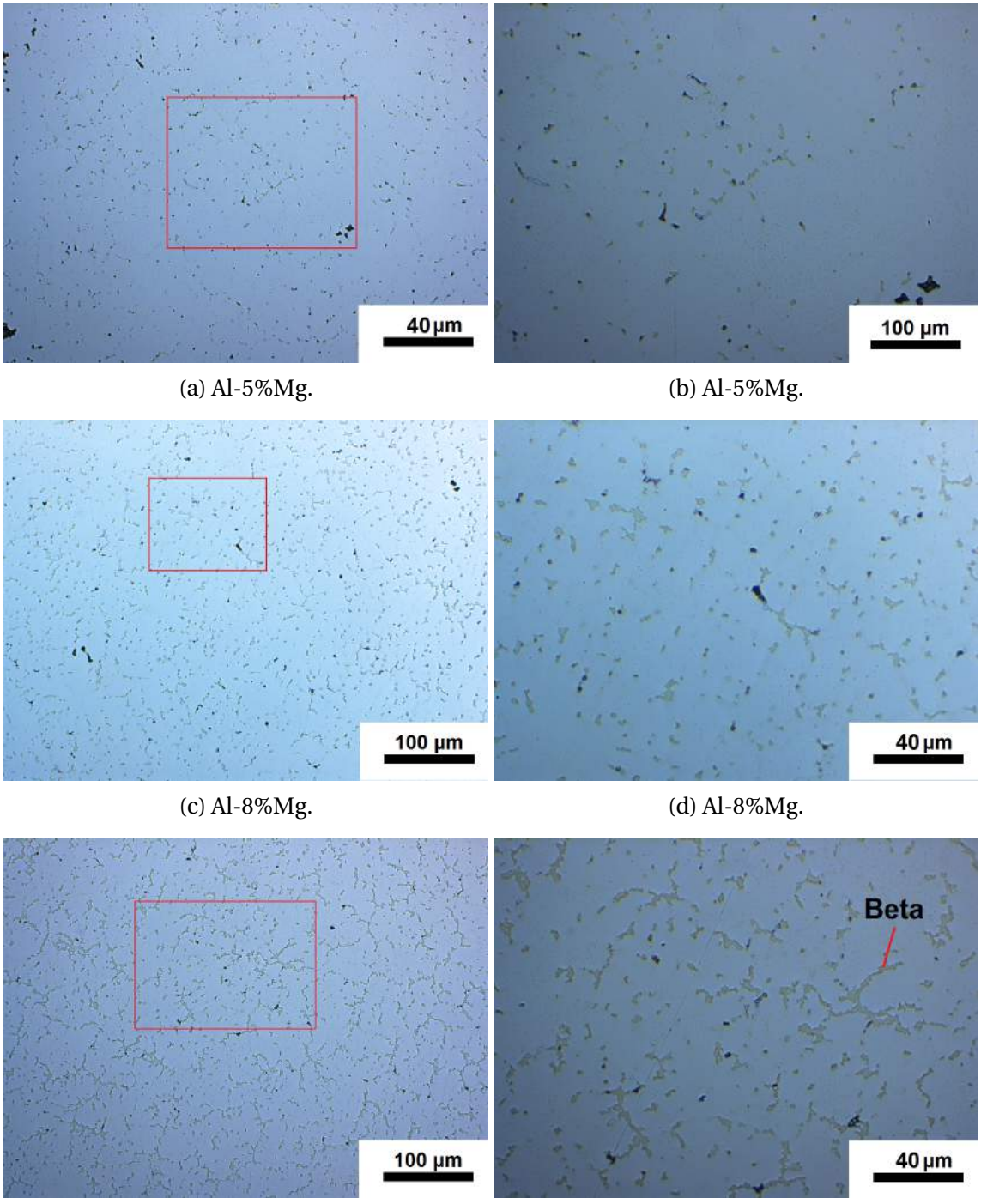

(a) Al-5%Mg. (b) Al-5%Mg.

(c) Al-8%Mg. (d) Al-8%Mg.

(e) Al-10%Mg. (f) Al-10%Mg.

Figure 4.2: Micrographs taken of as cast Al-XMg. The light grey particles are confirmed by SEM EDS to be beta particles, see figure 4.30. A clear increase of beta particles can be seen with increasing Mg content. Any differences in porosity is not seen.

AS CAST

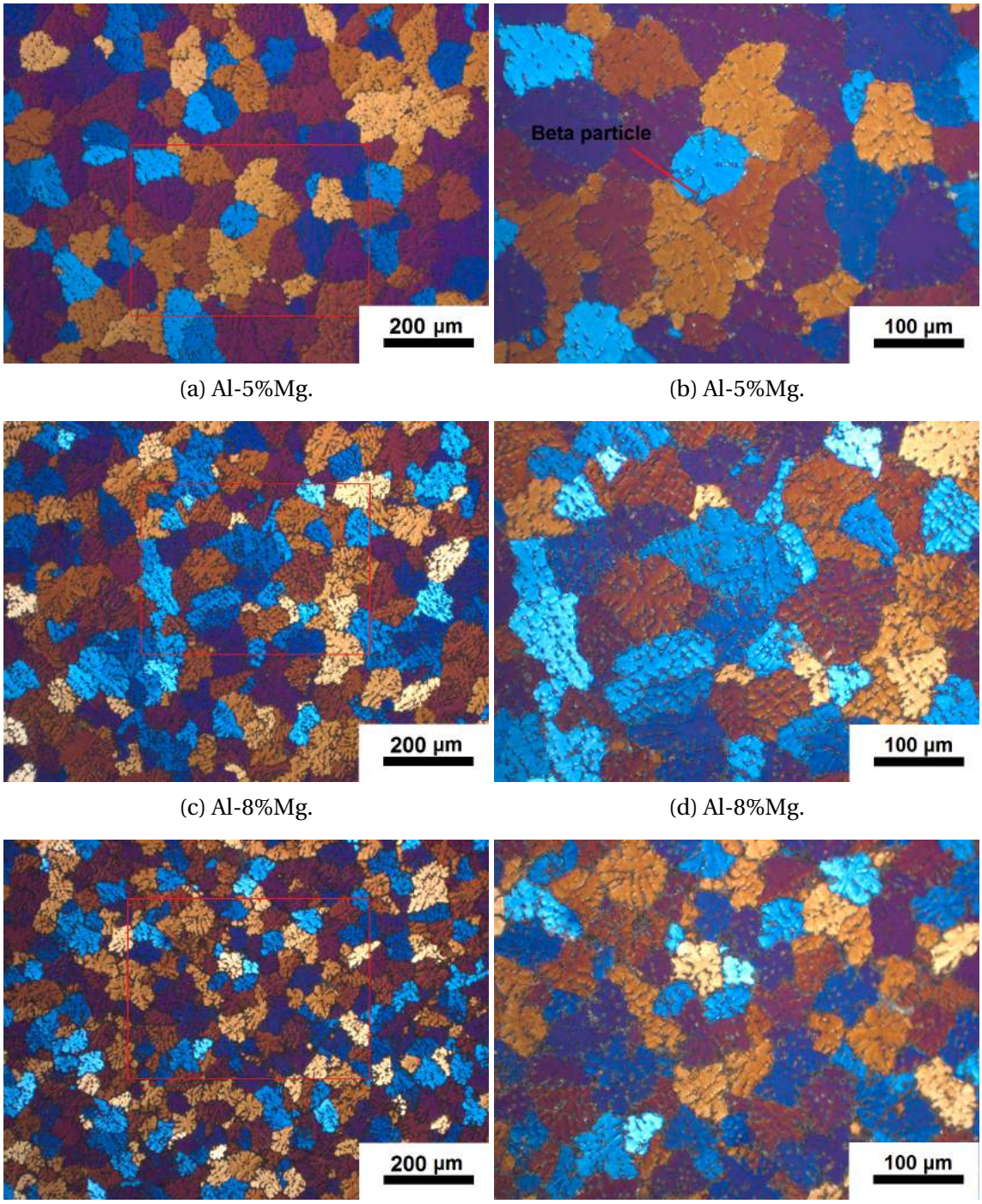

(a) Al-5%Mg. (b) Al-5%Mg.

(c) Al-8%Mg. (d) Al-8%Mg.

(e) Al-10%Mg. (f) Al-10%Mg.

Figure 4.3: Micrographs of anodized as cast Al-XMg. Some grain refinement and increasing amount of beta particles with increasing mg content can be seen.

Feed material for screw extrusion

In figures 4.4-4.5, micrographs of as cast and machined granules can be seen. Both beta particles and porosity can be seen, and the deformation direction is clearly seen by the way all the pores and beta particles are dragged out across the granules. Same conclusions for beta particles can be drawn for the granules, as for the as cast material. The deformation shows clearly in the anodized micrographs, with one side being jagged, but no differences between alloys are immediately seen. The grey spots seen in the Al-10%Mg granule in figure 4.5c, might be an art defect, i.e, an interaction during anodizing, that does not necessarily reflect the microstructure of the material, as they are seen in several of the anodized specimens, for no apparent reason. Other art effects will be pointed out when present.

The as melt spun ribbons can be seen in figures 4.6-4.7. The clusters of, most likely pores, occur typically near the air side, although they were seen near wheel side as seen in figure 4.6a. Some micro porosity was seen very faintly while adjusting focus, and best seen in 4.6f. The grain size of the ribbons is small, and decreases with increasing Mg content. Some places, especially in the Al-8%Mg in figure 4.7c-4.7d, the ribbons are so thin, that only one grain covers the entire cross section.

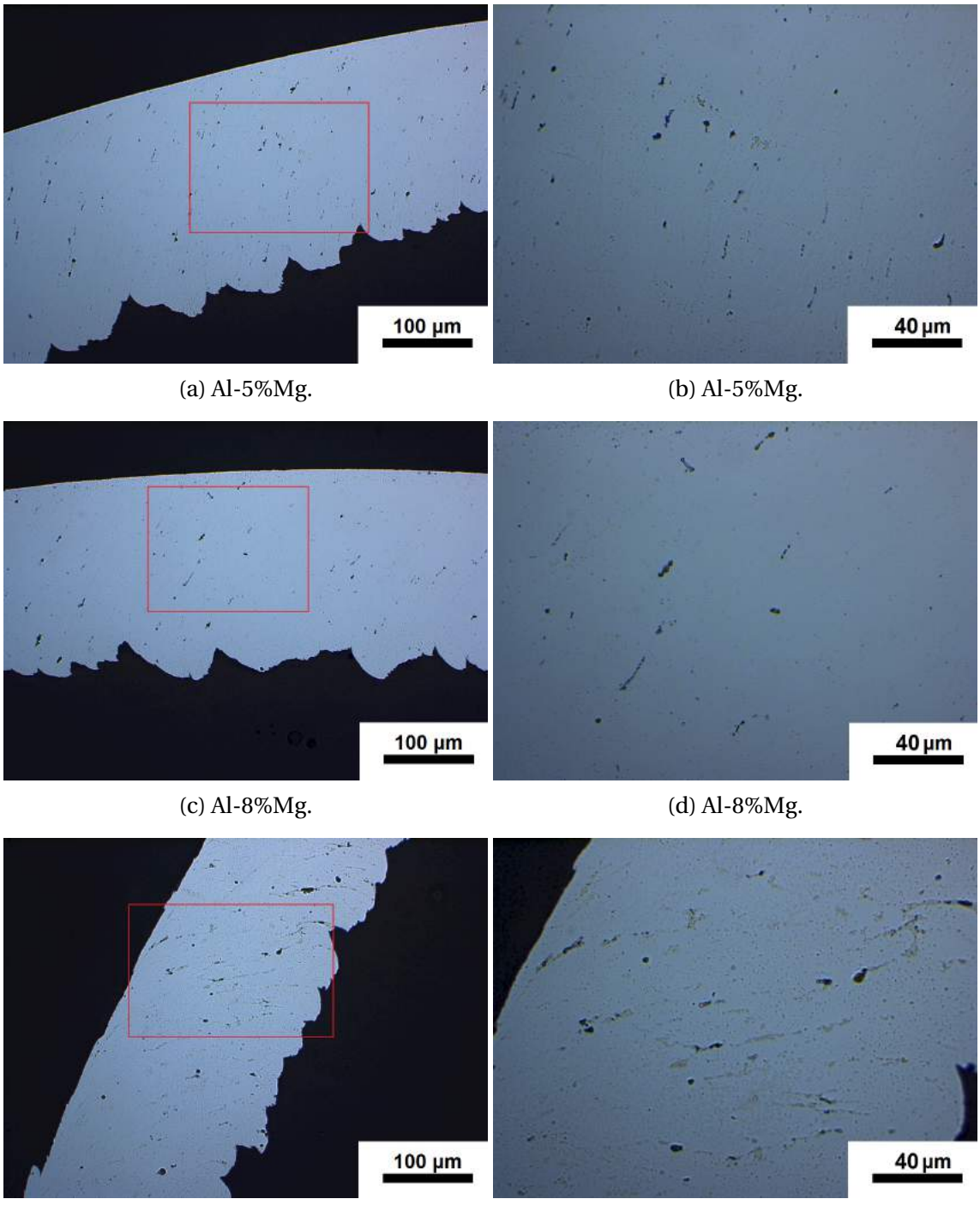

(a) Al-5%Mg. (b) Al-5%Mg.

(c) Al-8%Mg. (d) Al-8%Mg.

(e) Al-10%Mg. (f) Al-10%Mg.

Figure 4.4: Micrographs taken of as cast Al-XMg machines granulates. The deformation is clear to see, especially for the Al-10%Mg, where the beta particles are dragged out in the deformation direction.

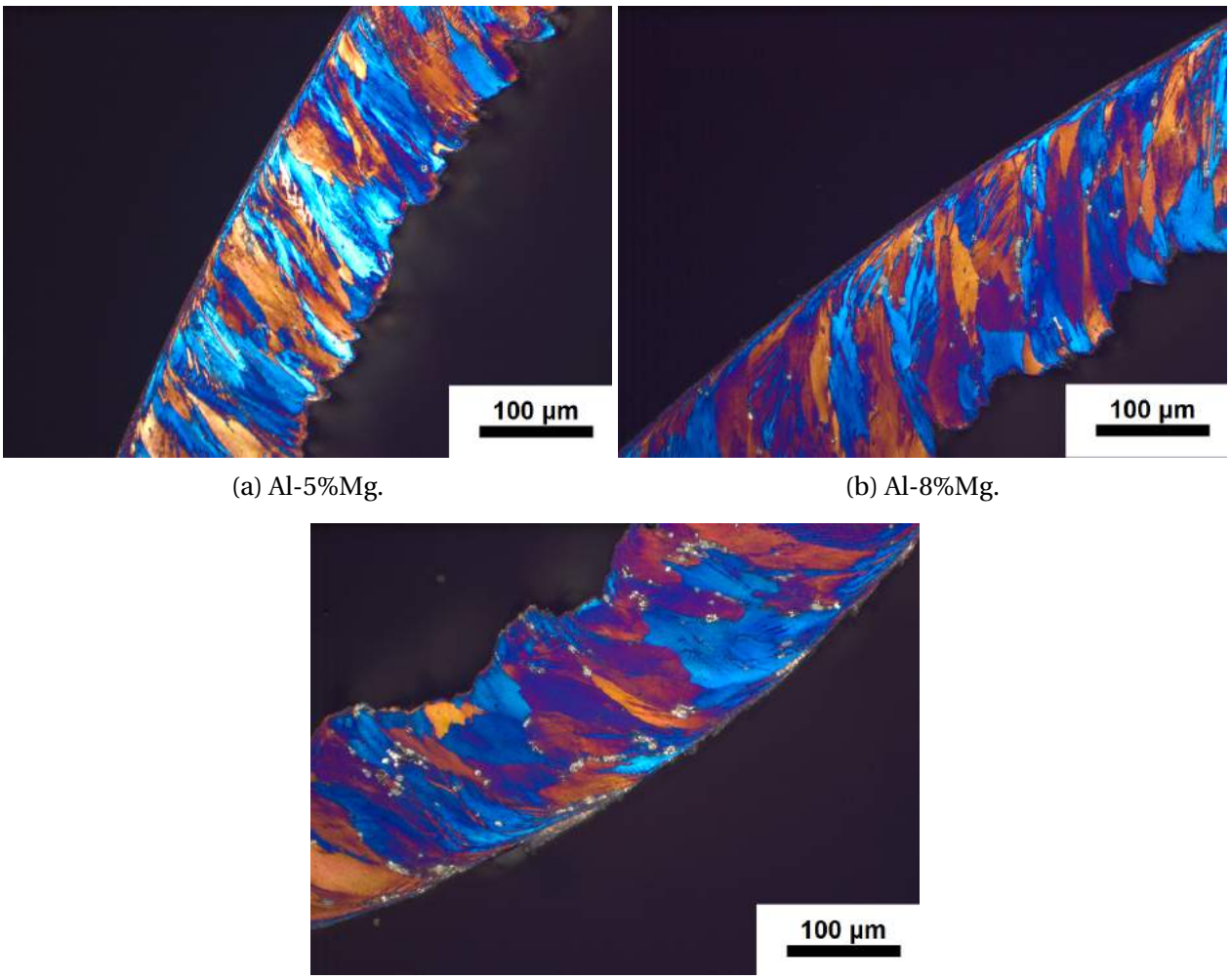

(a) Al-5%Mg.

(b) Al-8%Mg.

(c) Al-10%Mg.

Figure 4.5: Micrographs of anodized as cast Al-XMg machined granulates. The deformation as a result of cutting is clearly seen. The apparent increase in grey particles might be due to a difference in how the anodizing has affected the material.

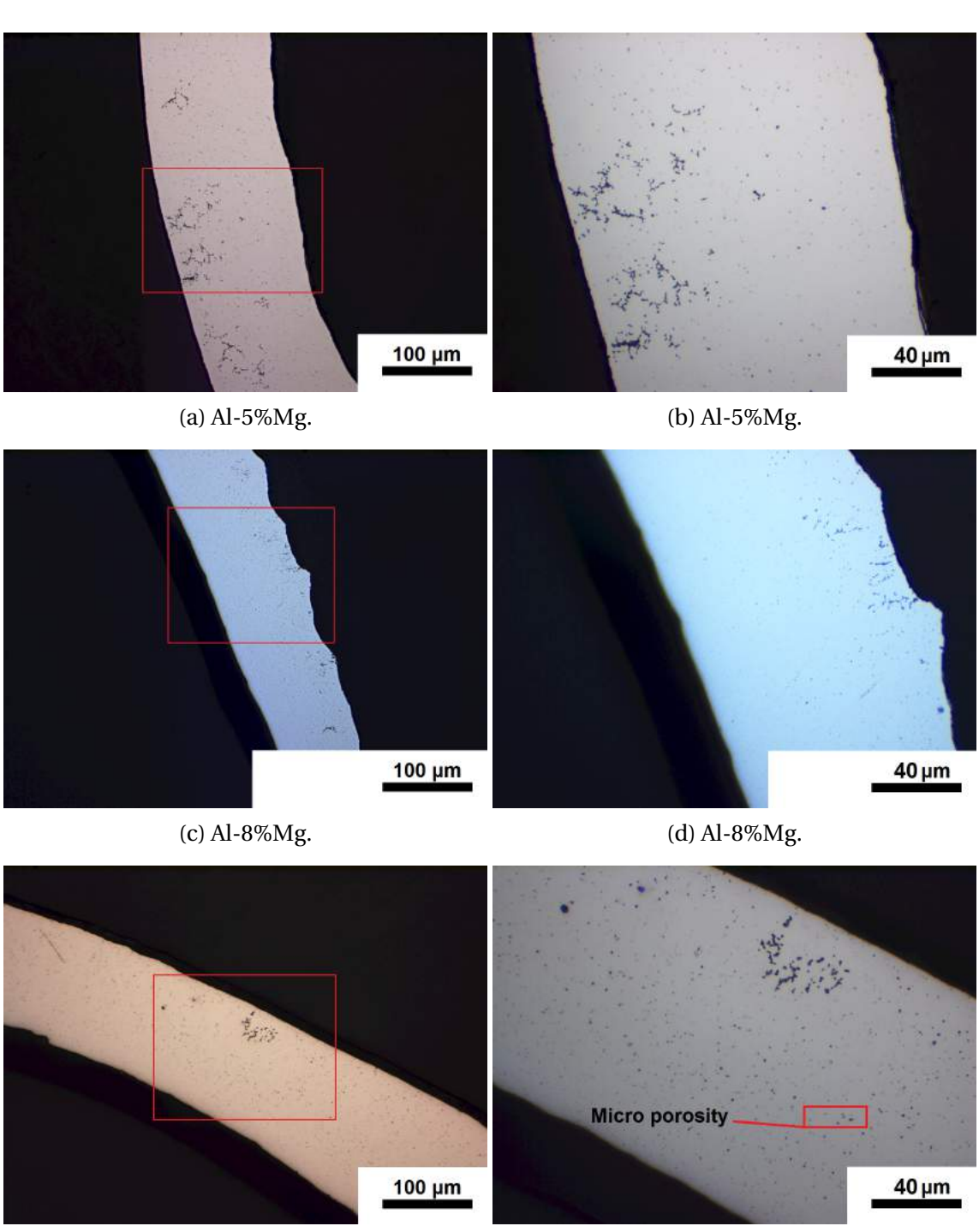

(a) Al-5%Mg. (b) Al-5%Mg.

(c) Al-8%Mg. (d) Al-8%Mg.

(e) Al-10%Mg. (f) Al-10%Mg.

Figure 4.6: The particle/pore clusters mostly congregate near the air side, although they were seen near the wheel edge, and seems more prominent in Al-5%Mg. Micro porosity can be seen distributed heterogeneously, with higher density with increasing Mg content. Copper side is to the left in all micrographs.

RS RIBBONS

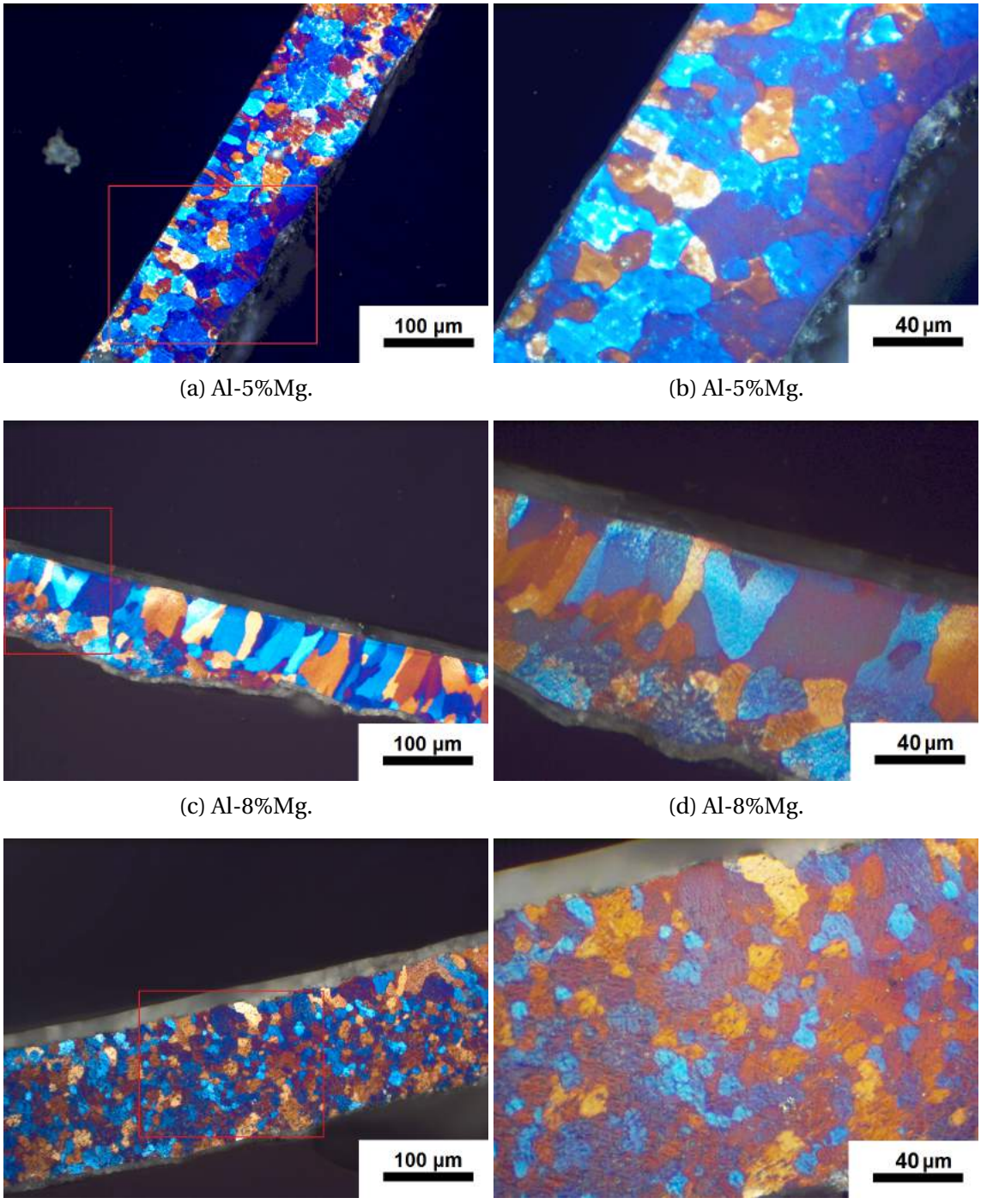

(a) Al-5%Mg. (b) Al-5%Mg.

(c) Al-8%Mg. (d) Al-8%Mg.

(e) Al-10%Mg. (f) Al-10%Mg.

Figure 4.7: Micrographs of anodized Al-XMg RS ribbons. Some grain refinement can be seen with increasing Mg content. A columnar structure is seen near the wheel side, on the left a) and b), and on the top c)-f). The thickness varies greatly, both between alloys, and within the same ribbon. The Al-8%Mg ribbon in c)-d) is very thin, and in the thinnest parts, the columnar section is seen stretching across the entire thickness.

Homogenized samples

Figure 4.8-4.9 shows the DC cast Al-XMg samples homogenized at 430 °C. A clear increase in density and size of porosity can be seen, compared to the as cast material. Notice especially the increased amount of non spherical porosity compared to the as cast material seen in figure 4.2. In the Al-5%Mg and Al-8%Mg samples, beta is difficult to see. There might be a beta particle seen in figure 4.8d, however, it is clear to see that a large amount of beta particles are still present in the Al-10%Mg sample. A general increase in size of porosity can be seen with increasing Mg content, however, the pore density change is inconclusive. One can see grain refinement with increasing Mg content, and some large porosity along grain boundaries, and in the middle of grains.The grey spots prevalent in the Al-5%Mg in figure 4.9a-4.9b, and visible in the Al-10%Mg in figure 4.9e-4.9f, might bean art effect, as no difference in the bright field images would suggest such differences in the anodized micrographs.

Samples homogenized at 430°C for 1 week, are seen in figures 4.10-4.11. An obvious change from the samples homogenized for 4 hours, is the decrease in beta particles in the Al-10%Mg samples. There might be a beta particle in figure 4.10f, but this is not conclusive. The same porosity size increase with increasing Mg content as samples homogenized for 4 hours can be seen. It is difficult to make a conclusion, on whether or not there is a difference in porosity density and size in the samples homogenized for 1 week, compared to the samples homogenized for 4 hours. Looking at figure 4.10c, compared to figure 4.8c, it might look like porosity density decreases, in addition to the pores being more spheroidal in the Al-8%Mg samples homogenized for 1 week. One can see the same grain refinement with increasing Mg content as for the samples following heat treatment schedule 1. There might be a stronger tendency for the pores to cluster on the grain boundaries and triple points in these samples, than for the samples following heat treatment schedule 1.

Micrographs of the DC cast samples homogenized to 490 °C is shown in figure 4.12-4.13. Porosity size increase with increasing Mg content. There might be a beta particle in 4.12f, however, it is most probably a cluster of pores, as it is similar in look to the micro pores surrounding it, only clustered. These micro pores increase markedly in density with increasing Mg content, which

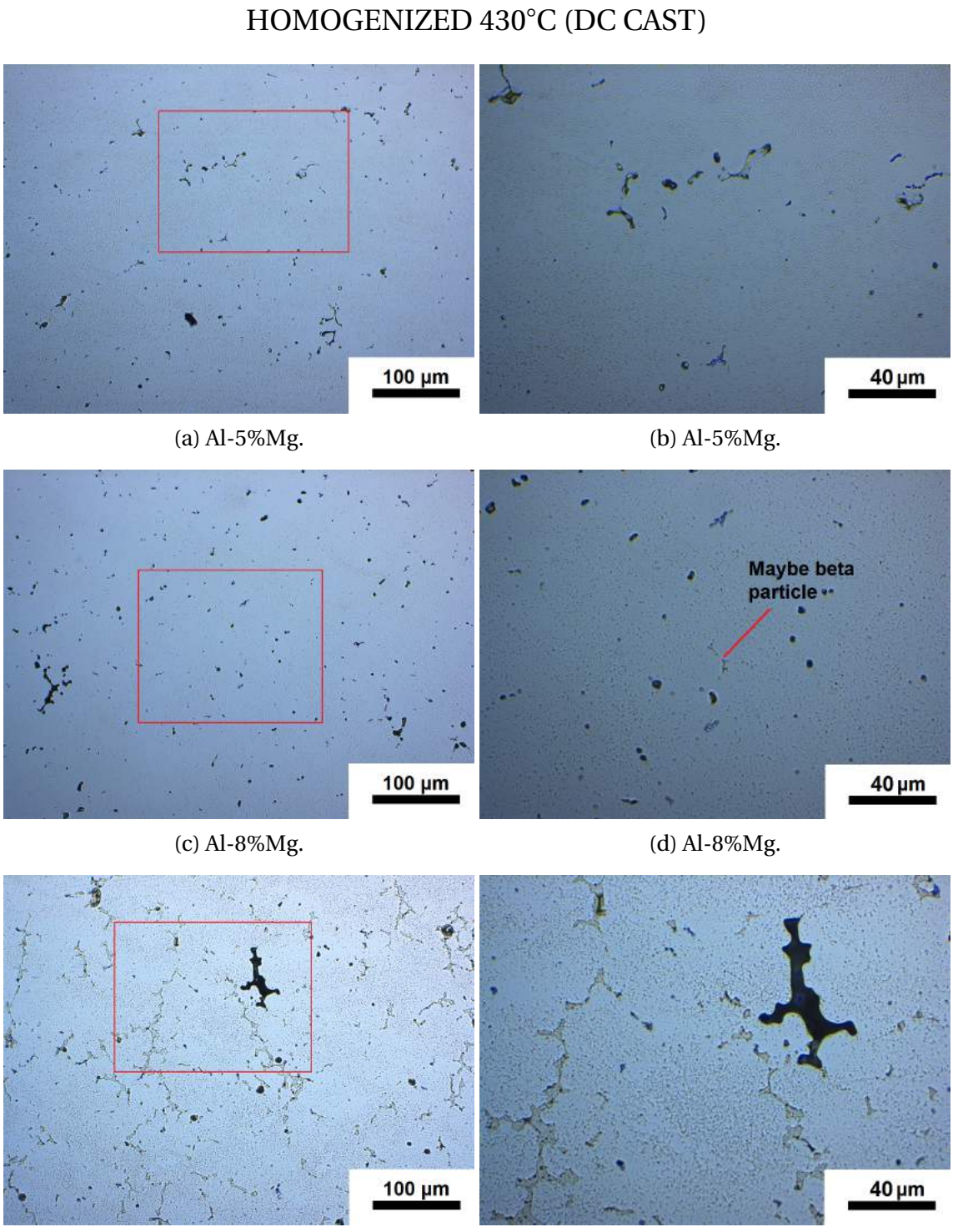

(a) Al-5%Mg. (b) Al-5%Mg.

(c) Al-8%Mg. (d) Al-8%Mg.

(e) Al-10%Mg. (f) Al-10%Mg.

Figure 4.8: Micrographs of DC cast Al-XMg, following heat treatment schedule 1. An increase in beta particles, and size of pores, with increasing Mg content can be seen. The density of pores might increase.

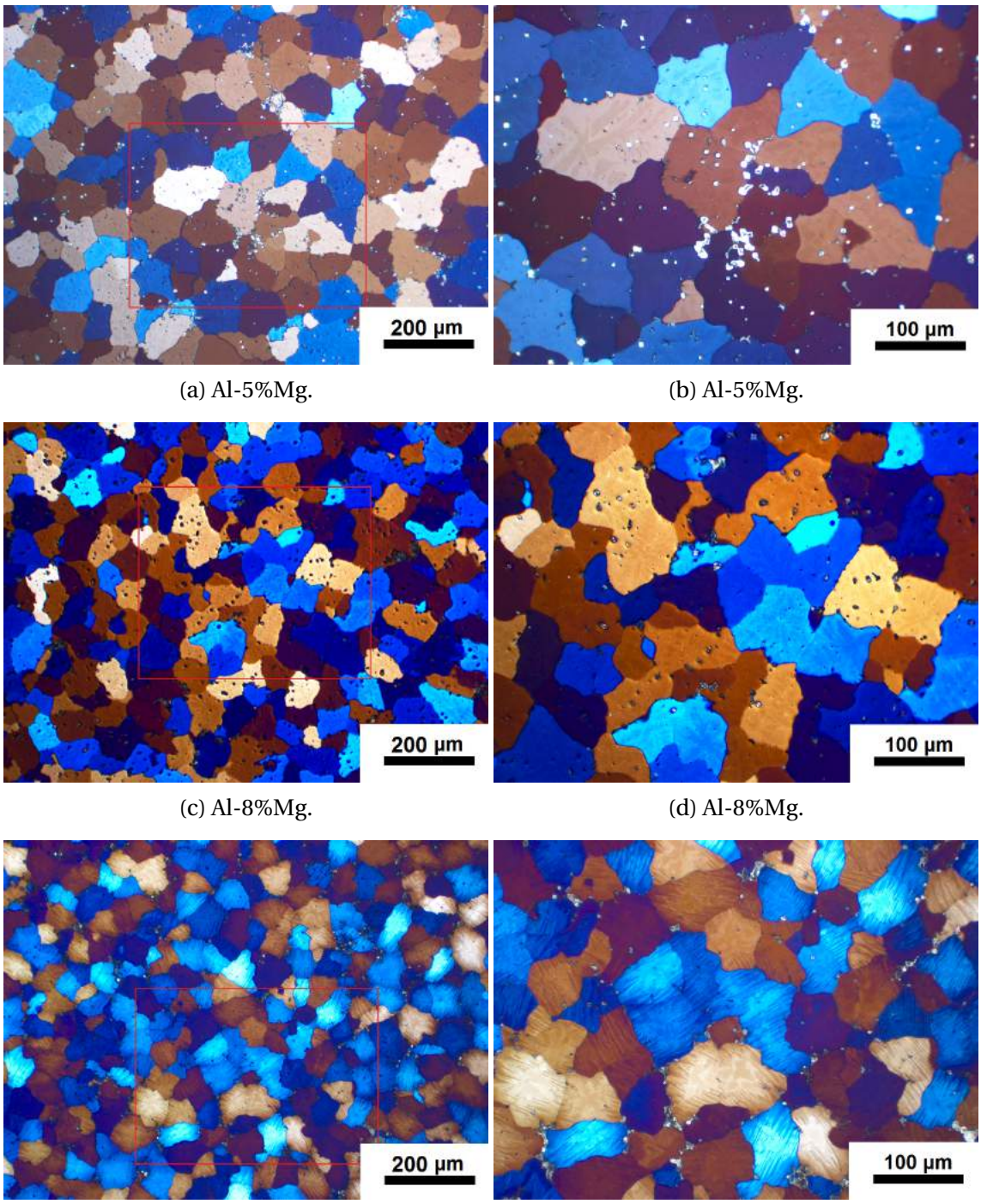

(a) Al-5%Mg. (b) Al-5%Mg.

(c) Al-8%Mg. (d) Al-8%Mg.

(e) Al-10%Mg. (f) Al-10%Mg.

Figure 4.9: Micrographs of anodized DC cast Al-XMg following heat treatment schedule 1. Grain refinement with increasing Mg content can be seen. The grey spots in a)-b) and some in e)-f), in addition to the stripes in e) and f) are believed to be art effects. Especially the grey spots, since bright field micrographs does not reveal such a difference between Al-5%Mg, and Al-8%Mg and Al-10%Mg. It might be an interaction with pores.

HOMOGENIZED 430°C, 1 WEEK (DC CAST)

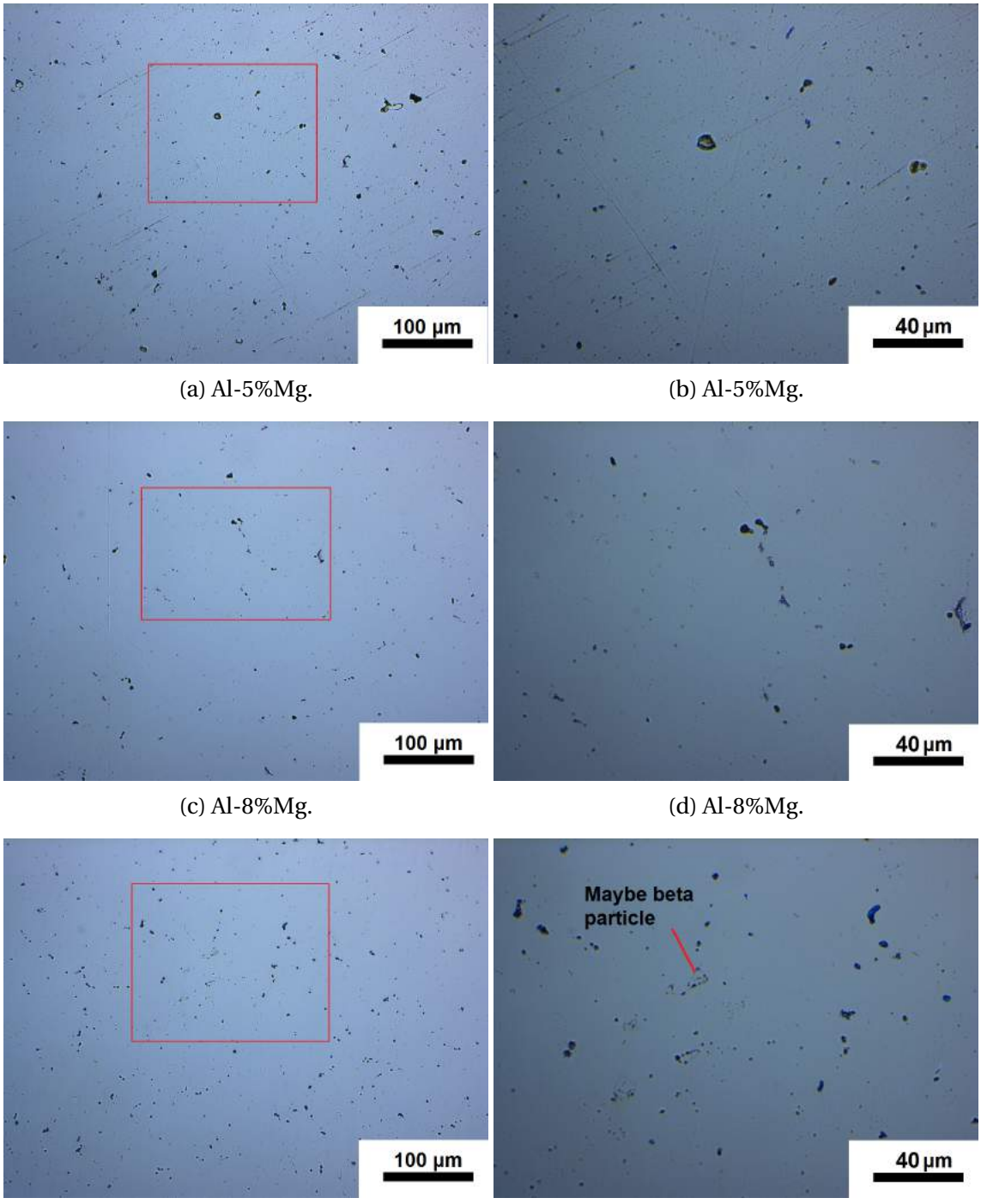

(a) Al-5%Mg. (b) Al-5%Mg.

(c) Al-8%Mg. (d) Al-8%Mg.

(e) Al-10%Mg. (f) Al-10%Mg.

Figure 4.10: Micrographs of DC cast Al-XMg, following heat treatment schedule 3. The very obvious beta particles seen in the samples heat treated for 4 hours in figure 4.8, are not seen in these samples. An increase in porosity size, with increasing Mg content can be seen. The density of pores might increase.

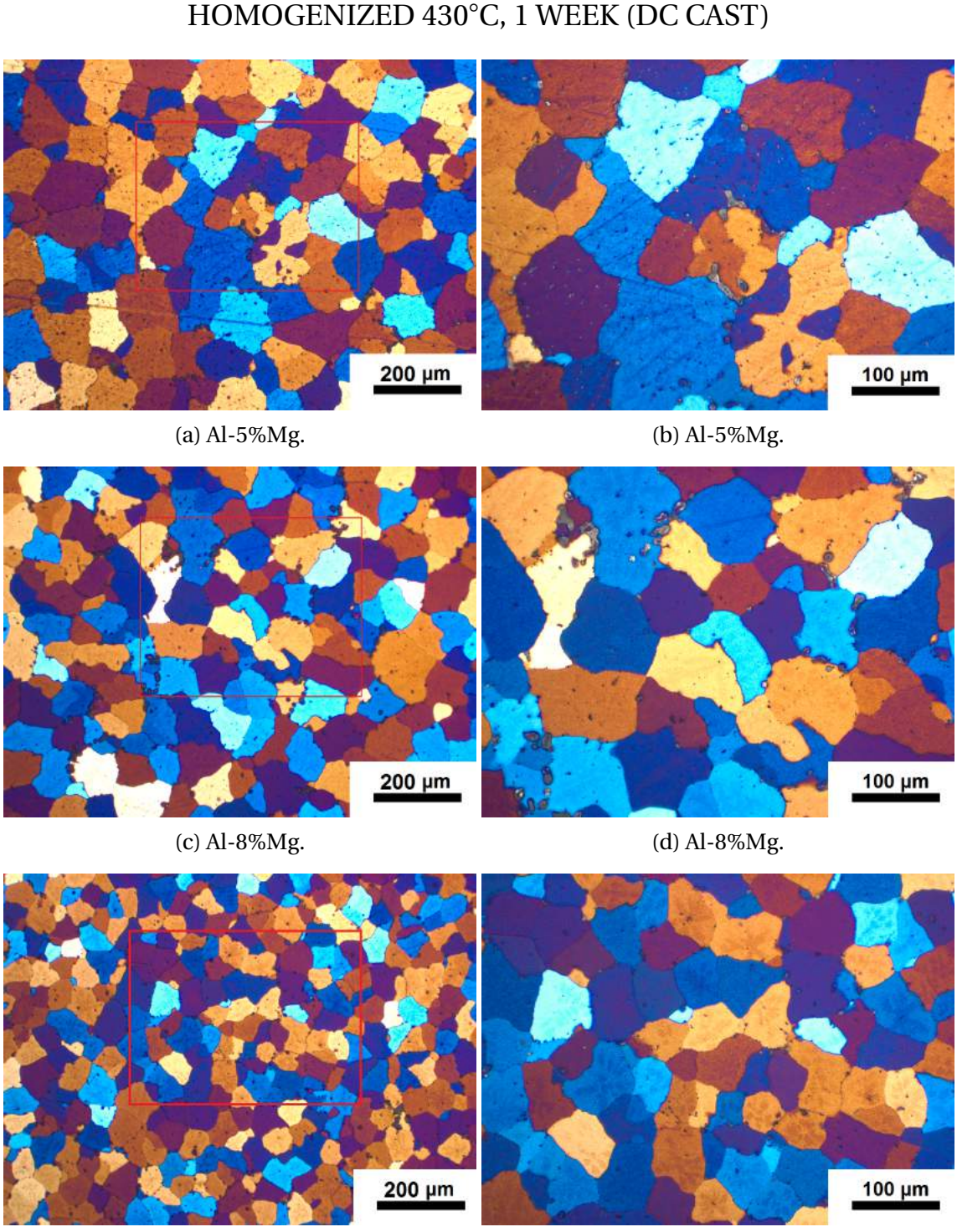

(a) Al-5%Mg. (b) Al-5%Mg.

(c) Al-8%Mg. (d) Al-8%Mg.

(e) Al-10%Mg. (f) Al-10%Mg.

Figure 4.11: Micrographs of anodized DC cast Al-XMg, following heat treatment schedule 1. Grain refinement with increasing Mg content can be seen, in addition to some large pores on the grain boundaries.

might be why the apparent micro pore clusters are seen most easily in the Al-10%Mg alloy, and not at all in the Al-5%Mg alloy. Compared to the samples homogenized at 430 °C, the samples homogenized to 490 °C show an increase in amount of spheroidal porosity, and since a no clear decrease in pore density seems to take place, a decrease in amount of non spheroidal porosity is also seen as a result. In addition, no clear signs of the beta phase can be seen. The same grain refinement tendency is seen as for the samples following heat treatment schedule 1 and 3, where it decreases with increasing Mg content. An increase in apparent porosity is seen from Al-5%Mg in figure 4.13a-4.13b, to Al-8%Mg in figure 4.13c-4.13c, however, this same increase is not seen in the bright field images in figure 4.12, and as such, these dark spots might be an unknown interaction with the anodizing electrolyte.

Micrographs of the edge of a homogenized DC cast Al-8%Mg sample following heat treatment schedule 2, is shown in figure 4.14a-4.14b. One can see that the grain size along the edge, is smaller by several hundred percent, in a layer that is about 10 microns in thickness. This edge effect was seen in all the heat treated samples, however, due to edge effects while anodizing, documenting this effect in all samples was not possible.

A micrograph of a homogenized DC cast Al-10%Mg sample following heat treatment schedule 3, is shown in figure 4.14c. This micrograph shows very small pores, which are not seen at a lower magnification, which are mainly situated on the grain boundaries and some triple points. This effect was also seen in all the heat treated samples.

HOMOGENIZED 490°C (DC CAST)

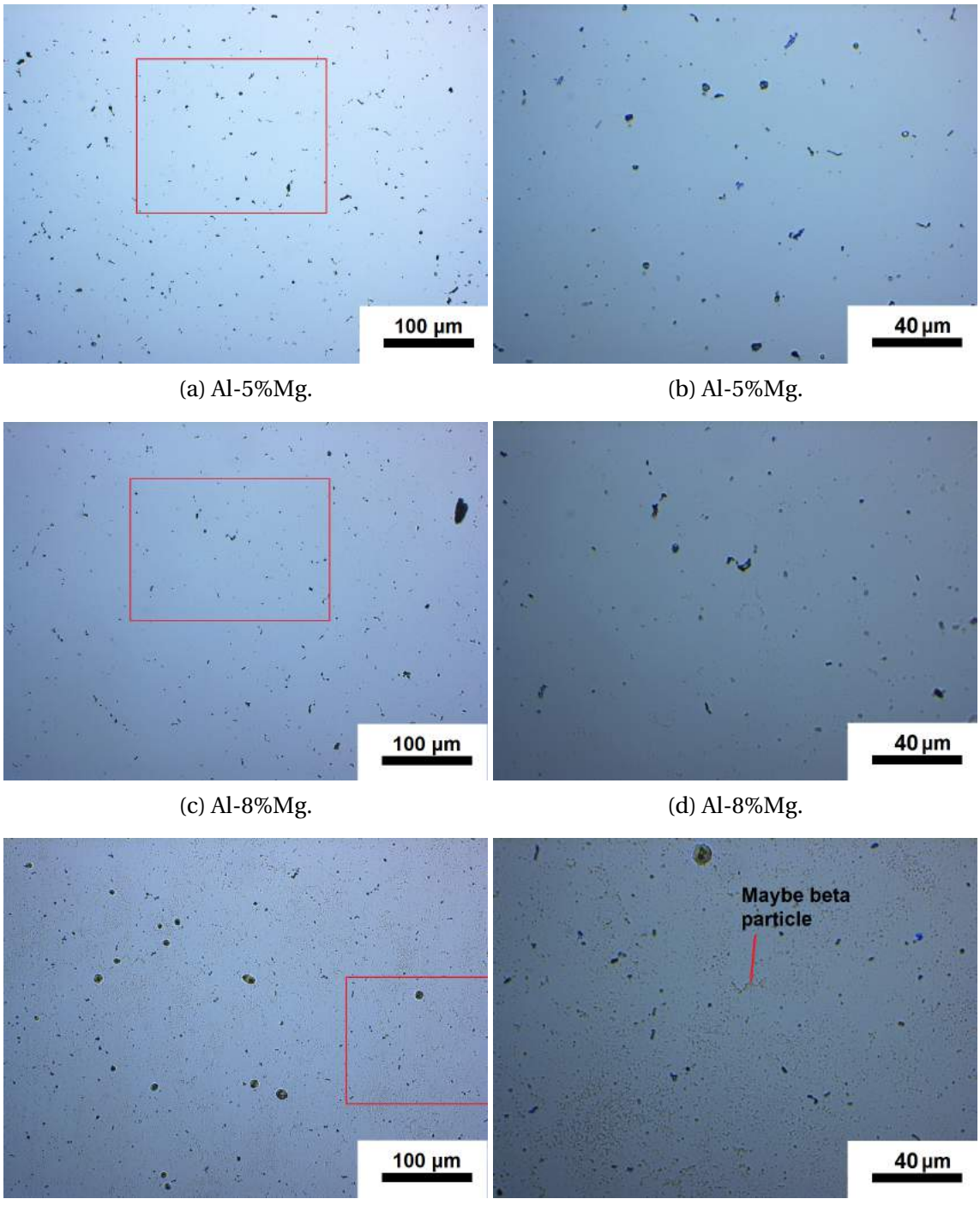

(a) Al-5%Mg. (b) Al-5%Mg.

(c) Al-8%Mg. (d) Al-8%Mg.

(e) Al-10%Mg. (f) Al-10%Mg.

Figure 4.12: Micrographs of DC cast Al-XMg, following heat treatment schedule 2. An increase in porosity size, with increasing Mg content can be seen. The density of pores might increase.

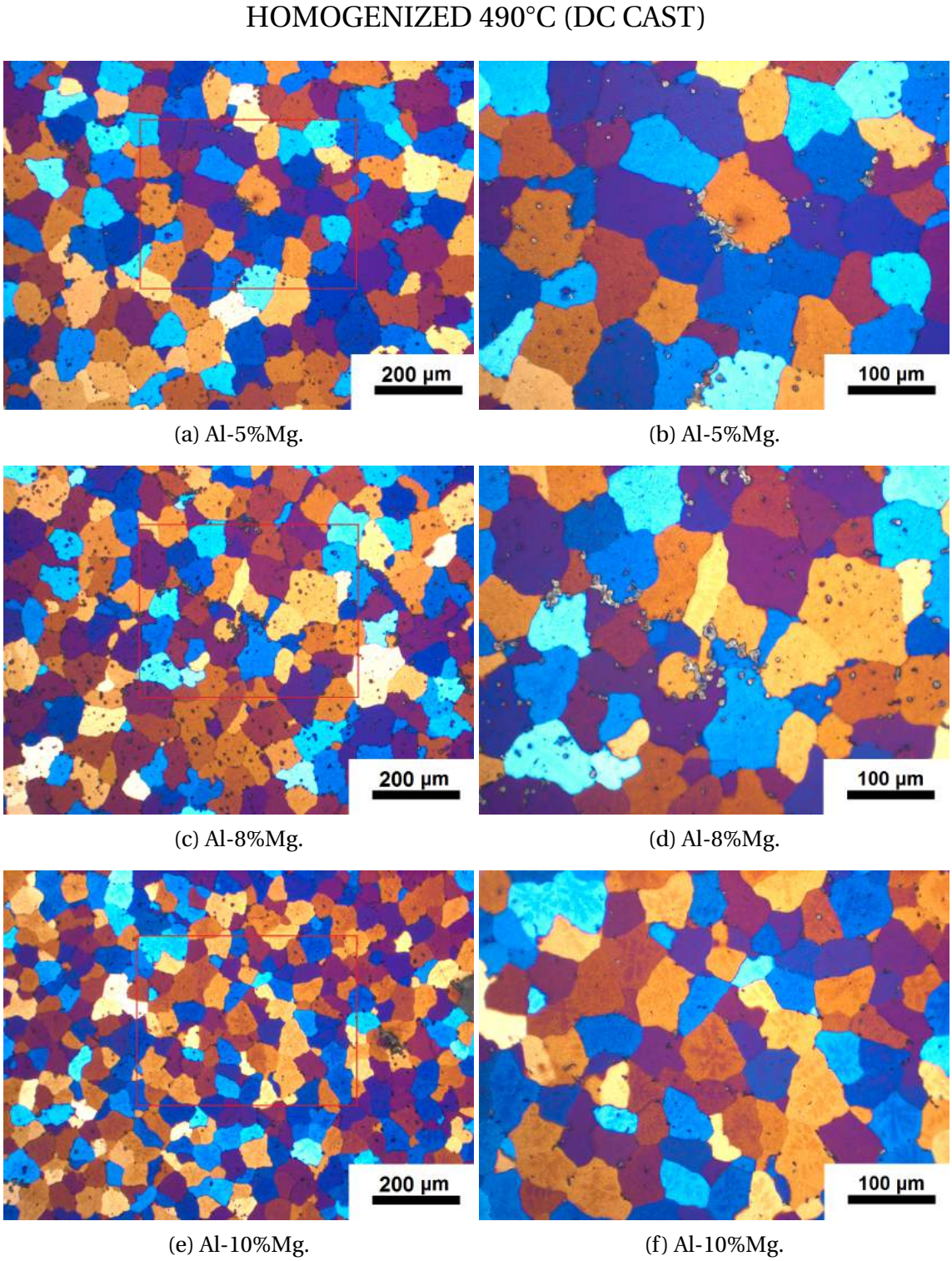

(a) Al-5%Mg. (b) Al-5%Mg.

(c) Al-8%Mg. (d) Al-8%Mg.

(e) Al-10%Mg. (f) Al-10%Mg.

Figure 4.13: Micrographs of anodized DC Al-XMg, following heat treatment schedule 2. An increase in porosity size, with increasing Mg content can be seen.

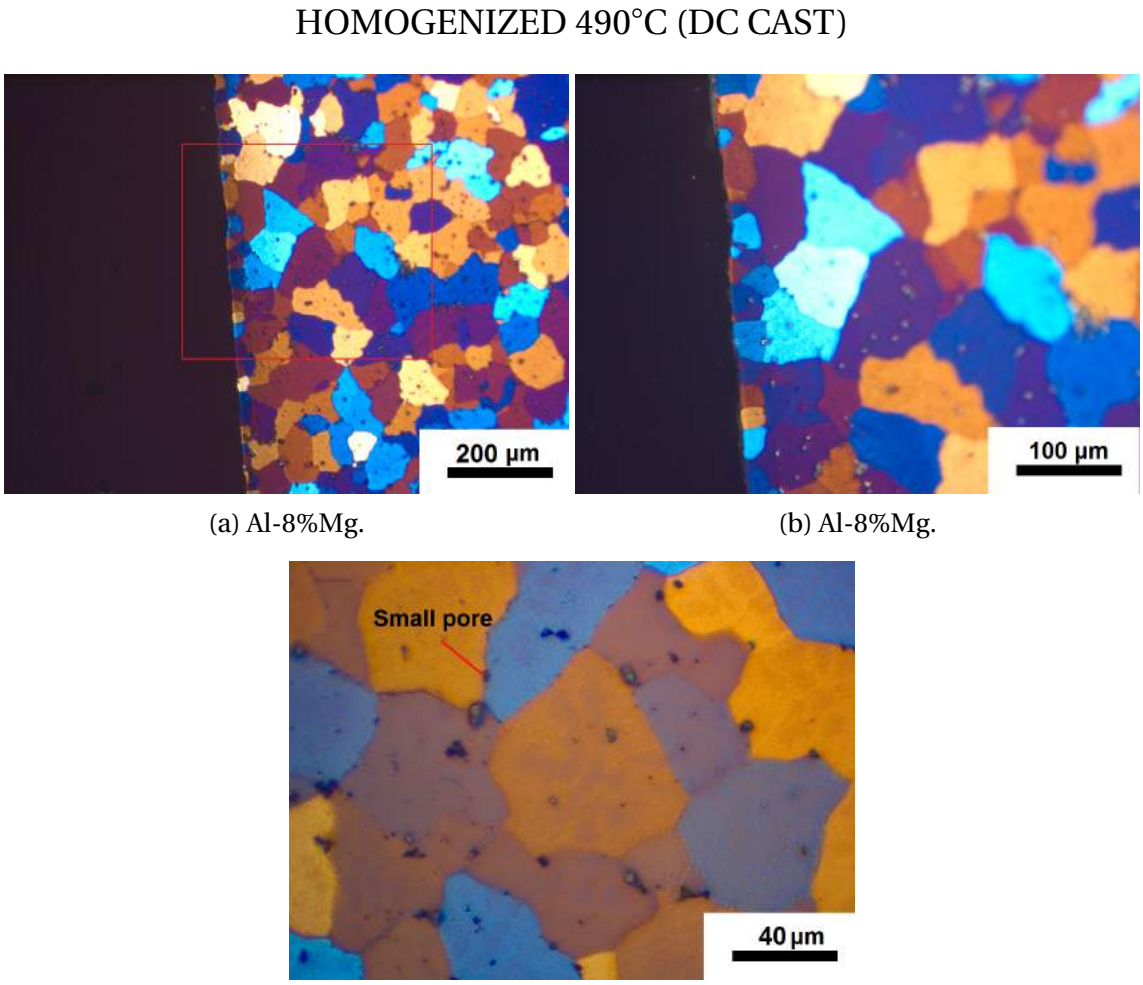

(a) Al-8%Mg.

(b) Al-8%Mg.

(c) Al-10%Mg.

Figure 4.14: Micrographs of anodized DC cast Al-XMg, following heat treatment schedule 2. Grain refinement can be seen near the edge, in a) and b). This was seen in all the heat treated samples. In addition, small pores can bee seen in c), which can not be seen at smaller magnifications. This was also seen in all the heat treated samples.

Conventional ram and screw extruded profiles

The following overview micrographs in figures 4.15-4.16,show the cross section of all the extruded profiles with the purpose of showing the amount of large scale porosity. They are 1 cm in diameter.

Figure 4.15 shows the conventional ram extruded profiles. The porosity decreases with increasing Mg content. Surface tearing can be seen along the edge, in the Al-5%Mg and Al-8%Mg profiles, much more pronounced in the Al-8%Mg profile, though not in the Al-10%Mg profile.

The screw extruded RS ribbons are shown in figure 4.17. The highest amount of porosity is seen in the Al-8%Mg profile, and a large amount of lamellar layers is seen in the Al-10%Mg profile. The micrographs are taken at 25X magnification, and at this magnification, dust on the lens easily obscures the vision, most easily seen in figure 4.17c. Information is missing from the middle of the Al-5%Mg profile, however, the overall impression stays the same.

In figure 4.16, the screw extruded granules are shown. Porosity decreases with increasing Mg content. No surface tearing or lamellar structure can be seen.

Comparing the profiles, conventional extrusion has the least amount of porosity and is the only method which sees surface tearing. All profiles see a decrease in large scale porosity with increasing Mg content. The only profile which has a lamellar structure is the Al-10%Mg screw extruded RS ribbon profile seen in figure 4.17c.

Figures 4.18-4.20, show panorama micrographs of the extruded material, conventional ram extruded, screw extruded machined granulates, and screw extruded RS ribbons respectively. It's easy to see that the screw extruded material has much smaller grains, in addition to no surface tearing. One can also see that the grains orientation is different. For conventional ram extruded profiles, the grains are mostly circular in shape, however, for the screw extruded material, the grains are longer in the extrusion direction. A discernible difference between the screw extruded material is not possible to see from these panorama micrographs.

The conventional ram extruded profile is shown in 4.22. No discernible grain refinement can be seen with increasing Mg content. Some grain refinement along the surface tearing in the Al-

CONVENTIONAL RAM EXTRUSION

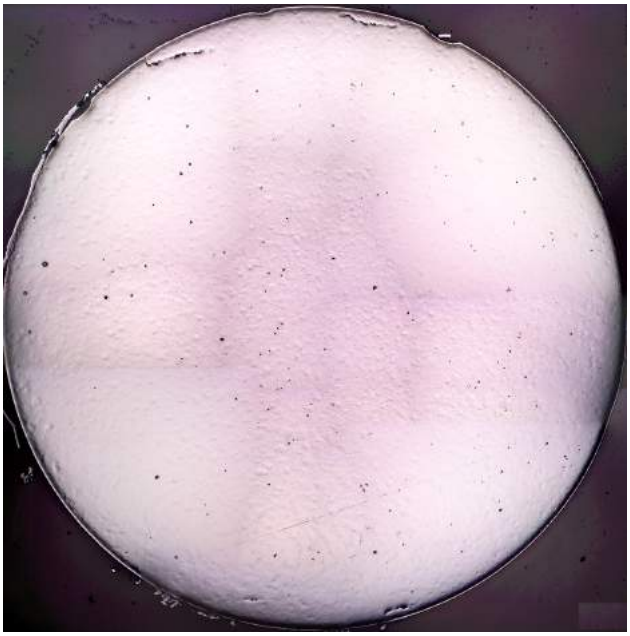

(a) Al-5%Mg.

(b) Al-8%Mg.

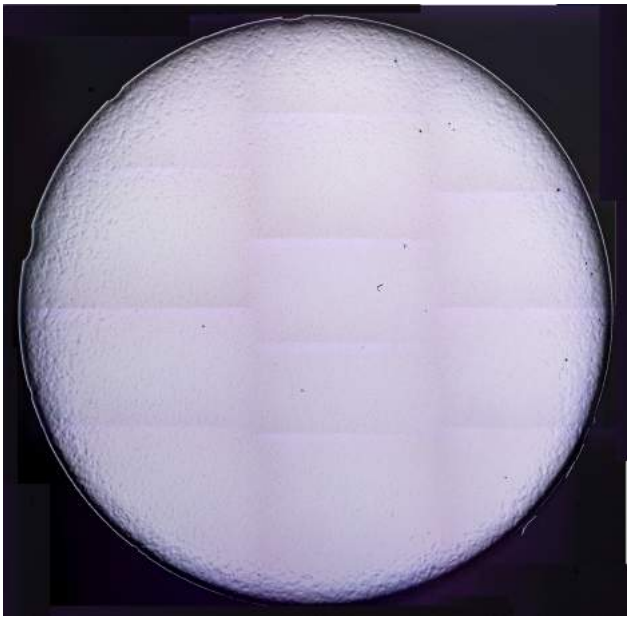

(c) Al-10%Mg.

Figure 4.15: A series of micrographs of the cross section of conventional ram extruded Al-X%Mg taken at 25X magnification merged together to form an overview image. The diameter is 1 cm. Higher density of large scale porosity can be seen in the Al-5%Mg profile, while the Al-8%Mg profile has experienced surface tearing to a high degree. The profiles have been press extruded at different parameters, so a direct comparison of the effect Mg has on the process, is not possible.

SCREW EXTRUDED MACHINED GRANULES

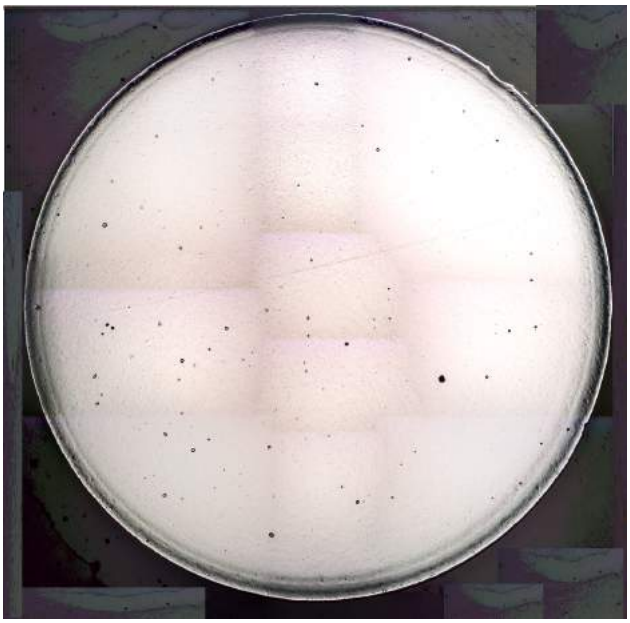

(a) Al-5%Mg.

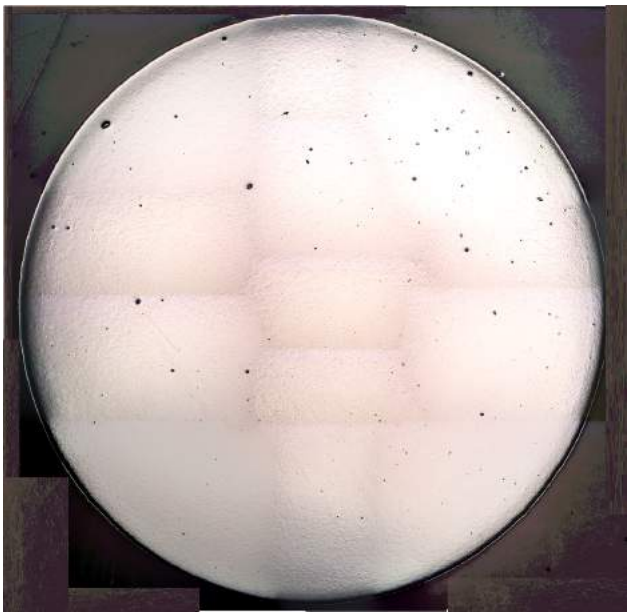

(b) Al-8%Mg.

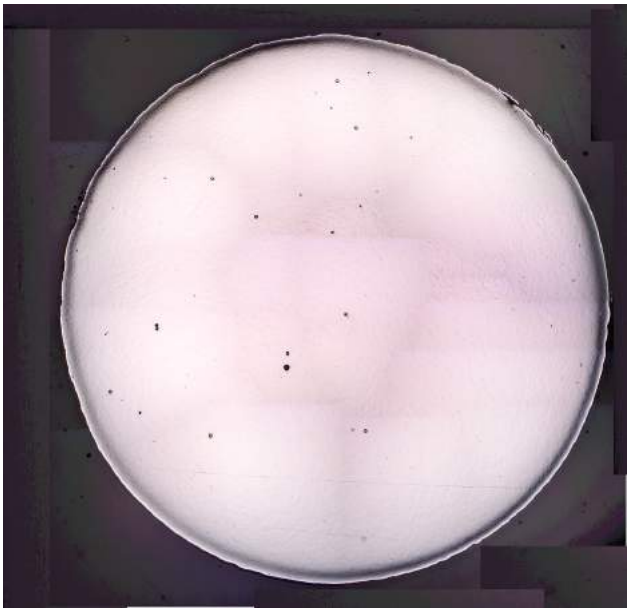

(c) Al-10%Mg.

Figure 4.16: A series of micrographs of the cross section of screw extruded Al-X%Mg machined granulates taken at 25X magnification merged together to form an overview image. The diameter is 1 cm. The Al-10%Mg has less large scale porosity.

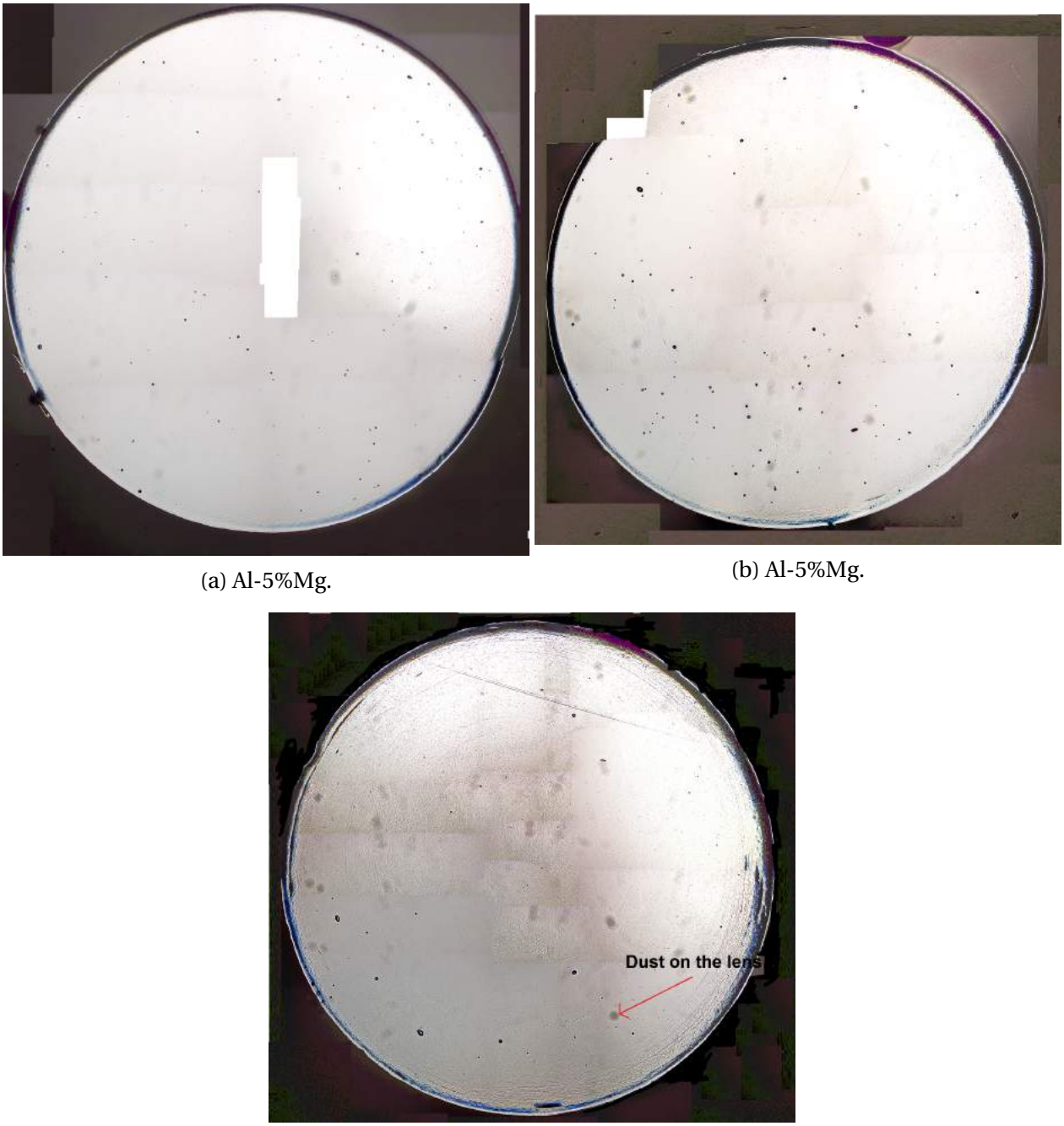

(a) Al-5%Mg.

(b) Al-5%Mg.

(c) Al-5%Mg.

Figure 4.17: A series of micrographs of the cross section of screw extruded Al-X%Mg RS ribbons taken at 25X magnification merged together to form an overview image. The diameter is 1 cm. The Al-8%Mg profile has larger pores than the other alloys, while the Al-10%Mg profiles has a lamellar structure. The dark spots indicated by an arrow in c) are spots on the lens.

8%Mg in 4.22c-4.22d can be seen. Some small rectangular porosity with the long side parallel with the extrusion direction can be seen. There might be an increase of this kind of porosity, with increasing mg content.

CONVENTIONAL RAM EXTRUDED

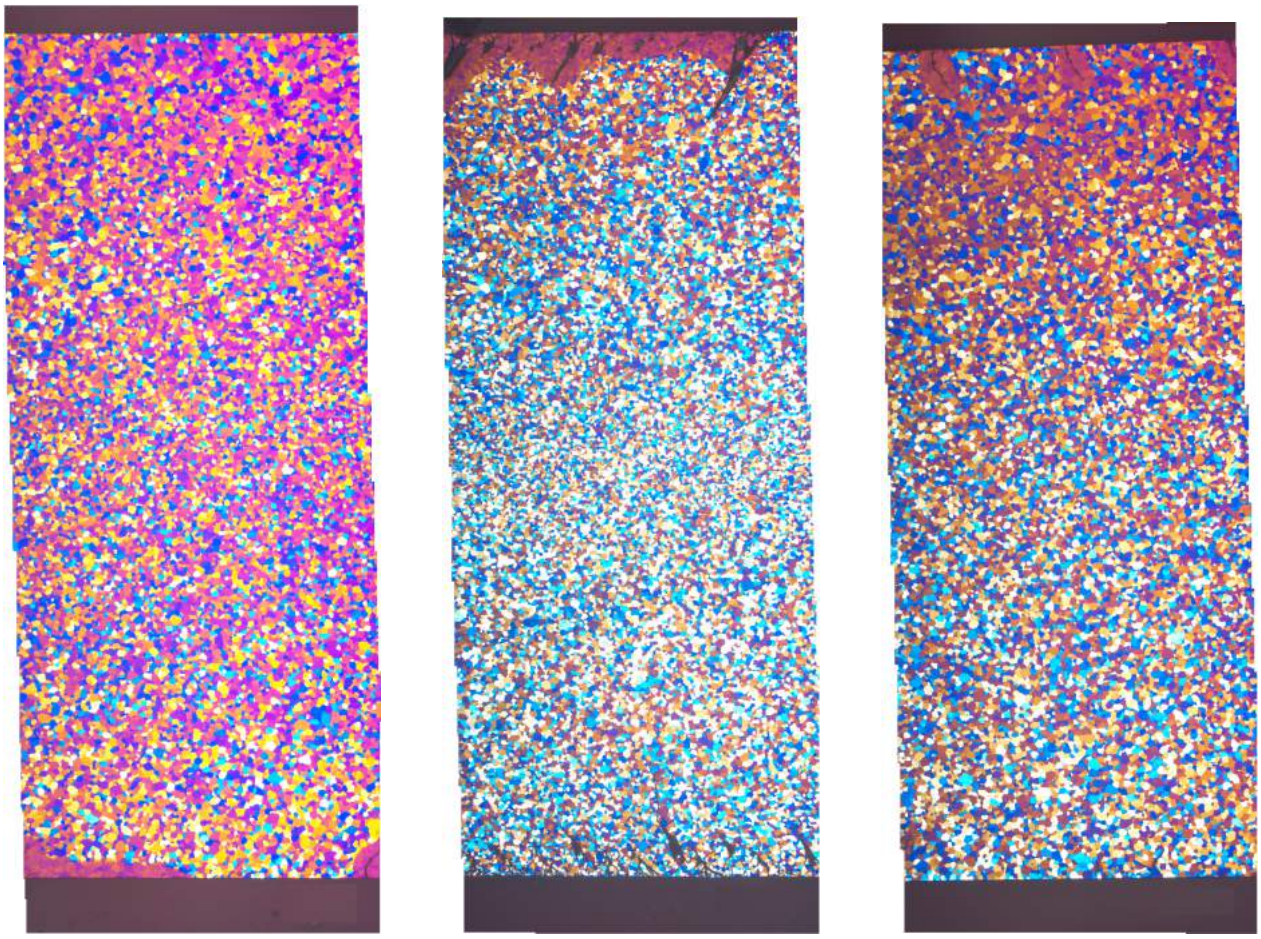

(a) Al-5%Mg. (b) Al-8%Mg. (c) Al-10%Mg.

Figure 4.18: Overview images of the conventional ram extruded profiles, each picture is taken at 25x, and put together to form an overview of the cross-section.

Figures 4.21-4.23 show micrographs of the longtitudal cross section, shown in figure 3.6, of the different extruded material. Anodized micrographs of the longtitudal cross sections of the extruded profile are seen in figures 4.22-4.26. Edge effects while anodizing happens very easily on these profiles, and a good micrograph of the edge is difficult to obtain, therefore, both edge, and middle micrographs are shown.

SCREW EXTRUDED MACHINED GRANULATES

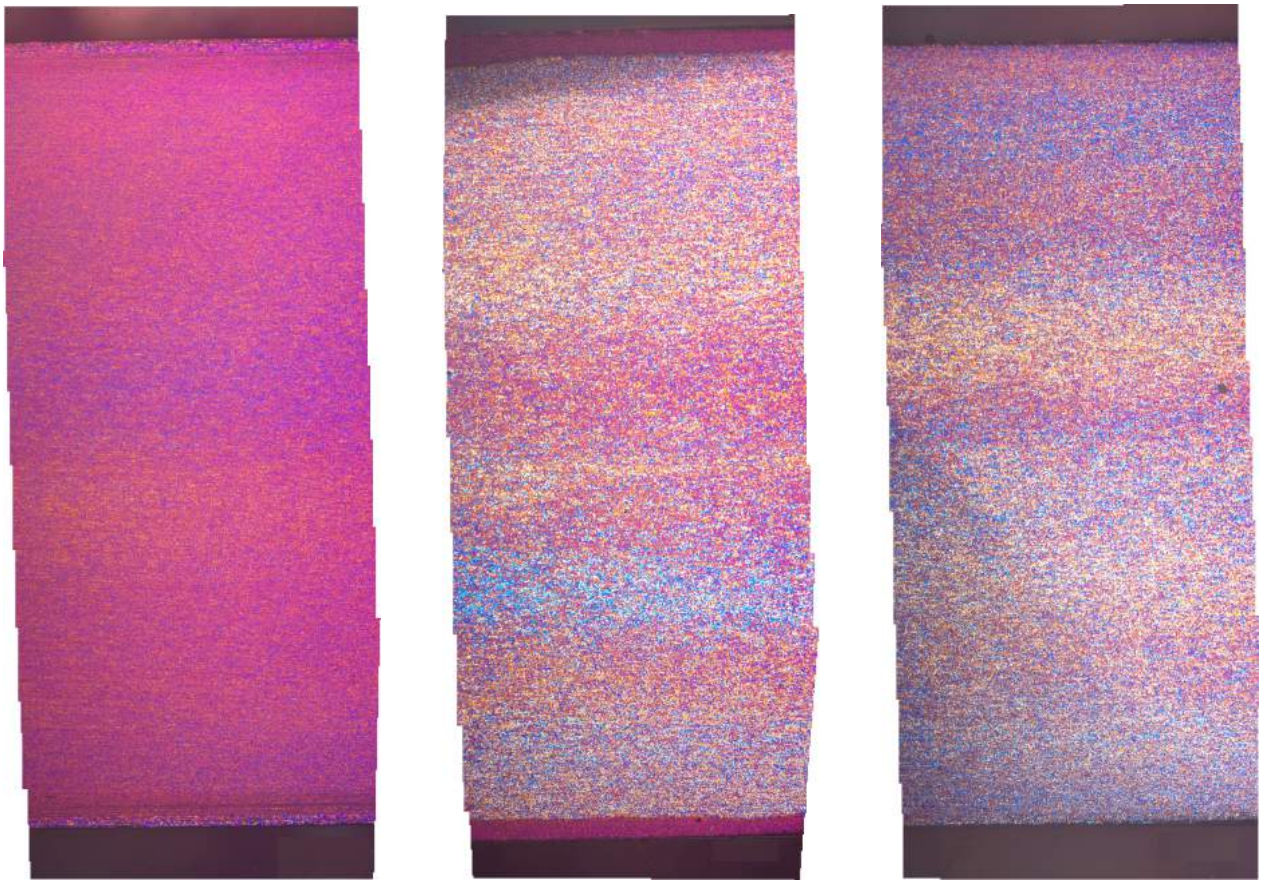

(a) Al-5%Mg. (b) Al-8%Mg. (c) Al-10%Mg.

Figure 4.19: Overview images of the screw extruded machined granulates profiles, each picture is taken at 25x, and put together to form an overview of the cross-section.

Micrographs of the conventional ram extruded profiles can be seen in figure 4.21. All the profiles exhibit large clusters of clusters/particles, often in a line, running parallel with the surface. The profiles all show signs of surface tearing, however, the Al-8%Mg profile in 4.21c and 4.21d, shows surface tearing to a large degree, even easily visible with the naked eye. The profiles were extruded at different speeds, which means one can not draw a direct conclusion to the effect of Mg on surface tearing.

The screw extruded machined granulates are shown in figure 4.23. The Al-5%Mg profile in figure 4.23a and 4.23b shows a large amount of porosity, which is absent in the Al-8%Mg and Al-10%Mg profiles. Some porosity/particle lines were seen in in these profiles as well, seen in figure 4.23e-

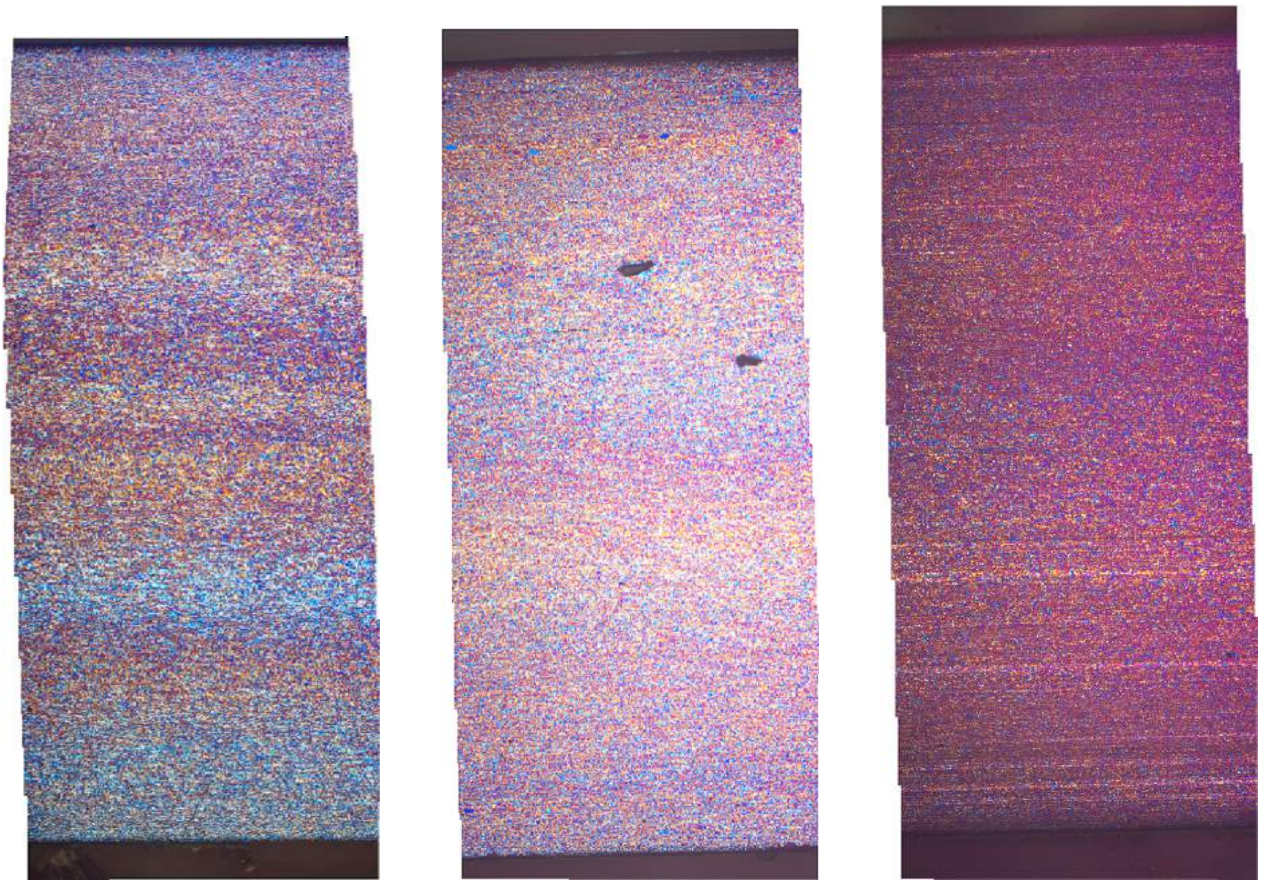

(a) Al-5%Mg. (b) Al-8%Mg. (c) Al-10%Mg.

Figure 4.20: Overview images of the screw extruded RS ribbons profiles, each picture is taken at 25x, and put together to form an overview of the cross-section.

4.23f, which is taken from the middle of the profile.

Figure 4.24 shows the screw extruded machined granulates. The Al-8%Mg profile in figure 4.24c-4.24d micrographs are taken in the middle, while the Al-5-and-10%Mg in figure 4.24a-4.24b, and 4.24e-4.24f respectively, are taken at the edge. This explains the apparent large difference in lamellarity in the extruding direction. There is however a difference between the AL-5%Mg and Al-10%Mg profiles in this regard, where the Al-5%Mg profile shows more lamellarity. One can also see a difference in grey lines in the extruding direction, which might be oxides. A large degree of grain refinement can be seen in the Al-10%Mg profile, near the edge, about 1-10 micron thick. Some grain refinement near the edge in the Al-5%Mg profile can also be seen, but not to

CONVENTIONAL RAM EXTRUDED

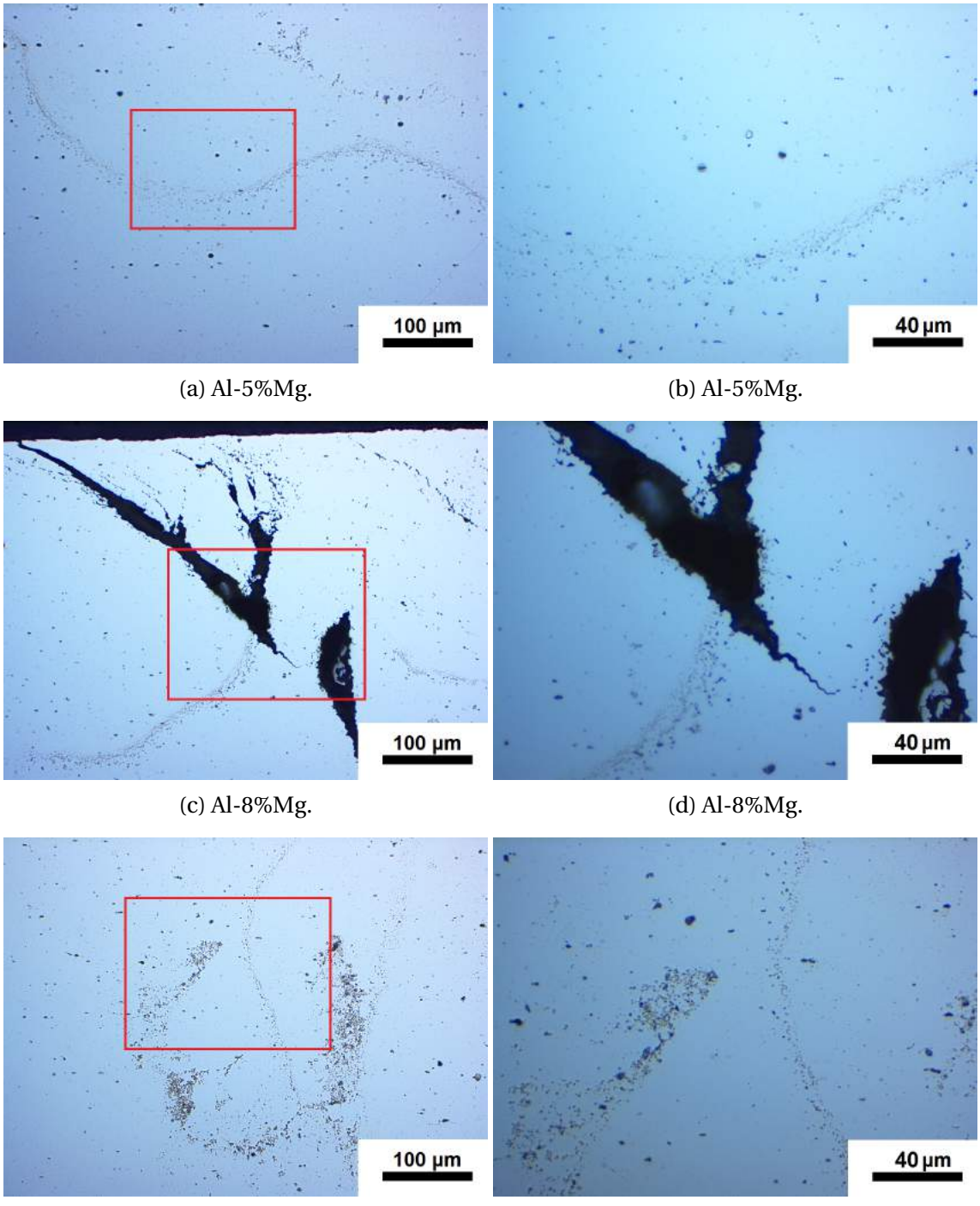

(a) Al-5%Mg. (b) Al-5%Mg.

(c) Al-8%Mg. (d) Al-8%Mg.

(e) Al-10%Mg. (f) Al-10%Mg.

Figure 4.21: Micrographs of the longtitudal cross section of conventional ram extruded Al-XMg profiles. The particle/porosity lines are seen in all the profiles, following the longtitudal direction. All the profiles had some degree of surface tearing, however, as seen in c) and d), the Al-8%Mg had experienced surface tearing to a severe degree.

CONVENTIONAL RAM EXTRUDED

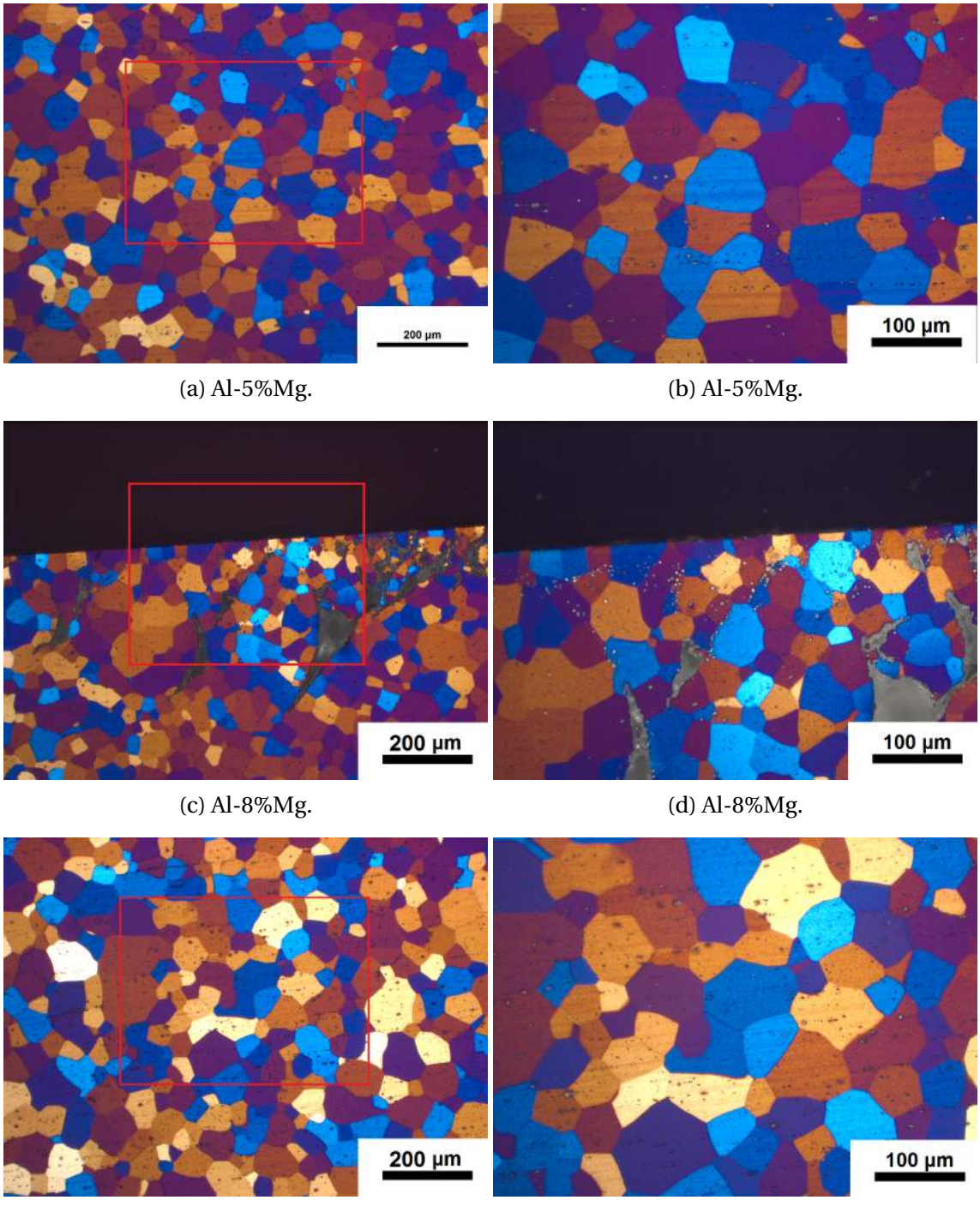

(a) Al-5%Mg. (b) Al-5%Mg.

(c) Al-8%Mg. (d) Al-8%Mg.

(e) Al-10%Mg. (f) Al-10%Mg.

Figure 4.22: Micrographs of conventional ram extruded Al-XMg profiles. No grain refinement with increasing Mg content can be seen. Some small porosity, and rectangular porosity with the long side in the extrusion direction is present. Some grain refinement near the edge, and along the surface tearing is also present.

the same degree.

Figure 4.25 shows the screw extruded RS ribbons. The porosity/particle lines seen in the conventional ram extruded profiles were also found in screw extruded RS ribbons, seen most clearly in figure 4.25a. Some cracks were also found, in the middle of the Al-8%Mg profile in figure 4.25c-4.25d, and along the edge of the Al-10%Mg in figure 4.25e-4.25f.

The screw extruded RS ribbons profile is shown in figure 4.26. All profiles show areas with increased grain size. The Al-8%Mg in figure 4.26c-4.26d profile has a straight line of grains with increases size going in the extruding direction.

SCREW EXTRUDED MACHINED GRANULATES

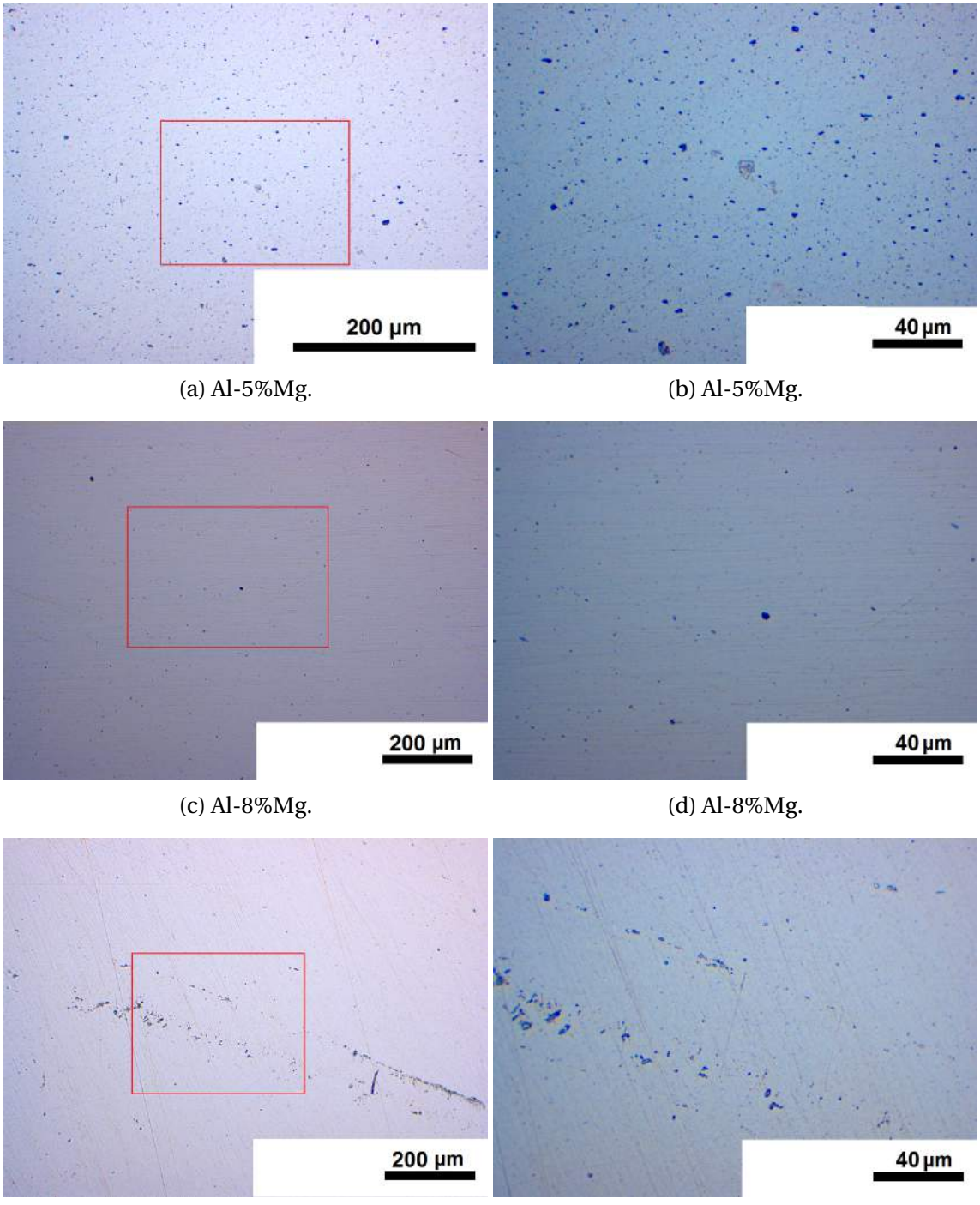

(a) Al-5%Mg. (b) Al-5%Mg.

(c) Al-8%Mg. (d) Al-8%Mg.

(e) Al-10%Mg. (f) Al-10%Mg.

Figure 4.23: Micrographs of the longtitudal cross section of screw extruded machined Al-XMg granulates. A large amount of porosity is seen in the Al-5%Mg profile in a) and b). Al-8%Mg in c) and d) is largely free of large scale porosity, but small pores can be seen. A line of porosity is seen in the middle of the Al-10%Mg profile, in e) and f).

SCREW EXTRUDED MACHINED GRANULATES

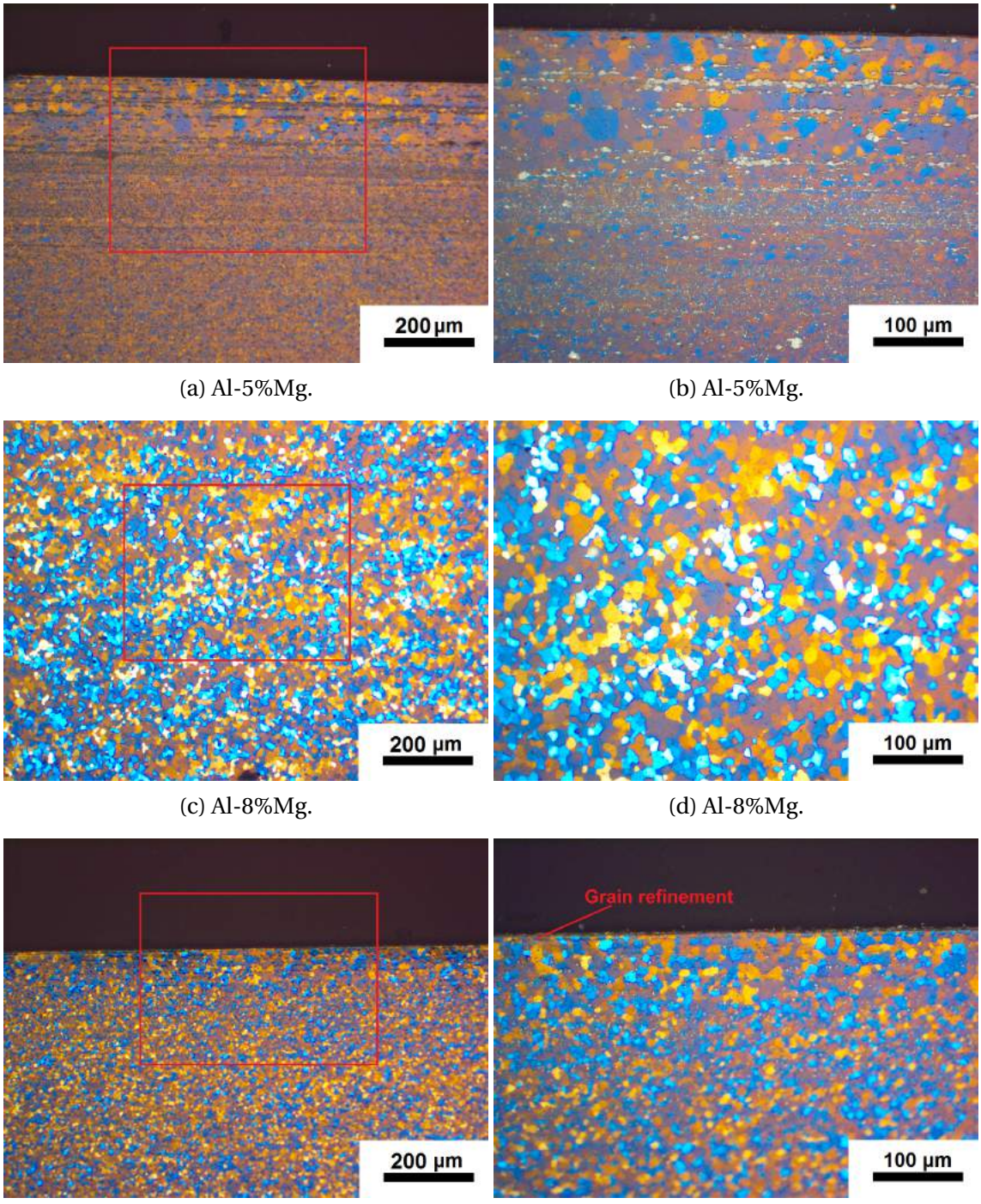

(a) Al-5%Mg. (b) Al-5%Mg.

(c) Al-8%Mg. (d) Al-8%Mg.

(e) Al-10%Mg. (f) Al-10%Mg.

Figure 4.24: Micrographs of screw extruded machined granulates. Some grain refinement at the edge can be seen, most pronounced in the Al-10%Mg profiles in e)-f). The difference in lamellarity in the Al-8%Mg profile in c)-d) compared to the Al-5-and-10%Mg profiles in a)-b), and e)-f), is mainly due to the picture being taken in the middle. However, there is a difference in lamellarity between the Al-5%Mg and Al-10%Mg profiles, with the former displaying more. This might be due to the grey lines, which might be oxides.

SCREW EXTRUDED RS RIBBONS

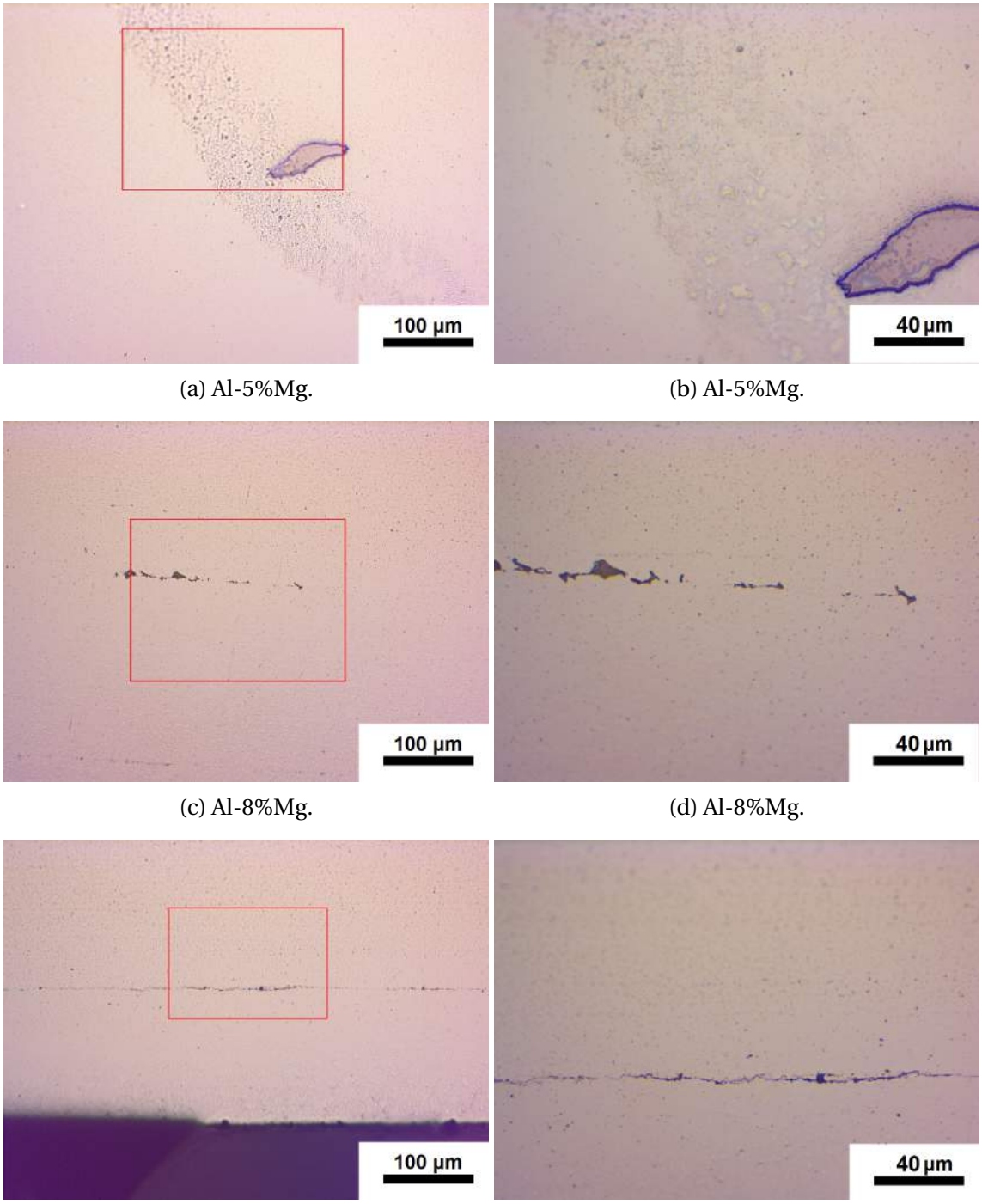

(a) Al-5%Mg. (b) Al-5%Mg.

(c) Al-8%Mg. (d) Al-8%Mg.

(e) Al-10%Mg. (f) Al-10%Mg.

Figure 4.25: Micrographs of the longtitudal cross section of screw extruded Al-XMg RS ribbons. Some particle/porosity lines were found in all the profiles, following the longtitudal direction, though not to the same degree as the conventional ram extruded profiles. Some cracks can be seen in the middle of Al-8%Mg profile in c) and d), and along the edge in the Al-10%Mg profile in e) and f).

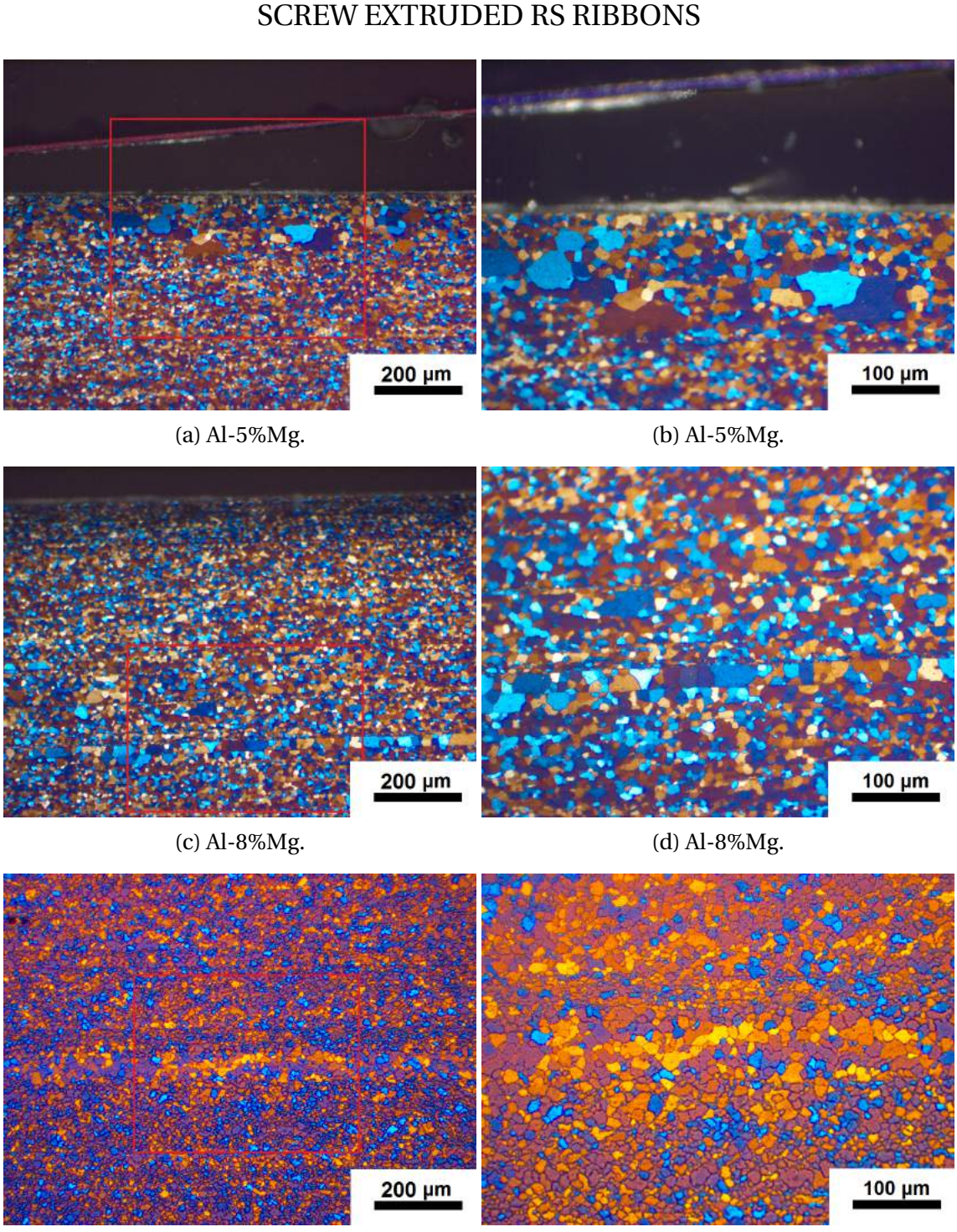

(a) Al-5%Mg. (b) Al-5%Mg.

(c) Al-8%Mg. (d) Al-8%Mg.

(e) Al-10%Mg. (f) Al-10%Mg.

Figure 4.26: Micrographs of screw extruded RS ribbons. Lines or areas of increased grain size are seen in all profiles. The Al-8%Mg profile in c)-d) has a very straight line of grains with increases size.

4.2 Grain size

Measured grain size of the investigated material is presented in this section. Note that the images of screw extruded machined granulates profiles were very difficult to measure grain size for, see the anodized images in figure 4.24, especially the Al-5%Mg profile. Keep this in mind when viewing the results.

The grain sizes of the investigated material can be seen in table 4.1. A general decrease in grain size with increasing Mg content can be seen. The lowest grain size is seen in the screw extruded Al-5%Mg RS ribbons, while the largest is seen in conventional ram extruded Al-5%Mg.

Table 4.1: Grain sizes for investigated material.

Material	Grain size [µm]		
	Al-5%Mg	Al-8%Mg	Al-10%Mg
As cast	80	70	52
RS ribbons	20	16	15
H 430 °C	64	46	55
H 430 °C, 1 week	67	81	43
H 490 °C	67	61	47
Conventional extruded	88	48	51
Screw extruded machined granulates	10	13	10
Screw extruded RS ribbons	11	10	12

4.3 Microprobe

This section presents microprobe line scans across the longtitudal section of the RS ribbons, to determine what phases are present. 2 scans were taken of each alloy. The beta phase contains 37wt% Mg, and this phase can not be seen in any of the linescans, figures 4.27-4.27.

Microprobe linescans of Al-5%Mg are shown in figure 4.27. The lines of Al and Mg are fairly smooth, no large drops or peaks are seen. Oxygen is slightly raised in figure 4.27a. Both oxygen

and silicon are above zero in the line scan in figure 4.27b.

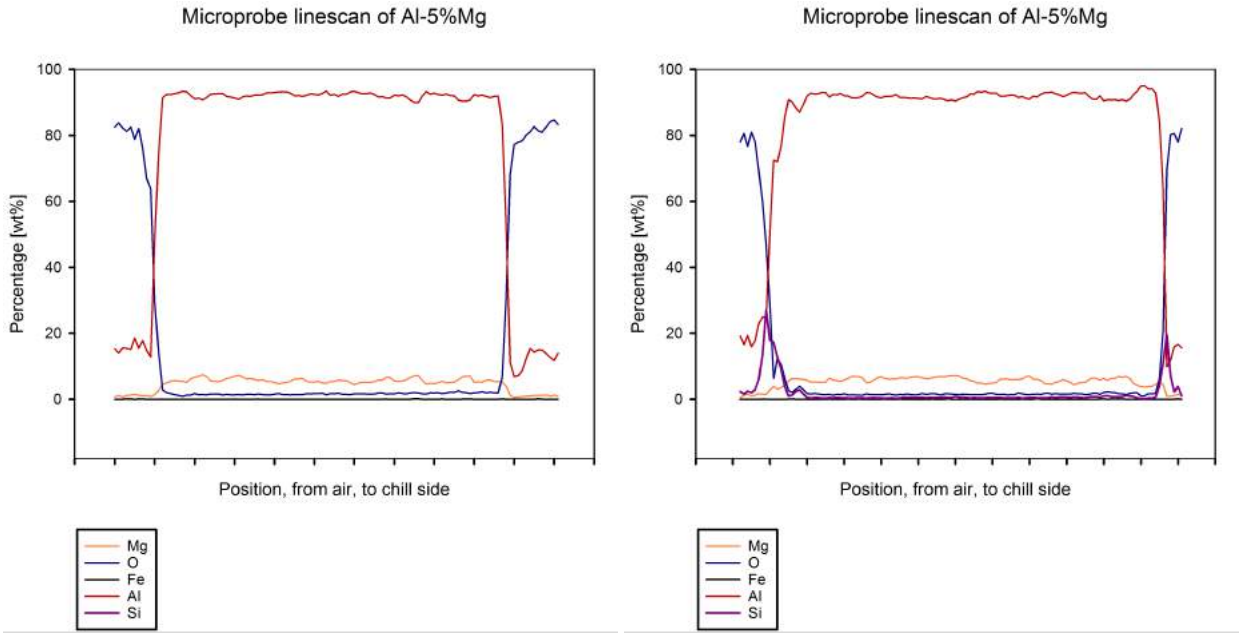

(a) (b)

Figure 4.27: Micro probe linescans of Al-5%Mg RS ribbons. End points were set outside the edge, which gives a drop off at the ends of the scans.

Microprobe linescans of AL-8%Mg ribbons are seen in 4.28. The lines of Mg and Al are slightly jagged, and the linescan in 4.28a has a peak of oxygen and silicon, but no peaks or drops in magnesium and aluminium are seen. Both oxygen and silicon are above zero.

Microprobe linescans of Al-10%Mg RS ribbons are shown in figure 4.29. The lines are markedly jagged, however, no peaks in the Mg line goes above 20wt%. The lines of oxygen and silicon are seen above zero, and the oxygen has several small peaks of about 1wt%.

Comparing all the linescans, a clear increase in jaggedness of the Al and Mg lines are seen from Al-5%Mg, to Al-8%Mg, to Al-10%Mg. All the linescans have some oxygen and silicon, as they are seen

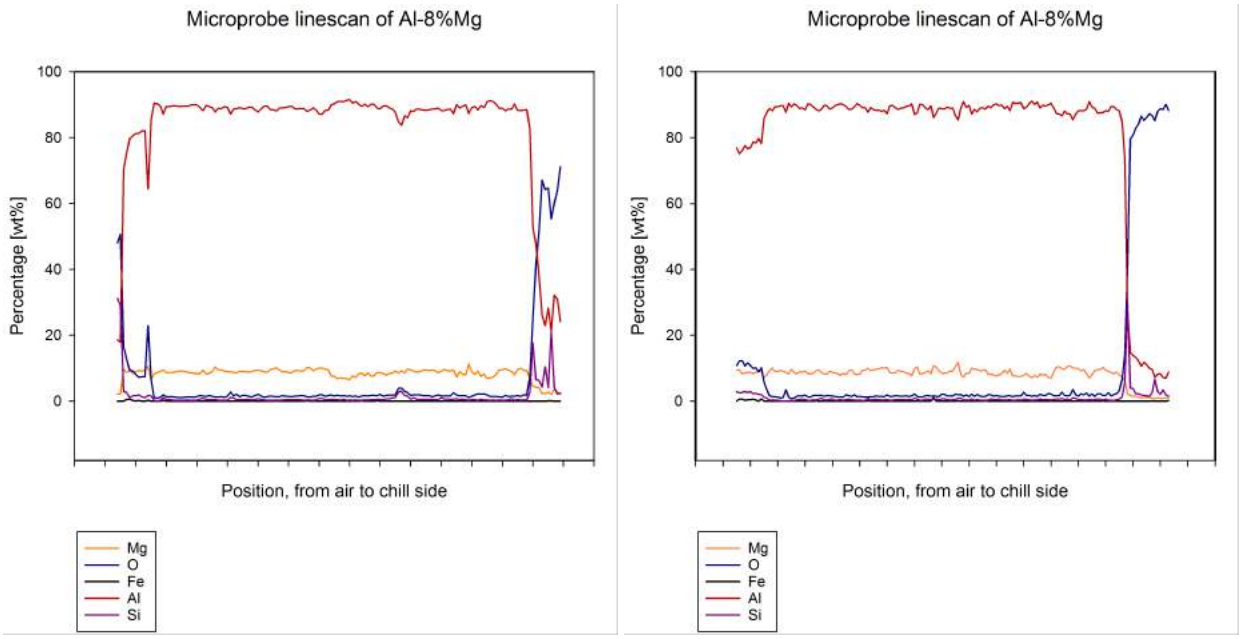

(a) (b)

Figure 4.28: Micro probe linescans of Al-8%Mg RS ribbons. End points were set outside the edge, which gives a drop off at the ends of the scans.

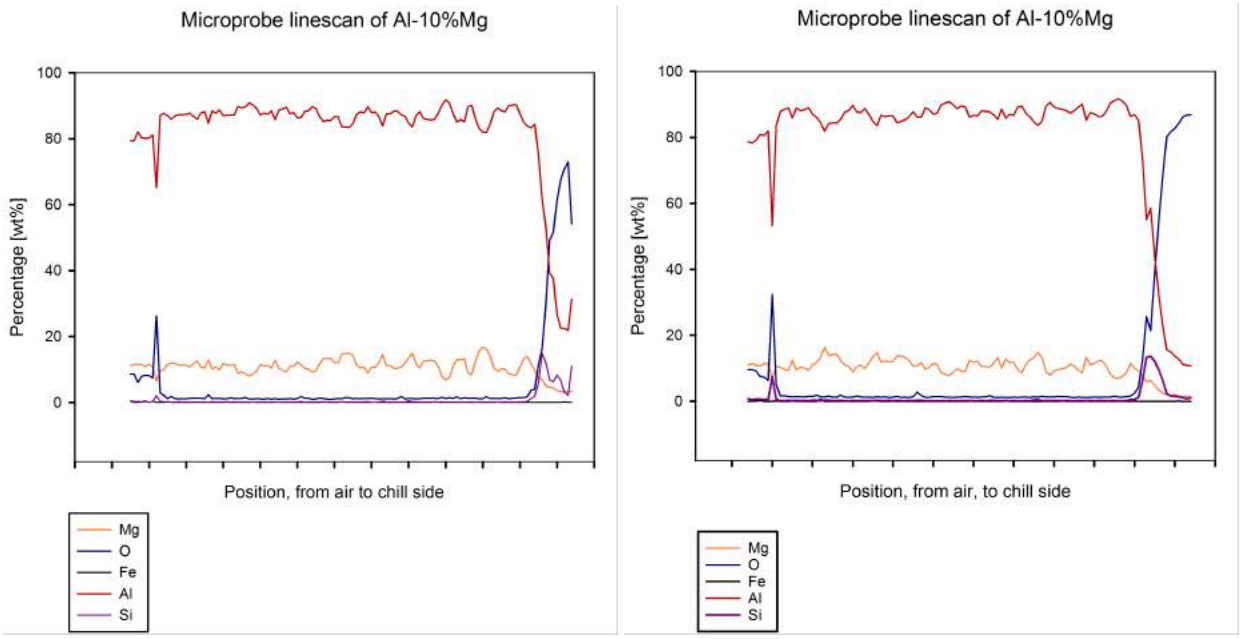

(a) (b)

Figure 4.29: Micro probe linescans of Al-10%Mg RS ribbons. End points were set outside the edge, which gives a drop off at the ends of the scans.

4.4 Energy-dispersive X-ray spectroscopy

This section presents various Energy-dispersive X-ray spectroscopy (EDS) point, and linescans, in addition to mappings, to determine the composition of the investigated DC cast and homogenized DC cast samples.

The EDS mapping in figure 4.30, shows an Mg rich particle. Doing a linescan over this particle, seen in figure 4.31, one can see that this particle has a approximately 35 wt% Mg. It is assumed this is a beta particle.

In figure 4.32, the only beta particle in the least likely specimen is presented. No beta particles further into the homogenization schedule was found with EDS. EDS of samples homogenized to 490°C was performed, but no beta particles were found.

Linescans of the samples homogenized at 430°C and to 490°C are shown in figures 4.33-4.38. The purpose of these scans were to determine if there was any difference in Mg content at the edge, but they also serve the purpose of gaining an overview of particle content. Representative linescans have been chosen. 3 linescans were taken at the edge and 3 linescans in the middle. The linescans at the edge were chosen as representative scans. No beta particles can be seen in these linescans, however, various other particles can be seen. Figure 4.35 shows an Mg, Si, and O rich particle in an Al-10%Mg sample homogenized at 430°C. The Al-5%Mg sample homogenized to 490°C in figure 4.36 shows an iron rich particle. The Al-10%Mg sample homogenized to 490°C in figure 4.38 shows a very Si and O rich particle.

AS CAST AL-5%Mg

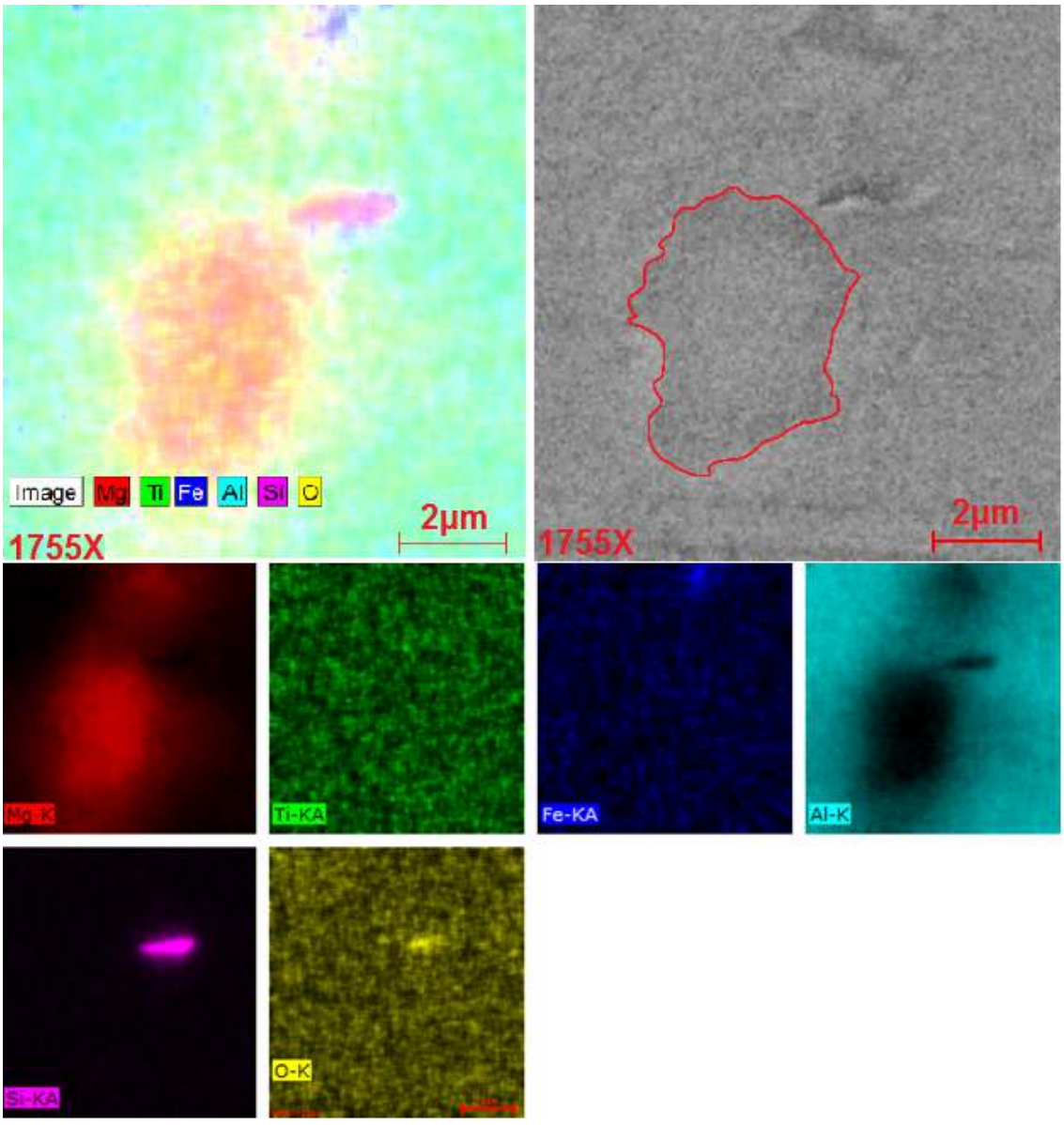

Figure 4.30

AS CAST AL-5%Mg

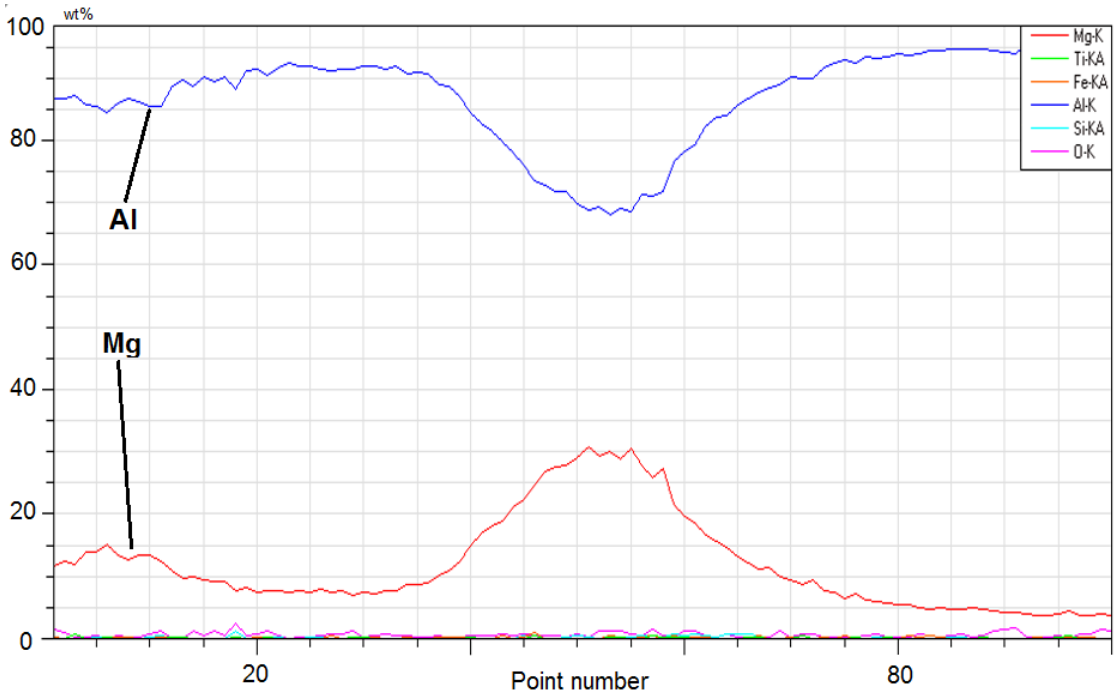

Figure 4.31

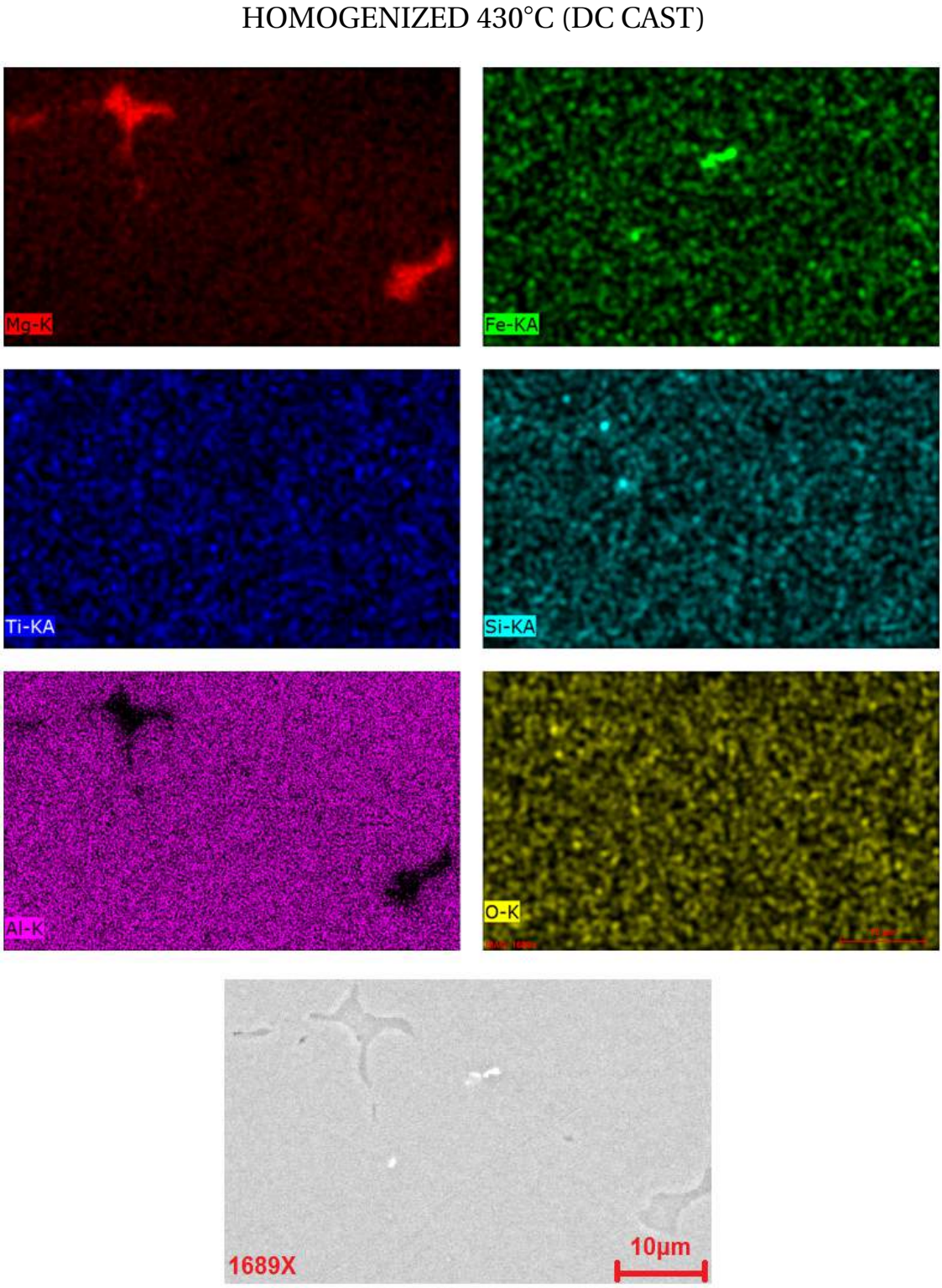

Figure 4.32: Mapping of sample homogenized at 430°C for 4 hours.

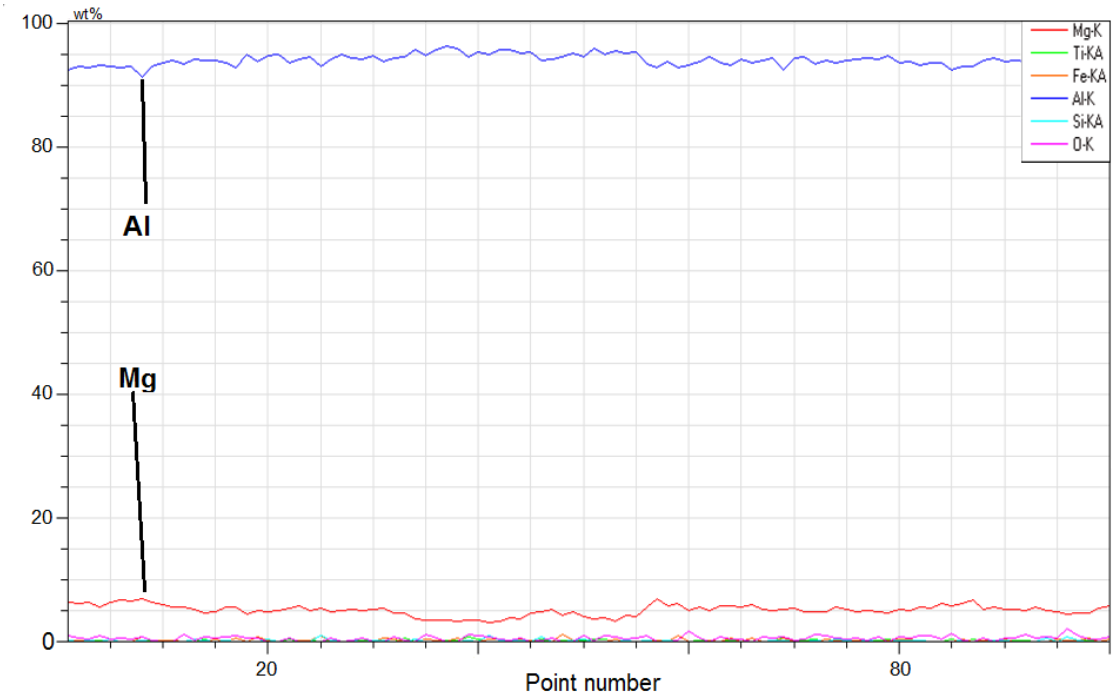

Figure 4.33: EDS line scan taken of heat treated Al-5%Mg at the edge, heat schedule following schedule 1.

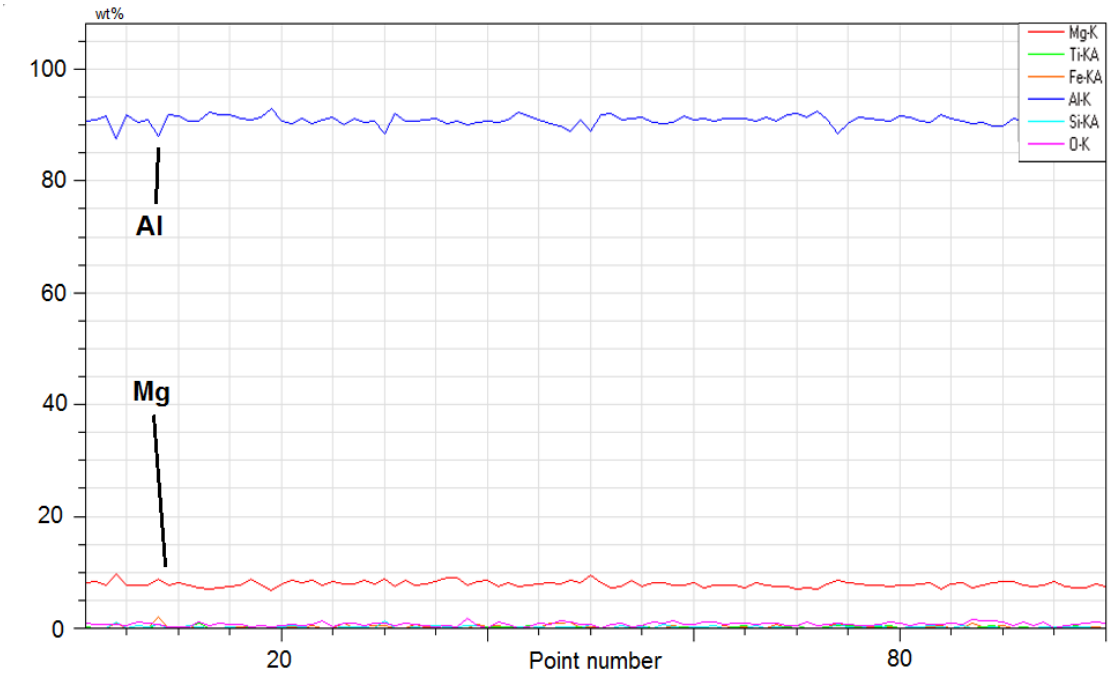

Figure 4.34: EDS line scan taken of heat treated Al-8%Mg at the edge, following heat schedule schedule 1.

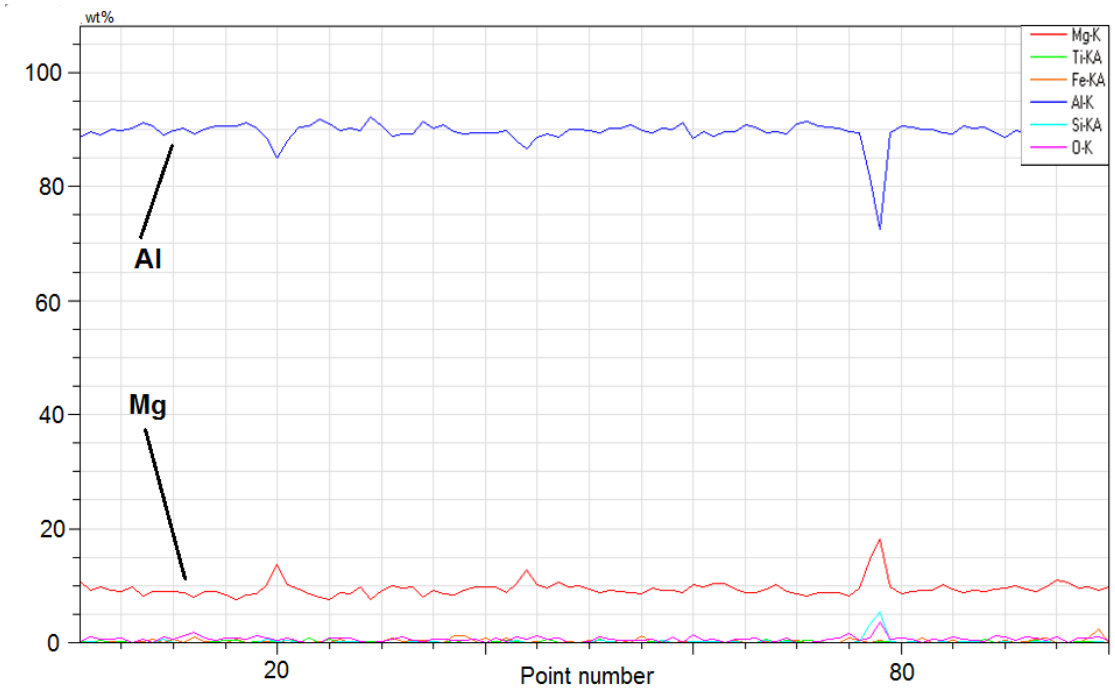

Figure 4.35: EDS line scan taken of heat treated Al-10%Mg at the edge, following heat schedule schedule 1.

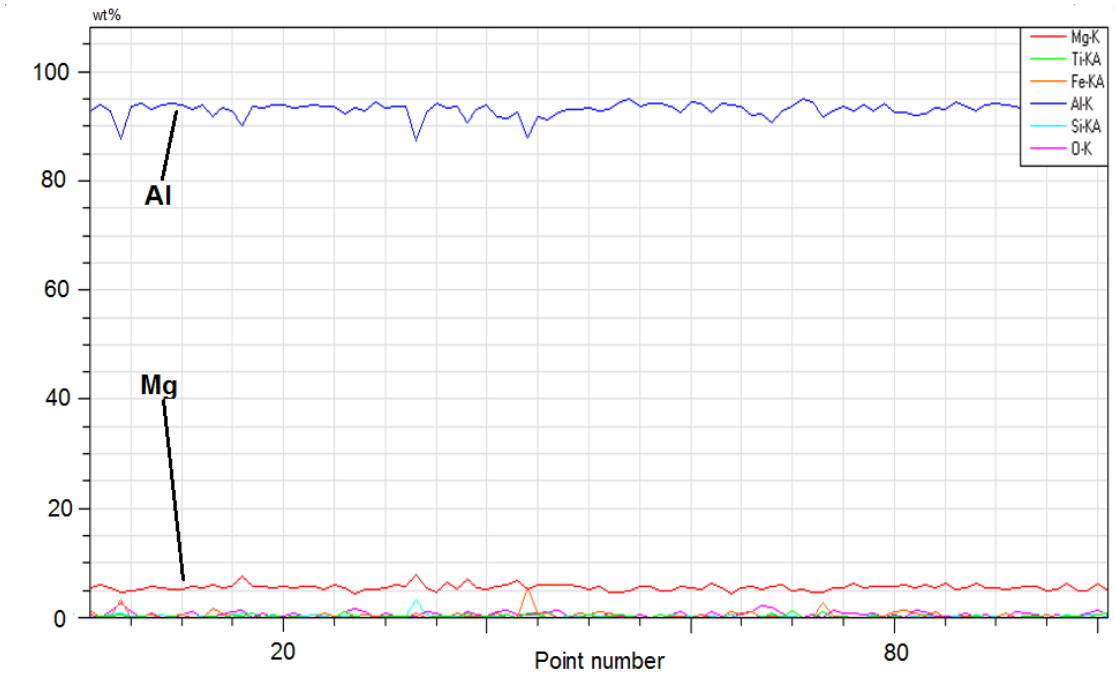

Figure 4.36: EDS line scan taken of heat treated Al-5%Mg at the edge, following heat schedule schedule 2.

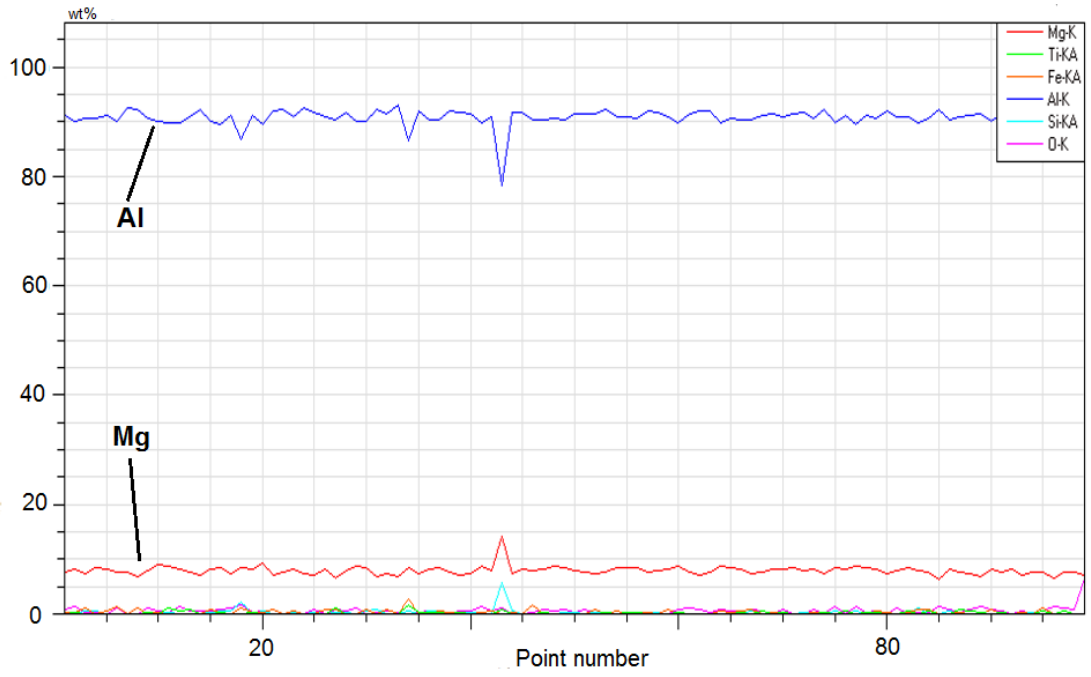

Figure 4.37: EDS line scan taken of heat treated Al-8%Mg at the edge, following heat schedule schedule 2.

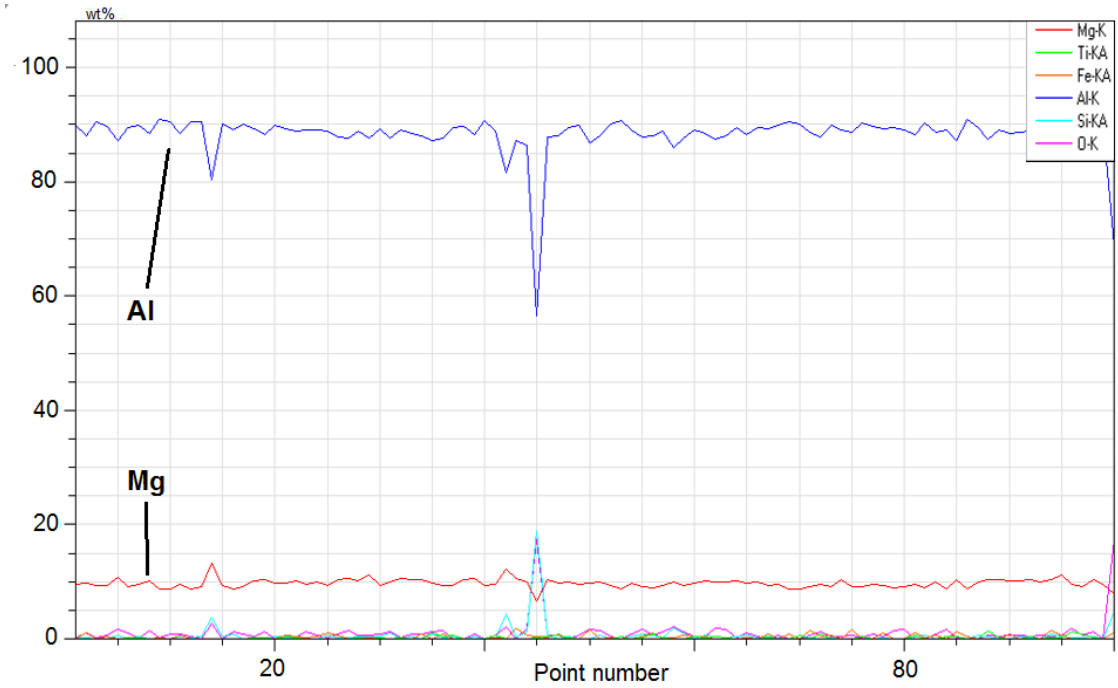

Figure 4.38: EDS line scan taken of heat treated Al-10%Mg at the edge, following heat schedule schedule 2.

4.5 Micro hardness

This sections presents hardness measurements, measured in vickers hardness. Hardness might depend on grain size, if the load is small enough, and the grain size large enough, the indentation might only cover 1 grain. From 2.8, there is inaccuracy when going below 200gf. Hardness measurements performed internally at the department by Kristian Grøtta Skorpen, at 500gf, showed a different trend regarding the hardness of conventional ram extruded profiles, where the hardness went up with increasing Mg content. This contradicts the results in this section, where the hardness of the conventional ram extruded profiles goes up from Al-5%Mg to Al-8%Mg, but then down again for Al-10%Mg. This means that there might be an interaction at lower loads that are unknown. Keep this in mind when viewing the results.

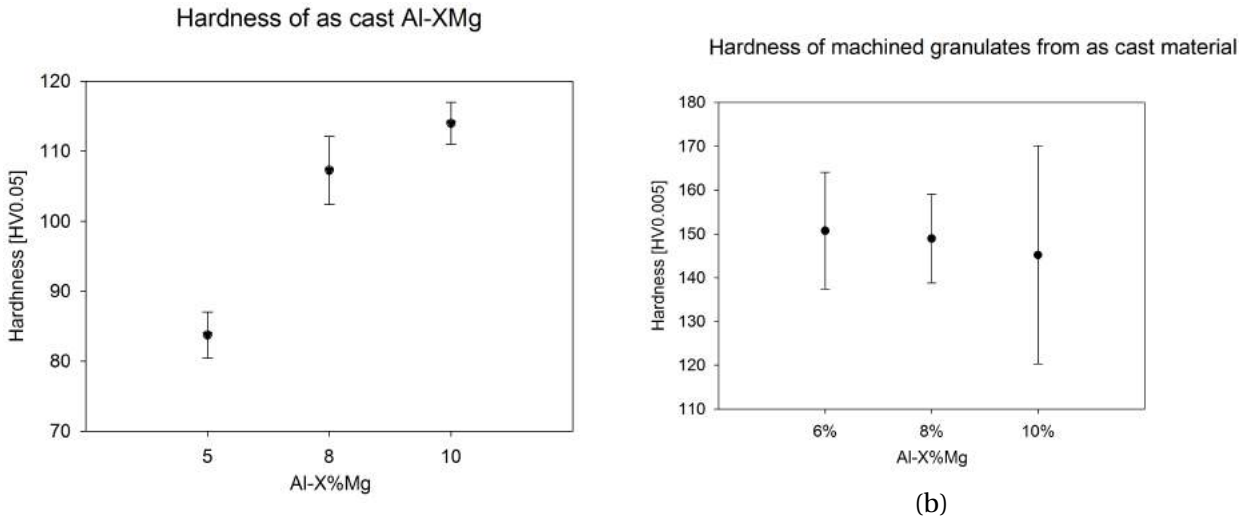

Figure 4.39: Microhardness of a) as cast and b) machined material (Berulfsen, 2015). The as cast material has a clear increase in hardness with increasing Mg content. The opposite is true for the machined granulates.

Figure 4.39 shows hardness of the 4.39a as cast material , and the 4.39b as cast machined granules. An increase in hardness for the as cast material with increasing Mg content can be seen, while the opposite is true for the machined granulates.

Hardness measurements of the RS ribbons, is shown in figure 4.40. Al-5%Mg in figure 4.40a shows no discernible difference between chill side and air side. Al-8%Mg in figure 4.40b shows

a decrease in hardness from air side to chill side. Al-10%Mg in figure 4.40c shows an increase in hardness from air side, to chill side. A high specific standard deviation is seen, due to low load and thin ribbons.

Figure 4.41 shows the hardness of the conventional ram extruded profiles, taken from center to edge. Both Al-5%Mg and Al-10%Mg show similar hardness, and no discernible difference between center and edge. Al-8%Mg shows a much higher hardness than both Al-5%Mg and Al-10%Mg, while also showing an increase in hardness from center to edge. As mentioned in the introduction to this chapter, hardness measurements performed internally at the department, showed an increase with Mg content, which is in disagreement with what is shown here.

Hardness measurements of the screw extruded machined granulates, taken from center to edge in the longtitudal direction, are shown in figure 4.42. Al-5%Mg and Al-10%Mg, in figure 4.42a and 4.42c, show a decrease in hardness from center to edge, while Al-8%Mg in 4.42b shows the opposite. An increase in hardness with increasing mg content can be seen.

In figure 4.43, hardness measurements from the center of the longtitudal direction, to the edge, of screw extruded RS ribbons are shown. Al-5%Mg in figure 4.43a, shows a slight increase in hardness from the center, to the edge. Al-8%Mg and Al-10%Mg in figure 4.43b-4.43c, shows a marked decrease in hardness from center to edge.

Hardness of the homogenized DC cast material is shown in figure 4.44. All of the alloys show a decrease in hardness when approaching the edge, and increasing hardness with Mg content.

RS RIBBONS

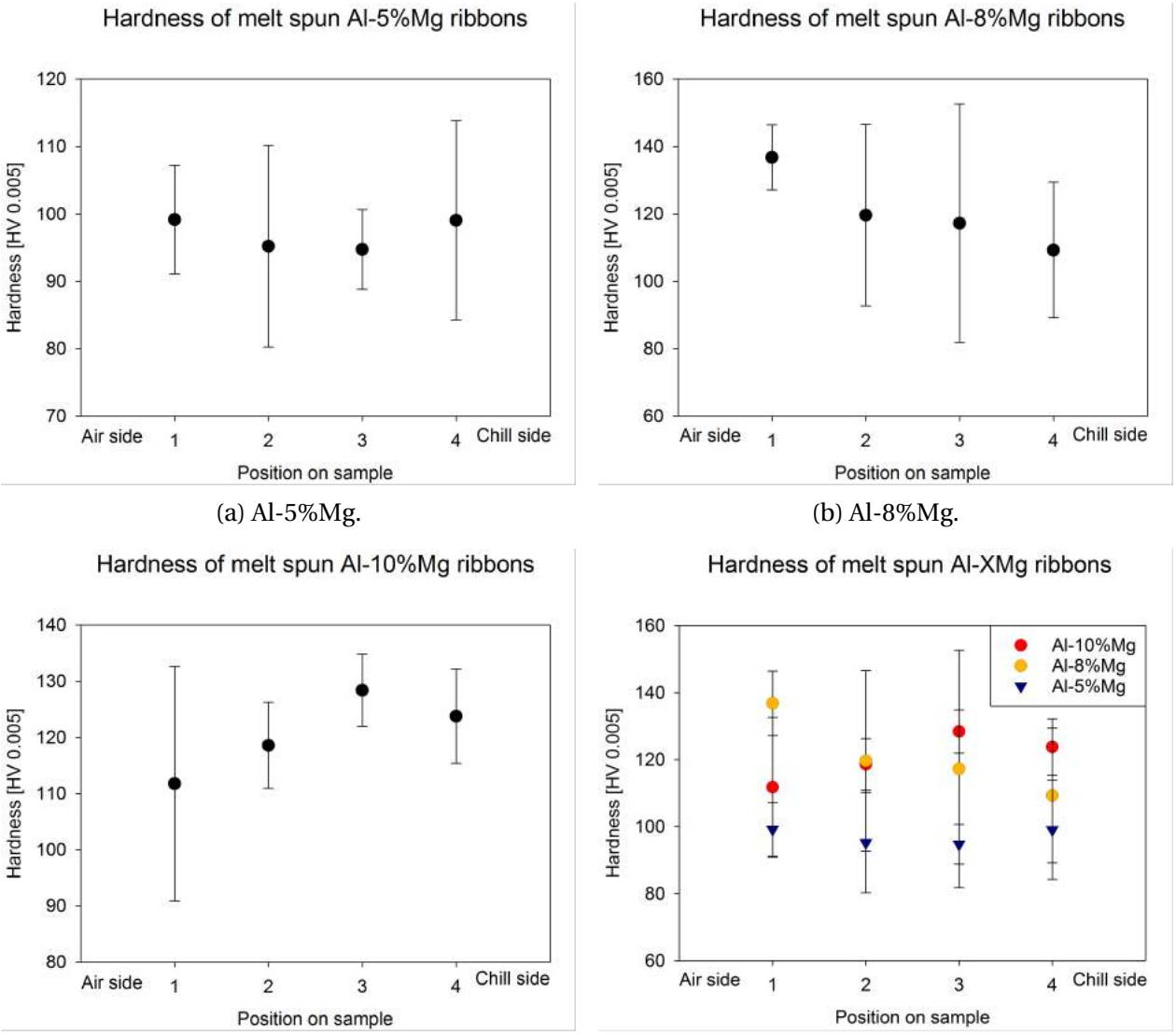

(a) Al-5%Mg.

(b) Al-8%Mg.

(c) Al-10%Mg.

(d) All alloys.

Figure 4.40: Microhardness of as melt spun ribbons. Position 1 is air side, and position 4 is wheel side. a) Al-5%Mg shows no difference between air and chill side, b) Al-8%Mg shows a decrease in hardness from air to chill side, and c) Al-10%Mg shows an increase in hardness from air to chill side (Berulfsen, 2015).

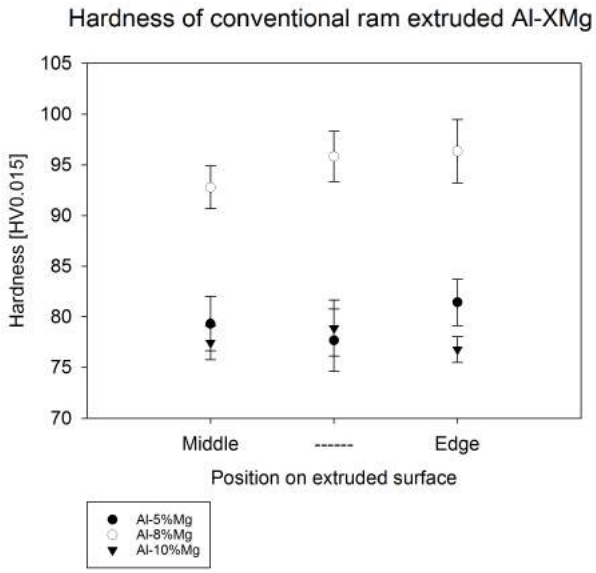

Figure 4.41: Microhardness of conventional ram extruded profiles, taken from the center of the longditudal direction, to the edge.

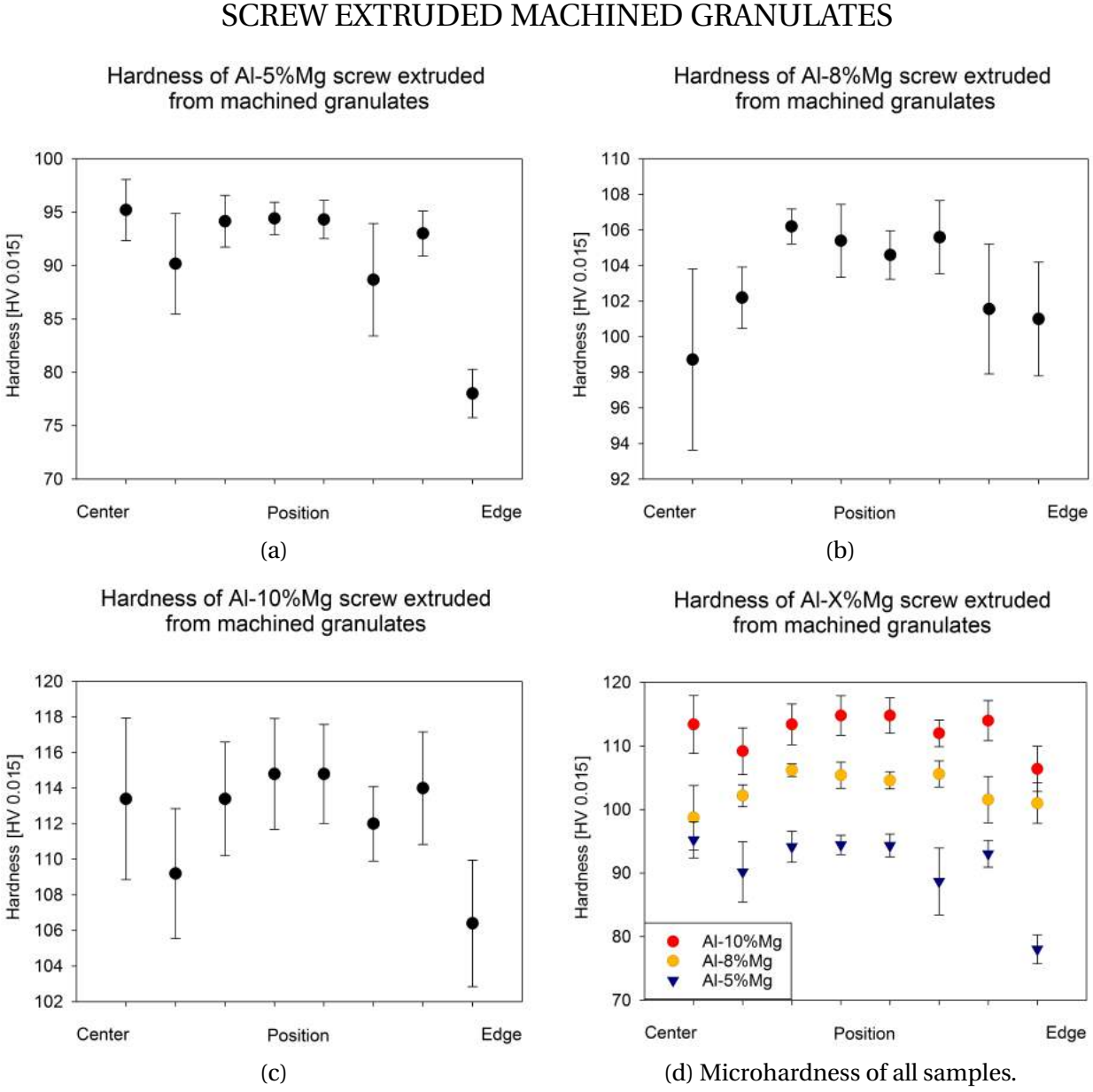

Figure 4.42: Microhardness of screw extruded machined granulated material, taken from the center of the longditudal direction, to the edge.

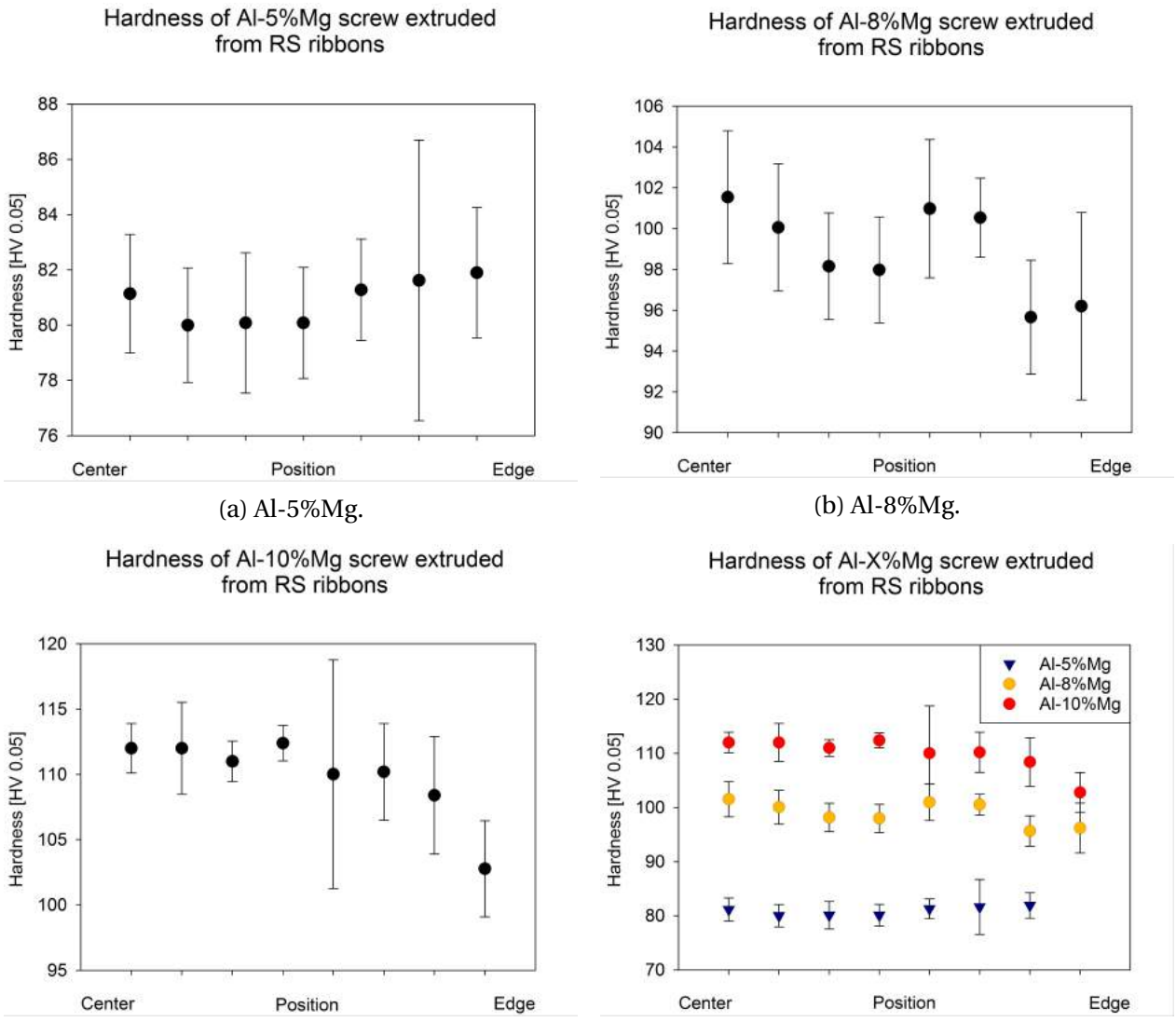

(a) Al-5%Mg.

(b) Al-8%Mg.

(c) Al-10%Mg.

(d) Average microhardness of all samples.

Figure 4.43: Microhardness of screw extruded melt spun material, taken from the center of the longditudal direction, to the edge (Berulfsen, 2015).

HOMOGENIZED DC CAST MATERIAL

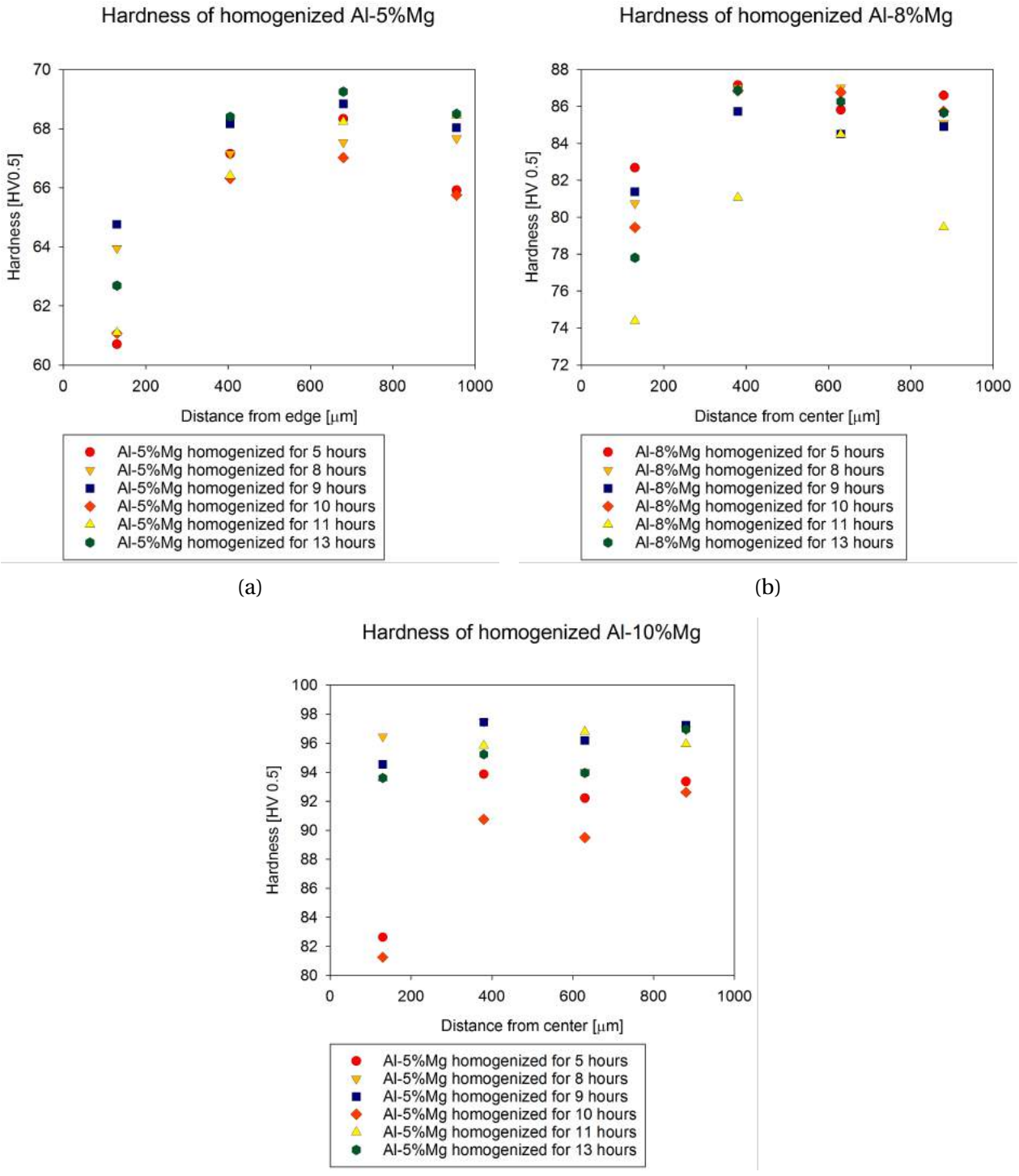

Figure 4.44: Microhardness of the homogenized DC cast Al-XMg material. See figure 3.12 to see what temperature the hours correspond to.

4.6 Tensile testing

This section presents representative room temperature stress-strain curves for the tensile tests performed on the investigated extruded materials. Complete data for tensile curves is shown in appendix A.

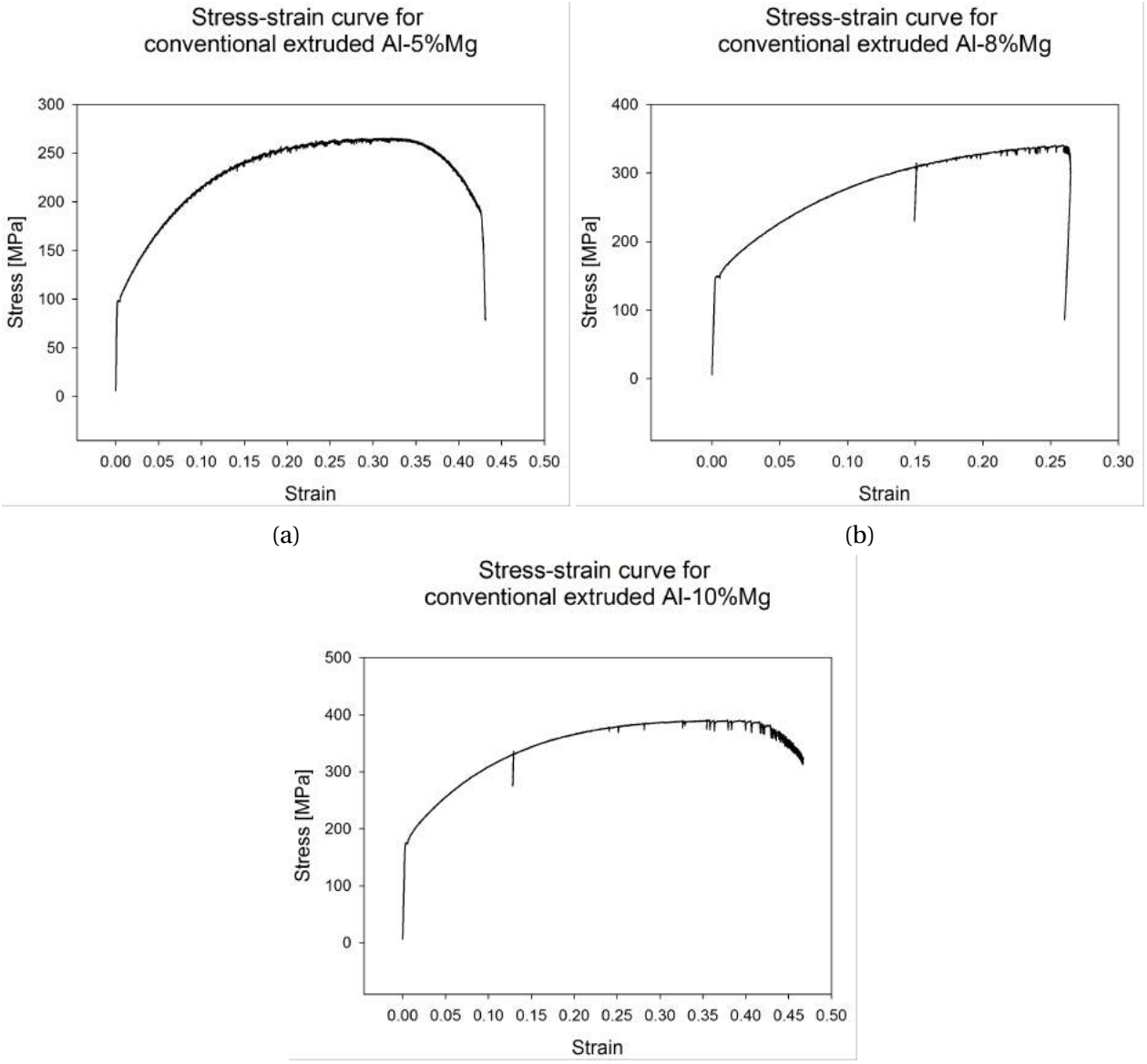

Figure 4.45: Representative stress-strain curves for conventional ram extruded Al-XMg.

The stress-strain curves for the conventional ram extruded profiles are shown in figure 4.45. The UTS increases with increasing Mg content, but more from Al-5%Mg in figure 4.45a to Al-8%Mg

in figure 4.45b, than from Al-8%Mg to Al-10%Mg in figure 4.45c. The strain at fracture for Al-8%Mg, at 0.25, is markedly lower than for the Al-5%Mg and Al-10%Mg profiles, at 0.43 and 0.47 respectively. The amount of serration in the graph increases with increasing Mg content.

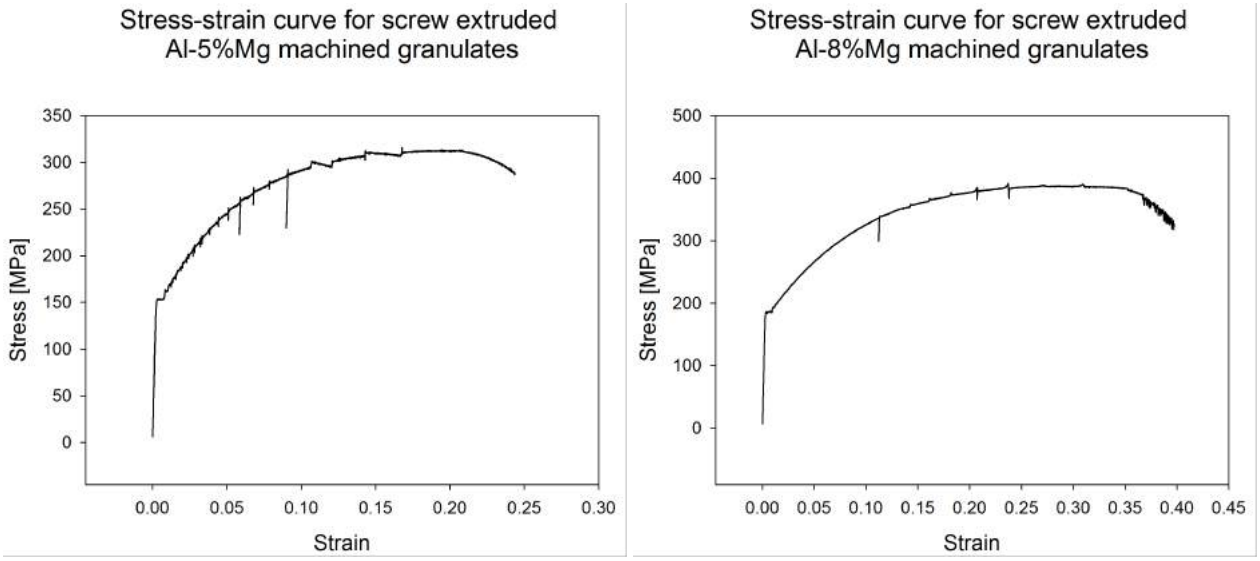

(a) (b)

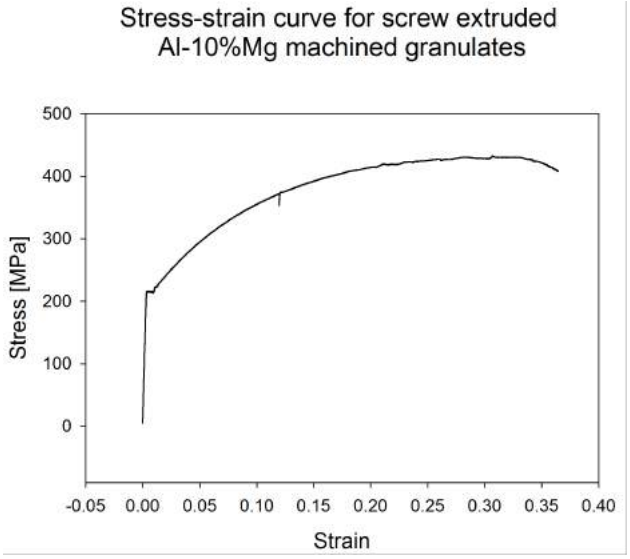

(c)

Figure 4.46: Representative stress-strain curves for screw extruded Al-XMg machined granulates.

Figure 4.46 shows the stress-strain curves for screw extruded Al-XMg machined granules. The UTS increases with increasing Mg content, but more from Al-5%Mg in figure 4.46a to Al-8%Mg in figure 4.46b, than from Al-8%Mg to Al-10%Mg in figure 4.46c, the same tendency as seen for

conventional ram extruded profiles. The strain at fracture is highest for Al-8%Mg at 0.4, and lowest for Al-5%Mg at 0.25. The amount of serration in the graphs decrease with increasing Mg content.

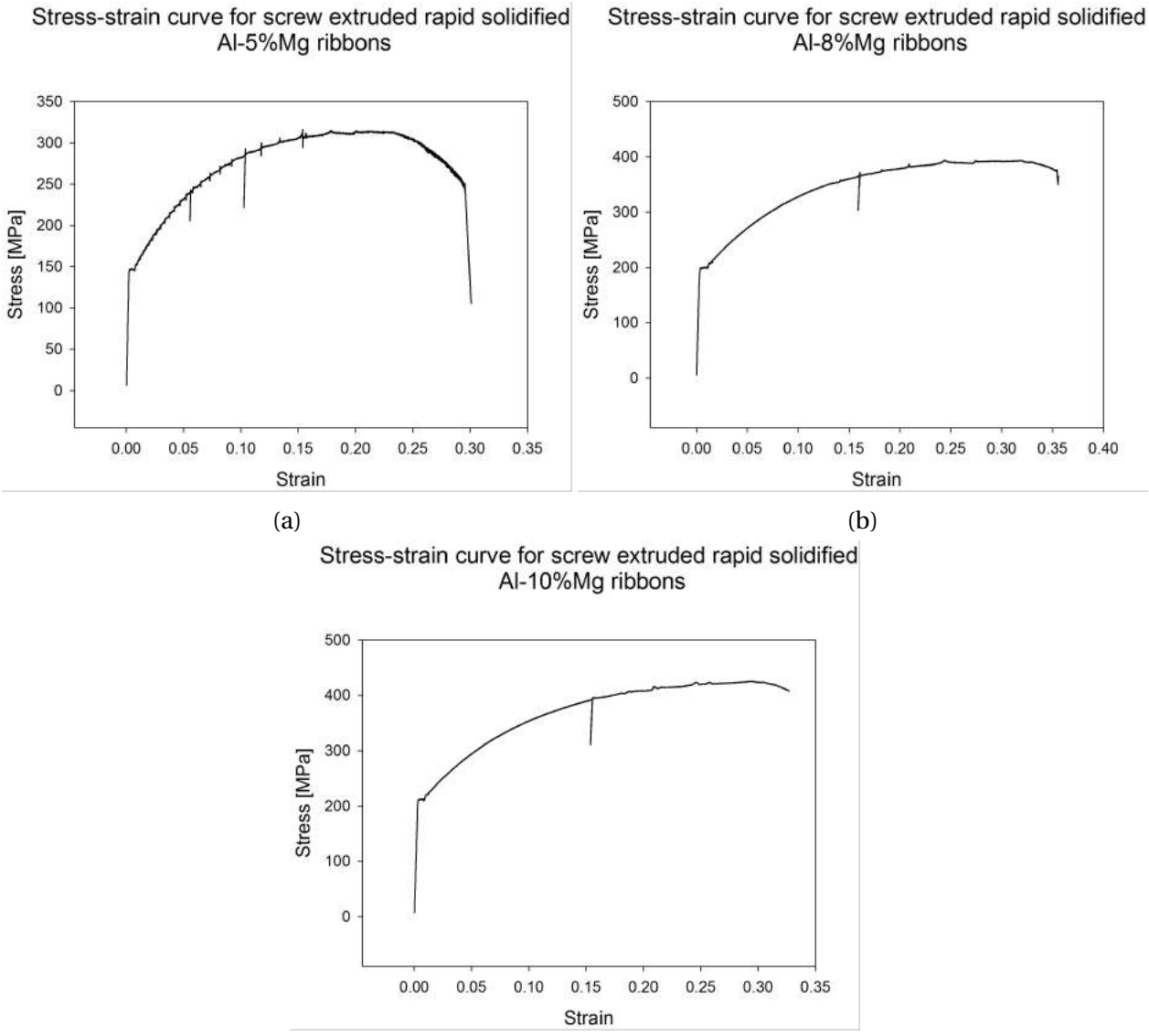

(a) (b)

(c)

Figure 4.47: Representative stress-strain curves for screw extruded RS ribbons.

The stress-strain curves for the screw extruded RS ribbons profiles are shown in figure 4.47. The UTS increases with increasing Mg content, but more from Al-5%Mg in figure 4.47a to Al-8%Mg in figure 4.47b, than from Al-8%Mg to Al-10%Mg in figure 4.47c, the same tendency as seen for conventional ram extruded, and screw extruded machined granulates profiles. The strain at fracture is highest for Al-8%Mg at 0.35, and lowest for Al-5%Mg at 0.3. The amount of serration

in the graph decreases with increasing Mg content.

Calculated UTS for all the extruded material is seen in figure 4.48. Conventional ram extruded profiles has markedly lower UTS for all alloys, screw extruded profiles show no discernible UTS, for all alloys. UTS increases with increasing Mg content.

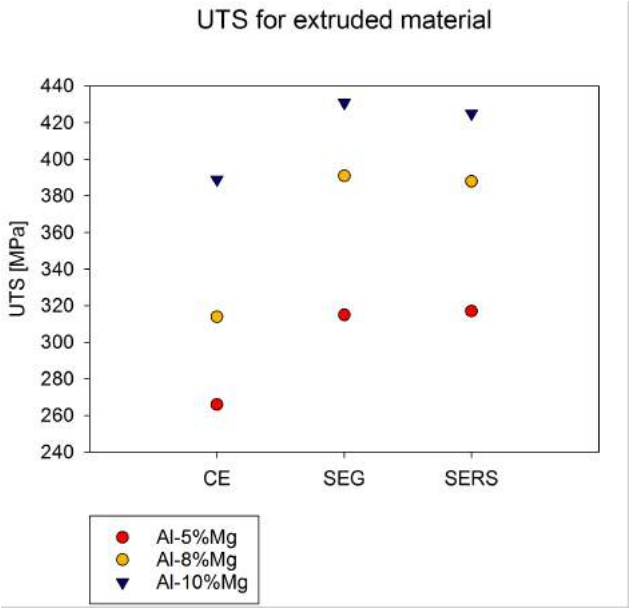

Figure 4.48: Calculated average UTS for conventional ram extruded (CE), screw extruded machined granulates (SEG), and screw extruded RS ribbons (SERS) profiles.

4.7 Hydrogen and magnesium measurement

A chemical analysis of the as cast, and screw extruded granules was performed by Sintef Molab, and the results are presented in this section.

Table 4.2 presents the chemical analysis of magnesium in the as cast and screw extruded machined granulates material. The Al-8%Mg and Al-10%Mg as cast and screw extruded material shows no discernible difference, considering some standard deviation is to be expected. The Al-5%Mg however, shows a decrease of 0.568 wt% from as cast, to screw extruded profile.

The chemical analysis of hydrogen in the as cast material, is given in table 4.3. There is 0.153 ppm more hydrogen in the Al-8%Mg sample, compared to the Al-5%Mg sample, while the Al-10%Mg at 0.644 ppm, has 0.181 ppm less hydrogen than Al-5%Mg. It should be remarked that

Table 4.2: Chemical analysis of Mg in the as cast and screw extruded granules profiles

Material	Alloy	wt%Mg
As cast	Al-5%Mg	5.119
	Al-8%Mg	7.805
	Al-10%Mg	9.585
Screw extruded machined granulates	Al-5%Mg	4.551
	Al-8%Mg	7.800
	Al-10%Mg	9.475

such hydrogen levels are not acceptable if one aims to produce low porosity and defect free extrusions.

Table 4.3: Chemical analysis of hydrogen content in the as cast material

Material	Alloy	H_2 ppm	ml/100g
As cast	Al-5%Mg	0.825	0.927
	Al-8%Mg	0.978	1.099
	Al-10%Mg	0.644	0.723

4.8 Fractography

This section presents SEM images of the fracture surfaces of tensile tested Al-5%Mg and Al-10%Mg profiles, to determine the characteristic fracture mechanisms of the different extruded profiles. Two profiles for each alloy were imaged, and representative images are shown.

Fracture surface of conventional ram extruded Al-5%Mg is shown in 4.49 and 4.50. From the overview in figure 4.49a, one can see a small circular section of voids in the middle, and large shear surfaces surrounding the area in the middle. The overview shows two places of interest pointed out. An area in the middle of the specimen in figure 4.49b-4.49d, and an area at the outer section of the specimen in figure 4.50. The area in the middle shows large voids in figures 4.49b-4.49c, and micro porosity in this void in figure 4.49d. These kinds of voids and micro porosity were found all along the ridge seen in the overview. The outer area shows a much smoother overall surface, with varying degrees of shear.

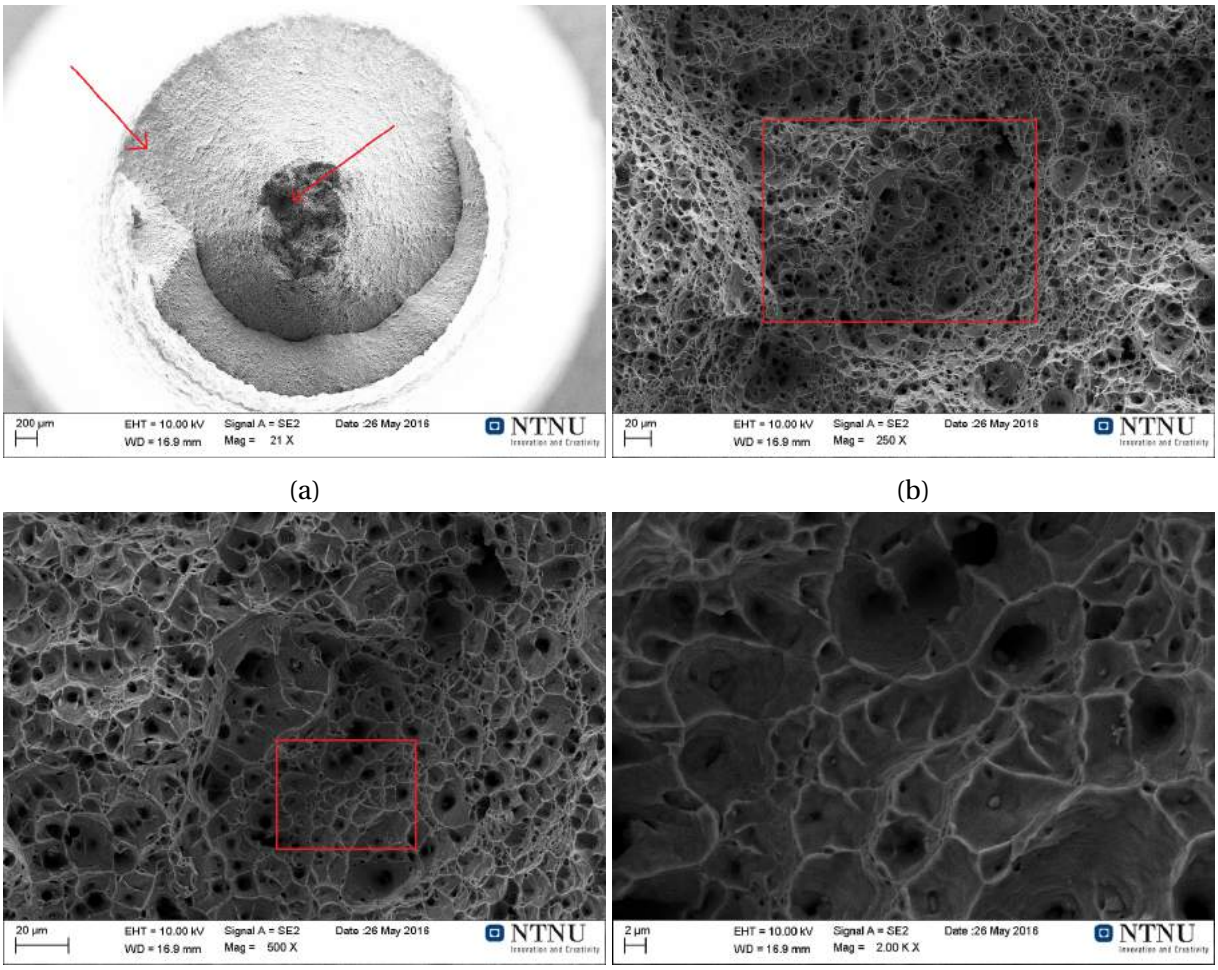

(a) (b)

(c) (d)

Figure 4.49: Fracture surface of conventional ram extruded Al-5%Mg.

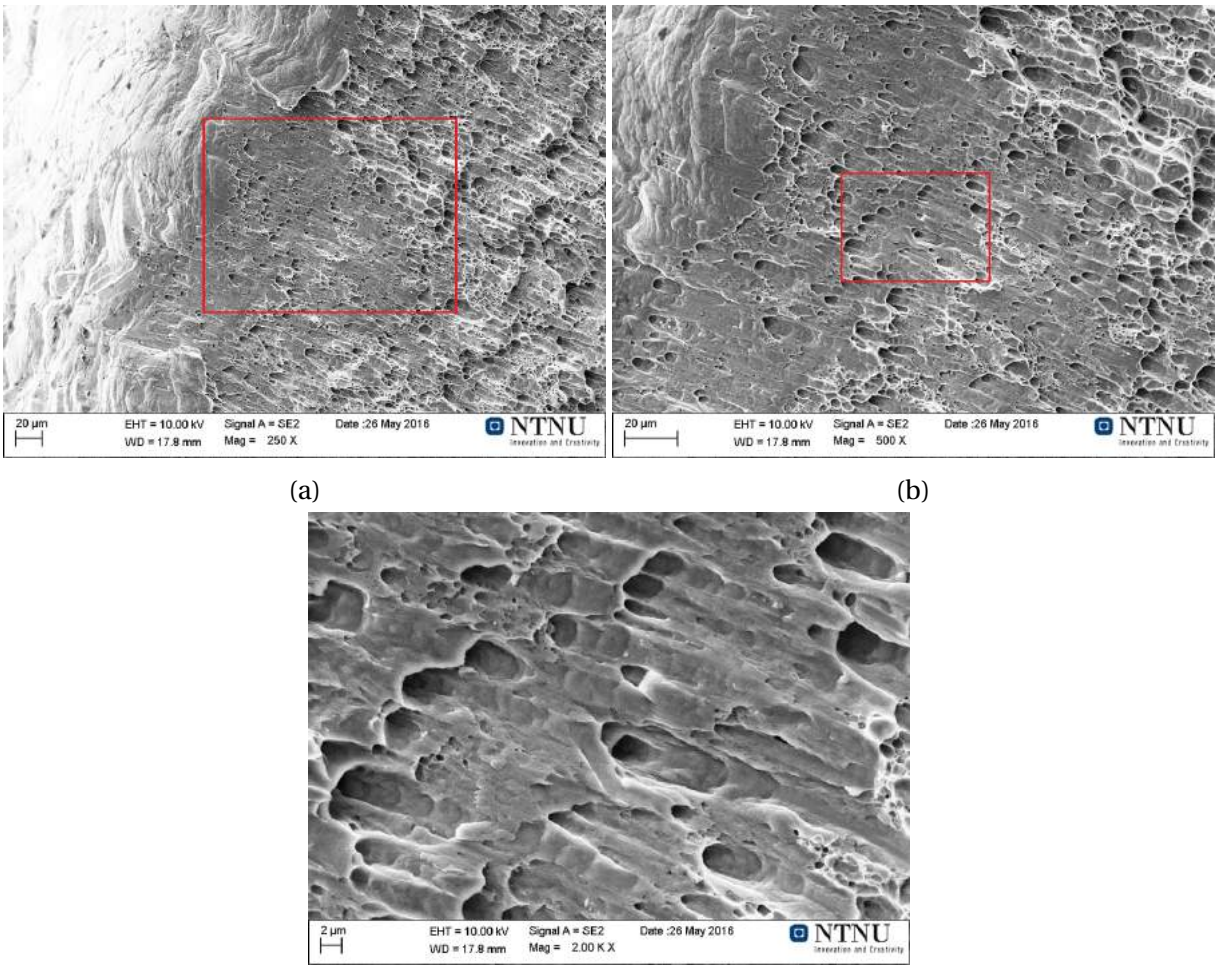

(a) (b)

(c)

Figure 4.50: Fracture surface of conventional ram extruded Al-5%Mg.

Figure 4.51 and 4.52 shows the fracture surface of conventional ram extruded Al-10%Mg. The overview in 4.51a shows a faceted surface, with large flat surfaces. Two areas of interest are pointed out in the overview image, an area in the middle where two faceted surfaces meet, and an area at the bottom of another faceted surface. The first area mentioned is shown in figures 4.51b-4.51d. Two faceted surfaces meet in the middle of the sample. Some large voids are seen, shear along the walls, and a complete separation of two 45°surfaces, in addition to micro porosity. The second area is shown in figures 4.52a-4.52c. The images show a shear surface, meeting a flat surface in the middle of the sample. The shear surface is much smoother, and complete separation of the two surfaces is seen.

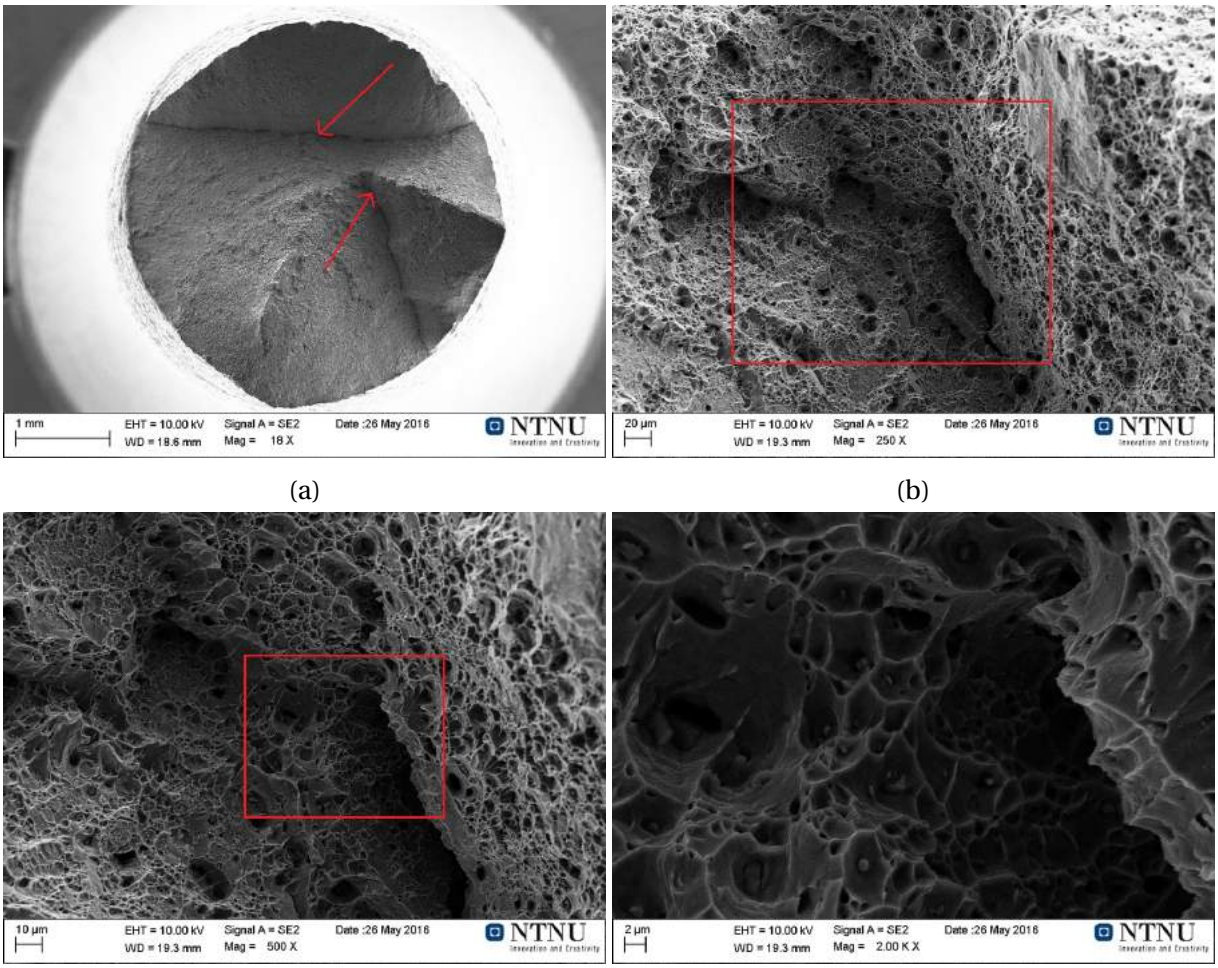

(a) (b)

(c) (d)

Figure 4.51: Fracture surface of conventional ram extruded Al-10%Mg.

The screw extruded Al-5%Mg machined granules profile is shown in figures 4.53-4.54. The

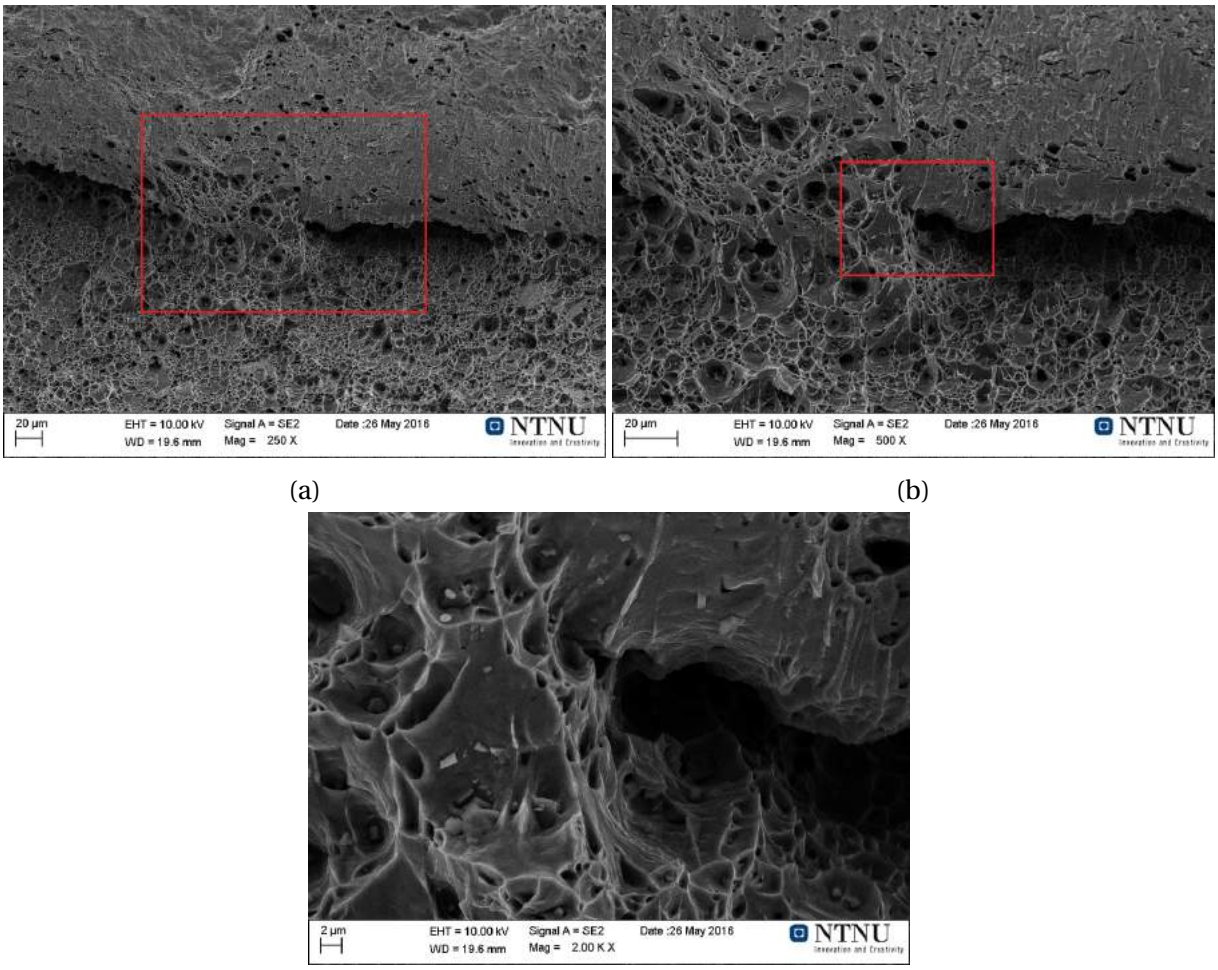

(a) (b)

(c)

Figure 4.52: Fracture surface of press extruded Al-10%Mg.

overview shows a ridge along the profile, with large voids, and faceted sides going away from this ridge. Two areas of interest are pointed out in the overview image, an area along the ridge, and an area at the outer part of the profile. The first area, shown in figures 4.53b-4.53d, show large voids, with micro porosity. The second area, shown in figures 4.54a-4.54c, show large degree shear, with some micro porosity in some areas.

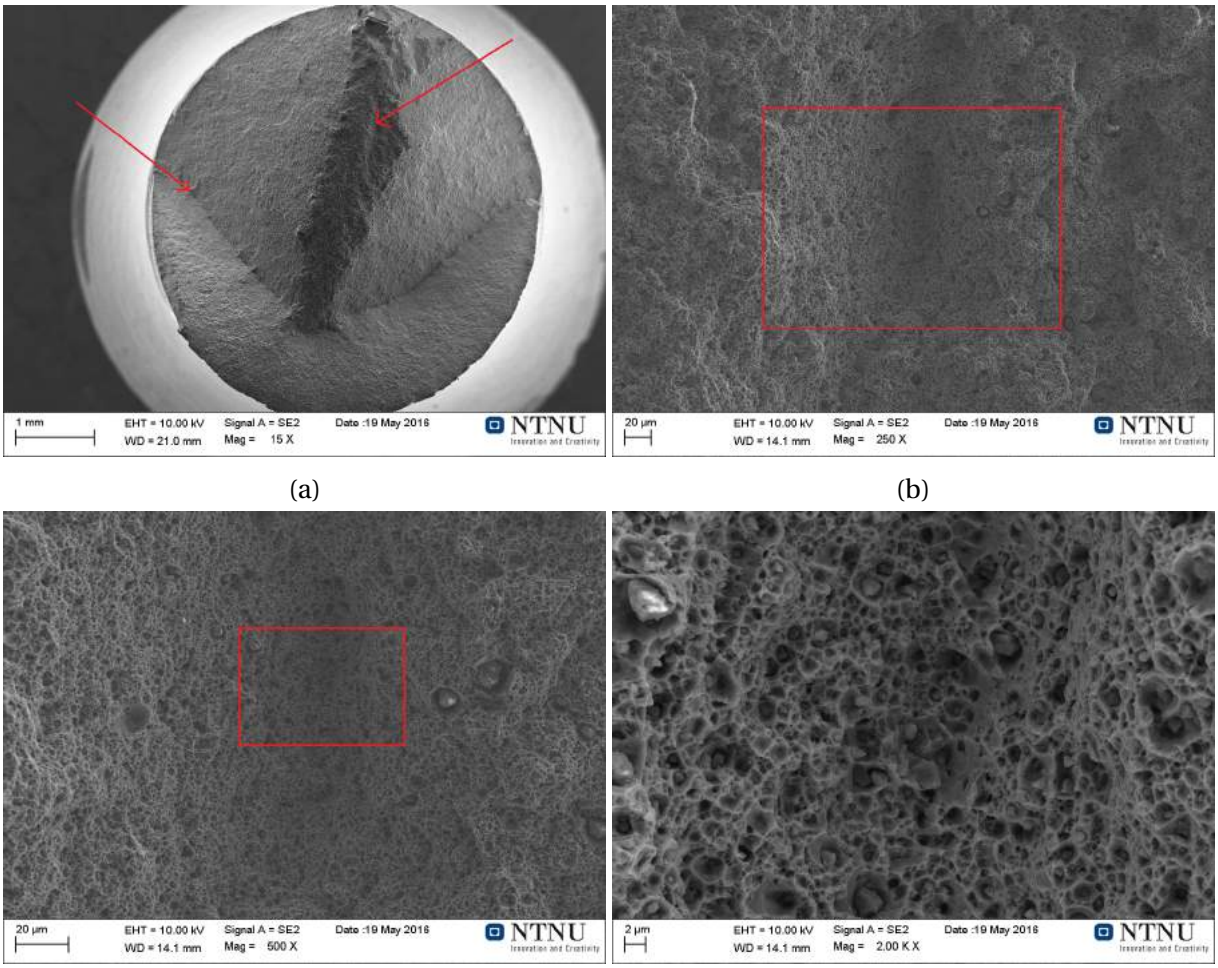

(a) (b)

(c) (d)

Figure 4.53: Fracture surface of Al-5%Mg screw extruded machined granulates.

Figures 4.55-4.56 show a screw extruded Al-10%Mg machined granules profile, and figure 4.56 shows another profile. Figure 4.55a shows a an overview of the first profile. Two areas of interest are pointed out in the overview image, an area in the middle, and one near the edge. The first area, seen in figure 4.55b-4.55c, is a swirl in the middle, with large gaps going in a spiral. The second area, in figure 4.56a-4.56c, is an intersection with a shear surface, and a flat surface.

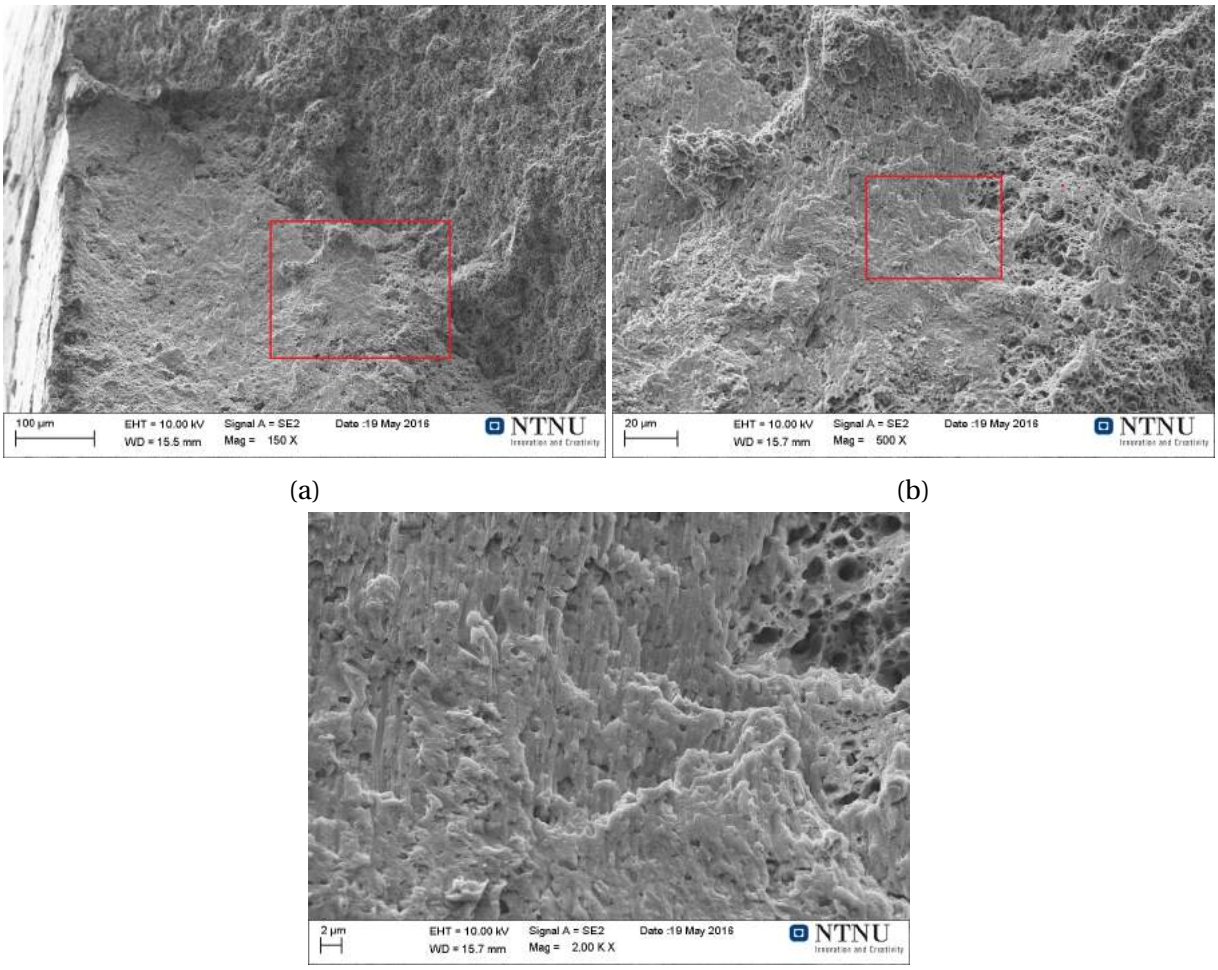

(a) (b)

(c)

Figure 4.54: Fracture surface of Al-5%Mg screw extruded machined granulates.

Micro porosity is seen at high magnification. The second profile is shown in figure 4.57. The overview image in figure 4.57a shows no swirl in the middle, but rather fracture rivers going away from a flatter surface, and a similar overall shape to that in the first profile is seen, with a flat surface in the middle, and 45°shear surfaces about two thirds away from the middle of the profile. A fracture river is shown in figures 4.57b-4.57c. The river wall shows a mix between shear and micro porosity.

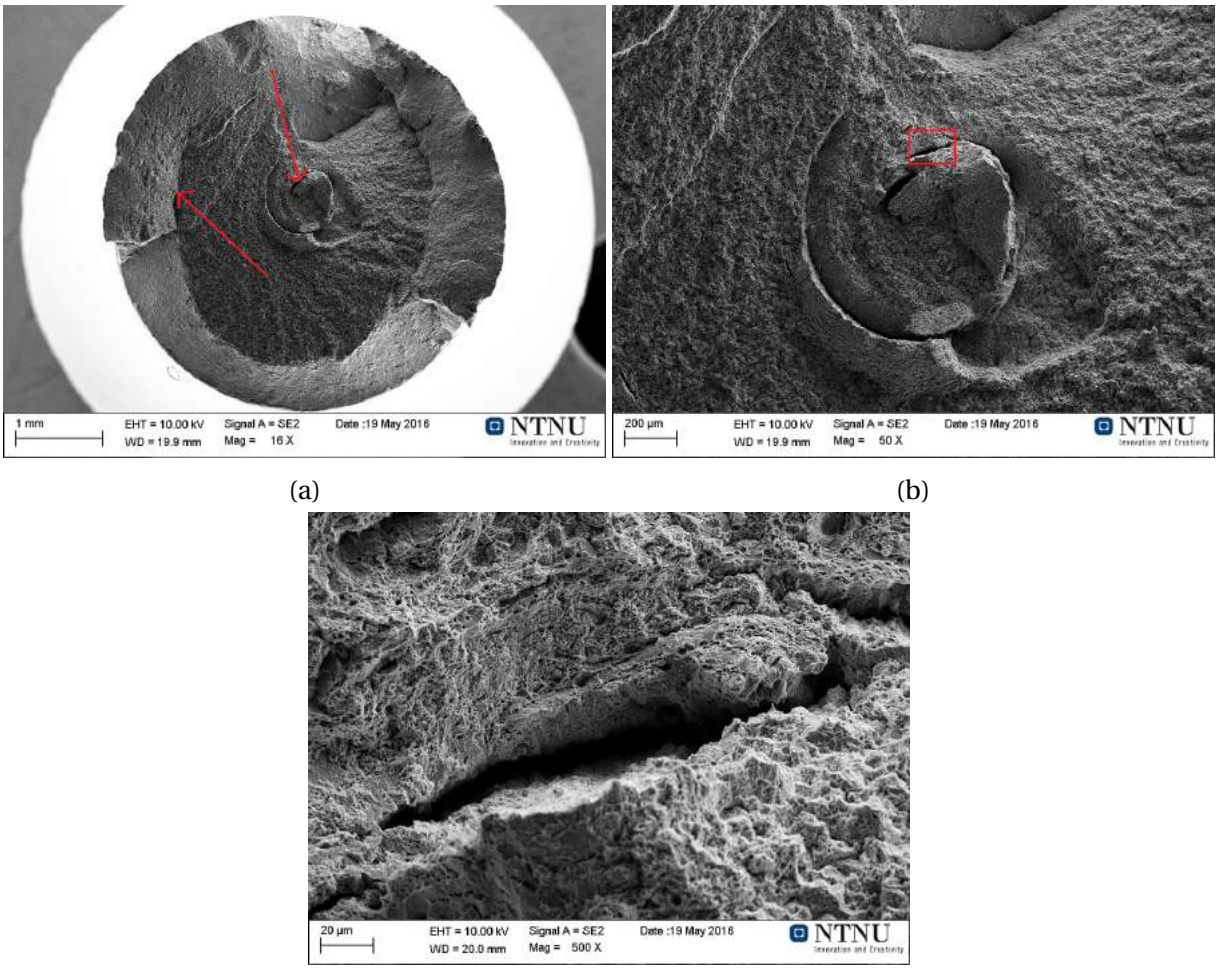

(a) (b)

(c)

Figure 4.55: Fracture surface of Al-10%Mg screw extruded machined granulates.

The screw extruded Al-5%Mg RS ribbons profile is shown in figures 4.53-4.54. The overview image in figure 4.58a shows a shear surface covering the entire middle of the specimen. Two areas of interest are pointed out in on this surface. A large pore with rivers running out from it, and the wall of one of these rivers. The first area is shown in figures 4.58b-4.58d, a large pore at

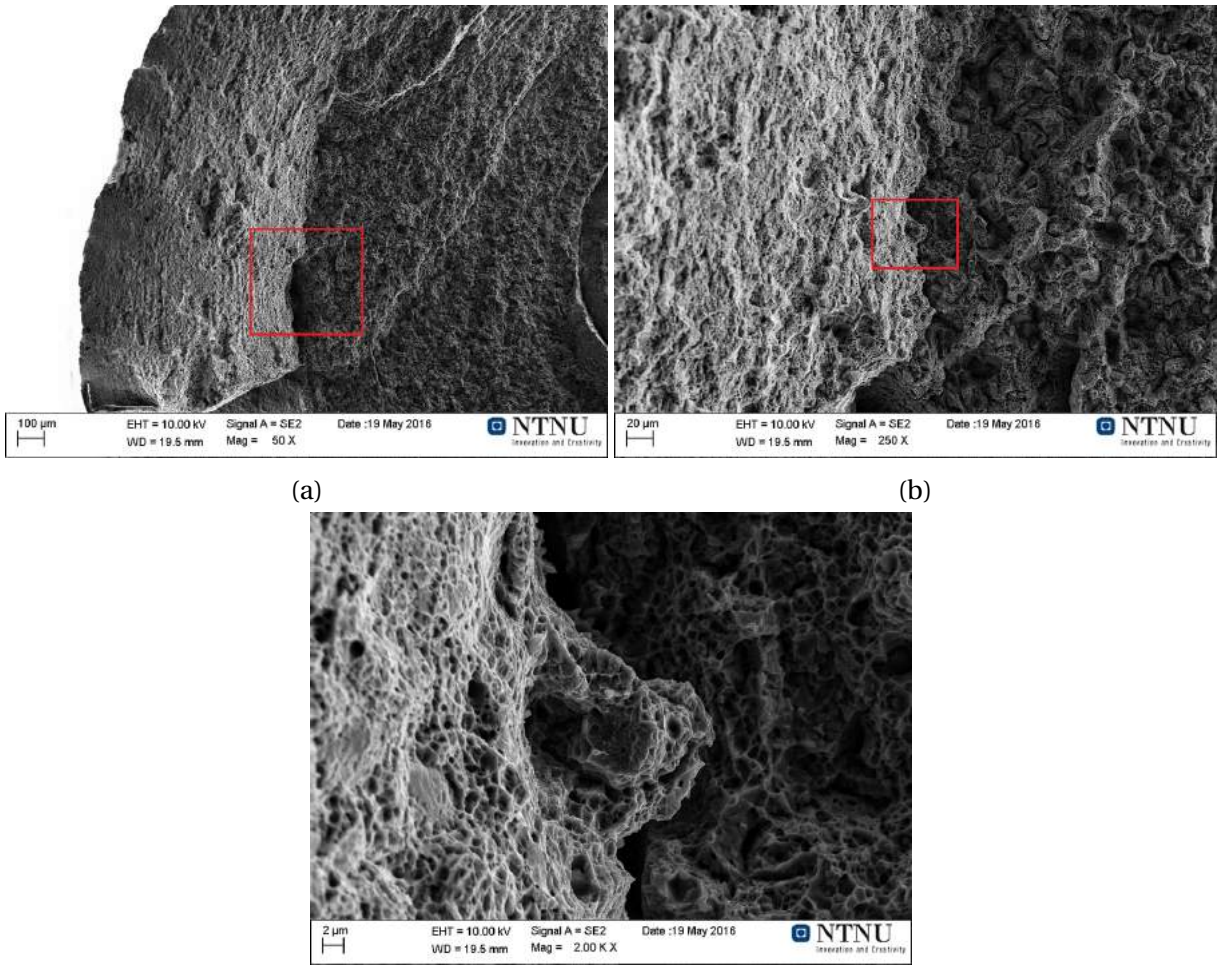

(a) (b)

(c)

Figure 4.56: Fracture surface of Al-10%Mg screw extruded machined granulates.

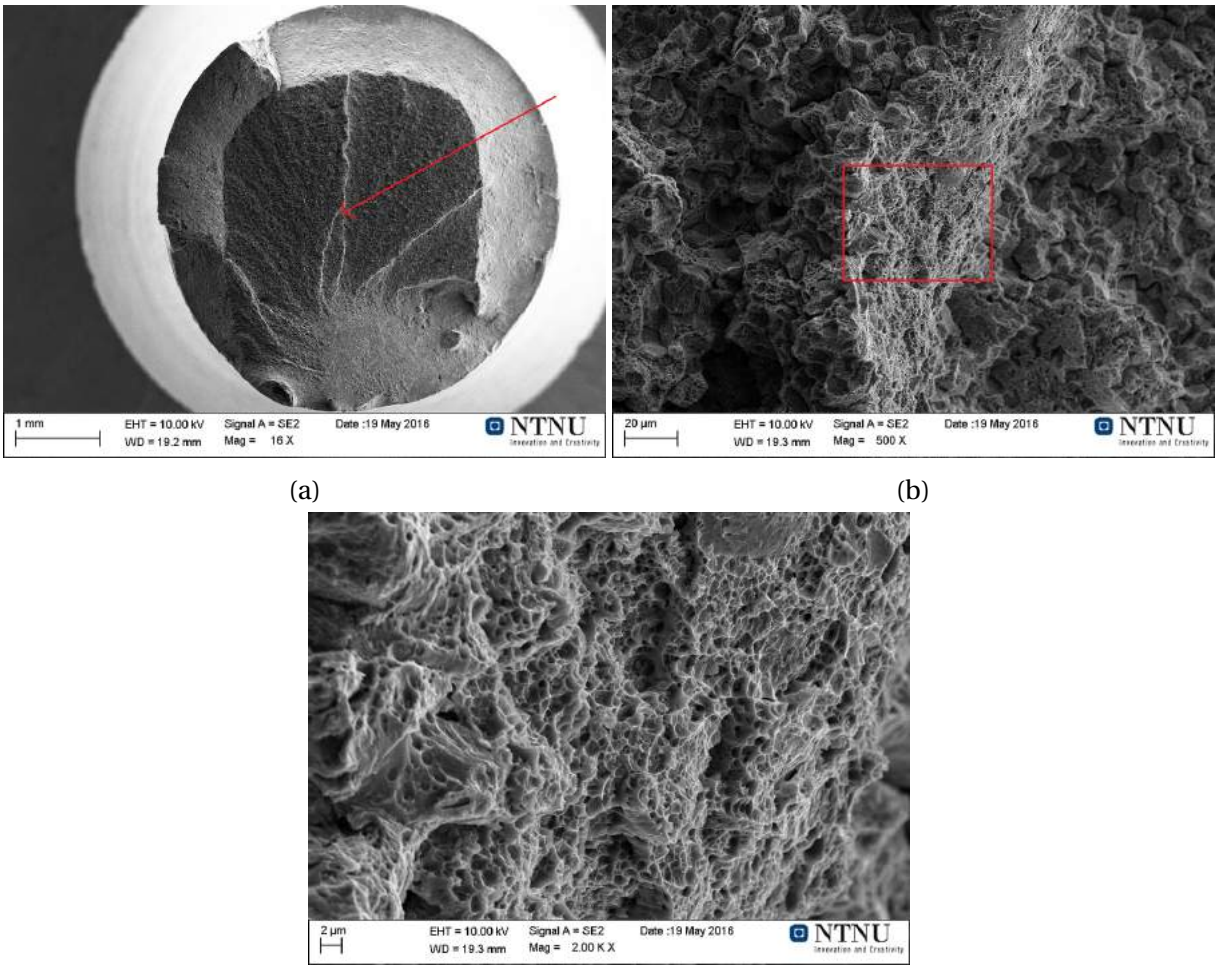

(a) (b)

(c)

Figure 4.57: Fracture surface of Al-10%Mg screw extruded machined granulates.

the base of the two largest rivers. The pore walls are heavily sheared, and surrounding the pore, micro porosity is seen. The second area is shown in figures 4.59a-4.59c. The river wall is seen to have a mix of shear and micro porosity.

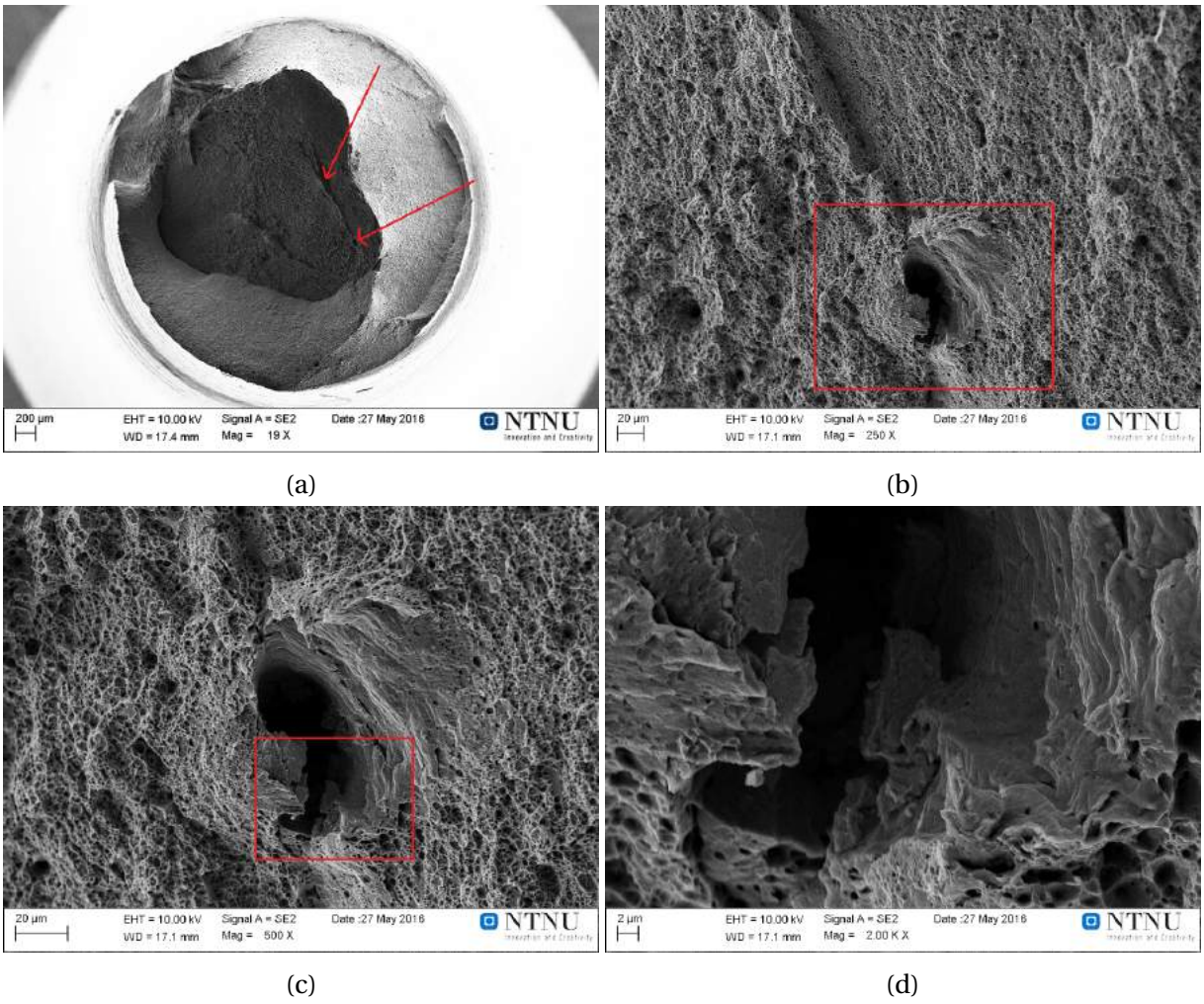

Figure 4.58: Fracture surface of screw extruded Al-5%Mg RS ribbons.

The screw extruded Al-10%Mg RS ribbons profile is shown in figures 4.60-4.61. The overview in figure 4.60a shows a heavily laminated profile. Two areas of interest are pointed out, an area of voids in the middle, and the edge of a crack wall. The first area in figures 4.60b-4.60d shows a large void, with some shear, and micro porosity. The second area in figures 4.61a-4.61c shows the edge of a large crack. Very large scale shear can be seen, with almost no micro porosity.

An overview image of a screw extruded Al-10%Mg RS ribbons profile is shown in figure 4.62. This image illustrates that not all screw extruded ribbons Al-10%Mg profiles were as heavily

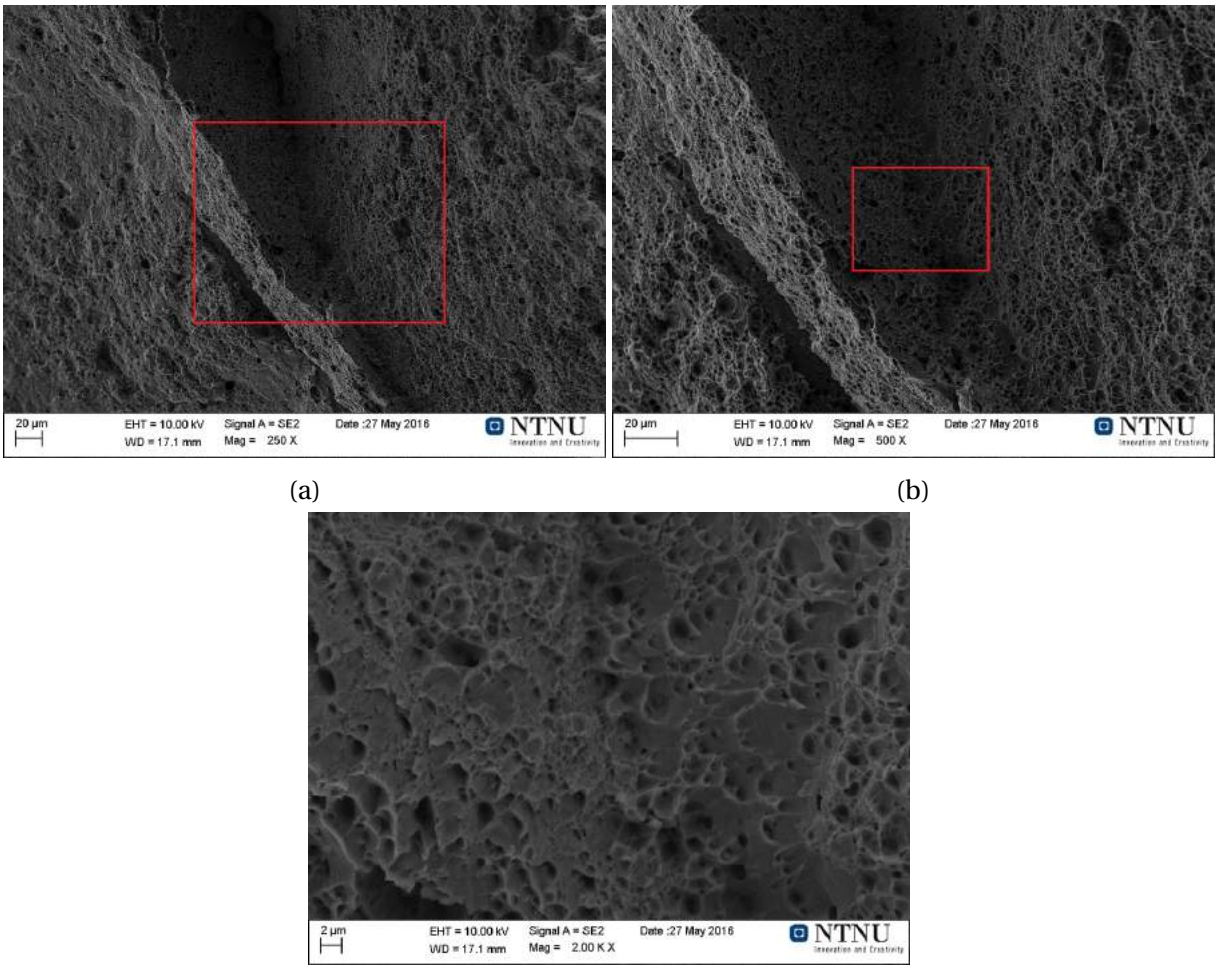

(a) (b)

(c)

Figure 4.59: Fracture surface of screw extruded Al-5%Mg RS ribbons.

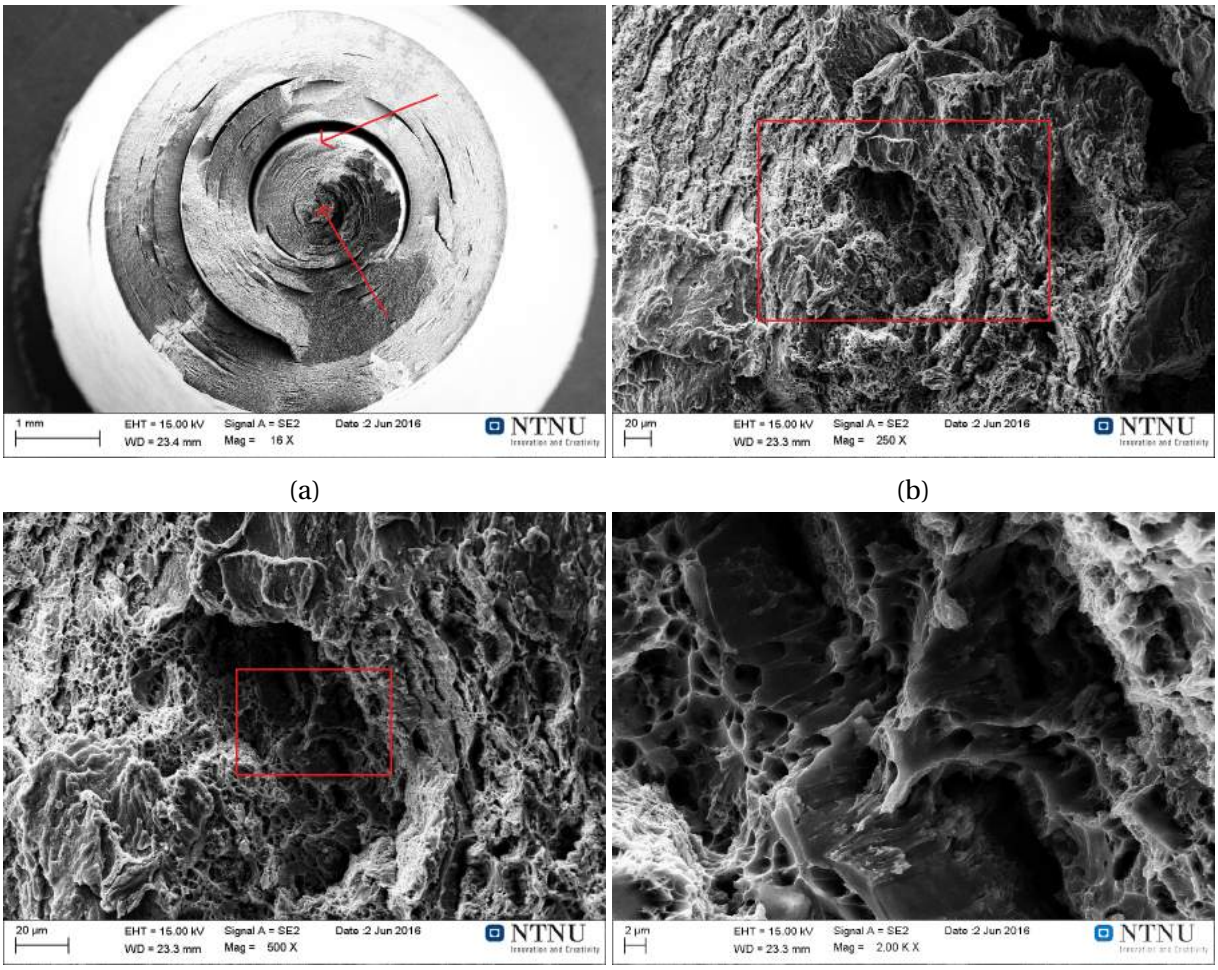

(a) (b)

(c) (d)

Figure 4.60: Fracture surface of screw extruded Al-10%Mg RS ribbons.

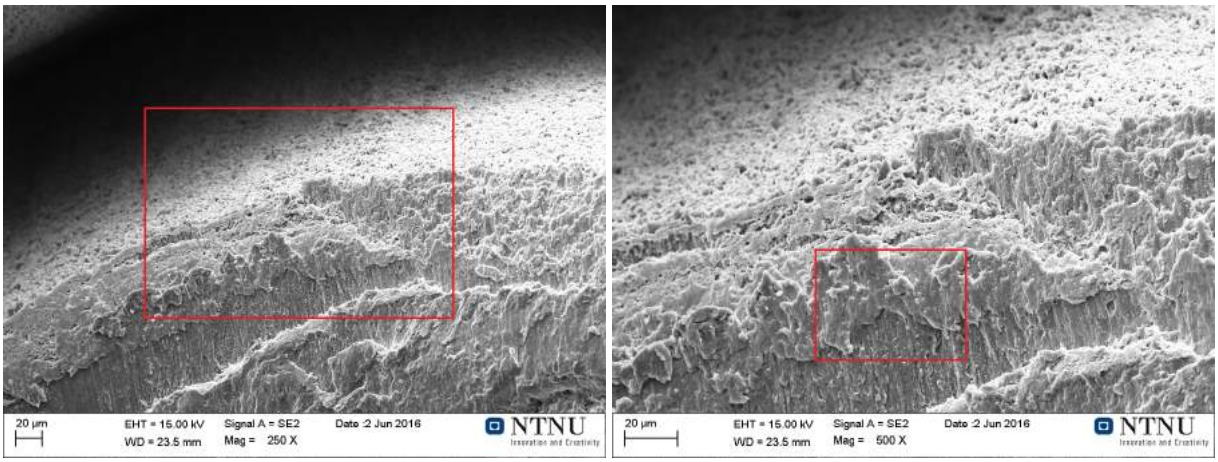

(a) (b)

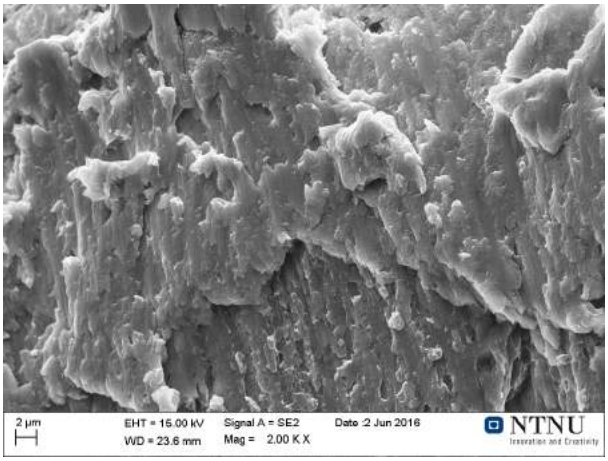

(c)

Figure 4.61: Fracture surface of screw extruded Al-10%Mg RS ribbons.

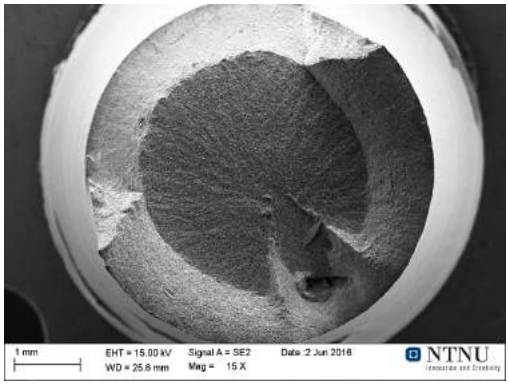

Figure 4.62: Overview image of screw extruded RS ribbons profile.

laminated as the one seen in figures 4.60-4.61.

4.9 X-ray diffraction

Table 4.4 shows the lattice parameters obtained by use of the Rietveld method, for most of the material characterized. An increase in lattice parameter can be seen with increasing Mg content. The highest lattice parameters obtained are 4.07757 Å, 4.09207 Å, and 4.09917 Å, for homogenized at 490°C Al-5%Mg, homogenized at 430°C Al-8%Mg, and conventional cast Al-10%Mg samples respectively.

Table 4.4: Rietveld refinement method calculated lattice parameters.

Material	Alloy	Lattice parameter [Å]
As cast	Al-5%Mg	4.06858
	Al-8%Mg	4.07942
	Al-10%Mg	4.08152
RS ribbons	Al-5%Mg	4.07245
	Al-8%Mg	4.08768
	Al-10%Mg	4.09564
Homogenized 430°C	Al-5%Mg	4.07651
	Al-8%Mg	4.09207
	Al-10%Mg	4.09558
Homogenized 490°C	Al-5%Mg	4.07757
	Al-8%Mg	4.09194
	Al-10%Mg	4.09910
Conventional ram extrusion	Al-5%Mg	4.07721
	Al-8%Mg	4.09105
	Al-10%Mg	4.09917
Screw extruded granules	Al-5%Mg	4.07363
	Al-8%Mg	4.08974
	Al-10%Mg	4.09768
Screw extruded RS ribbons	Al-5%Mg	4.07697
	Al-8%Mg	4.08983
	Al-10%Mg	4.09673

There are four characteristic peaks for pure aluminium in an XRD pattern. A tall peak at 38.6, and three smaller peaks at 44.8, 65.1, and 78.2. These peaks are matched with the XRD pattern of as cast Al-5%Mg in figure 4.63. One can see that the characteristic peaks match very well with four peaks of the Al-5%Mg pattern, however, the Al characteristic peaks are shifted slightly to

the right, due to the effect Mg in solid solution has on the lattice.

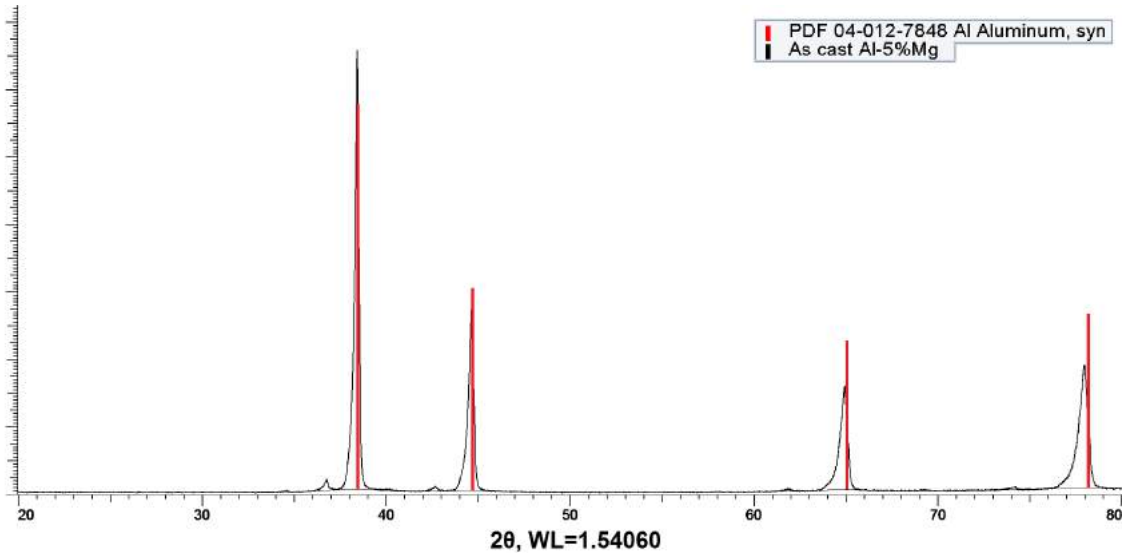

Figure 4.63: XRD pattern of as cast Al-5%Mg. Shift to the left of the characteristic aluminium pattern is due to Mg in solid solution.

The as cast XRD patters are presented normalized and stacked, in figure 4.64. The peaks shift to the left with increasing alloying content, in addition to broadening of the smaller peaks. The vertical red line is pure aluminium. Notice the increasing shift to the left of the vertical line, with increasing Mg content.

All investigated material are presented in the same normalized XRD patterns according to alloy composition, in figures 4.65-4.67. An increasing shift to the left of the vertical pure aluminium line can be seen with increasing Mg content. The shift in the two left tall peaks for all the extruded profiles, is due to the grain being oriented with the extrusion direction. The extension of the rightmost peak to the left has been identified by Rotan (2016) to be a different phase. This extension to the left is not markedly seen in any of the other investigated materials.

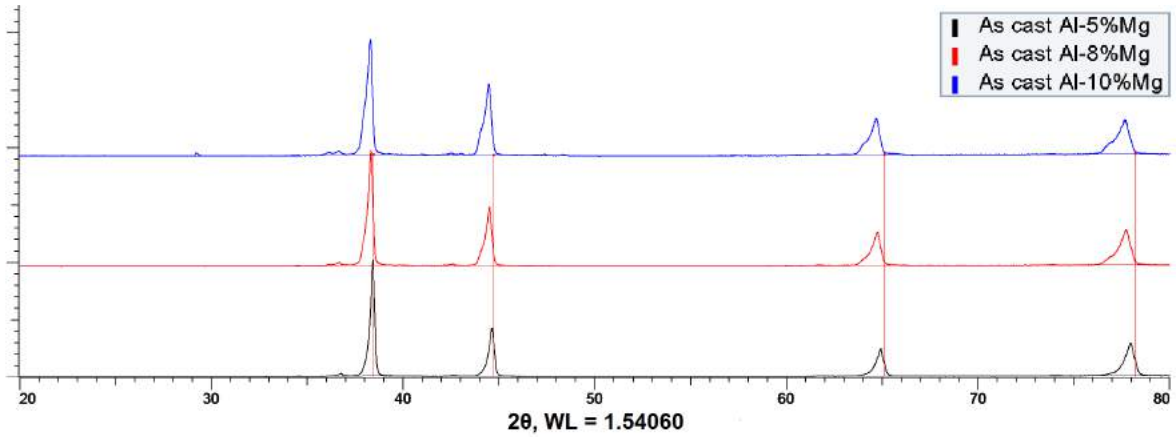

Figure 4.64: XRD pattern of as cast Al-XMG alloys. Notice the shift to the left, and the broadening of the smaller peaks, with increasing alloying elements.

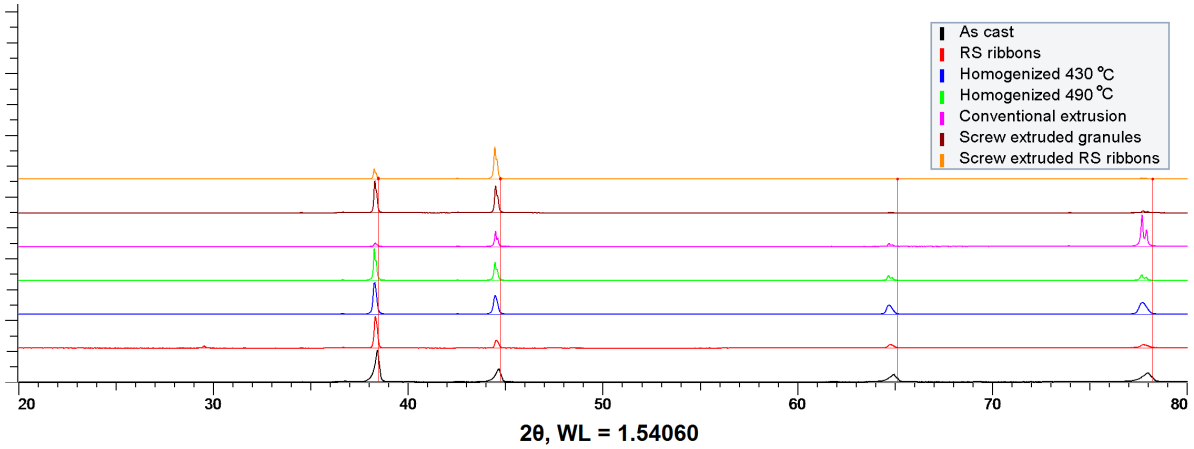

Figure 4.65: XRD pattern of Al-5%Mg investigated materials.

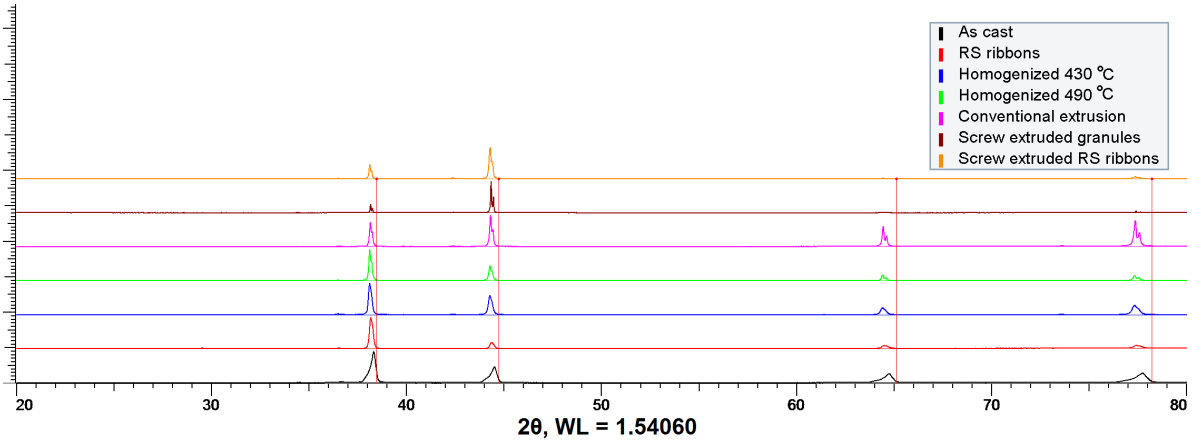

Figure 4.66: XRD pattern of Al-8%Mg investigated materials.

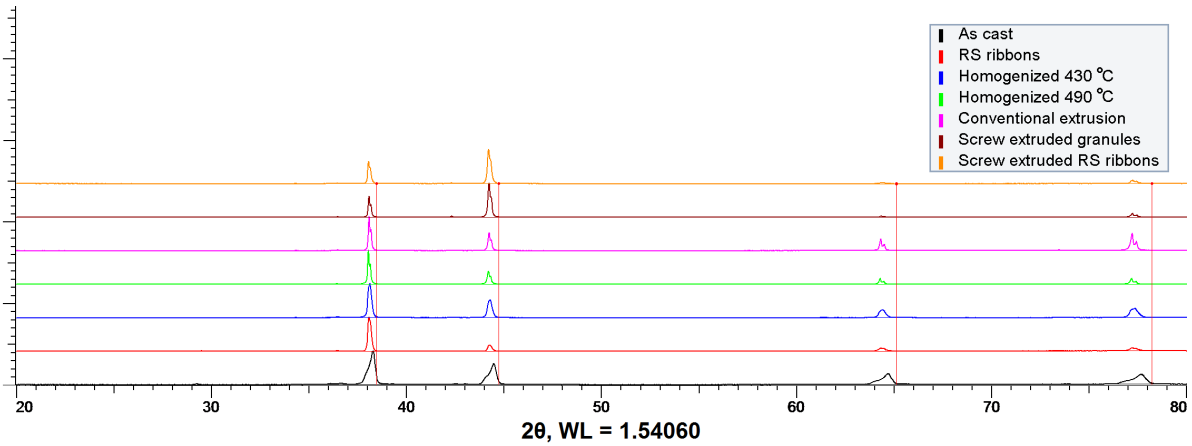

Figure 4.67: XRD pattern of Al-10%Mg investigated materials.

5 | Discussion

This chapter discusses the results presented in section 4, and takes aim to explain the results by use of theory presented in section 2.

5.1 Chemical analysis

The received DC billets have been chemically analyzed by Sintef Molab for hydrogen, and the results are seen in section 4.7. The hydrogen analysis shows a very high amount of hydrogen. The solubility of hydrogen in aluminium is 0.039 ppm, taken from section 2.7. The lowest hydrogen content seen in the as received DC cast billets, was 0.644 ppm. This is very high, and the reason for the large amounts of porosity seen in the DC cast billets and the subsequent homogenized samples. This has caused many problems. First during metallographic preparation, where porosity can easily cause the effects seen in appendix B. Second, in all the homogenized DC cast samples where porosity might have influenced hardness, or diffusion.

The received DC billets and screw extruded machined granulates have also been chemically analyzed for for Mg content. These results show no difference between the two materials, except from in the Al-5%Mg alloy. A marked loss of 0.568 wt%Mg from the DC cast billets, to screw extruded machined granulates is seen. As has been mentioned in section 3, the Al-5%Mg machined granulates were machined without an alcohol coolant, which resulted in large amounts of oxides. This could explain the loss of Mg content, as the analysis method might not detect Mg in oxides.

5.2 Microstructure

The defining microstructural features of the materials investigated in this work, are porosity, degree of presence of beta phase, and grain size. These features will be discussed in this section.

Porosity

The cast material contains a surprising amount of hydrogen. As mentioned in section 2.7, the solubility of hydrogen in 0.039. The amount of hydrogen in the cast material received, is 0.825, 0.975, 0.644 ppm in Al-5%Mg, Al-8%Mg, Al-10%Mg respectively. This means that most of the hydrogen in the as cast material must be trapped in the pores seen in the as cast micrographs in section 4.1. The porosity still remains in the machined granules, however, this is not seen as a problem, as the granules are heavily deformed during screw extrusion. If there was a problem with the hydrogen trapped in the pores, one might expect to see a drastic difference in porosity and mechanical properties between the screw extruded profiles machined granulates and screw extruded RS ribbons, where the feed material is expected to have drastically different hydrogen content. This is not seen, and one might assume that hydrogen in the granules does not have a negative effect on the outcome of the profile.

The tortuousity of pores in the DC cast homogenized material decreases with increasing Mg content, most easily seen in the DC cast samples homogenized at 430 °C for 4 hours, but true for all heat treated samples. In addition, pore size seems to increase with Mg content. From as cast, to DC cast homogenized for 4 hours, the porosity is in agreement with section 2.7, with increased pore size and density, however, from Chaijaruwanich et al. (2007) it should follow that the DC cast samples homogenized 1 week at 430°C, and to 490°C, would see the same trend, which they do not. From 4 hours, to 1 week, the pore size decreases, and the pore density looks like it decreases, although it's hard to tell without computer analysis. From 4 hours at 430°C to 490°C, the same tendency is seen, with the exception of some larger sized spheroid pores in DC cast Al-10%Mg homogenized to 490°C.

The conventional ram extruded material seen in section 4.1 has lines of porosity following the extrusion direction. This is seen in all the alloys. This porosity might be due to problems compacting the aluminium during extrusion, leading to small air pockets following the extrusion direction. With a ram/die opening ratio of 100/1, complex flow patterns will occur, and areas with lower density will occur. Upon cooling, shrinking might cause these areas to develop line porosity.

Regarding porosity in the screw extruded profiles seen in section 4.1, due to the high degree of deformation during extrusion, porosity in these profiles should not be due to porosity in feed material. Not much porosity is seen in the screw extruded profiles, disregarding the Al-5%Mg profile from machined granulates, which was machined wrongly, and contained large amounts of oxides. Some lines similar to the lines in conventional ram extruded profiles, are seen in the screw extruded profiles with Al-5 and 8%Mg RS ribbons, and Al-10%Mg machined granulates as feed material. Screw extrusion creates even more complex flow patterns than conventional extrusion, however, screw extrusion also compacts the feed material to a much larger degree, even so, difficulties compacting the feed material seems to persist. In Al-8 and 10%Mg profiles with RS ribbons feed material, larger cracks along the edge in the extrusion direction are seen, which is due to even larger problems of compacting. These cracks will cause large stress concentrations during use, and should be at a minimum.

Beta phase content

The Al_3Mg_2 beta phase is difficult to detect. In large amounts, it is easy to see in optical micrographs, as in section 4.1. In smaller amounts, it is possible to find and characterize through use of EDS in the SEM, however, beyond this, it is difficult to judge to what degree any beta phase is left. In hindsight, the micro probe should maybe have been used to a larger degree, as it has a greater resolution than EDS, and is operated by a professional.

Use of XRD was used, in hopes that the resulting XRD patters would be able to determine the beta phase. However, greater prior knowledge on the use of XRD and of the beta phase, would have revealed that the beta phase is extremely large, as mentioned in section 2.1. The beta

phase has a unit cell of 1168 atoms. The XRD results are matched with existing known elements, with known crystal structure, and known plane spacing, however, with a unit cell as large as 1168, atoms will have many different ways of arranging themselves, resulting in many different plane spacing. Too many to be able to differentiate between. No beta phase has therefore been matched with an existing XRD pattern.

The XRD results have therefore been used to calculate the lattice parameter by the Rietveld refinement method. As explained in section 2.10, more Mg in solid solution, gives a larger lattice parameter. The calculated lattice parameters can be seen in section 4.9, and addition plots are given in 5.1-5.2. That more Mg in solid solution gives a larger lattice parameter is clear from the figure in 5.1. All material with higher Mg content has a higher lattice parameter than material with lower Mg content. Comparing the different materials however, gives rather ambiguous results. An average of each material is seen in figure 5.2, and the DC cast samples homogenized to 490°C, has on average the highest lattice parameter, however, not far below, one can see conventional extrusion. Conventional extrusion should not be comparable to the DC cast samples homogenized to 490°C. With such a low rate of cooling, one would expect to see the conventional ram extruded profiles with one of the lowest lattice parameters. These results bring to question the validity of either lattice parameter as an indicator, or the results themselves. Comparing the XRD-patterns also give ambiguous results. The only definite conclusion that can be drawn, is that higher Mg content results in a shift to lower angles. It is however not possible to compare the different materials with the same base composition by looking at the XRD patterns.

Micro probe has regrettably only been used on the RS ribbons, results seen in section 4.3, and no beta phase was present. There might be beta phase below the resolution of the micro probe, for greater resolution, a transmission electron microscope should be used. From the XRD results, the RS ribbons has the second lowest lattice parameter, indicating a low fraction of Mg in solid solution, however, given the high rate of cooling, the Mg might be in several meta stable amorphous phases, not indicated by either micrographs or lattice parameter, which might be the cause of the low lattice parameter.

Homogenization shows progressively less visible beta with temperature, and time. EDS was performed on all DC cast homogenized samples up to 490°C, and beta was found in DC cast

Al-10%Mg homogenized for 4 hours at 430°C. No beta was found in the Al-5 or 8%Mg samples following the same homogenization schedule, or any of the DC cast samples homogenized to 490°C. This does not mean there isn't any beta, only that none was found.

EDS was unfortunately not performed on the extruded profiles. Knowledge on the restrictions of XRD was obtained too late. It was believed that XRD results might give a clearer picture on the presence of beta content than EDS. No beta can be seen in any of the extruded profiles by looking at optical micrographs, and the lattice parameter is markedly above as cast, and comparable to that of the DC cast homogenized samples.

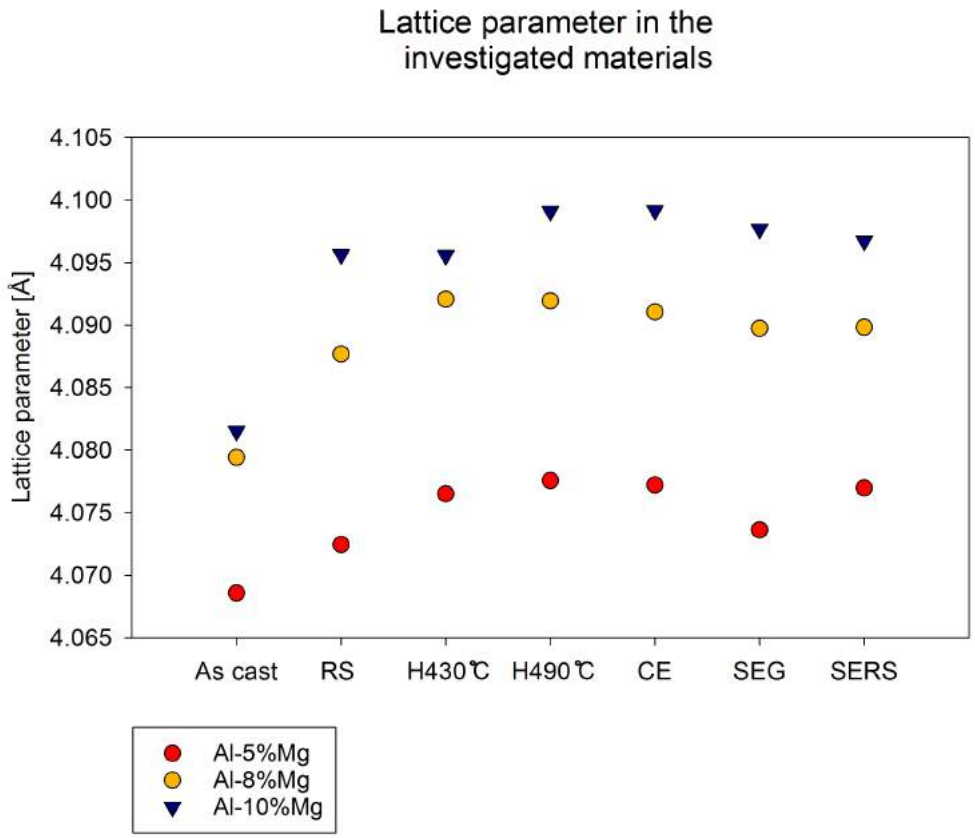

Figure 5.1: Lattice parameter in the investigated materials. H stands for homogenized. CE is conventional ram extrusion. SEG is screw extruded machined granulates. SERS is screw extruded RS ribbons.

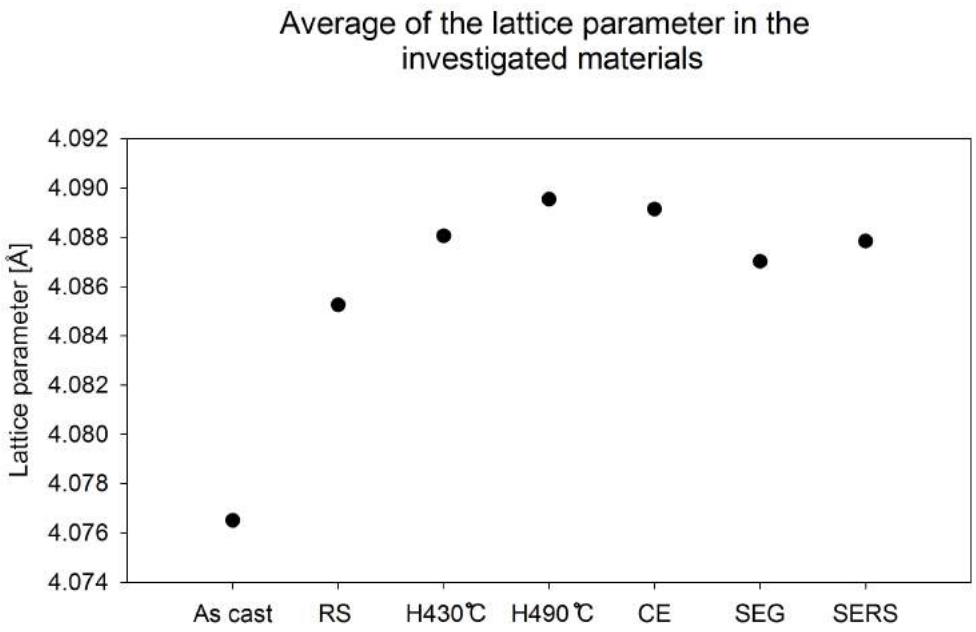

Figure 5.2: Lattice parameter as a function of production method.

Grain size

A figure with the grain size plotted against Mg content is seen in figure 5.3. A connection between high Mg content and low grain size is easy to see, there are only a few deviances from this trend, namely conventional ram extruded Al-10%Mg, which shows slightly higher than Al-8%Mg; DC cast Al-8%Mg homogenized at 430°C for 1 week, which shows higher grain size than Al-5%Mg; and DC cast Al-10%Mg homogenized samples at 430°C for 4 hours, which is higher than Al-8%Mg. Solid solution alloying elements are common grain refinement contributors, and the connection between Mg and grain size is well known (Kaneko et al., 2009).

Regarding the deviation in the Al-8%Mg conventional ram extruded profile, this profile was extruded at a much too high extrusion speed, as seen from the hot tearing. This might have resulted in large degree of deformation, which in turn will give a greater driving force for recrystallization. Time before quenching was sufficiently high for recrystallization to have a large effect, as seen in the equiaxed grains. The quench bath was several meters below the die, and time before quenching was high.

The deviances in homogenized DC cast material is less obvious. The DC cast Al-8%Mg alloy

homogenized for 1 week at 430°C has a much larger grain size than should be expected. A reason for this discrepancy in grain size, might be the amount of hydrogen that is seen. This alloy has the most hydrogen in the as cast condition of all the alloys. An unknown interaction caused by this hydrogen might be the cause.

The screw extruded and RS material has much smaller grain size compared to the other materials. This is due to very high rate of cooling for the RS ribbons, very high deformation, and relatively high rate of cooling for the screw extruded material. One can see signs of recrystallization near the edge in the anodized images in section 4.1, and also at other places of high deformation. Given a larger distance to the watercooling used, one might expect to see an even larger degree of recrystallization.

The grain size of the as cast material is higher on average, due to a long rate of cooling, and a large cross section of the bolt, which is 10 cm. Homogenized DC cast material is lower on average, especially if the outliers are not taken into account. The main grain refinement mechanism in DC cast homogenized material would be quenching, in addition to Mg in solid solution hindering grain growth upon cooling. If even colder water than room temp had been used, a greater difference between DC cast homogenized and as cast would almost certainly be seen.

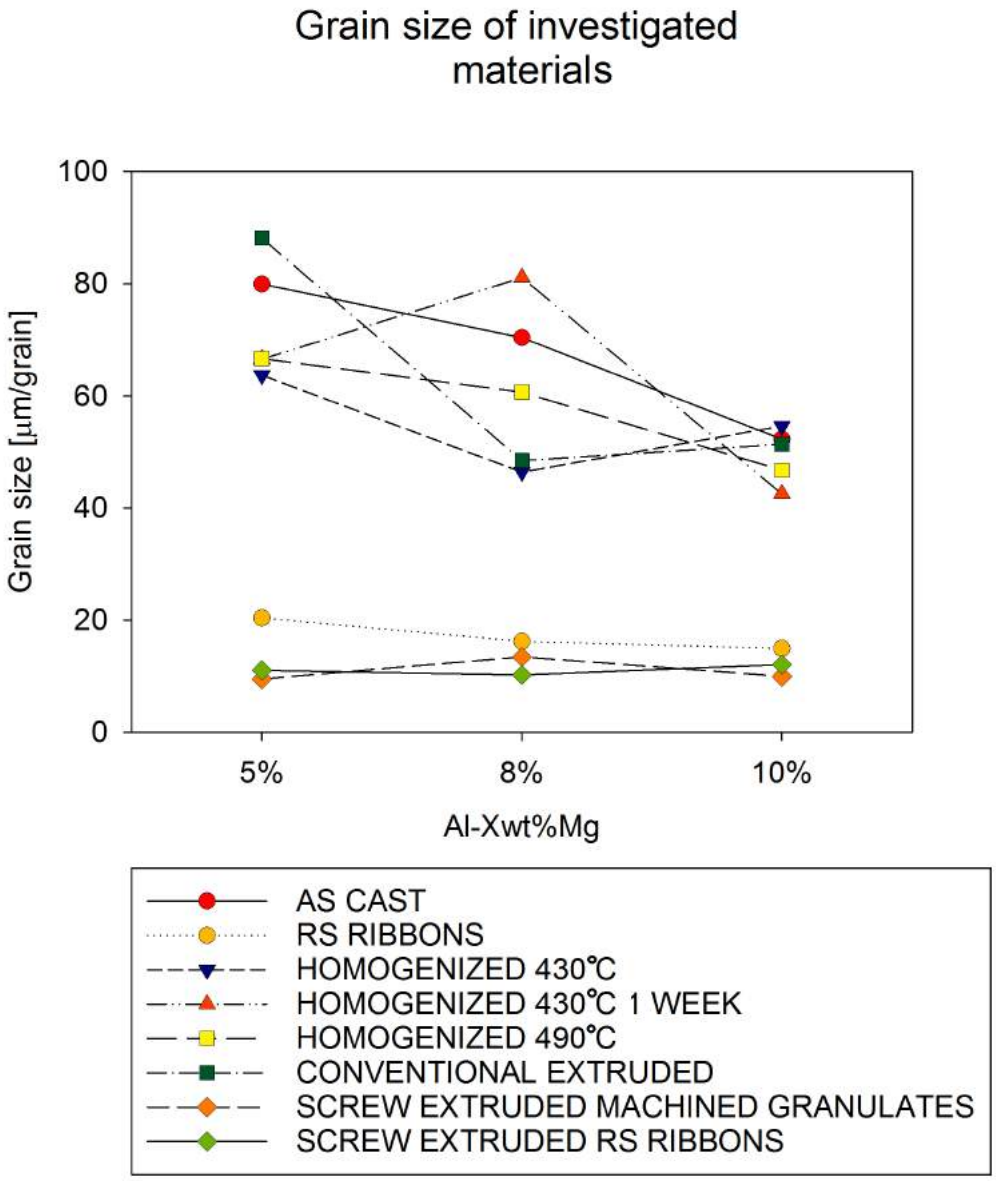

Figure 5.3: Grain size as a function of Mg content in the investigated materials. A connection between high Mg content, and low grain size can be seen.

5.3 Homogenization of DC cast materials

This section will discuss the difference between the different homogenization parameters.

Three different DC cast alloys were homogenized following the heat treatment schedule presented in section 3.8. They were imaged by optical microscopy, SEM, hardness tested, and analyzed by XRD.

Optical microscopy images showed differences in both grain size and porosity. Porosity in all investigated material was discussed in full in section 5.2. It was found that tortuousity decreased with Mg content, and pore size increased. Discrepancies with theory in section 2.7 were found for the DC cast samples homogenized for 1 week. For these samples, the pore size decreases compared to the DC cast samples homogenized for 4 hours, which is the opposite of what Chaijaruwanich et al. (2007) predicted.

The grain size decreases with increasing Mg content, which is to be expected. Solid solution is a common grain refinement contributor. There is an outlier when looking at effect Mg has on grain size. DC cast Al-8%Mg homogenized at 430°C for 1 week has markedly larger grain size than the other DC cast homogenized samples. An explanation for this might be the high hydrogen content in the as cast Al-8%Mg. There are no other obvious differences that might cause such a discrepancy between this alloy, and all the other alloys. The mechanism behind this interaction is unknown.

Hardness for the DC cast homogenized samples increases with increasing Mg content. Hardness increases with increasing degree of solid solution and is well established. From the hardness graphs in section 4.5, one can see a decrease in hardness towards the edge. Some grain refinement can be seen in the micrographs in section 4.1, which should yield higher hardness, not lower. No decrease in solid solution of Mg can be seen in the EDS linescans in section 4.4, which might mean that this decrease in hardness stems from an edge effect during metallographic preparation. Grinding and polishing a ductile specimen completely plane is very hard. Especially near the edge, and rounding would most likely have happened. This might explain the decrease in hardness, since no other results can help explain this decrease in hardness. No

connection between homogenization times and hardness can be seen. The purpose of homogenization is to eliminate the brittle beta phase. For DC cast samples homogenized for 4 hours at 430°C, beta is still seen. From the hardness measurements, it is evident that this amount of beta phase has little to no effect on hardness. Therefore, Mg in solid solution seems to be the greatest contributor hardness.

A thorough discussion on the beta phase content in all materials is seen in section 5.2. For the DC cast homogenized material, beta particles were clearly seen in the Al-10%Mg samples homogenized at 430°C for 4 hours, but disappeared to the extent that it was no longer visible in the optical microscope after homogenizing at 430°C for 1 week, as seen in section 4.1. Complete homogenization is a function of time and temperature, and it is evident from the visible beta particles in the DC cast samples homogenized at 430°C for 4 hours, that this is not enough time for complete homogenization. When the homogenization temperature was raised to 490°C, no beta was found with either optical or electron microscope.

5.4 Mechanical properties

The mechanical properties of the investigated material has been evaluated by hardness measurements, and tensile tests.

Tensile tests shows very similar UTS and stress-strain curves for screw extruded profiles, and much better UTS than the conventional ram extruded material. Ductility decreases, and strength increases with increasing Mg content across all profiles. Mg in solid solution is a major strength contributing mechanism for the 5xxx series, and with the added plastic deformation introduced by extrusion, this increase in strength with increasing Mg content is expected. The additional plasti deformation introduced by screw extrusion is part of the reason why screw extrusion sees a much higher UTS than conventional extrusion.

The Portevin Le'Chatelier (PLC) effect is seen to a varying degree in all samples. One might expect to see an increase in the amount of serration with increasing Mg content, due to more dislocation solute interactions. This is seen to some extent in the conventional ram extruded profiles,

but not in the screw extruded profiles. In the screw extruded profiles, the PLC effect decreases. Differences between the profiles beyond the Mg content are not immediately seen. Similar grain size is seen in the screw extruded profiles regardless of feed material and Mg content. A higher amount of cracks has been observed with higher Mg content, which should introduce a higher amount of stress concentrations, which in turn should give more solute-dislocation interaction, and more serration in the stress-strain curves. The field of PLC is very large, and regrettably beyond the scope of this work, but understanding the cause of this apparent discrepancy is of interest.

Hardness of the different materials is presented is section 4.5. A major strength contributor in the Al-Mg system is solid solution strengthening, as such, an increase on hardness with Mg is expected. This is mostly seen in all the samples. One deviation from this is the melt spun Al-8%Mg Ribbon, which has the highest hardness. This might be explained by the much thinner thickness, seen in micrographs in section 4.1, which is very small compared to the other alloys. Or it might be an effect of the uncertainty seen with such low loads and thin specimens. The Al-8%Mg ribbons have similar grain size to the Al-10%Mg ribbons, but the ribbon thickness also varied greatly. A thin thickness would affect the hardness by introducing more thermal stress, due to more rapid cooling. Another sample which deviates, is the conventional ram extruded Al-8%Mg. Reasons for this will be discussed in section 5.5.

A direct comparison of hardness across the different material will not be made, as it has been found that such low loads used in this work, introduces quite high uncertainty.

5.5 Correlation between microstructure and mechanical properties

In this section, a correlation between the microstructure and fracture surfaces, and mechanical properties in section 5.4 is discussed.

Screw extruded profiles from both feed materials show similar hardness, and similar UTS. This shows that both feed materials are compactable to a similar degree. The screw extruded Al-

5%Mg machined granulates profile which had large degrees of oxides on the surface of the transverse plane did not show much worse tensile properties due to this. Some loss of ductility can be seen in the stress-strain curves, compared to the profiles from RS ribbons. Similar hardness for this oxide rich profile compared to the profile from RS ribbons is also seen.

The fracture surfaces show decreasing ductility with increasing Mg content. Especially the conventional ram extruded Al-5%Mg profile shows large degree of ductility, with a very pronounced cup and cone shape, large voids in the middle, micro voids in the ductile areas, and large shear surfaces.

Screw extruded Al-10%Mg from both feed materials have fracture surfaces with circular areas with patterns of cracks. This might be due to low degree of compacting in these profiles, however, no apparent loss of strength is seen because of this. One might expect to see some profiles have markedly different tensile properties due to these compacting issues, but this is not seen. One difference in microstructure from the conventional ram extruded profiles to the screw extruded, is the much larger grain size. Grain size refinement is a common strength contributor, and one might reason that grain size is one of the main contributors to the increased strength for screw extruded profiles, alongside the high deformation.

The conventional ram extruded Al-8%Mg profile shows higher hardness than the Al-10%Mg profile. This is unexpected. Over all profiles, an increase in hardness with Mg content is seen, and is expected, due to the contribution from solid solution strengthening. Another contributor to strength in grain size. If The Al-8%Mg profile had a much smaller grain size, this difference in hardness might be explained. It does not have a smaller grain size. The two profiles show similar grain size in fact. The load for hardness measurements on the conventional ram extruded profiles is the same as for screw extruded machined granulates profiles, but the grain size is much larger for the conventional ram extruded profiles. There might therefore be an interaction other than solid solution strengthening an grain size which gives the conventional ram extruded Al-8%Mg the unexpectedly higher hardness. The low load is almost certainly a factor, as internal measurements at the department with a higher load, showed a linear increase of hardness with Mg content. However, since the grain size is so similar, the cause of the increased hardness is unknown. In the future however, a higher load for specimens such as these is recommended.

Comparing hardness of the different material is difficult. For the most part, micro hardness has been done, and as has been discussed in the previous paragraph, this might have a bigger influence on hardness than was originally thought. Instron (2016), a materials testing company, reports uncertainty below 200 gf. Measurements taken at 5 gf as is the case for RS ribbons, and at 500 gf, as is the case for the homogenized material, is therefore not directly comparable. It is therefor best to look at materials tested with similar gf, for comparisons.

6 | Summary and conclusions

The basis material of this work has been three DC cast Al-Mg alloys, with 5-8-and 10wt% magnesium. These base alloys have been used to produce two feed stock materials for a novel screw extrusion method. The first feed material produced was machined DC cast bolt granulates. The second feed material has been remelted DC cast billets that have been rapidly solidified by the melt spinning method.

These feed materials have been screw extruded. A novel method of extrusion developed by Hydro Aluminium in cooperation with the Department of Materials Science and Engineering at NTNU. This has been done in order to better the understanding of screw extrusion, and produce profiles with good mechanical properties.

In addition, a heat treatment schedule of the DC cast material has been done, in order to determine if full homogenization of Al-Mg alloys is possible. Heat treatment was performed in an air circulation furnace.

It has been found that screw extrusion produces profiles with good mechanical properties, compared to conventional extruded profiles. The grain size is much smaller, by approximately 50 µm, and the ultimate tensile strength of screw extruded Al-8%Mg is comparable to conventional extruded Al-10%Mg.

The homogenized DC cast samples shows presence of beta particles, confirmed by energy-dispersive x-ray spectroscopy (EDS), in the Al-10%Mg homogenized at 430°C for 4 hours, but none in Al-5 and 8%Mg samples. No beta particles were found in the samples homogenized to 490°C, though EDS linescans did show both iron, silicon, and oxygen rich particles. Time was found to have an effect on beta and porosity, as DC cast samples homogenized at 430°C for 1

week showed no visible beta, as seen in the optical microscope for the Al-10%Mg sample homogenized for 4 hours at the same temperature. Porosity was also found to change with time and temperature. Porosity tortuousity decreases with increasing magnesium content, and size increases. From as cast to 430°C for 4 hours porosity size and tortuousity increases, but from 430°C to 1 week and porosity size and maybe density decreases.

Progress has been made on characterization of the beta particle. It has been found that determining the amount or presence of beta directly by x-ray diffraction (XRD) is not possible, but the beta phase might be qualitatively compared by calculating the lattice parameter from the XRD results.

The conclusion regarding characterization of beta phase, is that a clear decrease in beta content can be seen for the homogenized particles with increasing temperature. However, a clearer image of the presence of beta phase might be made with greater use of the micro probe, and better knowledge of XRD data interpretation.

Progress has been made regarding production and preparation parameters for the melt spinning and screw extrusion methods. Homogeneous profiles with good mechanical properties have been produces, although some compacting issues, which is a weakness of the screw extrusion method, has been seen.

7 | Recommandations for further work

Screw extrusion is an ongoing field of study at NTNU, and further work is going to be made in this field. Determining the effects of heat treatment of the screw extruded profiles is needed in order to obtain more information on precipitation hardening in Al-Mg alloys, and maybe further improving the properties of the screw extruded profiles. In earlier work (Berulfsen, 2015), some age hardening effects on RS ribbons was found. This was unexpected, as Al-Mg alloys are generally not considered age hardenable, but there might be some positive effect seen still.

Fabricating Al-Mg RS ribbons with several different parameters, to obtain greater knowledge on the parameter effects is needed. The success rate of ribbon fabrication was approximately 50%, and understanding what the difference between a successful and unsuccessful run is limited. in addition, other alloying elements in addition to Mg might be of interest. Especially Zr, as this element has a great effect on the properties in an Al-Mg alloy.

References

Anderson, T. L. (2005). *Fracture Mechanics, Fundementals and Applications, Third Edition*. Taylor and Francis group.

Berulfsen, T. (2015). New rapidly solidified AlMg-x alloys, and their properties, micro- and nanostructures. Norwegian University of Science and Technology, Department of Materials Science and Engineering.

Bilsbak, A. (2012). Mikrostruktur og mekaniske egenskaper for skrueekstrudert aluminium. Master's thesis, Norwegian University of Science and Technology, Department of Materials Science and Engineering.

Birkholz, M. (2006). *Thin film analysis by X-ray scattering*. John Wiley & Sons.

Boettinger, W. J. and Coriell, S. R. (1986). *Science and Technology of the Undercooled Melt: Rapid Solidification Materials and Technologies*, chapter Microstructure Formation in Rapidly Solidified Alloys. Springer Netherlands.

Chaijaruwanich, A., Lee, P., Dashwood, R., Youssef, Y., and Nagaumi, H. (2007). Evolution of pore morphology and distribution during the homogenization of direct chill cast Al–Mg alloys. *Acta Materialia*, 55(1):285 – 293.

Chatterjee, A., Sarkar, A., Barat, P., Mukherjee, P., and Gayathri, N. (2009). Character of the deformation bands in the (A + B) regime of the Portevin-Le Chatelier effect in Al–2.5%Mg alloy. *Materials Science and Engineering: A*, 508(1–2):156 – 160.

Clark, K. (Visited 03/05/2016). http://www.doitpoms.ac.uk/miclib/full_record.php?id=141. Licence: http://creativecommons.org/licenses/by-nc-sa/2.0/uk/legalcode.

Duwez, P., Willens, R. H., and Klement, W. (1960). Continuous Series of Metastable Solid Solutions in Silver-Copper Alloys. *Journal of Applied Physics*, 31(6):1136–1137.

E92-16, A. (2016). *Standard Test Methods for Vickers Hardness and Knoop Hardness of Metallic Materials*. ASTM International. http://dx.doi.org/10.1520/E0092-16.

Friedrich, B., Kräutlein, C., and Krone, K. (2006). Melt treatment of copper and aluminium–the complex step before casting. In *Proceedings of The International Conference on Continous Casting of Non-Ferrous Metals, Wiley-Vch, DGM*, pages 3–22.

Grant, N. (1992). Recent trends and developments with rapidly solidified materials. *Metallurgical Transactions A*, 23(4):1083–1093.

Hjelen, J. (1986). *Scanning elektron-mikroskopi*. Metallurgisk Institttutt, NTH, Sør-Trønderlag, Trondheim, Norway.

Instron (Visited 13/05/2016). *http://www.instron.us/our-company/library/test-types/hardness-test/vickers-test*. Materials testing company.

Kaneko, K., Hata, T., Tokunaga, T., and Horita, Z. (2009). Fabrication and characterization of supersaturated Al-Mg alloys by severe plastic deformation and their mechanical properties. *Materials transactions*, 50(1):76–81.

Kaufmyn, W. (Visited 13/05/2016). http://fog.ccsf.cc.ca.us/%7ewkaufmyn/ENGN45 /ENGN45_Online_Homework/10_Homework_Kinetics_SOLUTIONS.htm.

Leibermann, H. H. (1993). *Rapidly Solidified Alloys : Processes, Structures, Properties, Applications Materials Engineering*. CRC Press.

Lin, Y., Wu, B., Li, S., Mao, S., Liu, X., Zhang, Y., and Wang, L. (2015). The quantitative relationship between microstructure and mechanical property of a melt spun al–mg alloy. *Materials Science and Engineering: A*, 621:212 – 217.

Mauland, E. (2013). Utherdbare bimetall materialer fremstilt ved skrueekstrudering. Master's thesis, Norwegian University of Science and Technology, Department of Materials Science and Engineering.

Míšek, K. (1968). Methods of quenching thin metallic specimens. *Czechoslovak Journal of Physics B*, 18(11):1402–1412.

Murray, J. L. (1982). The almg (aluminummagnesium) system. *Bulletin of Alloy Phase Diagrams*, 3(1):60–74.

Northeastern University (Visited 02/05/2016). http://www.northeastern.edu/nanomagnetism/downloads/Backscattered%20Electron%20Emission.ppt.pdf.

Pedersen, B. D. (2013). Preliminary investigations on the manufacture of AL-AZ31 bimetallic composites by the screw extrusion process. Master's thesis, Norwegian University of Science and Technology, Department of Materials Science and Engineering.

Polmear, I. J. and St. John, D. (2005). *Light Alloys, Fourth Edition*. Butterworth-Heinemann.

Porter, D. A., Easterling, K. E., and Sherif, M. (2009). *Phase Transformations in Metals and Alloys, Third Edition*. CRC press, Taylor and Francis group.

Rollett, A., Humphreys, F., Rohrer, G. S., and Hatherly, M. (2004). *Recrystallization and related annealing phenomena, Second Edition*. Elsevier.

Rotan, M. (2016). Personal communication. Norwegian University of Science and Technology, Department of Materials Science and Engineering.

Samson, S. (1965). The crystal structure of the phase β Mg_2Al_3. *Acta Crystallographica*, 19(3):401–413.

San-Martin, A. and Manchester, F. (1992). The Al-H (aluminum-hydrogen) system. *Journal of Phase Equilibria*, 13(1):17–21.

Sheppard, T. (2013). *Extrusion of aluminium alloys*. Springer Science & Business Media.

Singh, S. (1970). Diffusion coefficients in binary aluminum alloys. *Scripta Metallurgica*, 4(2):147 – 151.

Skorpen, K. G. (2011). Characterization of extruded aluminum. Master's thesis, Norwegian University of Science and Technology, Department of Materials Science and Engineering.

Skorpen, K. G., Mauland, E., Reiso, O., and Roven, H. J. (2014). Novel method of screw extrusion for fabricating Al/Mg (macro-) composites from aluminum alloy 6063 and magnesium granules. *Transactions of Nonferrous Metals Society of China*, 24(12):3886 – 3893.

Slámová, M., Očenášek, V., and Voort, G. V. (2004). Polarized light microscopy: Utilization in the investigation of the recrystallization of aluminum alloys. *Materials Characterization*, 52(3):165 – 177.

Stedje, T. J. (2014). Characterization of screw extruded rapid solidified AA6061. Master's thesis, Norwegian University of Science and Technology, Department of Materials Science and Engineering.

The Science Education Scenter at Carleston College (Visited 27/04/2016). http://serc.carleton.edu/research_feducation/geochemsheets/techniques/sem.html.

Werenskiold, J., Auran, L., Roven, H., Ryum, N., and Reiso, O. (2008). Screw extruder for continuous extrusion of materials with high viscosity. WO Patent App. PCT/NO2007/000,408.

Widerøe, F. and Welo, T. (2013). Using contrast material techniques to determine metal flow in screw extrusion of aluminium. *Journal of Materials Processing Technology*, 213(7):1007 – 1018.

Widerøe, Fredrik (2012). *Material flow in screw extrusion of aluminium*. PhD thesis, 2012:183, Norwegian University of Science and Technology, Department of Materials Science and Engineering.

Zha, M. (2014). *Development and characterizationof high solid solution Al-Mg alloysand an immiscible Al-Bi alloyprocessed by ECAP and annealing*. PhD thesis, 2014:149, Norwegian University of Science and Technology, Department of Materials Science and Engineering.

A | Stress-strain curves

This appendix present all stress-strain curves from the tensile tests performed in this work.

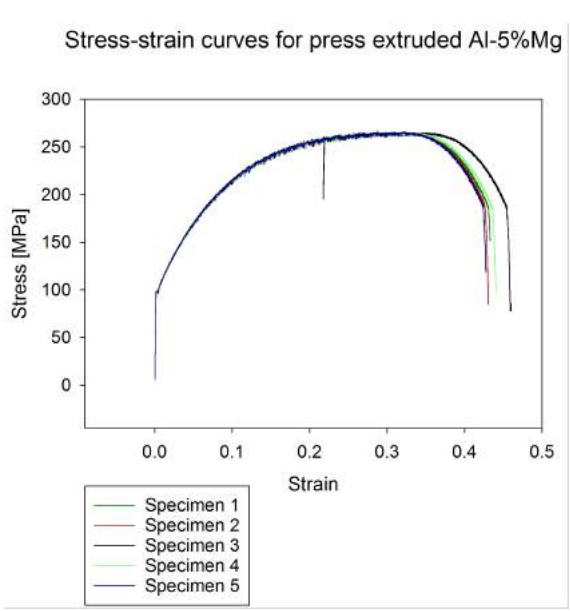

(a)

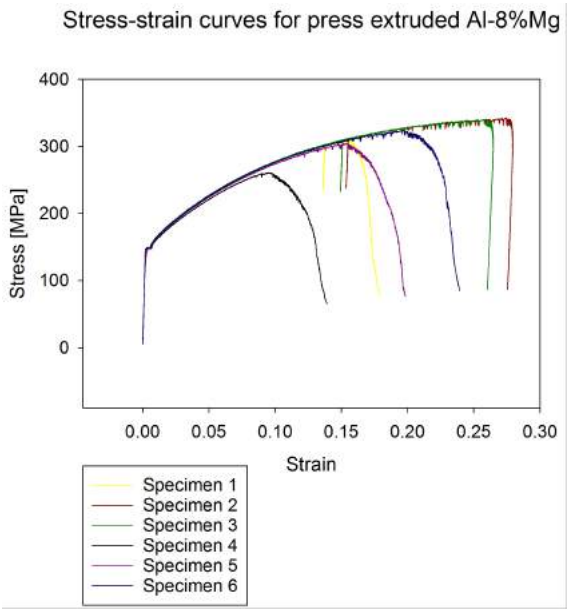

(b)

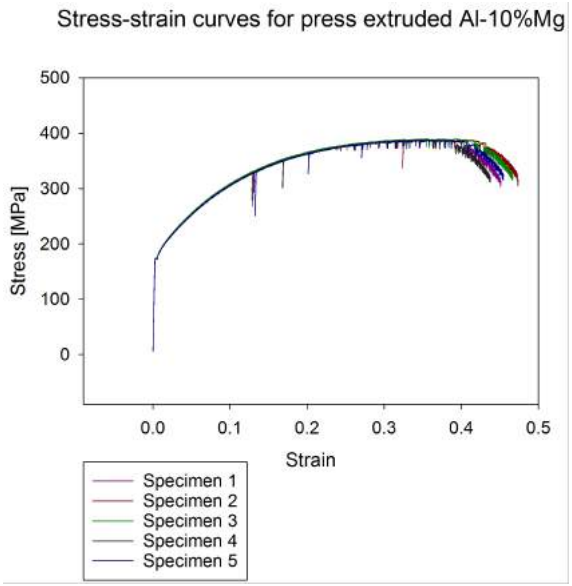

(c)

Figure A.1

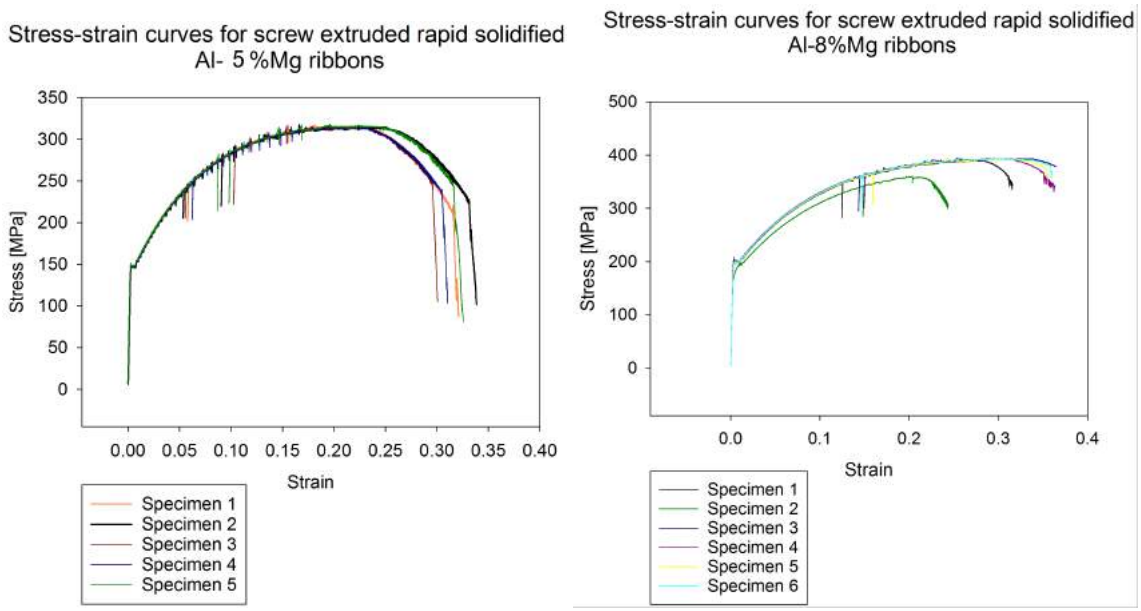

(a)

(b)

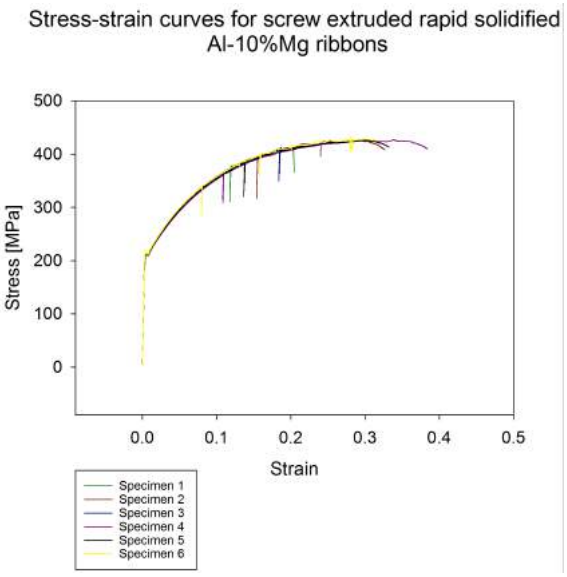

(c)

Figure A.2

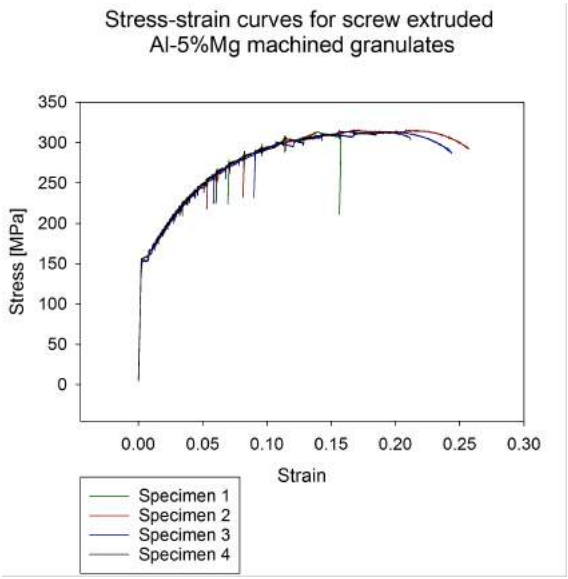

(a)

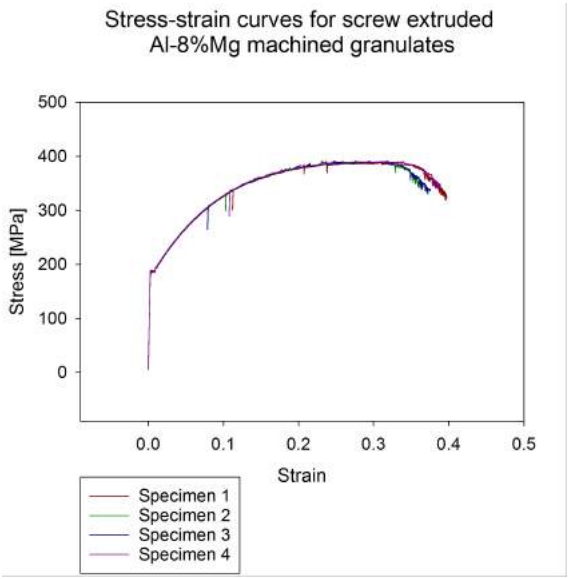

(b)

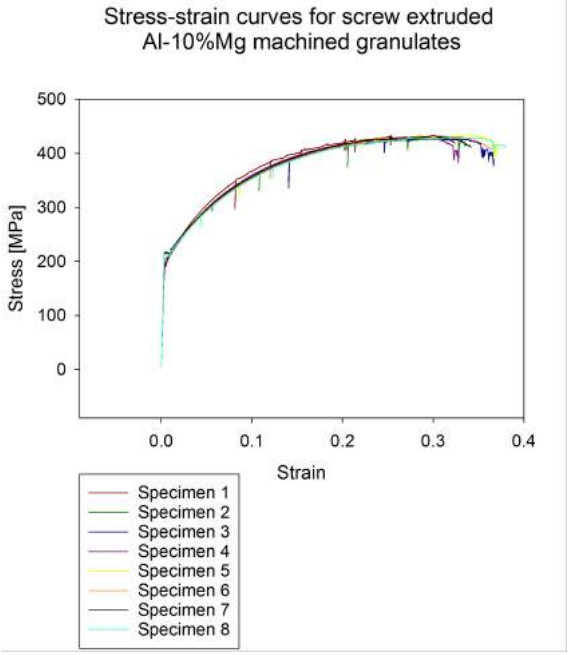

(c)

Figure A.3

B | Specimen preparation

The as cast material, and the heat treated as cast material especially, contained large amounts of porosity. Grinding and polishing by hand resulted in comet like tails emerging from the pores, which gave sub par images. An example of this is given in figure B.1a. Grinding with Streuers RotoPol-31 coupled with Struers RotoForce-4 and polishing with Streuers TegraPol-31 connected to a Streuers TegraForce-5 and TegraDoser-5 which rotates with the direction of the paper, gave much better results, as seen in figure B.1b.

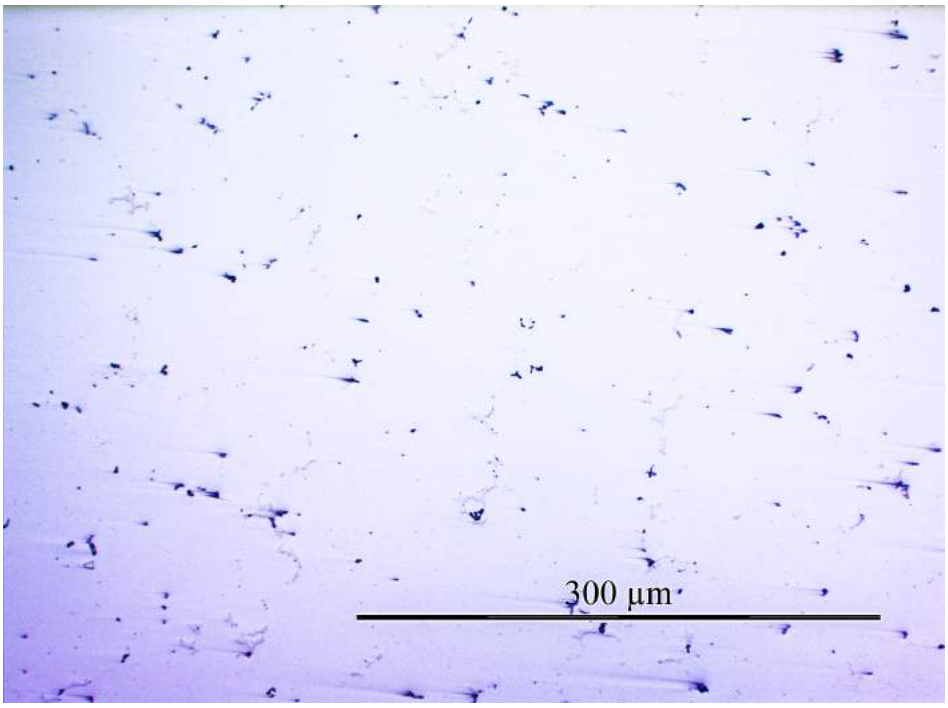

(a)

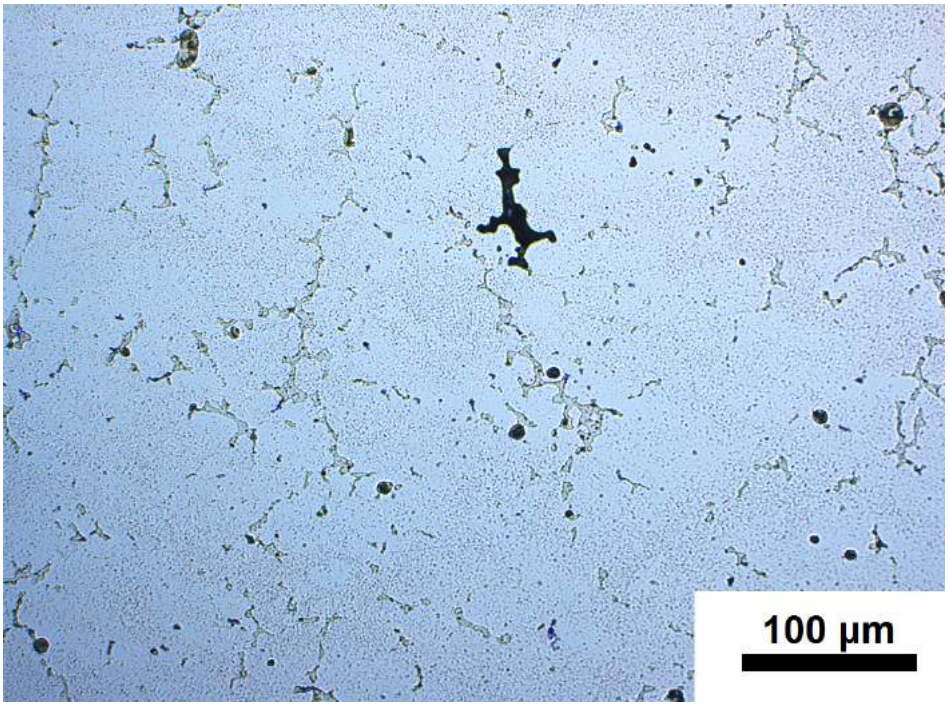

(b)

Figure B.1: .

C | Procedure parameters

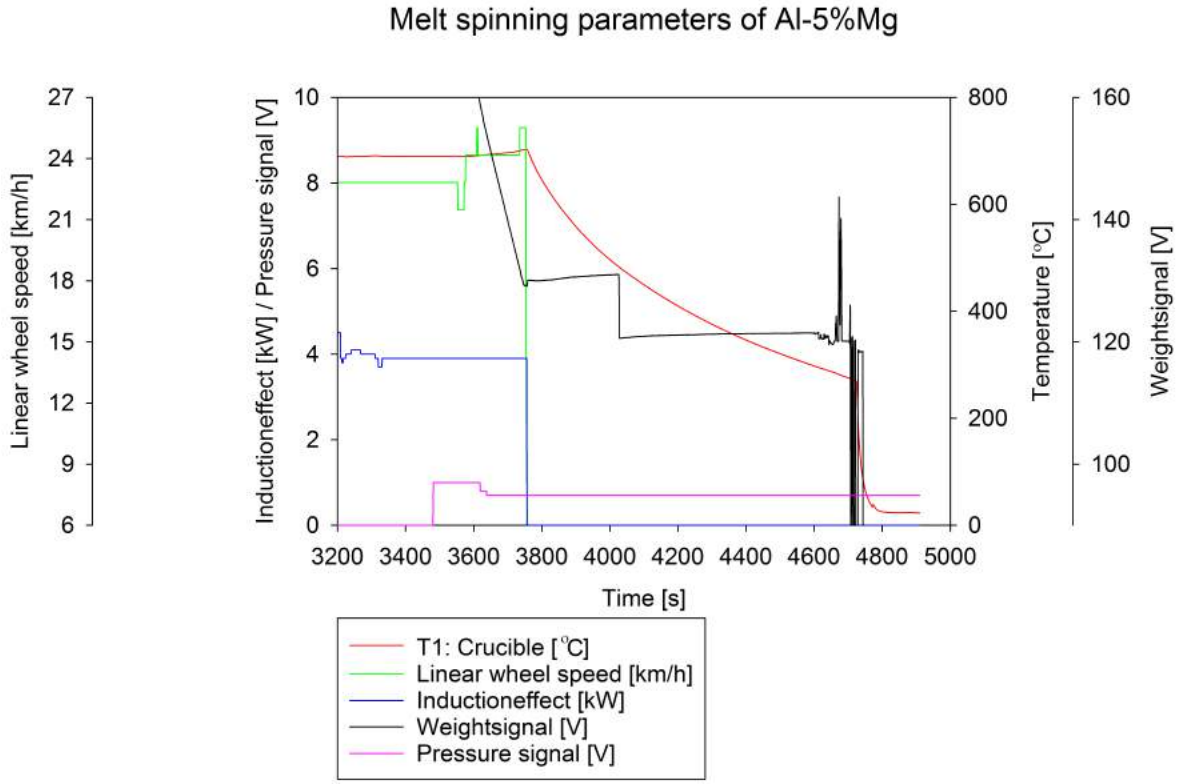

Figure C.1: Parameters used during melt spinning of Al-5%Mg alloys. When the pressuresignal goes above 0, the spinning process has started.

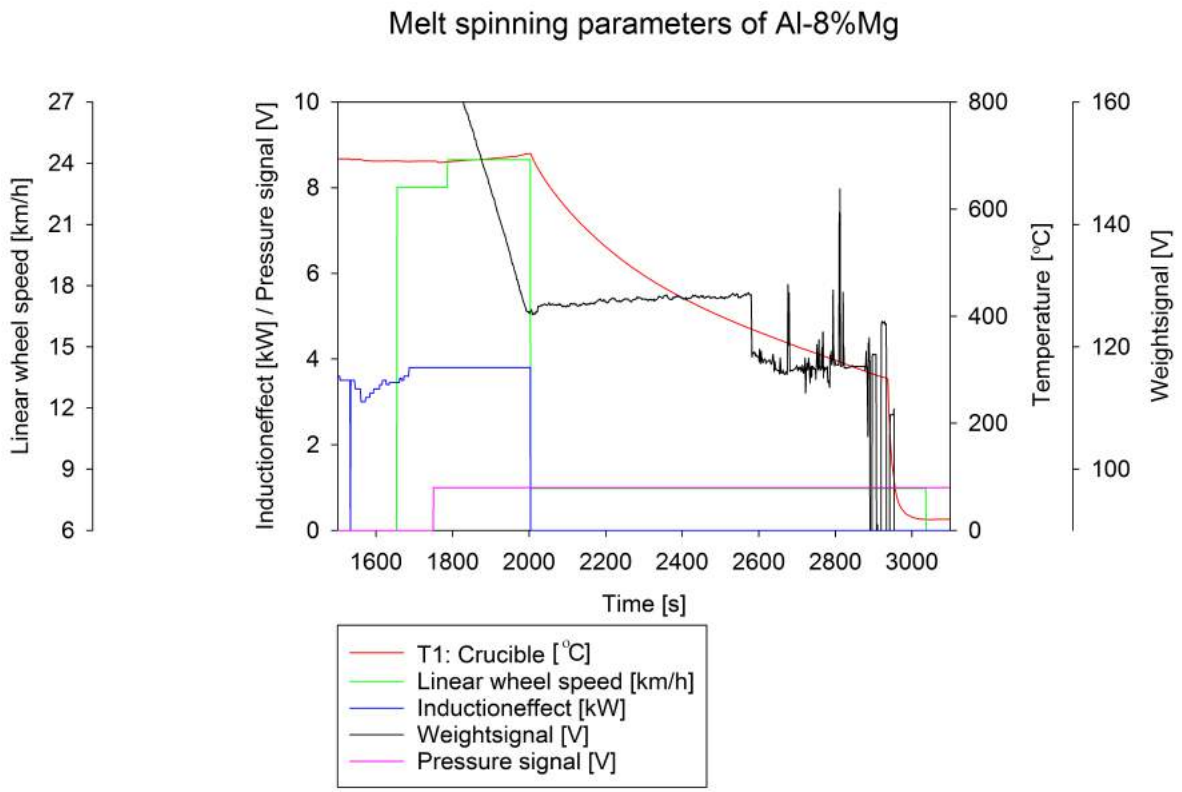

Figure C.2: Parameters used during melt spinning of Al-8%Mg alloys. When the pressure signal goes above 0, the spinning process has started.

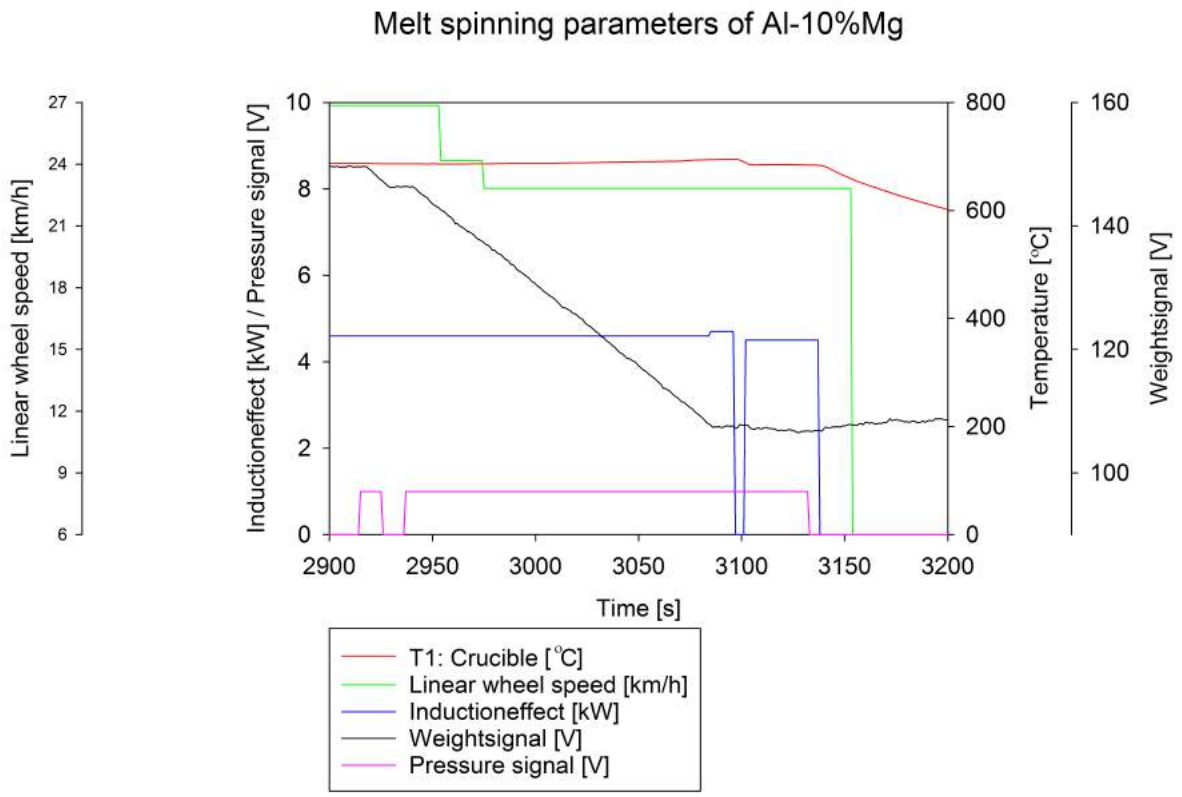

Figure C.3: Parameters used during melt spinning of Al-10%Mg alloys. When the pressuresignal goes above 0, the spinning process has started.

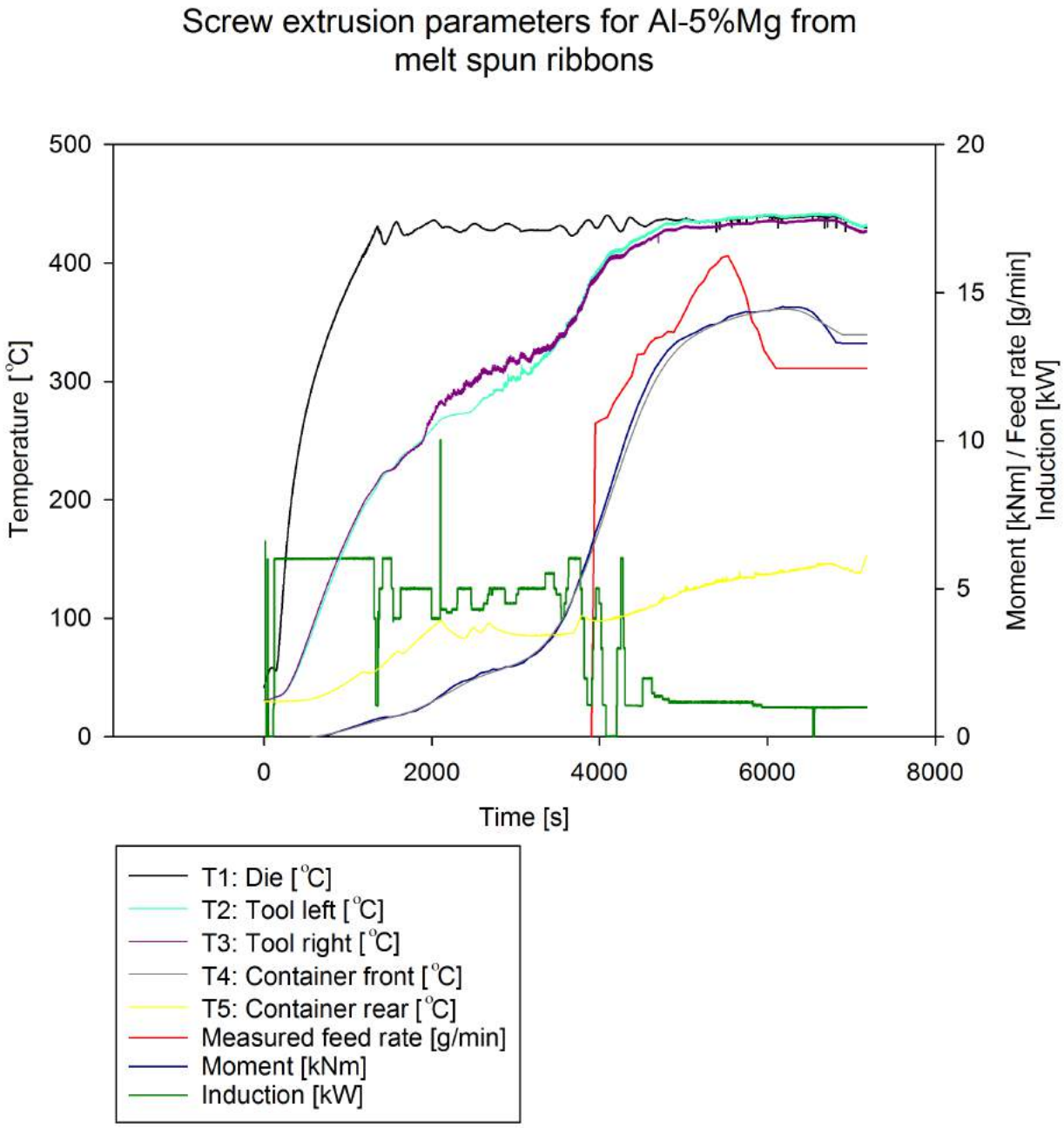
Screw extrusion parameters for Al-5%Mg from melt spun ribbons
Temperature [°C]
Moment [kNm] / Feed rate [g/min]
Induction [kW]
Time [s]
0
100
200
300
400
500
0
5
10
15
20
0
2000
4000
6000
8000
T1: Die [°C]
T2: Tool left [°C]
T3: Tool right [°C]
T4: Container front [°C]
T5: Container rear [°C]
Measured feed rate [g/min]
Moment [kNm]
Induction [kW]

Figure C.4

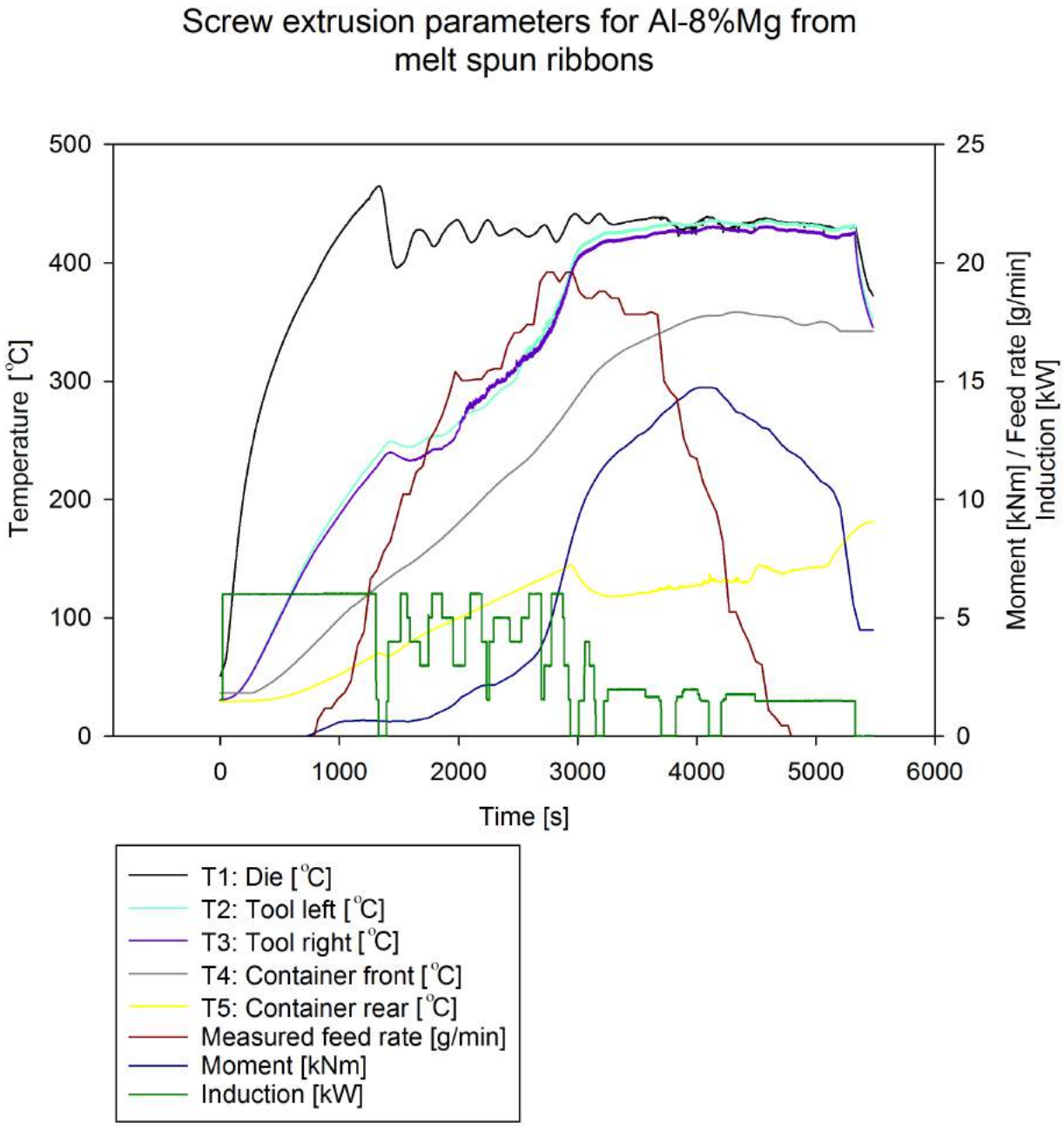
Screw extrusion parameters for Al-8%Mg from melt spun ribbons
Temperature [°C]
Moment [kNm] / Feed rate [g/min]
Induction [kW]
Time [s]
0
100
200
300
400
500
0
5
10
15
20
25
0
1000
2000
3000
4000
5000
6000
T1: Die [°C]
T2: Tool left [°C]
T3: Tool right [°C]
T4: Container front [°C]
T5: Container rear [°C]
Measured feed rate [g/min]
Moment [kNm]
Induction [kW]

Figure C.5

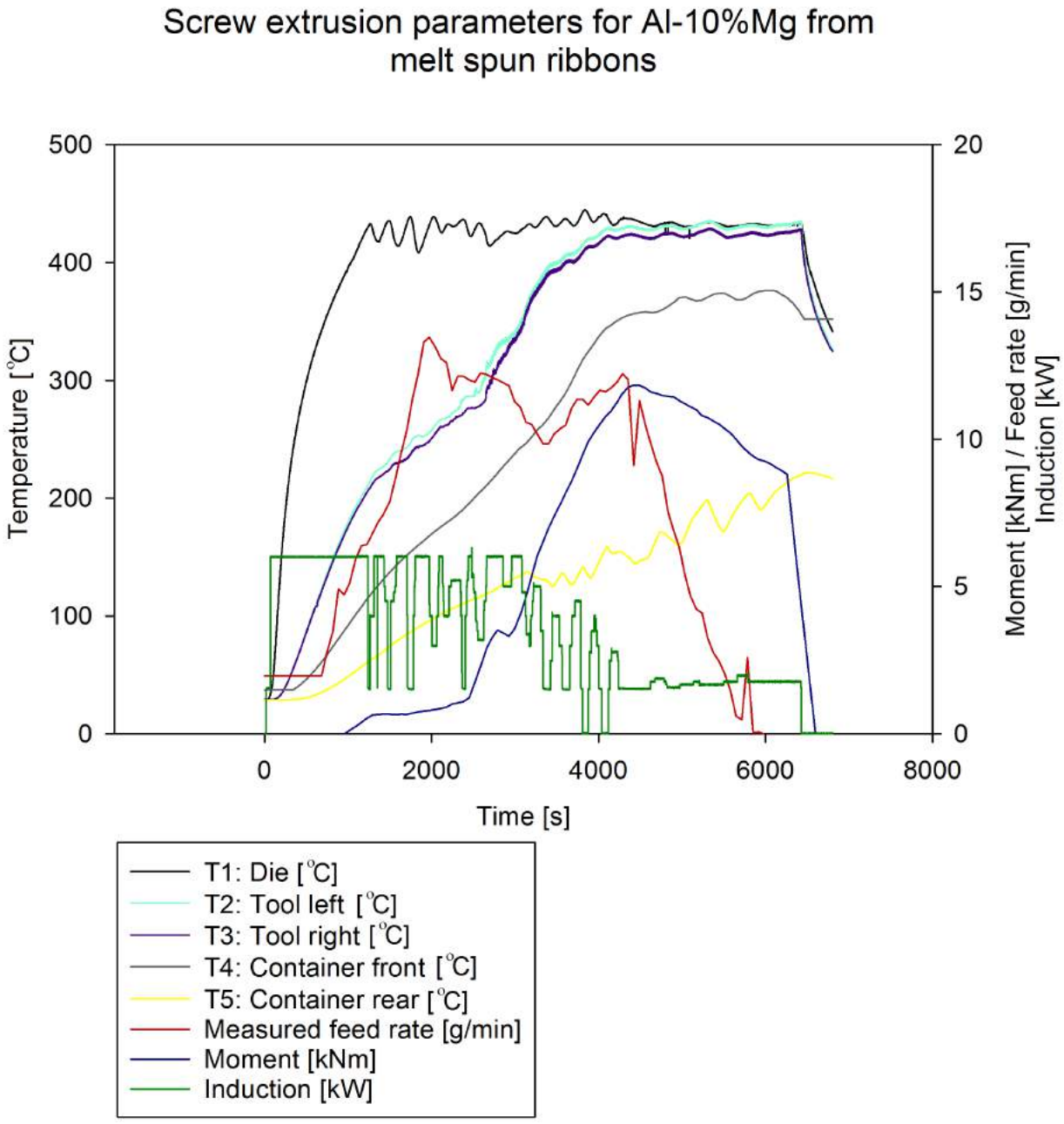
Screw extrusion parameters for Al-10%Mg from melt spun ribbons
Temperature [°C]
Moment [kNm] / Feed rate [g/min]
Induction [kW]
Time [s]
0
100
200
300
400
500
0
5
10
15
20
0
2000
4000
6000
8000
T1: Die [°C]
T2: Tool left [°C]
T3: Tool right [°C]
T4: Container front [°C]
T5: Container rear [°C]
Measured feed rate [g/min]
Moment [kNm]
Induction [kW]

Figure C.6

D | Specific STD of hardness measurements of homogenized material

Table D.1 shows the standard deviation for the hardness measurements seen in figure 4.44.

Table D.1: Specific standard deviation for the hardness values presented in figure 4.44.

	Standard deviation					
Distance [μm]	Heat treated 5 hours	Heat treated 8 hours	Heat treated 9 hours	Heat treated 10 hours	Heat treated 11 hours	Heat treated 13 hours
			Al-5%Mg			
130	3.11	1.77	1.39	5.62	2.86	1.38
405	2.20	1.82	1.89	2.46	1.85	0.92
680	1.94	2.36	1.50	1.10	0.87	1.69
955	2.11	1.89	0.39	1.79	0.82	1.37
			Al-8%Mg			
130	4.47	3.19	1.97	1.88	4.93	4.90
380	1.53	2.47	3.02	0.61	3.37	1.15
630	1.37	0.97	6.72	2.34	1.15	1.37
880	1.94	1.84	3.06	2.68	7.29	1.33
			Al-10%Mg			
130	7.68	2.79	3.21	3.81	1.69	2.66
380	4.36	2.64	0.66	1.11	2.13	5.69
630	3.65	4.03	1.98	3.71	0.72	2.28
880	3.29	1.48	2.22	1.85	1.39	1.27

E | Effect of covering samples with aluminium foil during homogenization

A comparison between covering the homogenized samples with foil, and not covering was performed. The samples were covered with normal aluminium foil by hand, and heat treated at 430°C together with samples that were uncovered. Bright field and polarized light microscopy, together with hardness was performed. No immediate difference could be seen, however, to be on the safe side, it was decided to homogenize with foil.

HOMOGENIZED

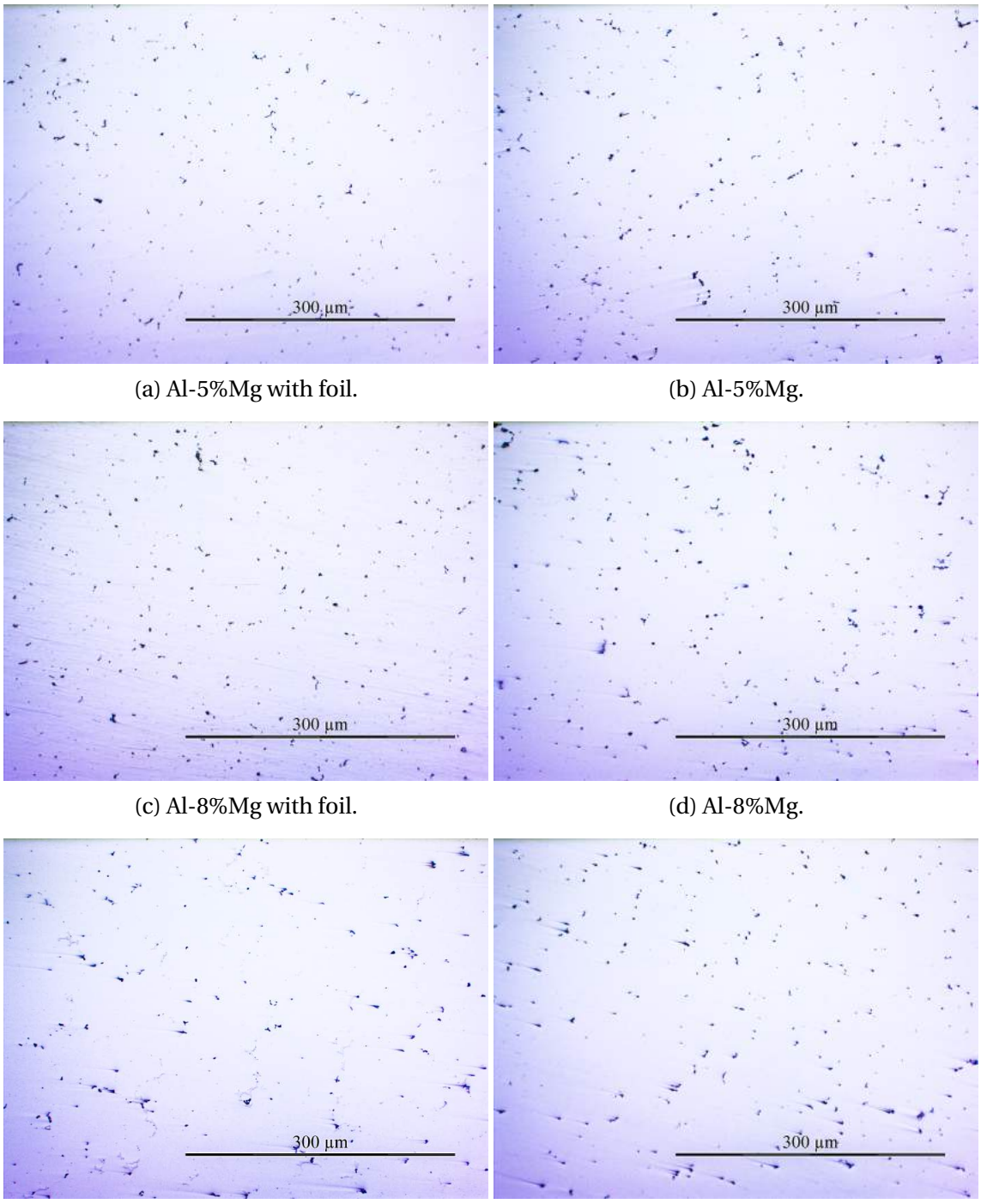

(a) Al-5%Mg with foil.

(b) Al-5%Mg.

(c) Al-8%Mg with foil.

(d) Al-8%Mg.

(e) Al-10%Mg with foil.

(f) Al-10%Mg.

Figure E.1: Micrographs of Al-XMg, following heat treatment schedule 1, covered in aluminium foil, and uncovered , at 200X magnification. No immeadiate difference between covered, and uncovered can be seen.

HOMOGENIZED

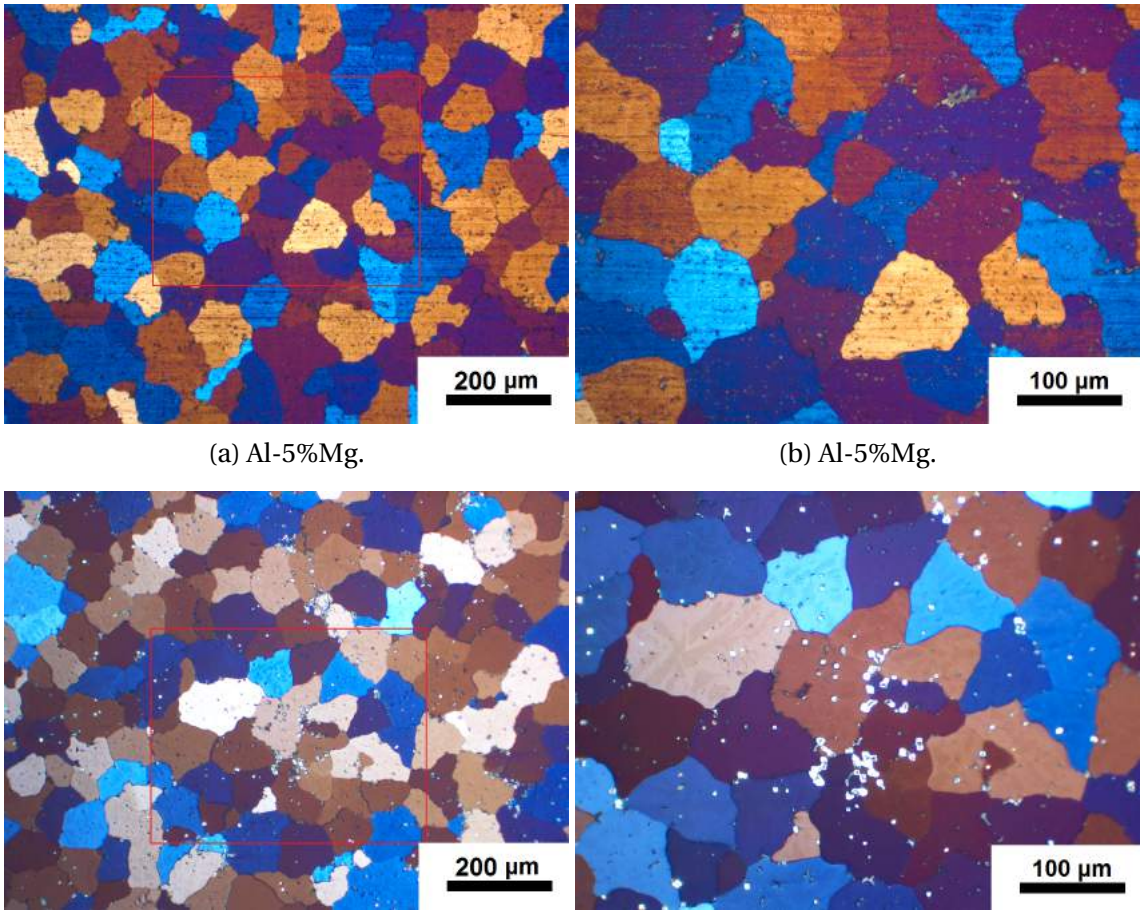

(a) Al-5%Mg.

(b) Al-5%Mg.

(c) Al-5%Mg with foil.

(d) Al-10%Mg with foil.

Figure E.2: Micrographs of Al-5%Mg, following heat treatment schedule 1, covered in aluminium foil, and uncovered. The light particles in the covered samples, might be a difference in anodizing effect, as this effect has been seen in other samples as well. A clear difference in grain size is not seen.

HOMOGENIZED

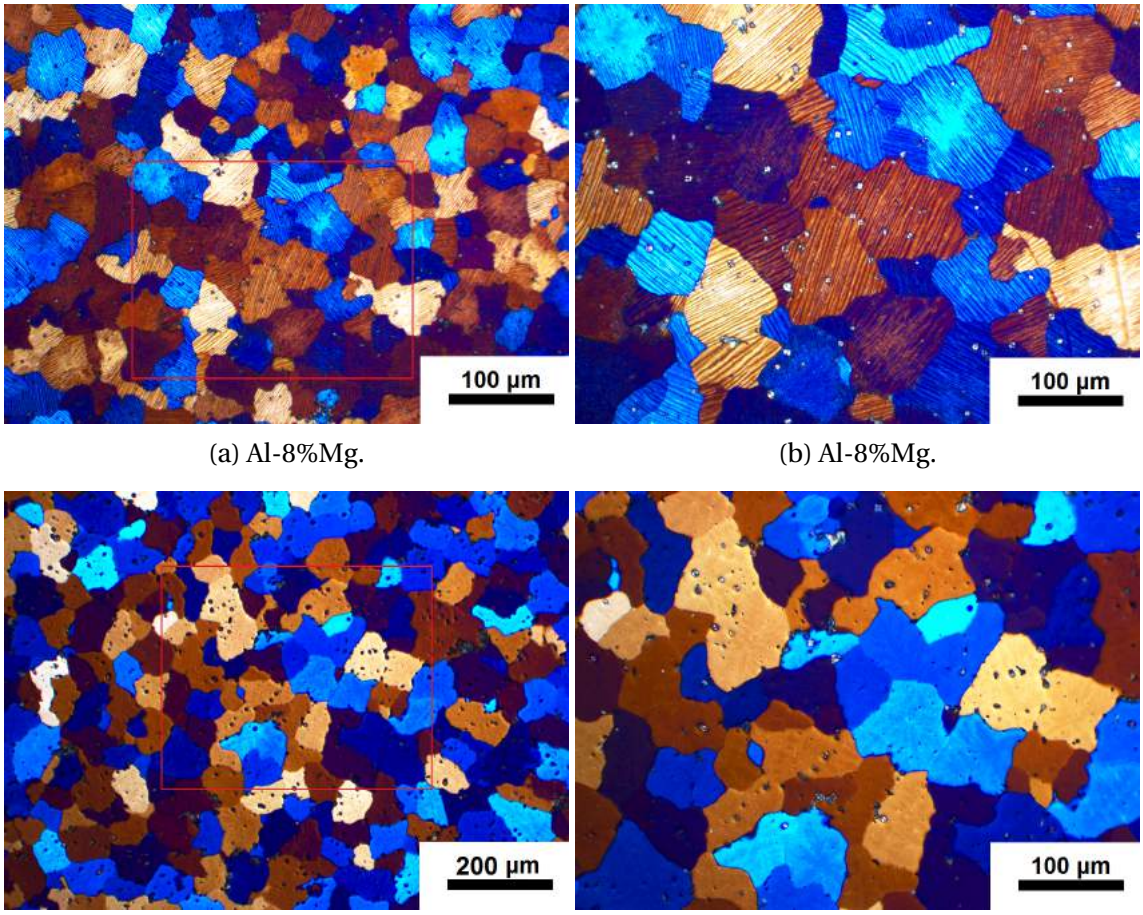

(a) Al-8%Mg.

(b) Al-8%Mg.

(c) Al-8%Mg with foil.

(d) Al-8%Mg with foil.

Figure E.3: Micrographs of Al-8%Mg, following heat treatment schedule 1, covered in aluminium foil, and uncovered. The uncovered samples have a different anodizing surface, with parallel stripes, in each grain. Other clear differences between covered and uncovered are not seen.

HOMOGENIZED

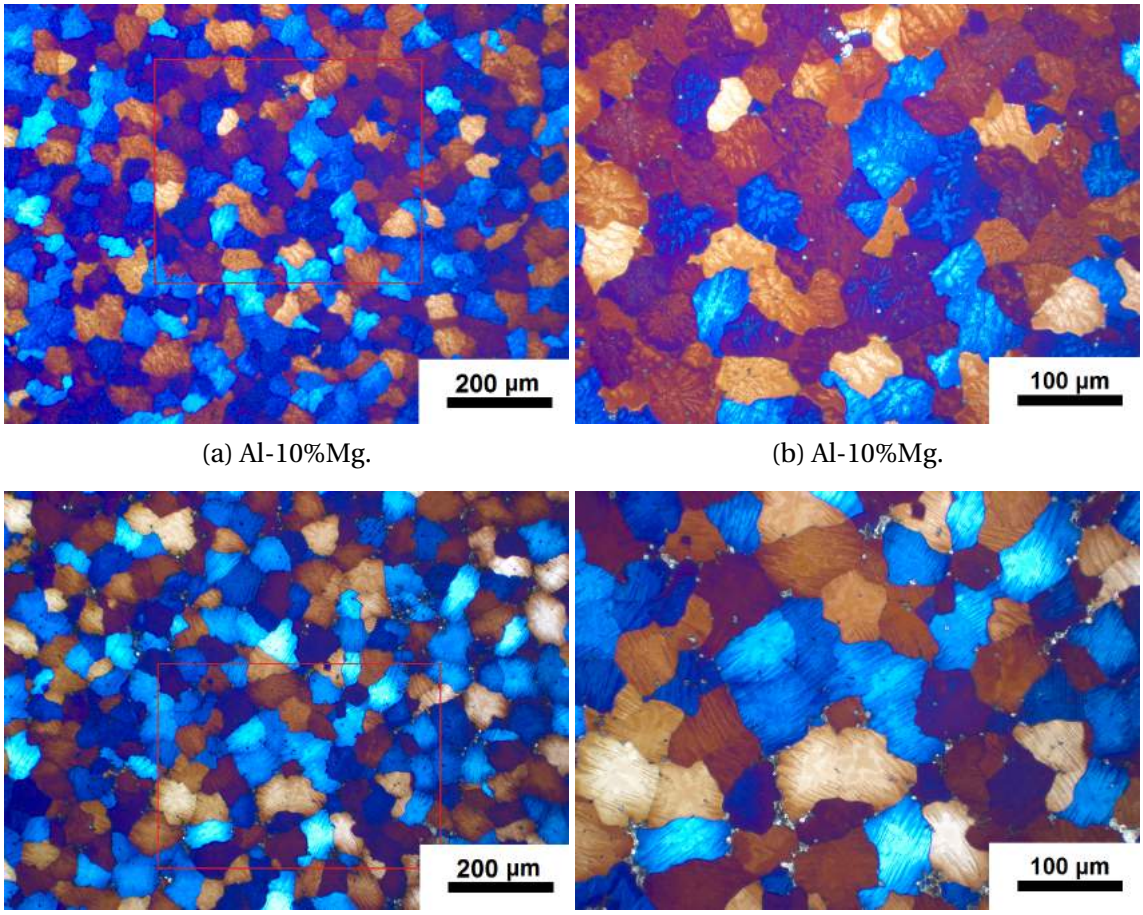

(a) Al-10%Mg.

(b) Al-10%Mg.

(c) Al-10%Mg with foil.

(d) Al-10%Mg with foil.

Figure E.4: Micrographs of Al-10%Mg, following heat treatment schedule 1, covered in aluminium foil, and uncovered. The uncovered samples have dendrite like light areas in each grain, while the covered samples have parallel stripes in each grain. The apparent increase in grey/intermetallic particles might be due to a difference in anodizing effect.

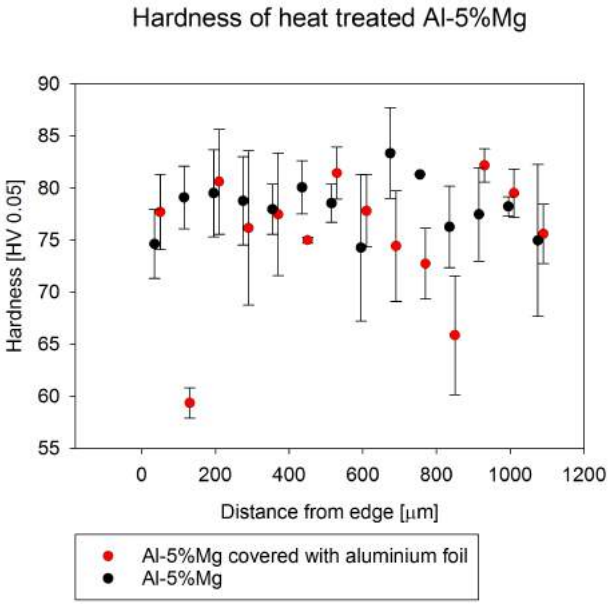

(a)

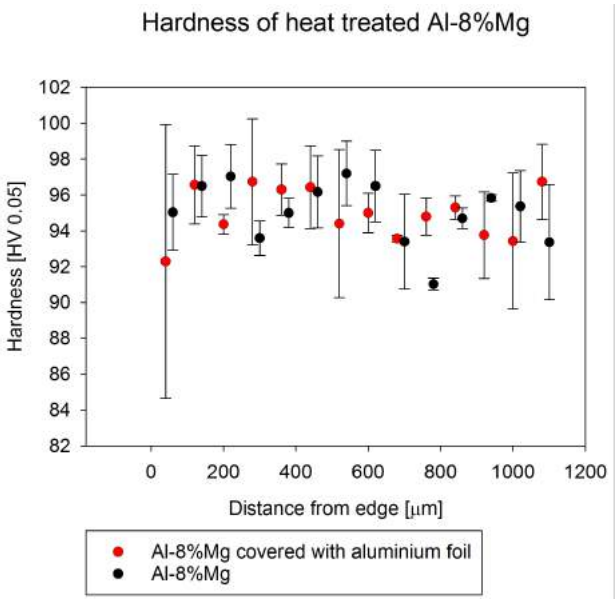

(b)

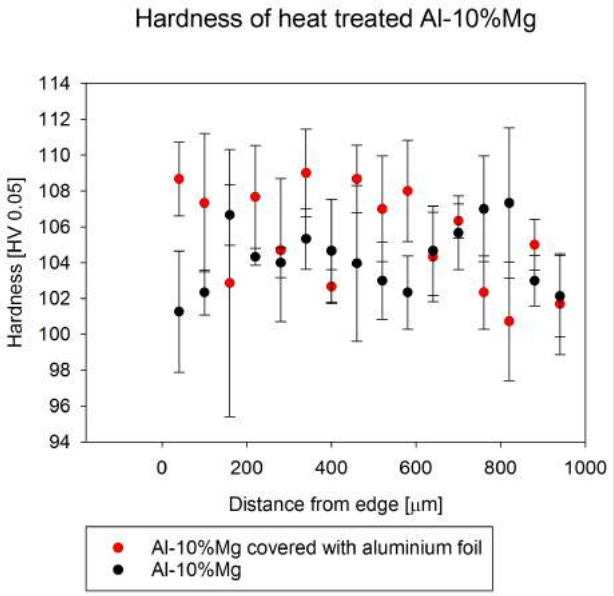

(c)

Figure E.5: .